Title
Micromechanical Framework for Mechanical Behavior of Asphalt Concrete Materials Featuring High Toughness, Low Viscosity Nano-molecular Resins

Author
Zhang, Hao

Publication Date
2019

Peer reviewed|Thesis/dissertation

UNIVERSITY OF CALIFORNIA

Los Angeles

Micromechanical Framework for Mechanical Behavior of Asphalt Concrete Materials Featuring High Toughness, Low Viscosity Nano-molecular Resins

A dissertation submitted in partial satisfaction of the

requirements for the degree Doctor of Philosophy

in Civil Engineering

by

Hao Zhang

2019

ABSTRACT OF THE DISSERTATION

Micromechanical Framework for Mechanical Behavior of

Asphalt Concrete Materials Featuring

High Toughness, Low Viscosity Nano-molecular Resins

by

Hao Zhang

Doctor of Philosophy in Civil Engineering

University of California, Los Angeles, 2019

Professor Jiann-Wen Ju, Chair

Innovative micromechanical-based isotropic formulations have been proposed to predict the mechanical behavior of the asphalt concrete materials featuring high toughness, low viscosity nano-molecular resins and employed for comparisons between model predications and experimental measurements. A class of isotropic elastic-damage model based on a continuum thermodynamic framework is developed within an initial elastic strain energy based formulation. A 3-D analytical modeling methodology is established by treating the revolutionary asphalt concrete material as an asphalt mastic composite matrix

containing fine aggregates, asphalt binder, polymerized DCPD and air voids with coarse aggregates inhomogeneities distributed in it . The effective elastic moduli of the asphalt mastic composites are homogenized by a newly proposed multilevel homogenization approach based on an ensemble-volume averaged pairwise interacting theory. The coarse aggregates are represented by spherical multilayer-coated particles in certain sizes. A governing damage evolution criterion is characterized through the net stress concept in conjunction with the hypothesis of strain equivalence.

An analytical formulation to predict the isotropic viscoelastic properties of the multiphase asphalt mastic composites is proposed within the micromechanical framework based on the concept of the correspondence principle along with the Laplace transform. The viscous behavior induced by the asphalt binder phase is characterized by a 4-parameter Burgers model, from where a multilevel homogenization approach similar to the elastic framework is employed to evaluate the effective viscoelastic mechanical properties of the heterogeneous asphalt mastic composites.

A class of isotropic elastoplastic-damage framework and isotropic thermo-elasto-viscoplastic-damage framework are developed following a similar methodology of the isotropic elastic-damage framework. The plastic and viscoplastic flows are introduced by means of an additive split of the stress tensor and the energy norm of strain tensor is redefined and employed as the equivalent strain. In particular, the Drucker-Prager yield condition is employed to characterize the plasticity behavior and a linear Perzyna type

associative flow rule and viscoplastic hardening law are characterized in terms of the effective quantities in the effective stress space. A rate-dependent damage evolution criterion is introduced within the initial elastic strain energy based micromechanical framework to implement the damage behavior. An Arrhenius-type temperature term, uncoupled with Helmholtz free energy potential, is introduced to account for the effect of temperature. The computation of coupled elastoplastic/ elasto-viscoplastic damage behaviors are realized by a two-step operator splitting methodology.

Numerical simulations are conducted based on the proposed formulations. Particularly, the 3-D modeling is achieved by Python scripting in ABAQUS to make sure there is no overlapping among spherical particle inclusions; while the two-step operator splitting computational algorithms are accomplished through Fortran UMAT. Prediction results are compared with suitably designed experimental data, showing reasonably good agreement.

The dissertation of Hao Zhang is approved.

Ajit K Mal

Ertugrul Taciroglu

Jian Zhang

Jiann-Wen Ju, Committee Chair

University of California, Los Angeles

2019

TABLE OF CONTENTS

LIST OF FIGURES

LIST OF TABLES

ACKNOWLEDGEMENTS

First of all, I would like to express my greatest appreciation and gratitude to my academic advisor, Professor Jiann-Wen Woody Ju, for his countless professional guidance, continuous encouragement, personal kindness and genuine care. Without Professor Ju's invaluable advice and significant support, this doctoral research would not have been possible to start and continue. Moreover, I have learned not only how to do research, but also how to treat people in great manners and deal with matters methodically from Professor Ju. He is my real advisor and mentor in my life.

I would also like to express my deepest appreciation to Professor Ajit Mal, Professor Ertugrul Taciroglu and Professor Jian Zhang who taught me during my M.S. program in UCLA and now serve in my Ph.D. dissertation committee.

I would like to express my sincere appreciation to Dr. Kuo-Yao Yuan for offering experimental data of indirect tension test conducted by him and Dr. Wei Yuan. Validations of my theoretical framework would not have been possible without these experimental data. I also owe special thanks to my office mates for their encouragement and unforgettable happy time together in and outside the office.

Finally, my gratitude and appreciation go to my parents, all other family members and friends. It is their endless love, encouragement and support that make my doctoral journey bright.

VITA

July 14, 1989	Born, Suihua, China
July, 2013	Bachelor of Science
	Department of Civil Engineering
	Harbin Institute of Technology, China
June, 2014	Master of Science
	Department of Civil and Environment Engineering
	University of California, Los Angeles
2014-2019	Graduate Student Researcher/ Teaching Assistant/
	Teaching Associate/ Teaching Fellow
	Department of Civil and Environmental Engineering
	University of California, Los Angeles

CHAPTER 1 : INTRODUCTION

1.1 Motivation

Roads are an integral part of our daily lives, while potholes on the roads are the lowly annoyance that cause millions of dollars in vehicle damages, national infrastructure repairing costs, business and economic loss, and a large portion of highway deaths every year. Potholes are formed by water, freezing and freeze-thaw cycles, excessive heat, wear and tear, and time. The areas that are most prone to pothole development are the poor drainage areas, particularly where roads dip, such as the trough under viaducts, where vehicular traffic is greatest and where poor maintenance allows small fissures to deteriorate. Pothole are not limited to cities in the Snowbelt, according to TRIP® (TRIP, 2016) and the Federal Highway Administration's annual survey (FHWA, 2014, 2017), the city of Los Angeles has 64% of roads ranked as poor, followed by San Francisco-Oakland with 60%, San Jose 56% and San Diego 55%. In 2014, the percentage of poor roads in Los Angeles and San Francisco even increased to 73% and 74%. The cost of repairing each pothole can be as high as $60, and the average annual cost for vehicle repairs due to potholes for individual motorists is $671.

Today, the nation annually invests about $68 billion to fix crumbling highway, roads and bridges. However according to the National Surface Transportation Policy and

Revenue Study Commission of the U.S. Congress, the annual investment required by all levels of government to simply MAINTAIN the nation's highways, roads, and bridges is estimated to be $185 billion per year for the next 50 years. The cost of bad roads to American business between now and 2022 is estimated to be $240 billion, according to the ASCE. Apart from that, personal injury lawsuits due to potholes are very expensive to public and private property owners. For instance, New York City paid out nearly $138 million over the past six years to settle more than 4000 lawsuits connected to personal injury and property damage from potholes.

The issue of fixing potholes is of great urgency. Various repairing materials and technologies were developed in the past several decades in order to solve the issue of potholes and there is a range of methods employed in different places at different times of year. For example, hot mix, hot box mix or recycled hot mix are used when the weather is warm and dry. Temporary cold patch is applied when the weather is cool but dry, whereas advanced polymer-modified cold patch is applied when the weather is cold and wet. Polyurethane-base systems, mobile infrared repair-recycle vehicles and "pothole killer" truck-mounted units are valid on dry road surfaces, no matter what the temperature is. Recently researchers at UCLA (Kao et al., 2011; W. Yuan et al., 2012; W. Yuan et al., 2013; W. Yuan et al., 2011) proposed a radically different solution by using a low viscosity, high toughness dicyclopentadiene (DCPD) resin as a binder or reinforcement in asphalt-aggregate pothole repair materials. After the DCPD resin is infiltrated, cured and hardened

under controlled conditions, it will form a continuous network of mechanical "cages" that lock in asphalt-aggregates, serve as load bearing component under repeated traffic stresses, provide compressive shear load strength, anchor patches with original pavement walls and sub-bases, prevent water infusion and serve as barrier for alligator cracks initiations and propagations.

A schematic of the infiltration of p-DCPD resin into the asphalt concrete mixture is illustrated in Figure 1.1, which shows the cured continuously caged network of DCPD polymer holding the aggregates together through the connected voids in a packed aggregate mixture. This caging effect provides strong confinement and dramatically improves the mechanical properties, rutting resistance, fatigue life and temperature stability of the patches.

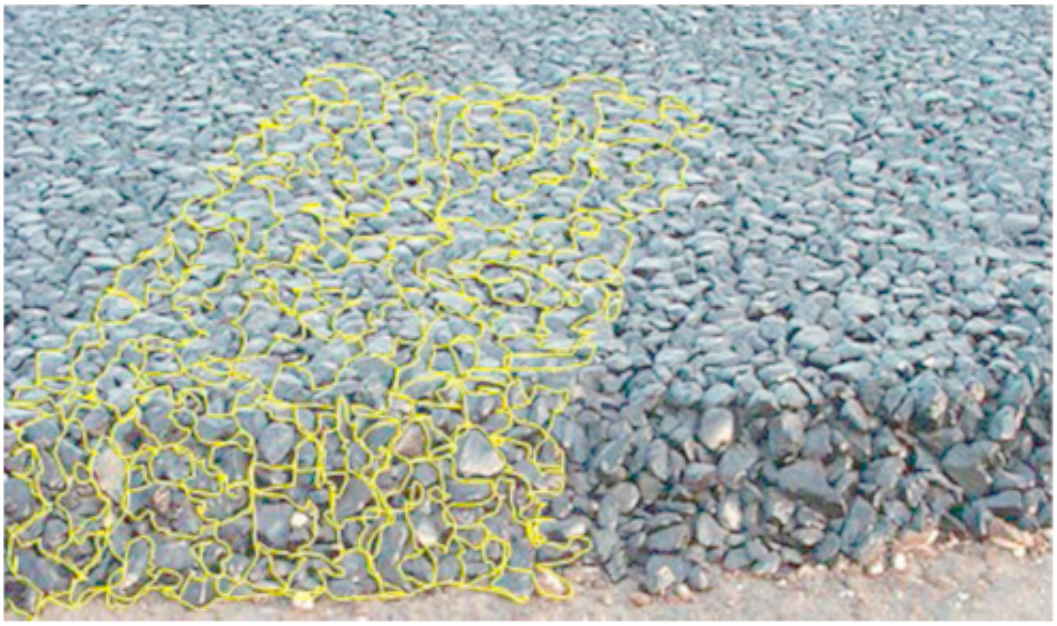

Figure 1.1 The schematic illustration of the caged asphalt concrete mixture with infiltrated p-DCPD (illustrated in yellow networks)

This revolutionary pothole patching technology will apparently provide extended endurance and serviceability of the repaired road surfaces thus reduce the maintenance costs, vehicle damages and personal injuries. X-ray computer tomography and a large amount of indirect tension and pine rutting tests were conducted to demonstrate that DCPD infiltration approach could greatly reduce the air voids and improve the mechanical properties of the asphalt concrete materials (W. Yuan et al., 2012; W. Yuan et al., 2011). Experiments also investigated the DCPD reinforcement for hot mix and cold mix during pothole repairs, as well as the bonding strength improvement enabled by DCPD between repair materials and original pavement (Colorado et al., 2014; W. Yuan et al., 2012; W. Yuan et al., 2013). Compared to the various experimental studies carried out on the DCPD infiltrated asphalt concrete materials, there is a lack of studies that physically described and explained the complex and instantaneous damage and repairing (healing) phenomena of the innovative asphalt concrete materials. Therefore, a rigorous computational framework needs to be established and a reliable mechanical modeling is required to predict the mechanical behavior of innovative asphalt concrete materials.

1.2 Objectives and Outline

The initial objective of this thesis research is to develop micromechanical-based multi-dimensional isotropic damage framework for innovative asphalt concrete materials

infiltrating high toughness, low viscosity nano-molecular resins. The major tasks of this research are concluded as follows:

1. **Development of a micromechanical-based isotropic elastic-damage framework of innovative asphalt concrete materials featuring high toughness, low viscosity nano-molecular resins**: A 3-D analytical modeling methodology is proposed based on the micromechanics framework, assuming that the innovative asphalt concrete materials are isotropic and behavior of the materials is within elastic range. The materials are separated into two parts, matrix and inhomogeneities, respectively: 1). asphalt mastic containing fine aggregates, asphalt binder, polymerized DCPD and air voids, 2). coarse aggregates. The effective elastic moduli of the asphalt mastic composites are homogenized by a newly proposed multilevel homogenization approach and validated employing bounds and inclusion theories. The coarse aggregates are represented by spherical multilayer-coated particles in certain sizes. A damage variable is introduced to predict the damage behavior of the materials with the initial elastic strain energy norm criterion. The elastic behavior and the damage behavior are uncoupled through the net stress concept in conjunction with the hypothesis of strain equivalence. Numerical simulations are then conducted based on the 3-D analytical modeling methodology.

2. **Development of a micromechanical-based isotropic elastoplastic-damage framework of innovative asphalt concrete materials featuring high toughness, low viscosity nano-molecular resins**: By employing the 3-D analytical modeling methodology

proposed in the previous task, where the asphalt concrete materials are separated into 4-phase asphalt mastic matrix and spherical inhomogeneities. The effective elastic moduli of the asphalt mastic composites are homogenized by the multilevel homogenization approach with the aid of a pairwise interacting inclusion theory. The coarse aggregates are represented by spherical multilayer-coated particles in certain sizes. The plastic flow is introduced by means of an additive split of the stress tensor. In particular, plastic flow and hardening law are characterized in terms of the effective quantities in the effective stress space. A damage variable is introduced to predict the damage behavior of the materials with the initial elastic strain energy norm criterion. A computational algorithm is systematically developed based on the operator splitting methodology. Numerical simulations are then conducted based on the 3-D analytical modeling methodology.

3. **Development of a micromechanical-based isotropic thermo-elasto-viscoplastic-damage framework of innovative asphalt concrete materials featuring high toughness, low viscosity nano-molecular resins**: The previous 3-D analytical modeling methodology is extended from elastoplastic range to elasto-viscoplastic range. The viscoplastic flow is introduced by means of an additive split of the stress tensor and the energy norm of strain tensor is redefined and employed as equivalent strain. In particular, a linear Perzyna type associative flow rule and viscoplastic hardening law are characterized in terms of the effective quantities in the effective stress space. A rate-dependent damage corrector is introduced within the initial elastic strain energy based

micromechanical framework to implement the damage behavior. The computational algorithm developed for elastoplastic damage framework is also extended to elasto-viscoplastic range based on the operator splitting methodology. An Arrhenius-type temperature term, uncoupled with Helmholtz free energy potential, is introduced to account for the effect of temperature. Numerical simulations are conducted based on the analytical modeling methodology.

4. **Development of a mechanical field application of Burgers model on predicting the viscoelastic properties of innovative asphalt mastic composites featuring high toughness, low viscosity nano-molecular resins**: An analytical modeling methodology is proposed to predict the isotropic viscoelastic properties of the 4-phase asphalt mastic composites. Viscous boundary value problems are structurally analogized with the classical elastic boundary value problems owning to the concept of the correspondence principle along with the Laplace transform. A multilevel homogenization approach is employed to evaluate the effective bulk and shear relaxation functions, creep compliance, and complex modulus of the composites based on a 4-parameter Burgers viscous model. 2-D creep simulations under the plane stress condition are conducted and numerical results are compared with theoretical derivations.

The content of the subsequent chapters is described as follows: Chapter 2 summarizes the review of related theories and literature. Chapter 3, 4, 5 and 6 develop the

aforementioned four major tasks, respectively. Chapter 7 summarizes the conclusions of this research and describes the future research plans.

1.3 References

Colorado, H. A., Yuan, W., Guo, Z., Juanri, J., & Yang, J. M. (2014). Poly-dicyclopentadiene-wollastonite composites toward structural applications. *Journal of Composite Materials, 48*(16), 2023-2031.

FHWA. (2014). Highway Statistics, Table HM-63, Miles by Measured Pavement Roughness / Present Serviceability Rating.Federal Highway Administration.

FHWA. (2017). U.S. Department of Transportation, 2015 Conditions and Performance Report to Congress: Status of the Nation's Highways, Bridges, and Transit: Conditions & Performance.Federal Highway Administration.

Kao, W. H., Carlson, L., Yang, J. M., & Ju, J. W. (2011). US9348024B2.

TRIP. (2016). Urban Roads TRIP Report: Bumpy roads ahead: America's roughest rides and strategies to make our roads smoother.TRIP.

Yuan, W., Yuan, K. Y., Zou, L., Yang, J. M., Ju, J. W., Kao, W., . . . Stephen, T. (2012). *DCPD resin catalyzed with Grubbs catalysts for reinforcing pothole patching materials.* Paper presented at the SPIE 8347, Nondestructive Characterization for Composite Materials, Aerospace Engineering, Civil Infrastructure, and Homeland Security 2012, San Diego, California.

Yuan, W., Yuan, K. Y., Zou, L., Yang, J. M., Ju, J. W., Kao, W., . . . Aktan, A. E. (2013). *Two layer structure for reinforcing pothole repair*. Paper presented at the Nondestructive Characterization for Composite Materials, Aerospace Engineering, Civil Infrastructure, and Homeland Security 2013.

Yuan, W., Yuan, M., Zou, L., Yang, J. M., Ju, W., Kao, W., . . . Solamon, R. (2011). *Development of high-toughness low-viscosity nano-molecular resins for*

reinforcing pothole patching materials. Paper presented at the SPIE 7983, Nondestructive Characterization for Composite Materials, Aerospace Engineering, Civil Infrastructure, and Homeland Security 2011, San Diego, California.

CHAPTER 2 : LITERATURE REVIEW

2.1 Overview of Continuum Damage Mechanics

Engineering materials such as metals, alloys, polymers, composites, asphalt, concrete, rocks, ceramics and wood share similar qualitative mechanical behavior despite their completely different physical microstructures. All of these materials show elastic behavior, yielding, some form of plastic or irreversible deformation. Other behaviors noted are anisotropy induced by strain, cyclic hysteresis loops, damage by monotonic loading or by fatigue, and crack growth under static or dynamic loads. These phenomena suggest that common mesoscopic properties can be interpreted by a few energy mechanisms that are similar for all these materials. Therefore, it is possible to successfully explain material behavior with the mechanics of continuous media and the thermodynamics of irreversible processes, which model the materials without detailed reference to the complexity of their physical microstructures.

Continuum damage mechanics, developed based on the assumption that the damaged material is a macroscopically homogeneous one, leads to the possibility of globally modeling the nucleation and the propagation of micro-defects including their effect on the mechanical behavior. It has been extensively introduced and employed for decades to describe the progressive degradation experienced by the mechanical properties of materials

prior to the initiation of macro-cracks. Palmgreen, Miner, and Robinson pioneered the concept of a variable related to the progressive deterioration prior to failure (Lemaitre, 1992). However, the starting point of continuum damage mechanics was in 1958, when L.M. Kachanov published the first paper on the creep of metals by introducing a field variable ψ called 'continuity' (Kachanov, 1958, 1999). Fifteen years later, a simple equation, $D=(1-\psi)$, received the status of an internal state variable in the thermodynamics sense where D $(0 \le D \le 1)$ depicts damage ($D=0$ denotes the undamaged state while $D=1$ signifies failure). However, during these fifteen years, this concept was practically ignored and only one important result appeared in 1968, which was the concept of effective stress introduced by Y.N. Rabotnov (Rabotnov, 1963). The basic developments of damage mechanics occurred during the 1970s, at least ten years after the tremendous development of fracture mechanics. In the 1980s, the theory was set up on a more rigorous basis using thermodynamics (Coleman & Gurtin, 1967; Germain et al., 1983; Hill & Rice, 1973; Rice, 1971) and micromechanics (Ju, 1989; Krajcinovic & Fanella, 1986; C. H. Wu, 1985), and applications of continuum damage mechanics to engineering began as many more people were involved in this discipline such as the applications to the modeling of creep damage (Krajcinovic, 1983; Levine, 1982), fatigue damage (Miner, 1945; Mould et al., 1994), elasticity coupled with damage (Krajcinovic & Fonseka, 1981; Lemaitre, 1971) and ductile plastic damage (Beremin, 1981; Krajcinovic & Fonseka, 1981; Rice & Tracey, 1969; Tai & Yang, 1986). Kachanov (Kachanov, 1958, 1999) was the first

to introduce the effective stress concept to model creep rupture. Later, the damage mechanics was widely used to model damage of fatigue and creep, ductile plastic damage (Chow & Wang, 1987) and damage of engineering materials such as concrete (Ortiz, 1985, 1987a, 1987b) soils (Ju & Yuan, 2012; Ju, Yuan, & Kuo, 2012; Ju, Yuan, Kuo, et al., 2012) composite materials (Ju et al., 2009; Ju & Yanase, 2009, 2010) and asphalt concrete (Hong et al., 2017; H. J. Lee et al., 2000; Park et al., 1996).

2.2 Continuum Damage Mechanics

2.2.1 Clarification of Damage

Material damage has been defined as a progressive, physical process by which materials break, and the study of the mechanics of such damage is based on internal variables and the mechanisms involved in the deterioration under the loading condition. Damage of materials can generally be classified in terms of scale. At the microscale level of the representative volume element, damage is induced by the accumulation of micro-stresses in the neighborhood of interfaces and/or defects, resulting in the breaking of bonds. At the mesoscale level, damage results from the growth and the coalescence of microcracks and/or microvoids that initiate one crack. At the macroscale level, the cracks that have been formed expand and grow. The first stage at microscale level requires micromechanical damage models in order to model microstructural change and individual microcracks or phenomenological continuum damage models to model distributed microcracks. The

second stage at mesoscale level may be studied by means of damage variables of the mechanics of continuous media defined at the mesoscale level. The third stage at macroscale level is usually studied using fracture mechanics with variables defined at the macroscale level. The consideration of a crack at the macroscopic level in the framework of fracture mechanics deduces a defect that substantially larger than the microscopic heterogeneities (grains, subgrains, other defects and microcracks, etc.). It is assumed that the main macroscopic crack is propagated through several grains to show a sufficient macroscopic homogeneity in size, geometry and direction, leading to possible treatment using the concepts of fracture mechanics. Chaboche's schematic illustration of these concepts is shown in Figure 2.1 and Figure 2.2.

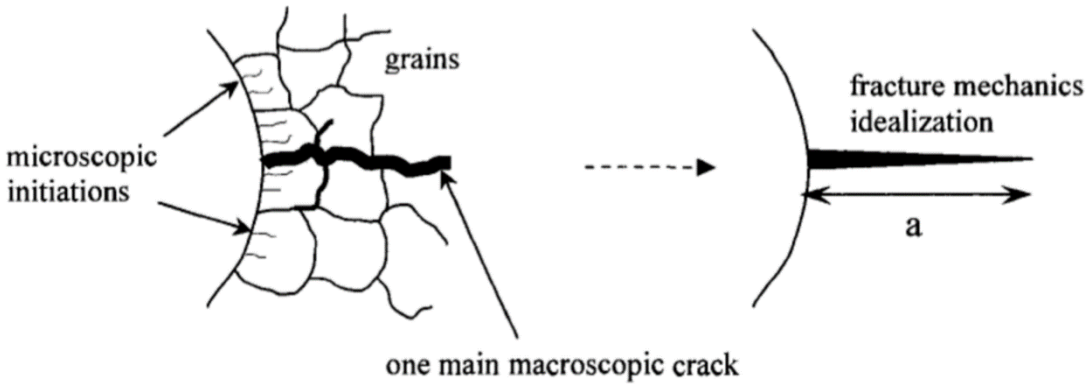

Figure 2.1 The schematic illustration of fatigue crack growth

In continuum mechanics, quantities defined at a mathematical point have been dealt with, and they represent averages on a certain volume from the physical perspective. The

representative volume element (RVE) is small enough to avoid smoothing of high gradients, but it is large enough to represent an average of the micro-processes. For the purposes of experiments and numerical analysis, various orders of magnitude of the RVE for different materials have been used, e.g., metals and ceramics $(0.1mm)^3$, polymers and most composites $(1mm)^3$, wood $(10mm)^3$, concrete $(100mm)^3$.

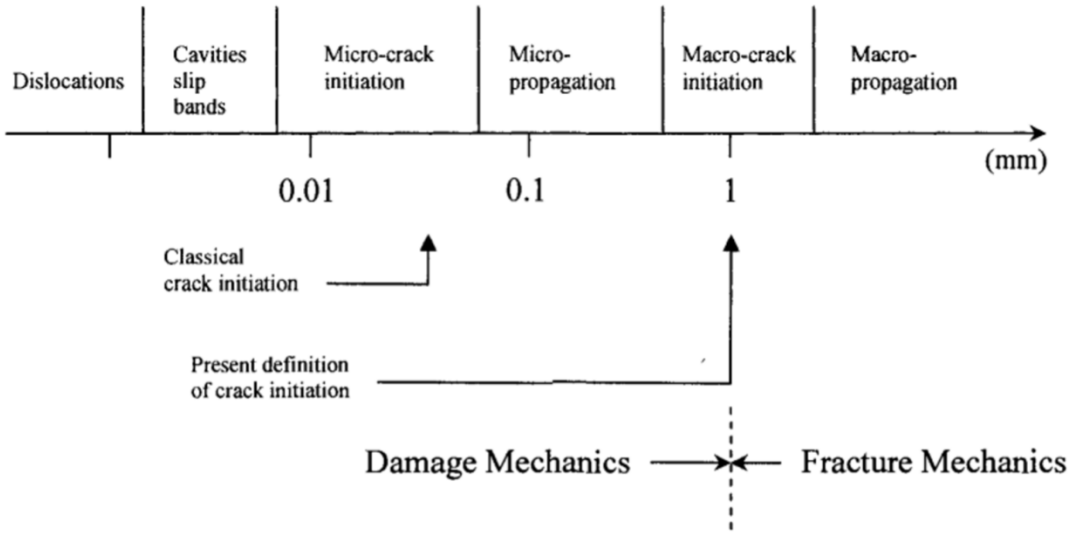

Figure 2.2 The Chaboche's crack initiation concept and classification of damage and fracture mechanics

2.2.2 The Effective Stress Concept and Hypothesis of Strain Equivalence

In order to avoid a micromechanical analysis for each type of defect and mechanism of damage, a principle should be postulated at the level of macroscale. In thermodynamics, the method of local state assumes that the thermo-mechanical state at a point can be

completely defined by the time values of a set of continuous state variables, which depend upon the point considered. This postulate introduced by Lemaitre (Lemaitre, 1971) imposes that the constitutive equations for the strain of a micro-volume element are not modified by a neighboring micro-volume element containing a microcrack. Extrapolating to the macroscale, it means that the strain constitutive equations written for the damaged surface are not modified by the damage or that the true stress loading on the material is the effective stress $\bar{\sigma}$ instead of σ.

Lemaitre pointed out the following principle results: "*Any strain constitutive equation for a damaged material may be derived in the same way as for a virgin material except that the usual stress is replaced by the effective stress*". A schematic representation of this principle is illustrated in Figure 2.3.

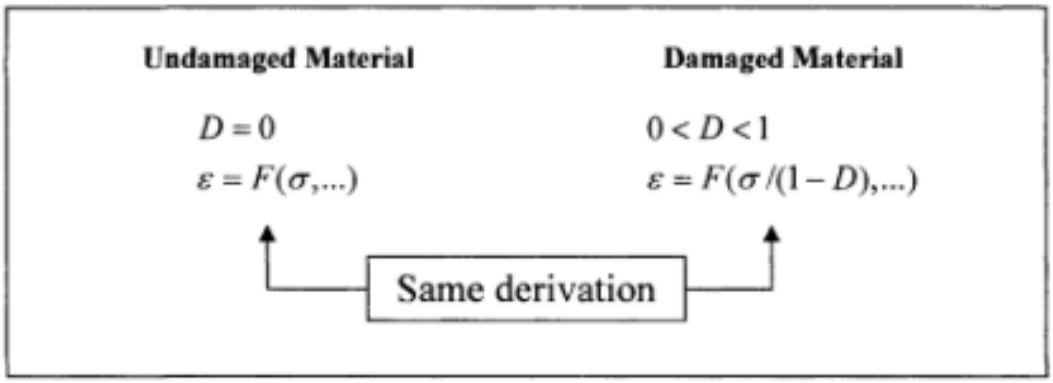

Figure 2.3 The schematic illustration of Lemaitre's derivation for undamaged and damaged materials

From the physical point of view, degradation of the material properties is the result of the initiation, growth and coalescence of microcracks or microvoids. Within the context of continuum mechanics, this process can be modeled by introducing an internal damage variable, which can be a scalar or a tensor quantity. A fourth-order tensor $\mathbf{M}$ is introduced to characterize the state of damage and transform the homogenized stress tensor σ into the effective stress tensor $\bar{\sigma}$ (Simo & Ju, 1987). Explicitly, it can be written as

$$\bar{\sigma} \equiv \mathbf{M}^{-1} : \sigma \tag{2.2.1}$$

For the isotropic damage case, the mechanical behavior of microcracks or microvoids is independent of their orientation and depends only on a scalar damage variable, d, where $0 \le d \le 1$. Accordingly, $\mathbf{M}$ will simply reduce to $(1-d)\mathbf{I}$, where $\mathbf{I}$ is the rank four identity tensor, and Eqn. (2.2.1) collapses to

$$\bar{\sigma} = \frac{\sigma(t)}{1-d(t)} \tag{2.2.2}$$

where $\sigma(t)$ is the Cauchy stress tensor, and $\bar{\sigma}(t)$ is the effective stress tensor, both at time t. The coefficient $1-d(t)$ dividing the stress tensor in Eqn. (2.2.2) results in a reduction factor associated with the amount of damage in the material first introduced by Kachanov (Kachanov, 1958, 1999). The damage parameter d may be interpreted physically as the ratio of damaged surface area over total surface area at a local material point. The value d =0 corresponds to the undamaged state, whereas other value of d corresponds to a damaged state.

In other words, the hypothesis of equivalent strain can be interpreted as "*The strain associated with a damaged state under the applied stress is equivalent to the strain associated with its undamaged state under the effective stress*" according to Simo and Ju (Simo & Ju, 1987). We can refer to Figure 2.4 for a schematic illustration of the hypothesis.

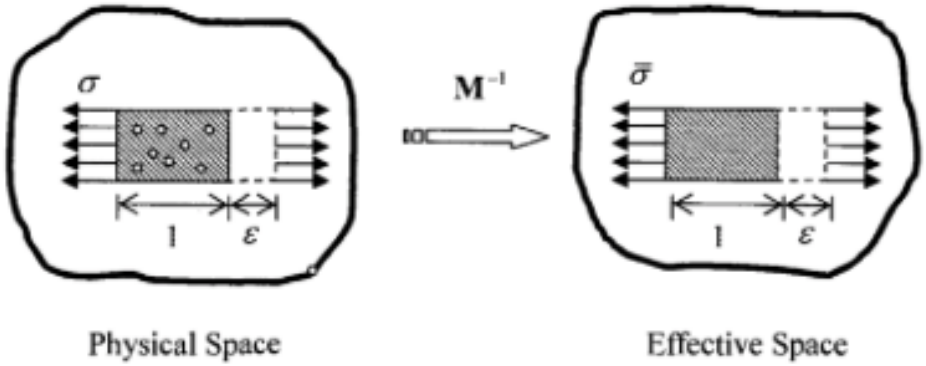

Figure 2.4 The schematic illustration of Simo and Ju's hypothesis of strain equivalence

2.2.3 The Effective Strain Concept and Hypothesis of Stress Equivalence

The concept of effective strain can be treated as an alternative to the concept of effective stress. We may use following notions of effective strain for anisotropic cases

$$\bar{\varepsilon} = \mathbf{M} : \varepsilon \tag{2.2.3}$$

whereas for isotropic cases

$$\bar{\varepsilon} = (1-d) : \varepsilon \tag{2.2.4}$$

Here $\varepsilon(t)$ is the strain tensor and $\bar{\varepsilon}(t)$ is the effective strain tensor.

Analogous to the hypothesis of strain equivalence and invoking similar homogenization techniques, the following dual hypothesis of stress equivalence was proposed by Simo and Ju (Simo & Ju, 1987):

"*The stress associated with a damaged state under the applied strain is equivalent to the stress associated with its undamaged state under the effective strain*". A schematic illustration is exhibited in Figure 2.5.

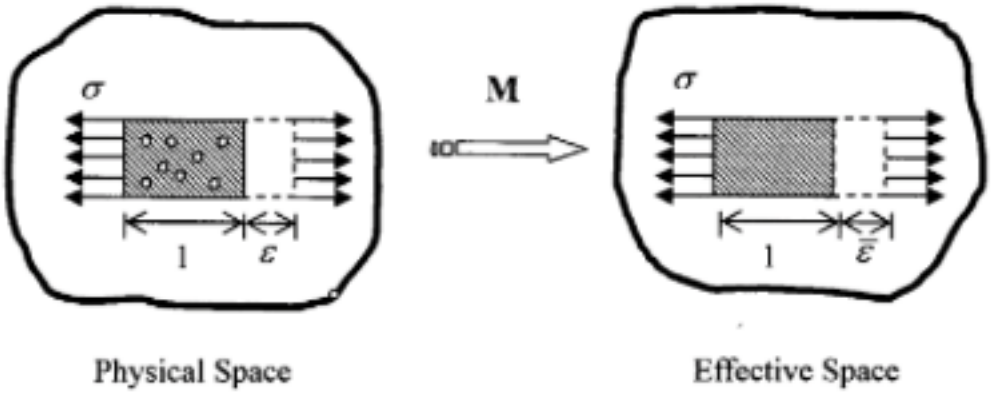

Figure 2.5 The schematic illustration of Simo and Ju's hypothesis of stress equivalence

2.2.4 Anisotropy of Damage and Projection Tensors

In many cases, it is practical to assume that damage is isotropic, especially under the conditions of proportional loading when the corresponding principal directions of the stresses remain constant. However, for some materials under special loading conditions or for most brittle materials, the damage is no longer independent of direction. In other words,

the damage is anisotropic and the damage variable is no longer to be a scalar.

The concept of the decomposition of stress and strain tensors into positive and negative projections has been introduced by Ladeveze and Lemaitre (Ladeveze & Lemaitre, 1984), Marzas and Lemaitre (Mazars & Lemaitre, 1985), Ortiz (Ortiz, 1985, 1987a), and Marzas (Mazars, 1986), and further developed by Simo and Ju (Simo & Ju, 1987), Yazdani and Schreyer (Yazdani & Schreyer, 1988), Ju (Ju, 1989), Stevens and Liu (Stevens & Liu, 1992) and others (Lubarda, 1994; Lubarda & Krajcinovic, 1994, 1995; Schreyer, 1995; Yazdani, 1993). The principal stresses of a stress tensor are defined by the characteristic equation

$$(\sigma - \lambda \mathbf{I})\mathbf{p} = 0 \tag{2.2.5}$$

where λ represent the eigenvalues of the stress tensor σ, $\mathbf{I}$ is the second rank identity tensor and $\mathbf{p}$ represent three unit (principle or eigen-) vectors defining the direction of the eigenvalues λ.

The stress tensor, written in terms of its eigenvalues in Eqn. (2.2.5), is

$$\sigma = \sum_{i=1}^{3} \lambda^i (p_i \otimes p_i) \tag{2.2.6}$$

where $|p_i| = 1$ and $\otimes$ stands for the dyadic (outer) tensor product. The magnitudes of the principle stresses are $\sigma^i = \lambda^i$. Eqn. (2.2.6) represents the spectral representation (decomposition) of a symmetric second order tensor. In 1994, Lubarda and Krajcinovic (Lubarda & Krajcinovic, 1994) introduced an orthogonal second order matrix $\mathbf{S}$, which satisfies the condition $\mathbf{S}^T\mathbf{S} = \mathbf{I}$ or $\mathbf{S}^T = \mathbf{S}^{-1}$ and has the following form

$$\mathbf{S} = \sum_{i=1}^{3} p_i \otimes e_i = p_1 \otimes \begin{Bmatrix} 1 \\ 0 \\ 0 \end{Bmatrix} + p_2 \otimes \begin{Bmatrix} 0 \\ 1 \\ 0 \end{Bmatrix} + p_3 \otimes \begin{Bmatrix} 0 \\ 0 \\ 1 \end{Bmatrix} \tag{2.2.7}$$

The vector $e_i = \begin{Bmatrix} \delta_{i1} & \delta_{i2} & \delta_{i3} \end{Bmatrix}$ has Kronecker delta functions for its components, defines the fixed coordinate system. The diagonal matrix can now be extracted from the matrix of stresses by the similarity transformation

$$\mathbf{a} = \mathbf{S}^T \bullet \sigma \bullet \mathbf{S} = \sum_{i=1}^{3} a^i (e_i \otimes e_i) = \begin{bmatrix} a^1 & 0 & 0 \\ 0 & a^2 & 0 \\ 0 & 0 & a^3 \end{bmatrix} \tag{2.2.8}$$

The elements of the diagonal matrix (2.2.8) are the eigenvalues of the stress tensor (2.2.7).

Motivated by the physics of the considered phenomenon, the stress tensor is decomposed into its positive and negative parts using the transformation

$$\sigma^+ = \mathbf{S}^+ \bullet \mathbf{a} \bullet (\mathbf{S}^+)^T \tag{2.2.9}$$

The matrix

$$\mathbf{S}^+ = \sum_{i=1}^{3} H(\sigma_i)(p_i \otimes e_i) \tag{2.2.10}$$

is used to eliminate the negative eigenvalues and the Heaviside function is denoted by $H(\sigma_i)$. The positive part of the diagonal matrix (2.2.8) can be written as

$$\sigma^+ = (\mathbf{S}^+ \bullet \mathbf{S}^T) \bullet \sigma \bullet (\mathbf{S} \bullet (\mathbf{S}^+)^T) = \sum_{i=1}^{3} \sigma_i^+ (p_i \otimes p_i) \tag{2.2.11}$$

where the positive eigenvalues

$$\sigma_i^+ = H(\sigma_i)\sigma_i \tag{2.2.12}$$

Define a second order symmetric tensor $\mathbf{Q}^+$

$$\mathbf{Q}^+ = \mathbf{S}^+ \bullet \mathbf{S}^T = \mathbf{S} \bullet (\mathbf{S}^+)^T = \sum_{i=1}^{3} H(\sigma_i)(p_i \otimes p_i) \tag{2.2.13}$$

and a fourth rank positive tensor $\mathbf{P}^+$, written in its symmetrized form, as a function of the second order symmetric tensor $\mathbf{Q}^+$

$$\mathbf{P}^+_{ijmn} = \frac{1}{2}(\mathbf{Q}^+_{im}\mathbf{Q}^+_{jn} + \mathbf{Q}^+_{in}\mathbf{Q}^+_{jm}) \tag{2.2.14}$$

Therefore Eqn. (2.2.11) can be rewritten in terms of tensor $\mathbf{P}^+$ in a compact form

$$\sigma^+ = \mathbf{P}^+ : \sigma \tag{2.2.15}$$

$\mathbf{P}^+$, now named as the positive projection operators, written in terms of the three principal directions $p_\sigma^{(i)}$ and $p_\varepsilon^{(i)}$ of the stress and strain tensors, are

$$\mathbf{P}^+_\sigma = \sum_{i=1}^{3} \left\langle \sigma^{(i)} \right\rangle p_\sigma^{(i)} \otimes p_\sigma^{(i)} \otimes p_\sigma^{(i)} \otimes p_\sigma^{(i)} \tag{2.2.16}$$

$$\mathbf{P}^+_\varepsilon = \sum_{i=1}^{3} \left\langle \varepsilon^{(i)} \right\rangle p_\varepsilon^{(i)} \otimes p_\varepsilon^{(i)} \otimes p_\varepsilon^{(i)} \otimes p_\varepsilon^{(i)} \tag{2.2.17}$$

where $\sigma^{(i)}$ and $\varepsilon^{(i)}$ are the principal stresses and strains, and $\left\langle \ \right\rangle$ denotes the McAuley brackets.

The positive parts of the stress and strain tensors can be written in a compact form using the positive projection operators

$$\sigma^+ = \mathbf{P}^+_\sigma : \sigma \tag{2.2.18}$$

$$\varepsilon^+ = \mathbf{P}^+_\varepsilon : \varepsilon \tag{2.2.19}$$

The remaining, negative part of the stress and strain tensors, are defined as

$$\sigma^- = \sigma - \sigma^+ \tag{2.2.20}$$

$$\varepsilon^{-} = \varepsilon - \varepsilon^{+} \tag{2.2.21}$$

Negative projection operators are defined in terms of the positive projection operators (2.2.16) and (2.2.17) by substituting (2.2.18) and (2.2.19) into (2.2.20) and (2.2.21) in a form analogous to (2.2.20) and (2.2.21) as

$$\sigma^{-} = \mathbf{P}_{\sigma}^{-} : \sigma \tag{2.2.22}$$

$$\varepsilon^{-} = \mathbf{P}_{\varepsilon}^{-} : \varepsilon \tag{2.2.23}$$

Thus, the negative projection operators can be derived as follows

$$\mathbf{P}_{\sigma}^{-} = \mathbf{I} - \mathbf{P}_{\sigma}^{+} \tag{2.2.24}$$

$$\mathbf{P}_{\varepsilon}^{-} = \mathbf{I} - \mathbf{P}_{\varepsilon}^{+} \tag{2.2.25}$$

In the case of anisotropic materials or damage-induced anisotropy, the positive and negative projection operators of the stress and strain tensors are not identical, however the symmetry holds for both positive and negative stress and strain projection tensors.

$$\mathbf{P}_{ijmn} = \mathbf{P}_{mnij} \tag{2.2.26}$$

2.3 Thermodynamic Approach to Constitutive Modeling

The classical thermodynamics has been extended to the thermo-mechanics of a continuum since the 1960s. Figure 2.6 shows the overview of general principles in order to describe continuum mechanics based on thermodynamics laws.

It can be stated that the two basic laws of thermodynamics provide simple but very clear theoretical foundations to describe dissipation and deformation in a continuum using

a suitable set of state variables. The first law of thermodynamics can be combined with balance of momentum and mechanical energy balance to present energy equation. The second law of thermodynamics is concerned with how the energy is transferred between systems. In continuum mechanics, another way of expressing the second law of thermodynamics is the Clausius-Duhem and Clausius-Planck inequality. This inequality is a statement concerning the irreversibility of natural processes, when energy dissipates, and particularly useful in the treatment of 'switch' conditions, such as loading-unloading conditions in plasticity.

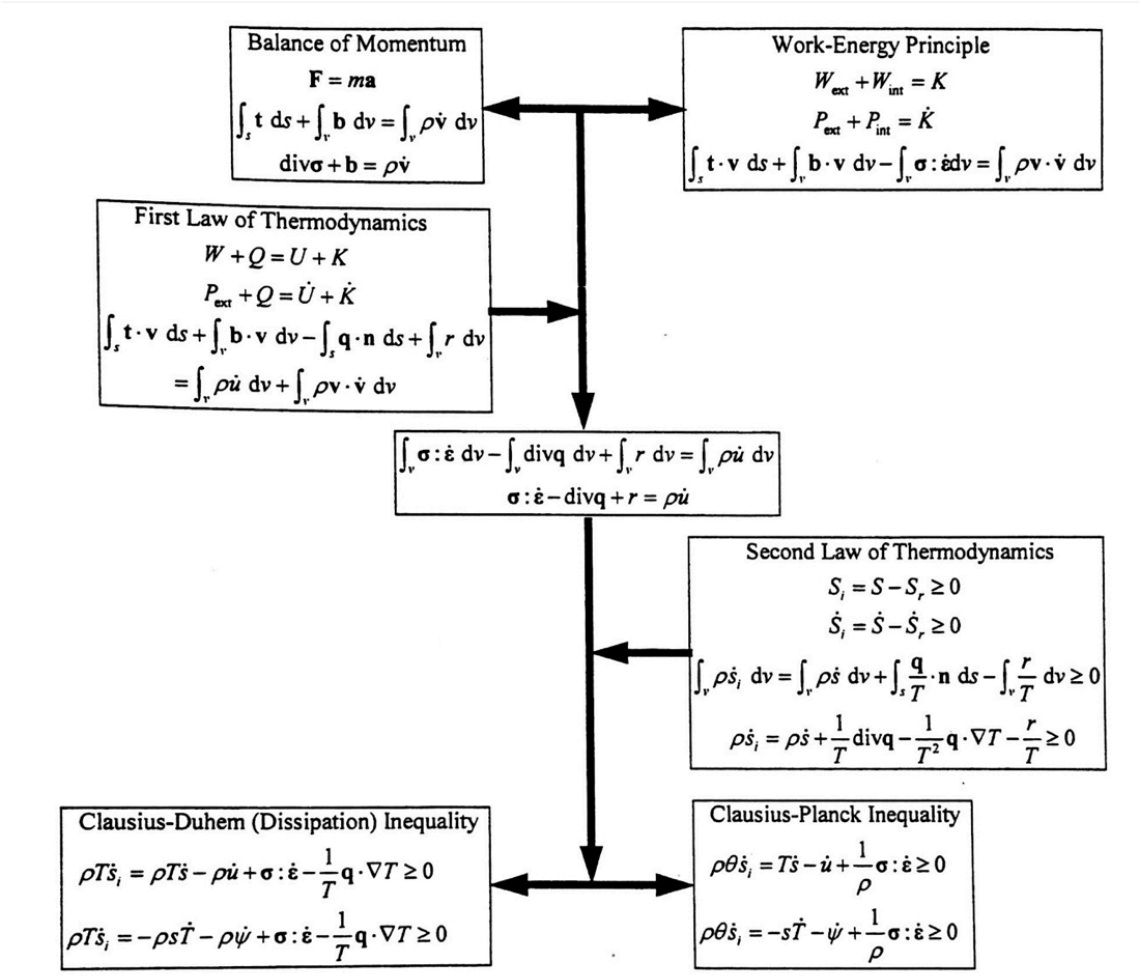

Figure 2.6 An overview of general principles of thermodynamic-based continuum mechanics

2.3.1 The First and Second Law of Thermodynamics

The first law of thermodynamics is a version of conservation of energy and its rate form is expressed as

$$P_{ext} + Q = \dot{U} + \dot{K} \tag{2.3.1}$$

where P_{ext} is the external power, Q is the rate at which heat is supplied, $\dot{U}$ is the rate of change of the internal energy and $\dot{K}$ is the rate form of kinetic energy.

If a solid body occupies a domain V and bounded by a surface S, then the energy equations can be expressed as follows

$$P_{ext} = \int_S \mathbf{t} \cdot \mathbf{v}\, dS + \int_V \mathbf{b} \cdot \mathbf{v}\, dV \tag{2.3.2}$$

$$Q = -\int_V \operatorname{div} \mathbf{q}\, dV + \int_V r\, dV \tag{2.3.3}$$

$$\dot{U} = \int_V \rho \dot{u}\, dV \tag{2.3.4}$$

$$\dot{K} = \int_V \rho \mathbf{v} \cdot \dot{\mathbf{v}}\, dV \tag{2.3.5}$$

where $\mathbf{t}$ is the tractions acting on the boundary surface, $\mathbf{v}$ is the velocity vector which is also the time derivative of displacement vector, $\mathbf{b}$ is the body force, $\mathbf{q}$ is the heat flux, r is the heat source of intensity, ρ is the density and $\dot{u}$ is the rate of the specific internal energy per unit mass.

The rate form of balance of mechanical energy can be expressed as

$$P_{ext} + P_{int} = \dot{K} \tag{2.3.6}$$

where P_{int} is the internal power, which can be expressed as

$$P_{int} = \int_V \rho \frac{du}{dt} dV = -\int_V \sigma : \dot{\varepsilon}\, dV \tag{2.3.7}$$

Therefore Eqn. (2.3.1) equals to

$$\int_V \sigma : \dot{\varepsilon}\, dV - \int_V \operatorname{div} \mathbf{q}\, dV + \int_V r\, dV = \int_V \rho \dot{u}\, dV \tag{2.3.8}$$

Eqn. (2.3.8) holds for any partial volume within the material body, therefore one has the local form of the first law

$$\sigma : \dot{\varepsilon} - \operatorname{div} \mathbf{q} + r = \rho \dot{u} \tag{2.3.9}$$

The second law of thermodynamics states that the entropy of isolated system never decreases because isolated systems always evolve toward thermodynamic equilibrium, i.e. the maximum entropy state.

The entropy and the entropy supply are defined as the scalar form

$$S = \int_V \rho s\, dV \tag{2.3.10}$$

$$S_r = -\int_S s_q \cdot \mathbf{n}\, dS + \int_V s^r\, dV \tag{2.3.11}$$

where s is the specific entropy or entropy density, s_q is the entropy flux through the element surface and s^r is the entropy supply due to sources within the element. The rate form of entropy supply Eqn. (2.3.11) can be expressed as

$$\dot{S}_r = -\int_S \frac{\mathbf{q}}{T} \cdot \mathbf{n}\, dS + \int_V \frac{r}{T} dV \tag{2.3.12}$$

where T is the non-negative scalar absolute temperature.

The entropy production is defined as the difference between entropy and entropy supply and is always a non-negative quantity.

$$S_i = S - S_r \geq 0 \tag{2.3.13}$$

$$\dot{S}_i = \dot{S} - \dot{S}_r \geq 0 \tag{2.3.14}$$

2.3.2 The Clausius-Duhem and Clausius-Planck Inequalities

From Eqn. (2.3.14) the Clausius-Duhem inequality is derived

$$\int_V \rho \dot{s}_i \, dV = \int_V \rho \dot{s} \, dV + \int_S \frac{\mathbf{q}}{T} \cdot \mathbf{n}\, dS - \int_V \frac{r}{T} dV \geq 0 \tag{2.3.15}$$

From Gauss-Green theorem, one can obtain

$$\int_S \frac{\mathbf{q}}{T} \cdot \mathbf{n}\, dS = \int_V div(\frac{\mathbf{q}}{T}) dV = \int_V \frac{1}{T} div\mathbf{q}\, dV - \int_V \frac{1}{T^2} \mathbf{q} \cdot \nabla T \, dV \tag{2.3.16}$$

Substituting Eqn. (2.3.16) into Eqn. (2.3.15) and the local form of the Clausius-Duhem inequality is obtained

$$\rho \dot{s}_i = \rho \dot{s} + \frac{1}{T} div\mathbf{q} - \frac{1}{T^2} \mathbf{q} \cdot \nabla T - \frac{r}{T} \geq 0 \tag{2.3.17}$$

Another way to express the Clausius-Duhem inequality is the dissipation inequality. The density of energy dissipation rate, D, is introduced to define the rate of internal entropy production per unit volume times the absolute temperature (Milan & Zdenek, 2001;

Thomson, 1852). By using Eqn. (2.3.9) and (2.3.17), the dissipation inequality can be expressed as

$$D \equiv \rho \dot{s}_i T = \rho \dot{s} T - \rho \dot{u} + \sigma : \dot{\varepsilon} - \frac{1}{T} \mathbf{q} \cdot \nabla T \geq 0 \tag{2.3.18}$$

If temperature is uniform in space, ∇T yields zero. Therefore Eqn. (2.3.18) becomes

$$\dot{s}_i T = \dot{s} T - \dot{u} + \frac{1}{\rho} \sigma : \dot{\varepsilon} \geq 0 \tag{2.3.19}$$

which is called the Clausius-Planck inequality (Astarita, 1989). In many applications, the thermal dissipation is very much smaller than the mechanical dissipation so that it is reasonable to assume that the thermal dissipation rate can be ignored. The Clausius-Duhem inequality becomes the Clausius-Planck inequality.

2.4 Effective Elastic Moduli on Composites

The modeling and estimation of effective elastic moduli of composites are of great interest to researchers and engineers in many science and engineering disciplines. The so-called "effective" elastic moduli of composites are obtained by some volume-averaging and ensemble-averaging processes over a "representative volume element" (RVE) featuring a "mesoscopic" length scale which is much larger than the characteristic length scale of particles (inhomogeneities) but smaller than the characteristic length scale of a macroscopic specimen.

There are many theoretical methods in the literature to tackle this class of problems. Whereas pioneering work in this field were stemming as early as in 1887 for the first ‘law

of mixtures', i.e. the well-known Voigt estimate and in 1929 for another one, the Reuss estimate, the actual foundations of homogenization techniques are only about half a century old. In the early 1960s, Hashin and Shtrikman (Hashin & Shtrikman, 1961, 1963) employed variational principle to obtain mathematical lower and upper bounds for effective elastic moduli of multiphase particulate composites. The Hashin-Shtrikman bounds have been derived for more general cases (Kröner, 1977; Walpole, 1966a, 1966b; Willis, 1977) based on the solution of the general equation for inhomogeneous elasticity by use of Green techniques and the description of random media by correlation functions of their elastic moduli. Nonlinear variational bounds for isotropic elastic and viscoelastic particulate composites were proposed by Castaneda and Willis (Castaneda, 1991; Castaneda & Willis, 1988; Willis, 1991, 1994). The second school for micromechanical estimation of effective elastic moduli of composites is known as the effective medium approach, including the self-consistent method proposed independently by Kröner, and Budianski and Wu (Budiansky & Wu, 1962), then generalized by Hill (Hill, 1965a, 1965b) and largely extended by other scholars (Berveiller & Zaoui, 1979; Hutchinson, 1970; Iwakuma & Nemat-Nasser, 1984; Lipinski et al., 1992; Molinari et al., 1987; Molinari et al., 2004), the differential scheme (Hashin, 1988; Laws & Dvorak, 1987; McLaughlin, 1977; Norris, 1985; Roscoe, 1952), the Mori-Tanaka method (Mori & Tanaka, 1973; Qiu & Weng, 1990; Taya & Chou, 1981; Taya & Mura, 1981), etc. The third school aims at direct determination of effective moduli of composites with randomly located particles by introducing some

approximations or by assuming certain special configurations for particles (inhomogeneities) dispersing in matrix materials. At dilute particle concentrations, some results were obtained by Dewey (Dewey, 1947), Kerner (Kerner, 1956), Eshelby (Eshelby, 1957) and Hashin (Hashin, 1959) by considering only effects due to single particles (i.e., no inter-particle interactions). These methods are suitable for low particle densities. In 1994, Ju and Chen (Ju & Chen, 1994a, 1994b) presented a series governing ensemble-volume averaged micromechanical field equations to relate ensemble-volume averaged stresses, strains, volume fractions, eigenstrains, particle shapes and orientations, and elastic properties of constituent phases of a linear elastic particulate composite. The concept and equations of ensemble-volume averaged micromechanical field relations have been borrowed and further developed by many researchers such as Sun (Ju & Sun, 2001; Sun & Ju, 2004; Sun et al., 2003), Lee and Pyo (H. Lee & Pyo, 2007), Ju and Yanase (Ju & Yanase, 2009, 2010), Ko and Ju (Ko & Ju, 2008, 2012). Numerical schemes are also largely studied for single and multiple inclusion problems (J. K. Lee et al., 2001; J. K. Lee et al., 2011; J. K. Lee & Mal, 1995, 1997). Under the assumptions that all particles are non-intersecting, embedded firmly into a homogeneous matrix material, i.e. perfect interfacial bonding, and that statistical homogeneity holds, effective (averaged) material properties remain the same for arbitrary averaging domains inside a composite medium. In this way, heterogeneous composites can be represented by equivalent homogeneous continuum media with appropriately defined effective properties.

2.4.1 The Voigt-Reuss Bounds

A general rule of mixtures is a weighted mean used to predict various properties of composite materials. On a strictly empirical basis, one can imagine defining a power law average of the constituents

$$\bar{M}^{\alpha} = f_i M_i^{\alpha} \tag{2.4.1}$$

where $\bar{M}$ is the effective modulus of the composite, M_i is the modulus of the *i*-th constituent, f_i is the volume fraction of the *i*-th constituent and α is a constant between -1 and +1. The special cases of Eqn.(2.4.1) yield Voigt upper bound and Reuss lower bound, i.e.

$$f_i^{-1} K_i \le \bar{K} \le f_i K_i \tag{2.4.2}$$

$$f_i^{-1} \mu_i \le \bar{\mu} \le f_i \mu_i \tag{2.4.3}$$

where K denotes the bulk modulus and μ denotes the shear modulus.

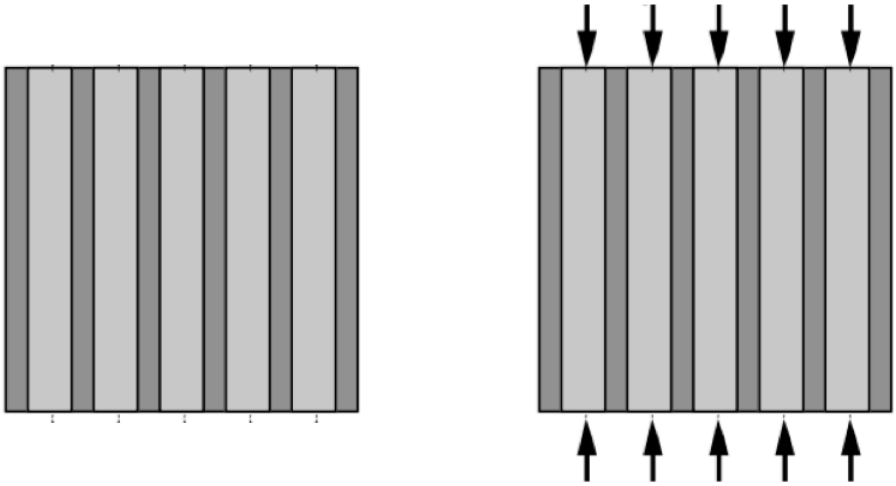

Figure 2.7 The schematic illustration of Voigt's iso-strain model

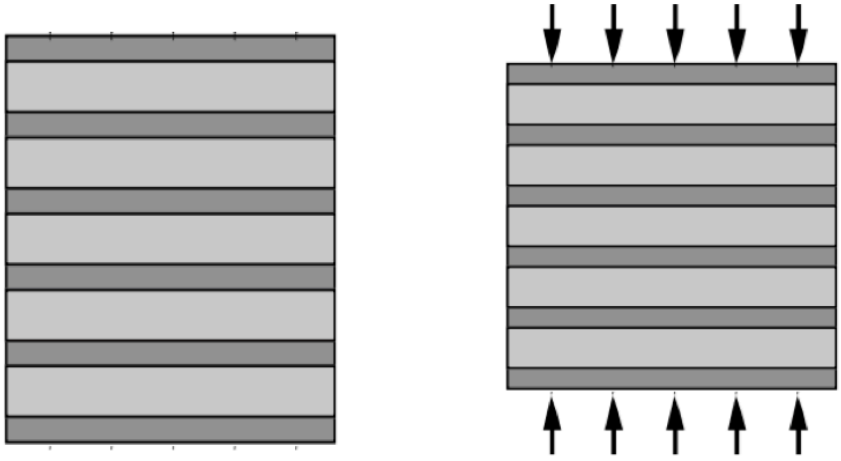

Figure 2.8 The schematic illustration of Reuss's iso-stress model

The Voigt and Reuss bounds are interpreted as the ratio of average stress and average stain within the composite. The stress and strain are generally unknown in the composite

and are expected to be nonuniform. The Voigt upper bound is found assuming that the strain is uniform, and the Reuss lower bound is found assuming that the stress is uniform. Figure 2.7 and Figure 2.8 are schematic illustrations of Voigt's and Reuss's models, models composed of series elements and parallel elements.

2.4.2 The Eshelby's Equivalent Inclusion Theory

When the elastic moduli of an ellipsoidal domain Ω of a material differ from those of the remainder (matrix), Ω is called an inhomogeneity. Eshelby (Eshelby, 1957) first pointed out that the stress disturbance in an applied stress due to the presence of an inhomogeneity can be simulated by an eigenstress caused by an inclusion when the eigenstrain is chosen properly. This equivalency is called *the equivalent inclusion method*. The principle premise of the equivalent inclusion method is to consider an infinitely extended material with the elastic moduli C^0_{ijkl}, containing an ellipsoidal domain Ω with the elastic moduli C_{ijkl}. The far-field stress σ^0_{ij} is applied at infinity and the corresponding strain is ε^0_{ij}, where $\sigma^0_{ij} = C^0_{ijkl}\varepsilon^0_{kl}$. The stress disturbance and the strain disturbance are denoted by σ'_{ij} and ε'_{ij}, respectively. A schematic illustration of Eshelby's premise is shown in Figure 2.9.

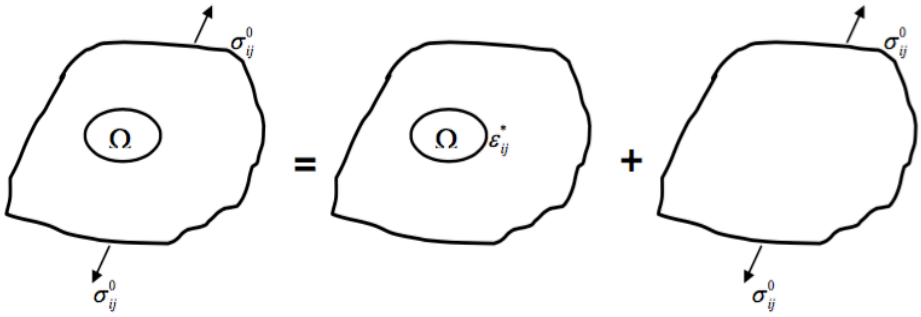

Figure 2.9 The schematic illustration of an infinitely extended material (matrix) containing an ellipsoidal domain (inhomogeneity) under far-field stress in Eshelby's equivalent inclusion theory

Based on the Hooke's law, the stress-strain relationships in the ellipsoidal domain and in matrix are

$$\sigma_{ij}^0 + \sigma'_{ij} = C_{ijkl}(\varepsilon_{kl}^0 + \varepsilon'_{kl}) \quad \text{in } \Omega \tag{2.4.4}$$

$$\sigma_{ij}^0 + \sigma'_{ij} = C_{ijkl}^0(\varepsilon_{kl}^0 + \varepsilon'_{kl}) \quad \text{in } \mathbf{D} - \Omega \tag{2.4.5}$$

Eqn. (2.4.4) and (2.4.5) can be related by the equivalent eigenstrain ε_{ij}^*, as shown in Figure 2.9. The new relationship becomes

$$C_{ijkl}(\varepsilon_{kl}^0 + \varepsilon'_{kl}) = C_{ijkl}^0(\varepsilon_{kl}^0 + \varepsilon'_{kl} - \varepsilon_{kl}^*) \quad \text{in } \Omega \tag{2.4.6}$$

The disturbing strain ε'_{ij} can be obtained as a known function of the eigenstrain ε_{ij}^* when the eigenstrain problem in the homogeneous material is solved. Namely

$$\varepsilon'_{kl} = S_{klmn}\varepsilon_{mn}^* \tag{2.4.7}$$

where S_{klmn} ($\mathbf{S}$) is the interior-point Eshelby's tensor. The Eshelby's tensor is symmetric in the first and second pair of indices, but in general it is not symmetric with regard to an exchange of these pairs (exhibits the minor but not the major symmetry)

$$S_{ijkl} = S_{jikl} = S_{ijlk} \neq S_{klij} \tag{2.4.8}$$

In case of an isotropic material, the components of $\mathbf{S}$ depend only on Poisson's ratio, the ratios of the principal axes, and their orientation with respect to some Cartesian coordinate system. The respective expressions are very long and can be found in Mura's book (Mura, 1987). Only in case of an isotropic material there exists a closed-form representation of the tensor $\mathbf{S}$, and the fields outside the inclusion. The Eshelby's solution for ellipsoidal inclusions is of fundamental importance for analytical homogenization techniques (e.g. Mori-Tanaka method, self-consistent method, the differential scheme, etc.).

From Eqn. (2.4.6) and (2.4.7), we have

$$C_{ijkl}(\varepsilon^0_{kl} + S_{klmn}\varepsilon^*_{mn}) = C^0_{ijkl}(\varepsilon^0_{kl} + S_{klmn}\varepsilon^*_{mn} - \varepsilon^*_{kl}) \quad \text{in } \Omega \tag{2.4.9}$$

from which the equivalent eigenstrain ε^*_{ij} is determined as

$$\varepsilon^*_{ij} = -(S_{ijkl} + A_{ijkl})^{-1}\varepsilon^0_{kl} \tag{2.4.10}$$

where the elastic mismatch tensor $A_{ijkl} = (C_{ijmn} - C^0_{ijmn})^{-1}C^0_{mnkl}$.

2.4.3 The Hashin-Shtrikman Bounds

The narrowest possible bounds on moduli that we can estimate for isotropic materials, knowing only the volume fractions of the constituents, are the Hashin-Shtrikman bounds(Hashin, 1962; Hashin & Shtrikman, 1961, 1963).

Under the same premise that Eshelby made, as mentioned in Section 2.4.2, consider composite materials which consist of matrix and inhomogeneities whose elastic moduli are $\mathbf{C^0}$ and $\mathbf{C}$ respectively, under an applied strain or stress ε^0 or σ^0 ($\sigma^0 = \mathbf{C^0} : \varepsilon^0$). The average strain of the composite materials can be shown as ε_{ij}^0.

The Eshelby's equivalent equation then reads

$$\mathbf{C} : (\varepsilon^0 + \varepsilon') = \mathbf{C^0} : (\varepsilon^0 + \varepsilon' - \varepsilon^*) \tag{2.4.11}$$

which is identical to Eqn. (2.4.6).

By introducing $\sigma^* = \mathbf{C^0} : \varepsilon^*$ and $\varepsilon' = \Gamma : \sigma^*$, we have

$$(\mathbf{C} - \mathbf{C^0})^{-1} : \sigma^* + (\varepsilon^0 + \Gamma : \sigma^*) = 0 \tag{2.4.12}$$

Based on the above equations, Hashin and Shtrikman have constructed an energy potential as

$$W^{**} = \frac{1}{2}[\sigma^*, (\mathbf{C} - \mathbf{C^0})^{-1} : \sigma^*] + [\sigma^*, \varepsilon^0] + \frac{1}{2}[\sigma^*, \Gamma : \sigma^*] \tag{2.4.13}$$

where the comparison function is σ^*, and the operation $[f, g] \equiv \frac{1}{V}\int_D f(x)g(x)\,dx$. Thus, the corresponding stationary equation becomes Eqn. (2.4.12) and its stationary value is

$$\frac{1}{2}[\sigma^*,\varepsilon^0]=\frac{1}{2}[\sigma^0,\varepsilon^*] \tag{2.4.14}$$

From the definition of elastic strain energy W^*, the stationary value of the potential also satisfies

$$\frac{1}{2}[\sigma^0,\varepsilon^*]=W^*-\frac{1}{2}[\sigma^0,\varepsilon^0] \tag{2.4.15}$$

Therefore, for a positive definite $\mathbf{C}-\mathbf{C^0}$

$$\frac{1}{2}[\varepsilon^0,\bar{\mathbf{C}}:\varepsilon^0]-\frac{1}{2}[\varepsilon^0,\mathbf{C}^0:\varepsilon^0]\le\frac{1}{2}[\sigma^*,(\mathbf{C}-\mathbf{C^0})^{-1}:\sigma^*]+[\sigma^*,\varepsilon^0]+\frac{1}{2}[\sigma^*,\Gamma:\sigma^*]$$

(2.4.16)

and for a negative definite $\mathbf{C}-\mathbf{C^0}$

$$\frac{1}{2}[\varepsilon^0,\bar{\mathbf{C}}:\varepsilon^0]-\frac{1}{2}[\varepsilon^0,\mathbf{C}^0:\varepsilon^0]\ge\frac{1}{2}[\sigma^*,(\mathbf{C}-\mathbf{C^0})^{-1}:\sigma^*]+[\sigma^*,\varepsilon^0]+\frac{1}{2}[\sigma^*,\Gamma:\sigma^*]$$

(2.4.17)

For a mixture of two materials, the Hashin-Shtrikman bounds for the bulk modulus K and shear modulus μ are given by

$$K^{HS\pm}=K_1+\frac{f_2}{(K_2-K_1)^{-1}+f_1(K_1+\frac{4}{3}\mu_1)^{-1}} \tag{2.4.18}$$

$$\mu^{HS\pm}=\mu_1+\frac{f_2}{(\mu_2-\mu_1)^{-1}+\frac{2f_1(K_1+2\mu_1)}{5\mu_1(K_1+\frac{4}{3}\mu_1)}} \tag{2.4.19}$$

where subscript 1 denotes the shell (matrix) and 2 denotes the sphere (inclusion/particle). A schematic illustration of the Hashin-Shtrikman spheres is shown in Figure 2.10.

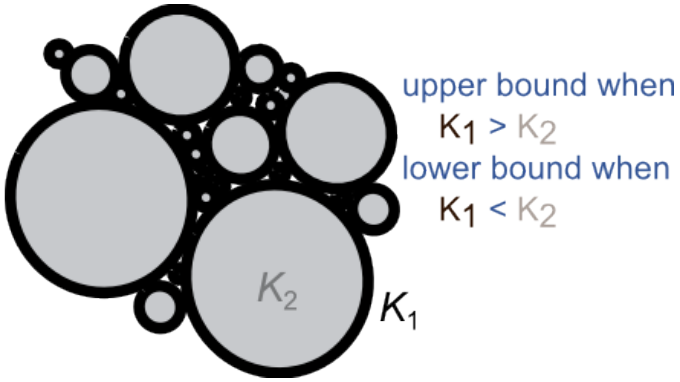

Figure 2.10 The schematic illustration of the Hashin-Shtrikman spheres

The upper bound is computed when $K_1 > K_2$, i.e. the shell is stiffer than the sphere; while the lower bound is computed when $K_2 > K_1$, i.e. the shell is softer than the sphere.

2.4.4 The Mori-Tanaka Method

The most common extensions of Eshelby's equivalent inclusion theory are the Mori-Tanaka method developed by Mori and Tanaka (Mori & Tanaka, 1973) and by Benvensite (Benveniste, 1987), and the self-consistent method pioneered by Kröner, by Budianski and Wu (Budiansky & Wu, 1962), and by Hill (Hill, 1965a, 1965b). The original Mori and Tanaka method and its subsequent modifications (Norris, 1989; Taya & Mura, 1981; Weng, 1984, 1990) is an effective field approximation based on Eshelby's elasticity solution for inhomogeneity in infinite medium. The effects of particle interactions are taken into account by a 'mean field approximation'. As is typical for mean field micromechanics

models, forth-order concentration tensors relate the average stress or average strain tensors in inhomogeneities and matrix to the average macroscopic stress or strain tensor, respectively; inhomogeneity "feels" effective matrix fields, accounting for phase interaction effects in a collective, approximate way.

Consider homogeneous ellipsoidal inclusions (with uniform eigenstrain ε_{ij}^{*}) randomly distributed in the matrix. Let us formally define the average stress field in the matrix as $\left\langle \sigma_{ij} \right\rangle_0$, the field in the inclusions as $\left\langle \sigma_{ij} \right\rangle_1$ and the volume fraction of inclusions as f_1. First of all, we have

$$f_1 \left\langle \sigma_{ij} \right\rangle_1 + \left(1 - f_1\right) \left\langle \sigma_{ij} \right\rangle_0 = 0 \tag{2.4.20}$$

Let us introduce a new single inclusion and assume this addition does not affect the volume fraction of inclusions f_1. Then the stress within the inclusion becomes

$$\sigma_{ij} = \sigma_{ij}^{\infty} + \left\langle \sigma_{ij} \right\rangle_0 \tag{2.4.21}$$

where σ_{ij}^{∞} is the Eshelby's interior-point stress in a single inclusion present in an infinite medium as

$$\sigma_{ij}^{\infty} = C_{ijkl} \left(S_{klmn} \varepsilon_{mn}^{*} - \varepsilon_{kl}^{*} \right) \tag{2.4.22}$$

Taking the average of σ_{ij}, we then have

$$\left\langle \sigma_{ij} \right\rangle_1 = \sigma_{ij}^{\infty} + \left\langle \sigma_{ij} \right\rangle_0 \tag{2.4.23}$$

Combining with the equilibrium equation we finally have

$$\left\langle \sigma_{ij} \right\rangle_0 = -f_1 \sigma_{ij}^{\infty} \tag{2.4.24}$$

$$\left\langle \sigma_{ij} \right\rangle_1 = \left(1 - f_1\right) \sigma_{ij}^{\infty} \tag{2.4.25}$$

It is shown that the average stresses are simply in terms of σ_{ij}^{∞}.

If the eigenstrain is not uniform, Mori-Tanaka's formula arrives as

$$\left\langle \sigma_{ij} \right\rangle_0 = -f_1 \left\langle \sigma_{ij}^{\infty} \right\rangle_1 \tag{2.4.26}$$

$$\left\langle \sigma_{ij} \right\rangle_1 = \left(1 - f_1\right) \left\langle \sigma_{ij}^{\infty} \right\rangle_1 \tag{2.4.27}$$

If the inclusions are inhomogeneous with uniform eigenstrain ε_{ij}^{t} ,the treatment is slightly different. The average stress in the matrix can be written as

$$\left\langle \sigma_{ij} \right\rangle_0 = C_{ijkl} \varepsilon_{kl}^{0} \tag{2.4.28}$$

where ε_{kl}^{0} is to be determined.

By introducing a new inhomogeneous inclusion, we have

$$\sigma_{ij} = C_{ijkl}^{*} \left(\varepsilon_{kl}^{0} + S_{klmn} \varepsilon_{mn}^{**} - \varepsilon_{kl}^{t} \right) = C_{ijkl} \left(\varepsilon_{kl}^{0} + S_{klmn} \varepsilon_{mn}^{**} - \varepsilon_{kl}^{**} \right) \tag{2.4.29}$$

From the equilibrium equation, we also have

$$f_1 C_{ijkl} \left(S_{klmn} \varepsilon_{mn}^{**} - \varepsilon_{kl}^{t} \right) + C_{ijkl} \varepsilon_{kl}^{0} = 0 \tag{2.4.30}$$

Combining Eqn. (2.4.29) and (2.4.30), we can determine ε_{kl}^{0} and ε_{mn}^{**} .

Approximately, Eqn. (2.4.29) can be split into two parts as

$$\begin{aligned}
&\sigma_{ij} = \sigma_{ij}^{\infty} + \sigma_{ij}^{'} \\
&\sigma_{ij}^{\infty} = C_{ijkl}^{*}\left(S_{klmn}\varepsilon_{mn}^{**1} - \varepsilon_{kl}^{t}\right) = C_{ijkl}\left(S_{klmn}\varepsilon_{mn}^{**1} - \varepsilon_{kl}^{**1}\right) \\
&\sigma_{ij}^{'} = C_{ijkl}^{*}\left(\varepsilon_{kl}^{0} + S_{klmn}\varepsilon_{mn}^{**2}\right) = C_{ijkl}\left(\varepsilon_{kl}^{0} + S_{klmn}\varepsilon_{mn}^{**2} - \varepsilon_{kl}^{**}\right)
\end{aligned} \tag{2.4.31}$$

in which $\varepsilon_{mn}^{**} = \varepsilon_{mn}^{**1} + \varepsilon_{mn}^{**2}$, and ε_{mn}^{**1} and ε_{mn}^{**2} are the respective equivalent eigenstrains for ε_{ij}^{t} and ε_{kl}^{0}.

By further assuming $\varepsilon_{mn}^{**1} \gg \varepsilon_{mn}^{**2}$, Eqn. (2.4.30) can be written as

$$\left\langle \sigma_{ij} \right\rangle_0 = C_{ijkl}\varepsilon_{kl}^{0} = -f_1\sigma_{ij}^{\infty} \tag{2.4.32}$$

Starting from the general ellipsoid shaped inclusions, various special cases can be derived. For a spherical inclusion in an isotropic material, the dependence on the principal axes and their orientation vanishes (geometric isotropy) and the Eshelby's tensor reduces to

$$S_{ijkl} = \alpha_0 \frac{1}{3}\delta_{ij}\delta_{kl} + \beta_0\left(I_{ijkl}^{S} - \frac{1}{3}\delta_{ij}\delta_{kl}\right) = \alpha_0\mathbf{I}_V + \beta_0\mathbf{I}_D \tag{2.4.33}$$

where

$$\alpha_0 = \frac{1+\upsilon_0}{3\left(1+\upsilon_0\right)} = \frac{3K_0}{3K_0 + 4G_0} \tag{2.4.34}$$

$$\beta_0 = \frac{2\left(4-5\upsilon_0\right)}{15\left(1-\upsilon_0\right)} = \frac{6\left(K_0 + 2G_0\right)}{5\left(3K_0 + 4G_0\right)} \tag{2.4.35}$$

In such case, the Mori-Tanaka scheme also yields an isotropic overall behavior, irrespective of the spatial locations and distributions of the inclusions (actually the elastic properties of composites predicted by all effective medium methods depends only on geometries). The effective bulk and shear moduli of the composites can be expressed as

$$\bar{K} = \frac{f_0 K_0 + \sum_{i=1}^{n} f_i K_i \gamma_K^i}{f_0 + \sum_{i=1}^{n} f_i \gamma_K^i} \tag{2.4.36}$$

$$\bar{\mu} = \frac{f_0 \mu_0 + \sum_{i=1}^{n} f_i \mu_i \gamma_\mu^i}{f_0 + \sum_{i=1}^{n} f_i \gamma_\mu^i} \tag{2.4.37}$$

where $f_0 = 1 - \sum_{i=1}^{n} f_i$ is the volume fraction of the matrix and

$$\gamma_K^i = \frac{K_0}{K_0 + \alpha_0 \left(K_i - K_0 \right)} \tag{2.4.38}$$

$$\gamma_\mu^i = \frac{\mu_0}{\mu_0 + \beta_0 \left(\mu_i - \mu_0 \right)} \tag{2.4.39}$$

2.4.5 Ju and Chen's Solutions

Inspired by Eshelby's equivalent inclusion theory, Ju and Chen (Ju & Chen, 1994a, 1994b) developed a series of ensemble-volume averaged micromechanical field equations. The concept of this ensemble-volume averaged micromechanical field is illustrated in Figure 2.11.

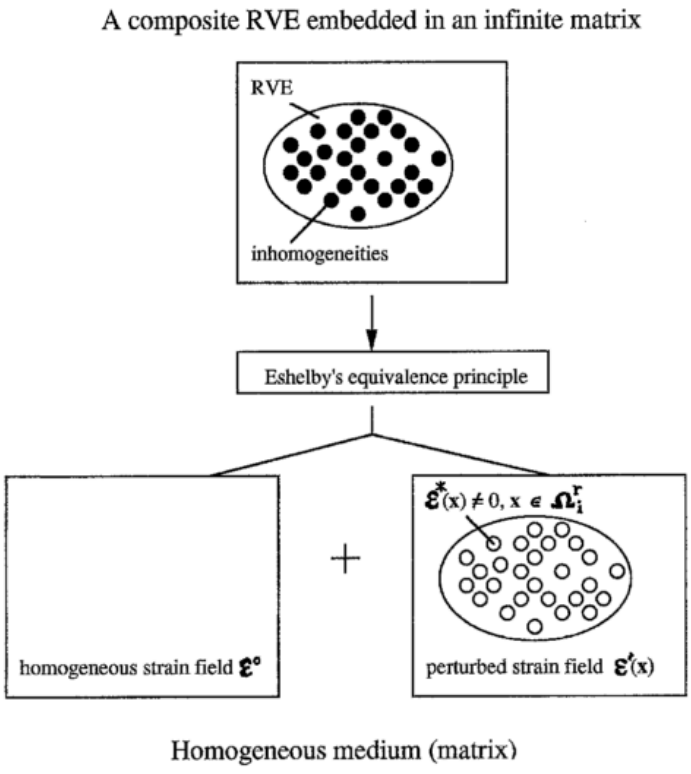

Figure 2.11 Schematic illustration of an ellipsoidal RVE containing inhomogeneities, and linear superposition treatment involving far-field strain and distributed eigenstrains in the Direct Eshelby's Method

To avoid the truncation errors of Greens' functions outside the domain of an RVE, an ellipsoidal RVE itself is embedded in an infinite and identical matrix material within the framework. The entire assembly is subjected to specified far-field stresses or strains. Furthermore, all particles are assumed to be nonintersecting (impenetrable).

Given a composite RVE subjected to specified far-field stresses or strains σ_{ij}^0, ε_{ij}^0, the volume-averaged total stress tensor reads

$$\bar{\sigma} = \frac{1}{V}\int_V \sigma(x)\,dx = \frac{1}{V}\left[\int_{V_m} \sigma(x)\,dx + \sum_{r=1}^{n}\int_{V_r} \sigma(x)\,dx\right] \tag{2.4.40}$$

where V, V_m, V_r are the volumes of the RVE, the matrix, and the r-th phase particles, respectively. Similarly, the volume-averaged strain tensor reads

$$\bar{\varepsilon} = \frac{1}{V}\int_V \varepsilon(x)\,dx = \frac{1}{V}\left[\int_{V_m} \varepsilon(x)\,dx + \sum_{r=1}^{n}\int_{V_r} \varepsilon(x)\,dx\right] = \frac{1}{V}\left[V_m\bar{\varepsilon}_m + \sum_{r=1}^{n} V_r\bar{\varepsilon}_r\right] \tag{2.4.41}$$

According to Eshelby's equivalence principle (Eshelby, 1957), the perturbed strain field $\varepsilon'(x)$ induced by inhomogeneities can be related to specified eigenstrains $\varepsilon^*(x)$ by replacing the inhomogeneities with the matrix material (or vice versa). That is, for the domain of the r-th phase particles with elastic stiffness tensor $\mathbf{C}_r$, we have

$$\mathbf{C}_r : [\varepsilon^0(x) + \varepsilon'(x)] = \mathbf{C}^0 : [\varepsilon^0(x) + \varepsilon'(x) - \varepsilon^*(x)] \tag{2.4.42}$$

where the disturbing strain $\varepsilon'(x)$ can be expressed as

$$\varepsilon'(x) = \int_V G'(x - x') : \varepsilon^*(x')\,dx' \tag{2.4.43}$$

where

$$G'_{ijmn}(x - x') = -\frac{1}{2}[G_{ik,lj}(x - x') + G_{jk,li}(x - x')]C^0_{klmn} \tag{2.4.44}$$

Based on the above equations, we can derive the three governing field equations as follows

$$\bar{\varepsilon} = \varepsilon^0 + \sum_{r=1}^{n} f_r \mathbf{S} : \bar{\varepsilon}_r^* \tag{2.4.45}$$

$$\bar{\sigma} = \mathbf{C^0} : \left(\bar{\varepsilon} - \sum_{r=1}^{n} f_r \bar{\varepsilon}_r^*\right) \tag{2.4.46}$$

$$-(\mathbf{A}_r + \mathbf{S}) : \overline{\varepsilon}_r^* = \varepsilon^0 \tag{2.4.47}$$

where $\mathbf{S}$ is the interior-point Eshelby's tensor and $\mathbf{A}_r$ is the elastic mismatch tensor, which can be calculated as

$$\mathbf{A}_r = (\mathbf{C}_r - \mathbf{C}^0)^{-1} \cdot \mathbf{C}^0 \tag{2.4.48}$$

The exact solution of the many-particle-interacting integral equations is an intricate task for arbitrary and random configurations of particles, and with the assumption that inter-particle interaction effects are neglected, a non-interacting approximate analytical solution of effective moduli for multiphase composites becomes

$$\overline{\mathbf{C}} = \mathbf{C}^0 \cdot [\mathbf{I} + \mathbf{B} \cdot (\mathbf{I} - \mathbf{S} \cdot \mathbf{B})^{-1}] \tag{2.4.49}$$

where $\mathbf{B} = \sum_{r=1}^{n} \phi_r (\mathbf{S} + \mathbf{A}_r)^{-1}$ $\mathbf{B} = \sum_{r=1}^{n} f_r \left(\mathbf{S} + \mathbf{A}_\mathbf{r}\right)^{-1}$.

Based on Eqn. (2.4.49), the non-interacting effective moduli for two-phase composites can be derived as

$$\overline{\mathbf{C}} = \mathbf{C}^0 \cdot \left\{ \mathbf{I} + f_1 \left[\left(\mathbf{C}_\mathbf{1} - \mathbf{C}^0 \right)^{-1} \cdot \mathbf{C}^0 + \left(1 - f_1\right)\mathbf{S} \right]^{-1} \right\} \tag{2.4.50}$$

If all particles are spherical and both the matrix and particles are isotropic, the effective bulk moduli and shear moduli are

$$\overline{K} = K_0 \left[1 + \frac{3(1-\upsilon_0)(K_1 - K_0) f_1}{3(1-\upsilon_0)K_0 + (1-f_1)(1+\upsilon_0)(K_1 - K_0)} \right] \tag{2.4.51}$$

$$\overline{\mu} = \mu_0 \left[1 + \frac{15(1-\upsilon_0)(\mu_1 - \mu_0) f_1}{15(1-\upsilon_0)\mu_0 + 2(1-f_1)(4-5\upsilon_0)(\mu_1 - \mu_0)} \right] \tag{2.4.52}$$

Subscript 0 denotes the matrix and 1 denotes the particles, υ_0 is Poisson's ratio of the

matrix and f_1 is the volume fraction of the particles.

It is noted that Eqn. (2.4.51) and (2.4.52) are identical to the Hashin-Shtrikman lower (or upper) bounds and the Mori-Tanaka method for isotropic composites, if the matrix is the softer (or harder) phase.

There exists a slight shortage in accuracy of this non-interacting solution despite its simplicity when involving eigenstrains in inhomogeneities and many-particle interaction problems. Therefore, Ju and Chen made another attempt to construct an approximate yet more accurate method to account for inter-particle interaction effects in two-phase composites. Compared to the non-interacting solution, a higher-order (in particle volume fraction) probabilistic approach is introduced to estimate effective elastic moduli of two-phase composites containing randomly located spherical inhomogeneities.

In comparison with Eqn. (2.4.51) and (2.4.52), the effective bulk modulus $\bar{K}$ and effective shear modulus $\bar{\mu}$ of the pairwise-interacting solution can be explicitly evaluated as

$$\bar{K} = K_0\left[1+\frac{30\left(1-v_0\right)f_1\left(3\gamma_1+2\gamma_2\right)}{3\alpha+2\beta-10\left(1+v_0\right)f_1\left(3\gamma_1+2\gamma_2\right)}\right] \tag{2.4.53}$$

$$\bar{\mu} = \mu_0\left[1+\frac{30\left(1-v_0\right)f_1\gamma_2}{\beta-4\left(4-5v_0\right)f_1\gamma_2}\right] \tag{2.4.54}$$

where

$$\gamma_1 = \frac{5f_1}{96\beta^2}\left[12v_0\left(13-14v_0\right)-\frac{96\alpha}{3\alpha+2\beta}\left(1-2v_0\right)\left(1+v_0\right)\right] \tag{2.4.55}$$

$$\gamma_2 = \frac{1}{2}+\frac{5f_1}{96\beta^2}\left[6\left(25-34v_0+22v_0^2\right)-\frac{36\alpha}{3\alpha+2\beta}\left(1-2v_0\right)\left(1+v_0\right)\right] \tag{2.4.56}$$

$$\alpha = 2\left(5v_0 - 1\right) + 10\left(1 - v_0\right)\left(\frac{K_0}{K_1 - K_0} - \frac{\mu_0}{\mu_1 - \mu_0} \right) \tag{2.4.57}$$

$$\beta = 2\left(4 - 5v_0\right) + 15\left(1 - v_0\right)\frac{\mu_0}{\mu_1 - \mu_0} \tag{2.4.58}$$

2.5 Behavior Modeling of Asphalt Materials

In order to establish the constitutive modeling of innovative asphalt composite material to describe its linear and nonlinear behaviors, theory of plasticity and viscoplasticity with yield criterions must be employed and incorporated with continuum damage mechanics. Several basic yield criteria or models are briefly reviewed in this section.

2.5.1 The von Mises Yield Criterion

The von Mises yield criterion, also known as the maximum distortion energy criterion, is based on the determination of the distortion energy in a given material, i.e., of the energy associated with changes in the shape in that material, as opposed to the energy associated with the changes in volume in the same material.

This statement suggests that yielding of a material begins when the second deviatoric stress invariant J_2 reaches a critical value, mathematically

$$f\left(J_2\right) \equiv \sqrt{J_2} - k = 0 \tag{2.5.1}$$

where k can be shown to be the yield stress of the material in pure shear.

Also, at the onset of yielding, the magnitude of the shear yield stress in pure shear is $\sqrt{3}$ times lower than the tensile yield stress in the case of simple tension. Thus, we have

$$k = \frac{\sigma_y}{\sqrt{3}} \tag{2.5.2}$$

where σ_y is the tensile yield strength of the material. If we set the von Mises stress equal to the yield strength and combine the above equations, the von Mises yield criterion can be expressed as

$$f(J_2) \equiv \sqrt{3J_2} - \sigma_v = \sqrt{3J_2} - \sigma_y = 0 \tag{2.5.3}$$

Substituting J_2 in terms of the principal stresses into the von Mises criterion equation we have

$$(\sigma_1 - \sigma_2)^2 + (\sigma_2 - \sigma_3)^2 + (\sigma_1 - \sigma_3)^2 = 6k^2 = 2\sigma_y^2 \tag{2.5.4}$$

or

$$(\sigma_1 + \sigma_2 + \sigma_3)^2 - \sigma_1\sigma_2 - \sigma_2\sigma_3 - \sigma_1\sigma_3{}^2 = 3k^2 = \sigma_y^2 \tag{2.5.5}$$

or as a function of the stress tensor components

$$(\sigma_{11} - \sigma_{22})^2 + (\sigma_{22} - \sigma_{33})^2 + (\sigma_{11} - \sigma_{33})^2 + 6(\sigma_{23}^2 + \sigma_{31}^2 + \sigma_{13}^2) = 6k^2 = 2\sigma_y^2 \tag{2.5.6}$$

This equation defines the yield surface as a circular cylinder whose yield curve, or intersection with the deviatoric plane, is a circle with radius $\sqrt{2}k$, or $\sqrt{\frac{2}{3}}\sigma_y$, as shown in Figure 2.12. This implies that the yield condition is independent of hydrostatic stresses.

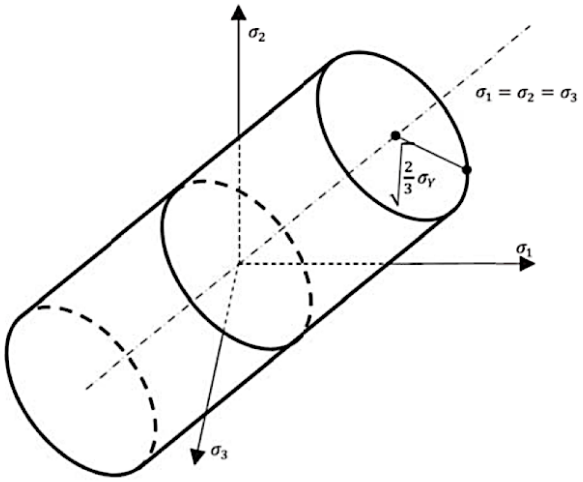

Figure 2.12 von Mises yield surface in principal stress space

2.5.2 The Drucker-Prager Plasticity Model

The Von Mises yield criterion is independent of hydrostatic pressure thus suitable for the modelling of plasticity in ductile materials such as metals. However, experimental results for materials such as rock, soils and concrete show that there is a strong dependence on the hydrostatic pressure. The extended criterion, whereby the hydrostatic-dependent first invariant is introduced to the Von Mises Eqn. (2.5.3), has been developed by Drucker and Prager (Drucker & Prager, 1952) as a simple modification of the von Mises model and is most frequently used in practical applications.

In terms of the stress invariants $\mathbf{I}_1$ and J_2, the Drucker-Prager criterion can be written as

$$f\left(\mathbf{I}_1, J_2\right) \equiv \sqrt{J_2} - \alpha \mathbf{I}_1 - k = 0 \tag{2.5.7}$$

where α is a material constant related to the theoretical cohesive strength of the material and k is the modified yield strength in absence of mean stress. When α is zero, Eqn. (2.5.7) reduces to the von Mises failure criterion. The Drucker-Prager yield surfaces in the principle stress space and the meridian planes are illustrated in Figure 2.13.

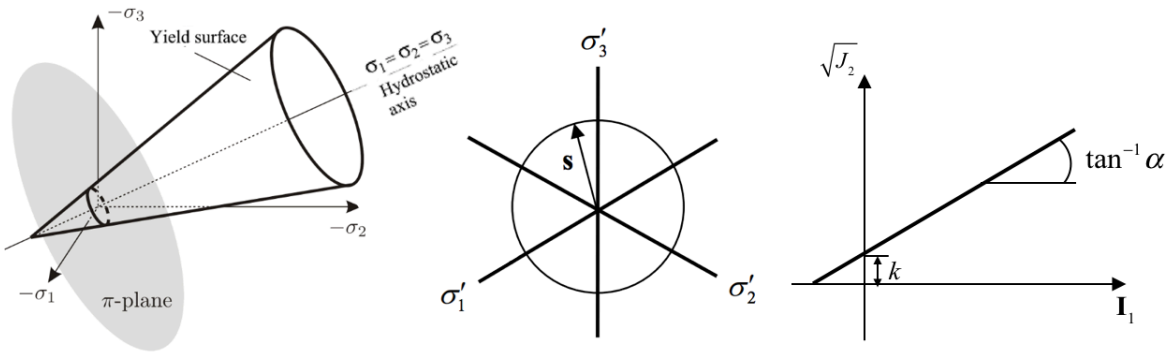

Figure 2.13 Yield surfaces of the Drucker-Prager plasticity model

The main characteristics the Drucker-Prager plasticity model includes: the yield criterion is simple and the yield surface is smooth and mathematically convenient to use in 3-D applications. Compared to the von Mises yield criterion, the Drucker-Prager model accounts for the effect of the hydrostatic pressure, at the same time, while the traces of the yield surface on the meridian planes are straight lines, reasonable results are expected only for a limited range of hydrostatic pressure, when the curvature in the failure envelope may be neglected. The influence of the intermediate principal stress is considered in the

Drucker-Prager model, however, there is no guarantee that this influence will be correctly represented unless the material parameters α and k are selected carefully.

2.5.3 The Perzyna Type Viscoplasticity Model

Viscoplastic models have been widely used to describe the rate-dependent inelastic mechanical behavior of materials. Among these models, Perzyna's theory (Olszak & Perzyna, 1969; Perzyna, 1966) is the basis of many viscoplasticity formulations. In this theory, the viscous behavior of a material is considered as a time-rate flow rule or loading function (comparing to the yield function in plasticity). The flow rule is assumed to be associative such that the viscoplastic potential is identical or at least proportional to the normal of the yield surface. The main feature of this model is that the rate-independent yield function used for describing the viscoplastic strain can become larger than zero, which effect is known as 'overstress'. In the small-strain theory, the strain rate vector in Perzyna viscoplasticity can be decomposed into the elastic and viscoplastic parts

$$\dot{\boldsymbol{\varepsilon}} = \dot{\boldsymbol{\varepsilon}}^{e} + \dot{\boldsymbol{\varepsilon}}^{vp} \tag{2.5.8}$$

where $\dot{\boldsymbol{\varepsilon}}^{e}$ is the elastic strain rate and $\dot{\boldsymbol{\varepsilon}}^{vp}$ is the viscoplastic strain rate, the superimposed dot denotes the time derivative. The stress rate $\dot{\boldsymbol{\sigma}}$ is related to the strain rate via the constitutive relation

$$\dot{\boldsymbol{\sigma}} = \mathbf{C}^{0} : \dot{\boldsymbol{\varepsilon}}^{e} = \mathbf{C}^{0} : \left(\dot{\boldsymbol{\varepsilon}} - \dot{\boldsymbol{\varepsilon}}^{vp} \right) \tag{2.5.9}$$

where $\mathbf{C}^0$ is the fourth-order elastic stiffness tensor.

The associative viscoplastic flow rule is given by the gradient to the yield surface (in the stress space)

$$\dot{\boldsymbol{\varepsilon}}^{vp} = \frac{1}{\eta}\left\langle g\left(f\left(\boldsymbol{\sigma},\mathbf{q}\right)\right)\right\rangle \frac{\partial f\left(\boldsymbol{\sigma},\mathbf{q}\right)}{\partial \boldsymbol{\sigma}} \tag{2.5.10}$$

where η is a scalar fluidity parameter or viscoplasticity consistency parameter with units of inverse seconds, the $\left\langle \ \right\rangle$ are McAuley brackets, and $g\left(f\right)$ is a dimensionless viscous flow function, commonly $g\left(f\right) = f^m$ where m is a material constant. For a linear Perzyna type viscoplasticity (associative flow rule), $m = 1$, whereas in other cases, non-associative flow rule.

The hardening law reads

$$\dot{\mathbf{q}} = \frac{1}{\eta}\left\langle g\left(f\left(\boldsymbol{\sigma},\mathbf{q}\right)\right)\right\rangle \tag{2.5.11}$$

The formulation can also be constructed in the strain space analogously.

If the viscoplasticity consistency parameter is very small, i.e. $\eta \to 0$, we recover the rate-dependent plasticity; whereas if the parameter goes to infinity, $\eta \to \infty$, we recover instantaneous elasticity.

2.6 The Mending Mechanism of DCPD

The densely cross-linked structures are the basis of superior mechanical properties such as high modulus, high fracture strength, and solvent resistance. Due to such properties,

highly cross-linked polymers have been widely applied and studied as matrices for composites, foamed structures, structural adhesives, insulators for electronic packaging, and other applications during past decades (X. Chen et al., 2003; Duenas et al., 2010; Kessler & White, 2001, 2002; White et al., 2001).

As one of the big family, dicyclopentadiene, abbreviated DCPD, is a liquid polymer with chemical formula $C_{10}H_{12}$. Its high toughness, low viscosity mechanical characteristic allows it to conduct as healing agent to restore and recover degradations asphalt concrete materials. Completion of this process requires a suitable chemistry to polymerize the DCPD liquid in the fracture plane. Researchers (Risse & Grubbs, 1991; Schrock, 1994) identified the living ring-opening metathesis polymerization (ROMP) as meeting the diverse set of requirements of the healing system, which includes long shelf life, low monomer viscosity and volatility, rapid polymerization at ambient conditions, and low shrinkage upon polymerization. Careful balance of catalyst, monomer, and other factors can offer excellent control of the polymer structure. In terms of homogeneous catalysts, most tungsten and molybdenum catalysts (Schrock's catalyst) have rapid initiation rates and can produce "living" polymerizations with excellent control of polydispersity and chain tactility, but the low functional group tolerance limits the monomers available. Ruthenium metathesis catalysts (Grubbs' catalyst) tend to have slower initiation rates, often leading to higher polydispersity, but their air stability and greater tolerance for

functional groups makes them "user friendly" and enables use of a wide range of functional monomers and additives.

The ROMP reaction, illustrated in Figure 2.14, invokes the use of a transition metal catalyst (for example, Grubbs' catalyst) that shows high metathesis activity while being tolerant of a wide range of functional groups as well as oxygen and water. The reaction polymerizes DCPD at room temperature in several minutes to yield a tough and highly cross-linked polymer network. The first generation DCPD-Grubbs' catalyst healing agent system is proposed by White et al. (White et al., 2001).

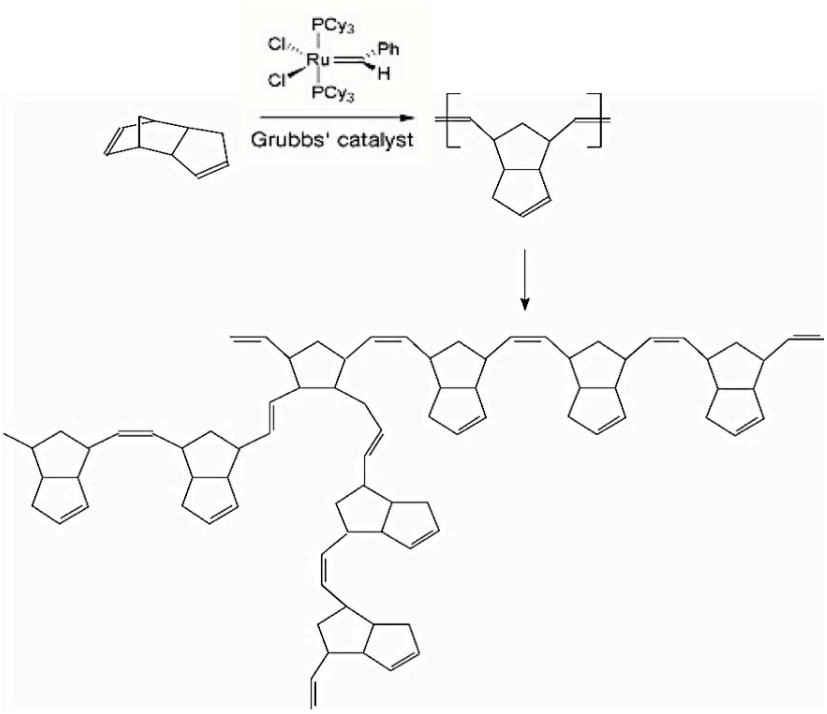

Figure 2.14 ROMP reaction of DCPD under Grubbs' catalyst

In White et al.'s healing agent system, DCPD is be filled in microcapsules and embedded into composites in the mixing process, and when stress concentration is induced by micro cracks, the microcapsules break and the liquid form DCPD is released into the cracks, which will begin its ROMP reactions under catalyst and repair the damage. Under such condition, repairing is not accomplished by external operations, so we can regard the system as 'self-healing'. This concept of self-healing materials are the next-generation materials for high-performance structures. To reduce the fatigue and subsequent probability of failure along with extended service life of polymer and polymer composites, the self-healing concept has great potential. However, none would have been accomplished without the ROMP reaction which allows the DCPD to form a network to bond with the materials, fill the cracks and air voids and restore mechanical properties and performance of the materials.

2.7 References

Astarita, G. (1989). *Thermodynamics: an advanced textbook for chemical engineers*. New York and London: Plenum Press.

Benveniste, Y. (1987). A new approach to the application of Mori-Tanaka's theory in composite materials. *Mechanics of Materials, 6*(2), 147-157.

Beremin, F. M. (1981). Experimental and numerical study of the different stages in ductile rupture: application to crack initiation and stable crack growth. North Holland.

Berveiller, M., & Zaoui, A. (1979). An Extension of the Self-consistent Scheme to Plastically Flowing Polycrystals. *Journal of the Mechanics and Physics of Solids, 26*, 325-344.

Budiansky, B., & Wu, T. T. (1962). Theoretical prediction of plastic strains of polycrystals. *Proceedings of the 4th U.S. National Congress of Applied Mechanics*, 1175.

Castaneda, P. P. (1991). The effective mechanical properties of nonlinear isotropic composites. *Journal of the Mechanics and Physics of Solids, 39*, 45-71.

Castaneda, P. P., & Willis, J. R. (1988). On the overall properties of nonlinearly viscous composites. *Proceedings of the Royal Society of London, Series A, 416*, 217-244.

Chen, X., Wudl, F., Mal, A. K., Shen, H., & Nutt, S. R. (2003). New Thermally Remendable Highly Cross-Linked Polymeric Materials. *Macromolecules, 36*(6), 1802-1807.

Chow, C. L., & Wang, J. (1987). An anisotropic theory of continuum damage mechanics for ductile fracture. *Engineering Fracture Mechanics, 27*(5), 547-558.

Coleman, B. D., & Gurtin, M. E. (1967). Thermodynamics with internal state variables. *Journal of Chemical Physics, 47*(2), 597-613.

Dewey, J. M. (1947). The elastic constants of materials loaded with non-rigid fillers. *Journal of Applied Mechanics, 18*, 578-581.

Drucker, D. C., & Prager, W. (1952). Soil Mechanics and Plastic Analysis or Limite Design. *Quarterly of Applied Mathematics, 10*, 157-175.

Duenas, T., Enke, A., Chai, K., Castellucci, M., Sundaresan, V. B., Wudl, F., . . . Ooi, T. K. (2010). Smart Self-Healing Material Systems Using Inductive and Resistive Heating. *Smart Coatings III, 1050*, 45-60.

Eshelby, J. D. (1957). The determination of the elastic field of an ellipsoidal inclusion, and related problems. *Proceedings of the Royal Society of London, Series A, 241*(1226), 376–396.

Germain, P., Nguyen, Q. S., & Suquet, P. (1983). Continuum thermodynamics. *Journal of Applied Mechanics, ASME, 50*(4B), 1010-1020.

Hashin, Z. (1959). *The moduli of an elastic solid, containing spherical particles of another elastic material*. Paper presented at the IUTAM Non-homogeneity in elasticity and plasticity symposium, Warsaw.

Hashin, Z. (1962). The elastic moduli of heterogeneous materials. *Journal of Applied Mechanics, 29*(2), 143-150.

Hashin, Z. (1988). The differential scheme and its applications to cracked materials. *Journal of the Mechanics and Physics of Solids, 36*(6), 719-734.

Hashin, Z., & Shtrikman, S. (1961). Note on a variational approach to the theory of composite elastic materials. *Journal of the Franklin Institute, 274*(4), 336-341.

Hashin, Z., & Shtrikman, S. (1963). A variational approach to the theory of the elastic behaviour of multiphase materials. *Journal of the Mechanics and Physics of Solids, 11*(2), 127-140.

Hill, R. (1965a). Continuum micro-mechanics of elastoplastic polycrystals. *Journal of the Mechanics and Physics of Solids, 13*, 89-101.

Hill, R. (1965b). A Self-Consistent Mechanics of Composite Materials. *Journal of the Mechanics and Physics of Solids, 13*(4), 213-222.

Hill, R., & Rice, J. R. (1973). Elastic potentials and structure of inelastic constitutive laws. *Siam Journal on Applied Mathematics, 25*(3), 448-461.

Hong, S., Yuan, K. Y., & Ju, J. W. (2017). New strain energy-based thermo-elastoviscoplastic isotropic damage–self-healing model for bituminous composites—Part I: Formulations. *International Journal of Damage Mechanics, 26*(5), 651-671.

Hutchinson, J. W. (1970). Elastic-plastic behavior of polycrystalline metals and composites. *Proceedings of the Royal Society of London, Series A, 319*, 247-272.

Iwakuma, T., & Nemat-Nasser, S. (1984). Finite elastic-plastic deformation of polycrystalline metals. *Proceedings of the Royal Society of London, Series A, 394*, 87-119.

Ju, J. W. (1989). On energy-based coupled elastoplastic damage theories-constitutive modeling and computational aspects. *International Journal of Solids and Structures, 25*(7), 803-833.

Ju, J. W., & Chen, T. M. (1994a). Effective elastic moduli of two-phase composites containing randomly dispersed spherical inhomogeneities. *Acta Mechanica, 103*(1-4), 123-144.

Ju, J. W., & Chen, T. M. (1994b). Micromechanics and effective moduli of elastic composites containing randomly dispersed ellipsoidal inhomogeneities. *Acta Mechanica, 103*(1-4), 103-121.

Ju, J. W., Ko, Y. F., & Zhang, X. D. (2009). Multi-level elastoplastic damage mechanics for elliptical fiber reinforced composites with evolutionary fiber debonding. *International Journal of Damage Mechanics, 18*(5), 419-460.

Ju, J. W., & Sun, L. Z. (2001). Effective elastoplastic behavior of metal matrix composites containing randomly located aligned spheroidal inhomogeneities, Part I: Micromechanics based formulation. *International Journal of Solids and Structures, 38*(2), 183-201.

Ju, J. W., & Yanase, K. (2009). Micromechanical elastoplastic damage mechanics for elliptical fiber reinforced composites with progressive partial fiber debonding. *Journal of Damage Mechanics, 18*(7), 639-668.

Ju, J. W., & Yanase, K. (2010). Micromechanics and effective elastic moduli of particle-reinforced composites with near-field particle interactions. *Acta Mechanica, 215*(1), 135-153.

Ju, J. W., & Yuan, K. Y. (2012). New strain-energy based coupled elastoplastic two-parameter damage and healing models for earth moving processes. *International Journal of Damage Mechanics, 21*(7), 989-1019.

Ju, J. W., Yuan, K. Y., & Kuo, A. W. (2012). Novel strain-energy-based coupled elastoplastic damage and healing models for geomaterials-Part I: Formulations. *International Journal of Damage Mechanics, 21*(4), 525-549.

Ju, J. W., Yuan, K. Y., Kuo, A. W., & Chen, J. S. (2012). Novel Strain Energy Based Coupled Elastoplastic Damage and Healing Models for Geomaterials - Part I: Formulations. *International Journal of Damage Mechanics, 21*(4), 551-576.

Kachanov, L. M. (1958). Time of the rupture process under creep conditions. [English Translation 1999]. *Izvestiia Akademii Nauk SSSR, 8*, 26-31.

Kachanov, L. M. (1999). Rupture time under creep conditions. *International Journal of Fracture, 97*(1-4), 11-18.

Kerner, E. H. (1956). The elastic and thermo-elastic properties of composite media. *Proceedings of the Royal Society of London, Series B, 69*, 807-808.

Kessler, M. R., & White, S. R. (2001). Self-activated healing of delamination damage in woven composites. *Composites Part A- Applied Science and Manufacturing, 32*(5), 683-699.

Kessler, M. R., & White, S. R. (2002). Cure kinetics of the ring-opening metathesis polymerization of dicyclopentadiene. *Journal of Polymer Science Part A: Polymer Chemistry, 40*(14), 2373-2383. doi:10.1002/pola.10317

Ko, Y., & Ju, J. W. (2008). Micromechanical Elastoplastic Damage Modeling of Evolutionary Interfacial Arc Debonding for Fiber Reinforced Composites. *International Journal of Damage Mechanics, 14*(4), 307-356.

Ko, Y., & Ju, J. W. (2012). Effects of fiber cracking on elastoplastic-damage behavior of fiber-reinforced metal matrix composites. *International Journal of Damage Mechanics, 22*(1), 48-67.

Krajcinovic, D. (1983). Creep of structures - a continuous damage mechanics approach. *Journal of Structural Mechanics, 11*(1), 1-11.

Krajcinovic, D., & Fanella, D. (1986). A micromechanical damage model for concrete. *Engineering Fracture Mechanics, 25*(5-6), 585-596.

Krajcinovic, D., & Fonseka, G. U. (1981). The continuous damage theory of brittle materials: Part 1: General theory. *Journal of Applied Mechanics, 48*(4), 809-815.

Kröner, E. (1977). Bounds for effective elastic moduli of disordered materials. *Journal of the Mechanics and Physics of Solids, 25*(2), 137-155.

Ladeveze, P., & Lemaitre, J. (1984). *Damage effective stress in quasi-unilateral conditions.* Paper presented at the 16th International congress of theoretical and applied mechanics, Lyngby, Denmark.

Laws, N., & Dvorak, G. J. (1987). The effect of fiber breaks and aligned penny-shaped cracks on

the stiffness and energy release rates in unidirectional composites. *International Journal of Solids and Structures, 23*(9), 1269-1283.

Lee, H., & Pyo, S. (2007). Micromechanics-based elastic damage modeling of particulate composites with weakened interfaces. *International Journal of Solids and Structures, 44*(25), 8390-8406.

Lee, H. J., Daniel, J. S., & Kim, Y. R. (2000). Continuum damage mechanics-based fatigue model of asphalt concrete. *Journal of Material in Civil Engineering, 12*(2), 105-112.

Lee, J. K., Choi, S. J., & Mal, A. K. (2001). Stress analysis of an unbounded elastic solid with orthotropic inclusions and voids using a new integral equation technique. *International Journal of Solids and Structures, 38*(16), 2789-2820.

Lee, J. K., Ku, D. Y., & Mal, A. K. (2011). Elastic analysis of a half-plane with multiple inclusions using volume integral equation method. *Engineering Analysis with Boundary Elements, 35*(3), 564-574.

Lee, J. K., & Mal, A. K. (1995). A volume integral equation technique for multiple scattering problems in elastodynamics. *Applied Mathematics and Computation, 67*(1-3), 135-159.

Lee, J. K., & Mal, A. K. (1997). A Volume Integral Equation Technique for Multiple Inclusion and Crack Interaction Problems. *Journal of Applied Mechanics, 64*(1), 23-31.

Lemaitre, J. (1971). *Evaluation of dissipation and damage in metals submitted to dynamic loading.* Paper presented at the Proceedings of International Congress of Methametics, Kyoto, Japan.

Lemaitre, J. (1992). *A Course on Damage Mechanics*. Berlin: Springer-Verlag.

Levine, H. S. (1982). A two-surface plastic and micro cracking model for plain concrete. *Nonlinear Numerical Analysis of Reinforced Concrete, Proceedings Winter Annual Meeting, ASME*, 27-47.

Lipinski, P., Naddari, A., & Berveiller, M. (1992). Recent results concerning the modelling of polycrystalline plasticity at large strains

Author links open overlay panel. International Journal of Solids and Structures, 29, 1873-1881.

Lubarda, V. A. (1994). An analysis of large-strain damage elastoplasticity. *International Journal of Solids and Structures, 31*(21), 2951-2964.

Lubarda, V. A., & Krajcinovic, D. (1994). Tensorial representation of the effective elastic properties of the damaged material. *International Journal of Damage Mechanics, 3*(1), 38-56.

Lubarda, V. A., & Krajcinovic, D. (1995). Constitutive structure of rate theory of damage in brittle elastic solids. *Applied Mathematics and Computation, 67*(1-3), 81-101.

Mazars, J. (1986). A description of micro- and macroscale damage of concrete structures. *Engineering Fracture Mechanics, 25*(5-6), 729-737.

Mazars, J., & Lemaitre, J. (1985). Application of Continuous Damage Mechanics to Strain and Fracture Behavior of Concrete. In S. S.P. (Ed.), *Application of Fracture Mechanics to Cementitious Composites. NATO ASI Series (Series E: Applied Sciences)* (Vol. 94, pp. 507-520): Springer, Dordrecht.

McLaughlin, R. (1977). A study of the differential scheme for composite materials. *International Journal of Engineering Science, 15*(4), 237-244.

Milan, J., & Zdenek, P. B. (2001). *Inelastic Analysis of Structures*: John Wiley& Sons.

Miner, M. A. (1945). Cumulative damage in fatigue. *Journal of Applied Mechanics, 12*(3), A159-A164.

Molinari, A., Canova, G. R., & Ahzi, S. (1987). A self consistent approach of the large deformation polycrystal viscoplasticity. *Acta Metallurgica, 35*(12), 2983-2994.

Molinari, A., Houdaigui, F., & Tóth, L. S. (2004). Validation of the tangent formulation for the solution of the non-linear Eshelby inclusion problem. *International Journal of Plasticity, 20*(2), 291-307.

Mori, T., & Tanaka, T. (1973). Average stress in matrix and average elastic energy of materials with misfitting inclusions. *Acta Metallurgica, 21*(5), 571-574.

Mould, J. C. J., Levine, H. S., & Tennant, D. (1994). *Evaluation of a rate-dependent three invariant softening model for concrete.* Paper presented at the Fracture and Damage in Quasibrittle Structures, Chapman and Hall, London.

Mura, T. (1987). *Micromechanics of defects in solids* (2nd ed.): Springer Netherlands.

Norris, A. N. (1985). A differential scheme for the effective moduli of composites. *Mechanics of Materials, 4*(1), 1-16.

Norris, A. N. (1989). An examination of the Mori-Tanaka effective medium approximation for multiphase composites. *Journal of Applied Mechanics, ASME, 56*, 83-88.

Olszak, W., & Perzyna, P. (1969). On thermal effects in viscoplasticity. *Journal of Applied Mathematics and Physics, 20*, 676–680.

Ortiz, M. (1985). A constitutive theory for the inelastic behavior of concrete. *Mechanics of Materials, 4*, 67-93.

Ortiz, M. (1987a). An analytical study of the localized failure modes of concrete. *Mechanics of Materials, 6*, 159-174.

Ortiz, M. (1987b). A method of homogenization of elastic media. *International Journal of Engineering Science, 25*(7), 923-934.

Park, S. W., Kim, Y. R., & Schapery, R. A. (1996). A viscoelastic continuum damage model and its application to uniaxial behavior of asphalt concrete. *Mechanics of Materials, 24*(4), 241-255.

Perzyna, P. (1966). Fundamental problems in viscoplasticity. *Advances in Applied Mechanics, 9*(2), 243-377.

Qiu , Y. P., & Weng, G. J. (1990). On the application of Mori-Tanaka's theory involving transversely isotropic spheroidal inclusions. *International Journal of Engineering Science, 289*, 1121-1137.

Rabotnov, Y. N. (1963). On the Equation of State of Creep. *Proceedings of the Institution of Mechanical Engineers, 178*(1), 2-117-112-122.

Rice, J. R. (1971). Inelastic constitutive relations for solids: An internal-variable theory and its application to metal plasticity. *Journal of the Mechanics and Physics of Solids, 19*(6), 433-455.

Rice, J. R., & Tracey, D. M. (1969). On the ductile enlargement of voids in triaxial stress fields. *Journal of the Mechanics and Physics of Solids, 17*(3), 201-217.

Risse, W., & Grubbs, R. H. (1991). Block and graft copolymers by living ring-opening olefin metathesis polymerization. *Journal of Molecular Catalysis, 65*(1-2), 211-217.

Roscoe, R. (1952). The viscosity of suspensions of rigid spheres. *British Journal of Applied Physics, 3*, 267-269.

Schreyer, H. L. (1995). Continuum Damage Based on Elastic Projection Operators. *International Journal of Damage Mechanics, 4*(2), 171-195.

Schrock, R. R. (1994). Recent Advances in the Chemistry and Applications of High-Oxidation State Alkylidene Complexes. *Pure and Applied Chemistry, 66*(7), 1447-1454.

Simo, J. C., & Ju, J. W. (1987). Strain- and stress-based continuum damage model - I. Formulation. *International Journal of Solids and Structures, 23*(7), 821-840.

Stevens, D. J., & Liu, D. (1992). Strain-based constitutive model with mixed evolution rules for concrete. *Journal of Engineering Mechanics, ASCE, 118*(6).

Sun, L. Z., & Ju, J. W. (2004). Elastoplastic Modeling of Metal Matrix Composites Containing Randomly Located and Oriented Spheroidal Particles. *Journal of Applied Mechanics, 71*(6), 774-785.

Sun, L. Z., Ju, J. W., & Liu, H. T. (2003). Elastoplastic modeling of metal matrix composites with evolutionary particle debonding. *Mechanics of Materials, 35*(3), 559-569.

Tai, W. H., & Yang, B. X. (1986). A new microvoid-damage model for ductile fracture. *Engineering Fracture Mechanics, 25*, 377-384.

Taya, M., & Chou, T. W. (1981). On two kinds of ellipsoidal inhomogeneities in an infinite elastic body: an application to a hybrid composite. *International Journal of Solids and Structures, 17*(6), 553-563.

Taya, M., & Mura, T. (1981). On stiffness and strength of an aligned short-fiber reinforced composite containing fiber-end cracks under uniaxial applied stress. *Journal of Applied Mechanics, 48*(2), 361-347.

Thomson, W. (1852). On the universal tendency in nature to the dissipation of mechanical energy. *Philosophical Magazine, 4*(25), 304-306.

Walpole, L. J. (1966a). On bounds for overall elastic moduli of inhomogeneous systems-I. *Journal of the Mechanics and Physics of Solids, 14*, 151-162.

Walpole, L. J. (1966b). On bounds for overall elastic moduli of inhomogeneous systems-II. *Journal of the Mechanics and Physics of Solids, 14*, 289-301.

Weng, G. J. (1984). Some elastic properties of reinforced solids, with special reference to isotropic ones containing spherical inclusions. *International Journal of Engineering Science, 22*, 845-856.

Weng, G. J. (1990). The theoretical connection between Mori-Tanaka's theory and the Hashin-Shtrikman-Walpole bounds. *International Journal of Engineering Science, 28*, 1111-1120.

White, S. R., Sottos, N. R., Geubelle, P. H., Moore, J. S., Kessler, M., Sriram, S. R., . . . Viswanathan, S. (2001). Autonomic healing of polymer composites. *Nature, 409*(6822), 794-797.

Willis, J. R. (1977). Bounds and self-consistent estimates for the overall properties of anisotripic composites. *Journal of the Mechanics and Physics of Solids, 25*, 185-202.

Willis, J. R. (1991). On methods for bounding the overall properties of nonlinear composites. *Journal of the Mechanics and Physics of Solids, 39*, 73-86.

Willis, J. R. (1994). Upper and lower bounds for nonlinear composite behavior. *Materials Science and Engineering: A, 175*, 7-14.

Wu, C. H. (1985). *Tension-compression test of a concrete specimen via a structure damage theory.* Paper presented at the Damage Mechanics and Continuum Modeling, Detroit.

Yazdani, S. (1993). On a Class of Continuum Damage Mechanics Theories. *International Journal of Damage Mechanics, 2*(2), 162-176.

Yazdani, S., & Schreyer, H. L. (1988). An Anisotropic Damage Model with Dilatation for Concrete. *Mechanics of Materials, 7*(3), 231-244.

CHAPTER 3 : MICROMECHANICS-BASED ISOTROPIC ELASTIC-DAMAGE FRAMEWORK OF ASPHALT CONCRETE MATERIALS FEATURING HIGH TOUGHNESS, LOW VISCOSITY NANO-MOLECULAR RESINS

3.1 Introduction

Researchers at UCLA School of Engineering (Kao et al., 2011; W. Yuan et al., 2012; W. Yuan et al., 2013; W. Yuan et al., 2011) brought up a revolutionary pothole patching technology for asphalt concrete pavements by employing an ultra-high toughness, low viscosity nano-molecular resin, dicyclopentadiene (DCPD), as a binder or additive in the traditional asphalt concrete materials. Certain classes of DCPD resin can be cured to (polymerized) p-DCPD by a commercially available catalyst (e.g., the ruthenium-based Grubbs' catalysts) to form an ultra-tough material with many of the desirable properties for pothole repair technology. Furthermore, the viscosity of DCPD resin is controllable by the catalyst for different curing times. This important feature allows DCPD to infiltrate the asphalt/concrete–aggregate mixtures in the beginning like water and enables p-DCPD to occupy most air voids.

In order to take full advantage of this revolutionary technology, the mechanical behavior of the innovative asphalt concrete pothole patching materials needs be studied

based on the well-developed continuum damage mechanics. The fundamental assumption for continuum damage mechanics is the assumption that the damaged material is a macroscopically homogeneous one, makes it possible for global modeling of the nucleation and the propagation of micro-defects including their effects on the mechanical behavior.

The theory of continuum damage mechanics has been employed for decades to describe the progressive degradation of material properties from a micromechanical aspect. Initiated by Kachanov (Kachanov, 1958, 1999) and Rabotnov (Rabotnov, 1963), the theory was developed based on the assumption that the damaged material is a macroscopically homogeneous one (Chaboche, 1981). Later the theory was set up on a more rigorous basis using thermodynamics and micromechanics, and its applications to engineering began as many more people were involved in this discipline such as the applications to the modeling of elasticity coupled with damage (Krajcinovic & Fonseka, 1981; Ladeveze & Lemaitre, 1984; Lubarda & Krajcinovic, 1994; Ortiz, 1987b), elastoplastic damage (Kiefer et al., 2018; Y. Wu & Ju, 2017; Yan et al., 2019), creep damage (Krajcinovic, 1983; Mould et al., 1994; Murakami & Ohno, 1981; Pandey et al., 2019), fatigue damage (Abu Al-Rub et al., 2010; Chaboche & Lesne, 1988; Chow & Wang, 1987; Sermage et al., 2000), etc.

In this chapter, a 3-D homogenous-matrix with spherical multilayer-coated inclusions (particles) model was employed to simulate the materials. The concept under this 3-D model is that the materials can be decomposed into two parts: irregular coarse aggregates; and asphalt mastic composed of fine aggregates, asphalt binder, p-DCPD and air voids.

The irregular coarse aggregates are replaced and simulated by spherical multilayer-coated particles of different sizes (three in this model), and then the effective elastic moduli of the asphalt mastic, which is treated as the matrix of the model, are homogenized using various homogenization methods.

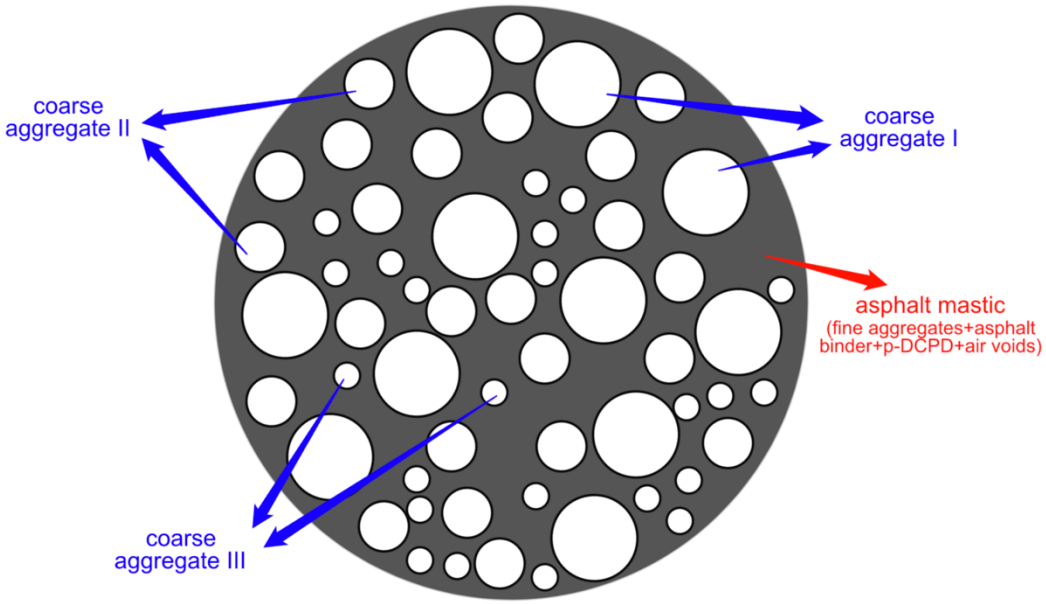

Figure 3.1 The schematic illustration of a cross section of the 3-D innovative asphalt concrete cylinder model (plan view)

Figure 3.1 shows a schematic illustration of a cross section view (plan view) of the 3-D model, with irregular coarse aggregates replaced by spherical particles in three sizes and asphalt mastic treated as homogeneous. Figure 3.2, taken before an indirect tension test, is a plan view of a real asphalt concrete cylinder cast with the innovative materials (D2 64-10 mix was used). By comparing Figure 3.1 and Figure 3.2, the 3-D model looks reasonable.

Furthermore, we may replace the spherical particles by the ellipsoidal particles or even irregular shaped particles, which may better simulate the real case to some extent. A new variable involved when replacing the spherical particles by the ellipsoidal particles is the orientation of the principle axes. The introducing of irregular shaped particles, which can be generated by image processing technology, requires more work.

Figure 3.2 Plan view of asphalt concrete cylinder cast with innovative asphalt materials

3.2 Overview of the Micromechanical Framework

The starting point to tackle a new problem is always to start from the fundamental step. In the micromechanical framework of these innovative asphalt concrete materials infiltrated with DCPD, the very first and fundamental step is to assume the behavior of the materials is within elastic range. Once we have a meaningful and effective elastic model,

we can further develop the elastic model into plastic, viscoplastic, thermo-elasto-viscoplastic models and so on. In this section, the 3-D model, which can be decomposed into two parts, as illustrated in Section 3.1, is assumed to be under elastic behavior, and an analytical method to describe this elastic behavior is derived in detail.

3.3 Equivalent Multilayer-coated Particles

The irregular coarse aggregates in the innovative asphalt concrete materials are simulated by spherical multilayer-coated particles of different sizes. Concepts similar to the multilayer coats have been used in many researches (Martínez et al., 2003; Puissant et al., 1994; Yang & Mal, 1995; K. Y. Yuan et al., 2014). A schematic illustration of the multilayer-coated particle is shown in Figure 3.3. Inspired by the concept of micromechanics, we assume such an outmost layer is applied to the original coated particle that its elastic properties are equivalent to the overall properties of the coated particle. We call this outmost layer the equivalent coated layer. Under such assumption, the coated particle can be treated as a macroscopically homogeneous material.

To calculate the elastic moduli of this multilayer-coated particle, we can assume that the particle is made up of several spherical shells with different radii and derive constitutive equations for each shell separately. The boundary conditions for these constitutive equations would be that pressure and displacement at each surface are the same. Figure 3.4

shows a schematic illustration of a general spherical shell under both internal and external pressures (Bower, 2009).

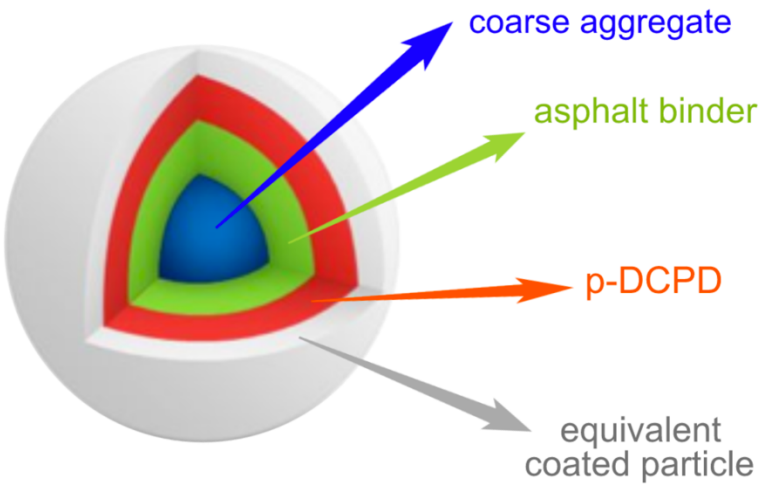

Figure 3.3 The schematic illustration of a spherical multilayer-coated particle

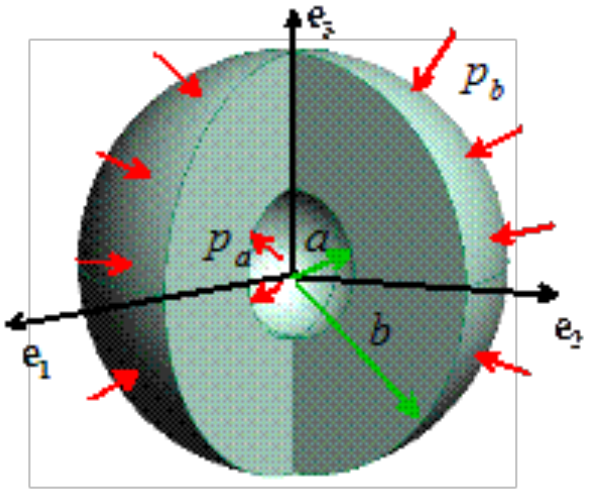

Figure 3.4 A 3-D hollow spherical shell under both internal and external pressures

Assuming that the inner surface ($R = a$) is subjected to pressure p_a, the outer surface

($R = b$) is subjected to pressure p_b, while no body forces act on the shell and the temperature is uniform. The displacement field (Bower, 2009) within the body of shell ($a \le R \le b$) is

$$u_{(R)} = \frac{1}{2E(b^3 - a^3)R^2}\left[2(p_a a^3 - p_b b^3)(1-2\upsilon)R^3 + (p_a - p_b)(1+\upsilon)a^3 b^3\right] \qquad (3.1)$$

where E denotes the Young's modulus of the shell, and υ denotes the Poisson's ratio.

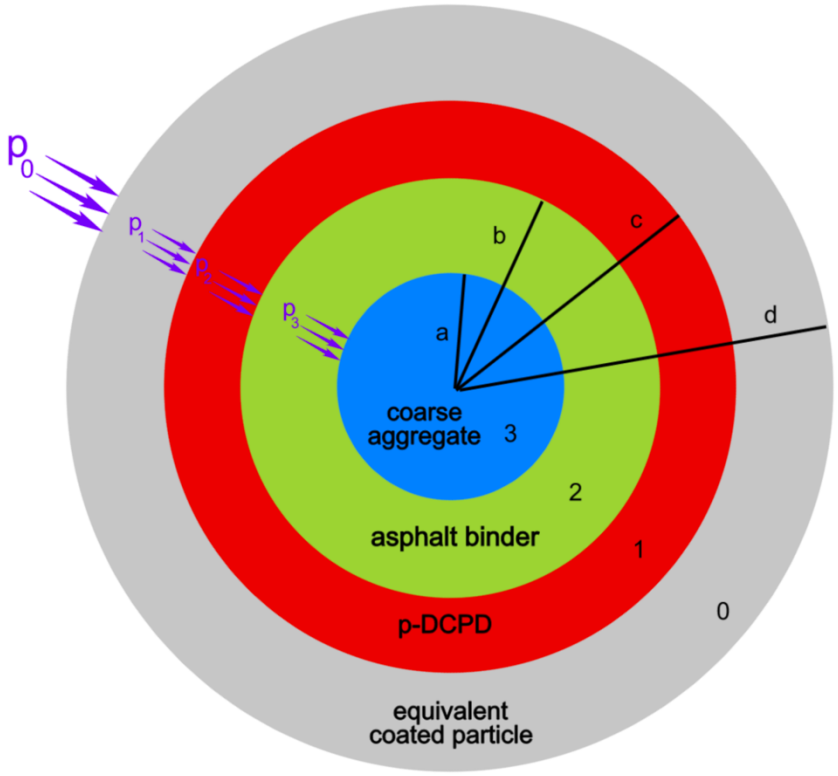

Figure 3.5 Boundary conditions for the multilayer-coated particle (cross section cutting through center of particle)

Based on the boundary conditions given in Figure 3.5, the displacement on each layer will be

$$u_{(od)} = \frac{1}{2E_0(d^3-c^3)d^2}\left[2(p_1c^3-p_0d^3)(1-2\upsilon_0)d^3+(p_1-p_0)(1+\upsilon_0)c^3d^3\right] \quad (3.2)$$

$$u_{(oc)} = \frac{1}{2E_0(d^3-c^3)c^2}\left[2(p_1c^3-p_0d^3)(1-2\upsilon_0)c^3+(p_1-p_0)(1+\upsilon_0)c^3d^3\right] \quad (3.3)$$

$$u_{(1c)} = \frac{1}{2E_1(c^3-b^3)c^2}\left[2(p_2b^3-p_1c^3)(1-2\upsilon_1)c^3+(p_2-p_1)(1+\upsilon_1)b^3c^3\right] \quad (3.4)$$

$$u_{(1b)} = \frac{1}{2E_1(c^3-b^3)b^2}\left[2(p_2b^3-p_1c^3)(1-2\upsilon_1)b^3+(p_2-p_1)(1+\upsilon_1)b^3c^3\right] \quad (3.5)$$

$$u_{(2b)} = \frac{1}{2E_2(b^3-a^3)b^2}\left[2(p_3a^3-p_2b^3)(1-2\upsilon_2)b^3+(p_3-p_2)(1+\upsilon_2)a^3b^3\right] \quad (3.6)$$

$$u_{(2a)} = \frac{1}{2E_2(b^3-a^3)a^2}\left[2(p_3a^3-p_2b^3)(1-2\upsilon_2)a^3+(p_3-p_2)(1+\upsilon_2)a^3b^3\right] \quad (3.7)$$

$$u_{(3a)} = -\frac{a(1-2\upsilon_3)}{E_3}p_3 \quad (3.8)$$

Here, 0, 1, 2, 3 denotes the index of the layer, where both the displacement field u, and the Young's modulus and the Poisson's ratio would follow. a, b, c, d denotes the radius of each interface of the layers.

As mentioned previously, the entire particle is macroscopically homogeneous, so the displacement at the outer surface should be

$$u_{(d)} = -\frac{d(1-2\upsilon_0)}{E_0}p_0 \quad (3.9)$$

By applying the continuity conditions of displacement on each interface, i.e. $u_{(0d)} = u_{(d)}$, $u_{(0c)} = u_{(1c)}$, $u_{(1b)} = u_{(2b)}$, $u_{(2a)} = u_{(3a)}$, and eliminating all the unknown pressures, Eqn. (3.2)-(3.8) will merge into one equation, which can be expressed in a way that the Young's modulus of the equivalent entire particle, E_0, is a function of the Young's moduli and the Poisson's ratios of the equivalent coated layer, p-DCPD, asphalt binder and coarse aggregate, and radii of layers' interfaces. The workload is massive by hand calculation, so computational software (Mathematica) is used here. The expression of the equivalent Young's modulus of the entire particle given by Mathematica is

$$E_0 = E_1 \frac{1-2\upsilon_0}{1-2\upsilon_1} \frac{Ca^3\left(2Ab^3+2Bc^3\right)+Nb^3\left(Dc^3+2Mb^3\right)}{Ca^3\left(\Lambda Ab^3+2Bc^3\right)+Nb^3\left(Dc^3+\Lambda Mb^3\right)} \tag{3.10}$$

where

$$\begin{aligned} A &= E_1\left(1+\upsilon_2\right)+2E_2\left(1-2\upsilon_1\right) \\ B &= E_2\left(1+\upsilon_1\right)-E_1\left(1+\upsilon_2\right) \\ C &= E_3\left(1-2\upsilon_2\right)-E_2\left(1-2\upsilon_3\right) \\ D &= E_2\left(1+\upsilon_1\right)+2E_1\left(1-2\upsilon_2\right) \\ M &= E_2\left(1-2\upsilon_1\right)-E_1\left(1-2\upsilon_2\right) \\ N &= E_3\left(1+\upsilon_2\right)+2E_2\left(1-2\upsilon_3\right) \\ \Lambda &= -\frac{1+\upsilon_1}{1-2\upsilon_1} \end{aligned} \tag{3.11}$$

The Young's moduli and the Poisson's ratios of p-DCPD, asphalt binder and coarse aggregate and the radius (size) of the coarse aggregate, E_1, E_2, E_3, υ_1, υ_2, υ_3, a(notice that we've categorized the coarse aggregates into several different sizes, so a is not a fixed value but depends on the size of aggregates), are known values, while the Poisson's ratio of the equivalent coated layer, which is also the equivalent Poisson's ratio of the entire

particle, and the radii of equivalent coated layer-p-DCPD interface and p-DCPD-asphalt binder, υ_0, b, c are yet unknown. Notice that d vanishes in Eqn. (3.11), which indicates that the dimension of the equivalent coated layer has nothing to do with the Young's modulus of the entire particle, which meets the concept of micromechanics and validate the assumption of equivalent coated layer.

The unknown Poisson's ratio of the entire particle, υ_0, can be solved by the empirical formula given by Ahmed and Jones (Ahmed & Jones, 1990)

$$\upsilon_0 = \frac{\upsilon_1 f_1 E_1 + \upsilon_2 f_2 E_2 + \upsilon_3 f_3 E_3}{f_1 E_1 + f_2 E_2 + f_3 E_3} \tag{3.12}$$

where f_1, f_2 and f_3 denote the volume fraction of p-DCPD, asphalt binder and coarse aggregate respectively. Notice that for different sizes of coarse aggregates, the volume fractions are different. The value of b and c can be derived from the thicknesses of p-DCPD layer and asphalt binder layer. As mentioned before, coarse aggregates are categorized into several different sizes. Yet we assume the multilayer-coated particles, whatever sizes of coarse aggregates they contain, share the same thicknesses of p-DCPD layer and asphalt binder layer. The thicknesses of p-DCPD layer and asphalt binder layer are defines as

$$t_1 = c - b; \qquad t_2 = b - a \tag{3.13}$$

which can be solved by the following formulas

$$\sum_{i=1}^{n} f_{3i} \frac{(a_i + t_1 + t_2)^3 - a_i^3}{(a_i + t_1 + t_2)^3} = \frac{f_1}{f_1 + f_2 + f_{3i}} \tag{3.14}$$

$$\sum_{i=1}^{n} f_{3i} \frac{(a_i + t_2)^3 - a_i^3}{(a_i + t_2)^3} = \frac{f_2}{f_2 + f_{3i}} \tag{3.15}$$

Attentions need to be paid to Eqn. (3.14) and (3.15), since they consider all coarse aggregates of different sizes, while previously we consider only one particle/one coarse aggregate at a time. f_{3i} denotes the volume fraction of coarse aggregate with size a_i. On the left side of the equation, all coarse aggregates are taken into consideration, while on the right side only a certain size of coarse aggregate is considered.

Based on Eqn. (3.11)- (3.15) and the Young's moduli and the Poisson's ratios of p-DCPD, asphalt binder and coarse aggregate and sizes of coarse aggregates, the Young's modulus and the Poisson's ratio of the entire multilayer-coated particle can be calculated.

3.4 Homogenization of Effective Elastic Properties

Traditional asphalt concrete pavement materials are complex and heterogeneous, they consist of coarse aggregates, fine aggregates, asphalt binder (tar and additives) and air voids. To investigate the mechanical behavior of asphalt concrete, the heterogeneous asphalt mastic can be represented by equivalent homogeneous continuum media with appropriately defined effective properties. The theory of micromechanics (Mura, 1987; Qu & Cherkaoui, 2006) has been widely employed to predict the overall properties. For instance, a circular two-layer built-in micromechanical model was proposed by Li et al. (G. Q. Li et al., 1999) or a more general framework of micromechanical modeling of an arbitrary ellipsoidal multicoated inclusion by Lipinski et al. (Lipinski et al., 2006).

As mentioned in Chapter 2, there are various methods to estimate the elastic properties of composite materials. In the three methods particularly emphasized in Section 2.4, the Hashin-Shtrikman variational bounds are efficient when no specific geometries of the constituents are given; Mori-Tanaka method takes an effective medium approach by considering an average internal stress in the matrix; and Ju and Chen provide analytical solutions of effective elastic properties of the composite materials by taking variations of Eshelby's inclusion theory. In this section, all three methods are developed to be applicable to homogenize composites that have more than two phases. Results and comparison will be made in Section 3.6.

For an isotropic material, the relationships between Young's modulus E, Poisson's ratio υ, bulk modulus K and shear modulus μ are

$$K = \frac{E}{1-2\upsilon} \qquad \mu = \frac{E}{2(1+\upsilon)} \tag{3.16}$$

3.4.1 The Hashin-Shtrikman Bounds

The Hashin-Shtrikman bounds may be one of the remarkable achievements in mechanics of composites. They are the tightest bounds (Hashin, 1962; Hashin & Shtrikman, 1961, 1963) possible from range of composite moduli for a mix of two-phase materials that are independent of the geometries of the constituents.

The detailed derivation of the Hashin-Shtrikman bounds has been shown in Section

2.4.3, whose tensor form is as Eqn. (2.4.16) and (2.4.17) and a case of mix of two isotropic materials in Eqn. (2.4.18) and (2.4.19). However, in our model, the materials are more than two phases. So we need to apply a more general form of the Hashin-Shtrikman bounds, which is derived by Berryman (Berryman, 1995), can be written as

$$K^{HS+} = \Lambda(\mu_{\max}), \qquad K^{HS-} = \Lambda(\mu_{\min}) \tag{3.17}$$

$$\mu^{HS+} = \Gamma(\zeta(K_{\max}, \mu_{\max})), \qquad \mu^{HS-} = \Gamma(\zeta(K_{\min}, \mu_{\min})) \tag{3.18}$$

where

$$\Lambda(z) = \left\langle \frac{1}{K(r) + \frac{4}{3}z} \right\rangle^{-1} - \frac{4}{3}z \tag{3.19}$$

$$\Gamma(z) = \left\langle \frac{1}{\mu(r) + z} \right\rangle^{-1} - z \tag{3.20}$$

$$\zeta(K, \mu) = \frac{\mu}{6}\left(\frac{9K + 8\mu}{K + 2\mu}\right) \tag{3.21}$$

The brackets $\langle\ \rangle$ in Berryman's equations indicate volume average over the constituents, weighted by their volume fractions. In order to make the equations more accessible, I modified them into Eqn. (3.22)-(3.24), which are identical to the original equations, Eqn. (3.17)-(3.21).

$$K^{HS+} = \left(\sum_{i=1}^{n} \frac{f_i}{K_i + \frac{4}{3}\mu_{\max}} \right)^{-1} - \frac{4}{3}\mu_{\max}, \qquad K^{HS-} = \left(\sum_{i=1}^{n} \frac{f_i}{K_i + \frac{4}{3}\mu_{\min}} \right)^{-1} - \frac{4}{3}\mu_{\min} \tag{3.22}$$

$$\mu^{HS+} = \left(\sum_{i=1}^{n} \frac{f_i}{\mu_i + \zeta_{\max}} \right)^{-1} - \zeta_{\max}, \qquad \mu^{HS-} = \left(\sum_{i=1}^{n} \frac{f_i}{\mu_i + \zeta_{\min}} \right)^{-1} - \zeta_{\min} \tag{3.23}$$

where

$$\zeta_{\max} = \frac{\mu_{\max}}{6}\left(\frac{9K_{\max} + 8\mu_{\max}}{K_{\max} + 2\mu_{\max}}\right), \qquad \zeta_{\min} = \frac{\mu_{\min}}{6}\left(\frac{9K_{\min} + 8\mu_{\min}}{K_{\min} + 2\mu_{\min}}\right) \tag{3.24}$$

The Hashin-Shtrikman bounds are very reliable in homogenizing the elastic properties of the interim asphalt mastic, as mentioned before.

3.4.2 The Mori-Tanaka Method

The original Mori and Tanaka method (Benveniste, 1987; Mori & Tanaka, 1973) and its subsequent modifications (Norris, 1989; Taya & Mura, 1981; Weng, 1984, 1990) is an effective field approximation based on Eshelby's elasticity solution for inhomogeneity in infinite medium. The effects of particle interactions are taken into account by a ‘mean field approximation’. As is typical for mean field micromechanics models, forth-order concentration tensors relate the average stress or average strain tensors in inhomogeneities and matrix to the average macroscopic stress or strain tensor, respectively; inhomogeneity "feels" effective matrix fields, accounting for phase interaction effects in a collective, approximate way.

The detailed derivation of Mori-Tanaka method is shown in Section 2.4.4. For a special case where isotropic spherical inclusions are randomly dispersed in an isotropic

matrix, the Mori-Tanaka scheme also yields an isotropic overall behavior, and the effective bulk and shear moduli of the composites can be expressed as

$$\bar{K} = \frac{f_0 K_0 + \sum_{i=1}^{n} f_i K_i \gamma_K^i}{f_0 + \sum_{i=1}^{n} f_i \gamma_K^i} \tag{3.25}$$

$$\bar{\mu} = \frac{f_0 \mu_0 + \sum_{i=1}^{n} f_i \mu_i \gamma_\mu^i}{f_0 + \sum_{i=1}^{n} f_i \gamma_\mu^i} \tag{3.26}$$

where f_i is the volume fraction of the i-th inclusion, $f_0 = 1 - \sum_{i=1}^{n} f_i$ is the volume fraction of the matrix, K_0, K_i, μ_0, μ_i are the bulk and shear moduli of the matrix and inclusions respectively and

$$\gamma_K^i = \frac{K_0}{K_0 + \alpha_0 \left(K_i - K_0 \right)}$$
$$\alpha_0 = \frac{3K_0}{3K_0 + 4\mu_0} \tag{3.27}$$

$$\gamma_\mu^i = \frac{\mu_0}{\mu_0 + \beta_0 \left(\mu_i - \mu_0 \right)}$$
$$\beta_0 = \frac{6\left(K_0 + 2\mu_0 \right)}{5\left(3K_0 + 4\mu_0 \right)} \tag{3.28}$$

3.4.3 The Multilevel Homogenization Approach Employing Ju and Chen's Pairwise Interacting Solutions

Taking the inspiration from Eshelby's equivalent inclusion theory, Ju and Chen proposed a micromechanical framework to investigate effective mechanical properties of two-phase composite materials containing randomly dispersed spherical inhomogeneities, which is proved to be one of the current best ways to theoretically predict (instead of mathematical bounds) the effective moduli. In their works, Ju and Chen considered both non-interacting and pairwise-interacting conditions and gave corresponding solutions (Ju & Chen, 1994a, 1994b), which can be applied to a wider range of conditions and offer significant improvement in precision of predictions.

The exact solution of the many-particle-interacting integral equations is intricate, so approximations are made in Ju and Chen's non-interacting solution (Ju & Chen, 1994b) that the inter-particle interaction effects can be neglected, all particles are spherical, and both the particles and matrix are isotropic. Under such approximations, one can arrive at the effective moduli for two-phase composites as derived in Eqn. (2.4.51) and (2.4.52).

Ju and Chen have also provided a variation of non-interacting solution, which takes the inter-particle interaction effects into consideration and allows one to homogenize the elastic moduli of multiphase composites containing randomly distributed particles using the pairwise-interacting solutions (Ju & Chen, 1994a). Not adding much complicity to the

work of non-interacting solution, the pairwise-interacting solution increased the accuracy of estimation when involving eigenstrains in inhomogeneities and many-particle interaction problems.

The proposed approximate and probabilistic pairwise particle interaction formulation coupled with the general ensemble-volume average field equations leads to a novel, higher-order (in volume fraction), and accurate method for the prediction of effective elastic moduli of two-phase composites containing randomly located spherical particles.

Based on Ju and Chen's work, for a two-phase (inclusions and matrix) composite, if the inclusions (particles) are assumed to be identical and spherical in an elastic matrix, the effective bulk modulus $\bar{K}$ and effective shear modulus $\bar{\mu}$ of this composite can be explicitly evaluated as

$$\bar{K} = K_0\left[1+\frac{30\left(1-v_0\right)f_1\left(3\gamma_1+2\gamma_2\right)}{3\alpha+2\beta-10\left(1+v_0\right)f_1\left(3\gamma_1+2\gamma_2\right)}\right] \tag{3.29}$$

$$\bar{\mu} = \mu_0\left[1+\frac{30\left(1-v_0\right)f_1\gamma_2}{\beta-4\left(4-5v_0\right)f_1\gamma_2}\right] \tag{3.30}$$

where

$$\gamma_1 = \frac{5f_1}{96\beta^2}\left[12v_0\left(13-14v_0\right)-\frac{96\alpha}{3\alpha+2\beta}\left(1-2v_0\right)\left(1+v_0\right)\right] \tag{3.31}$$

$$\gamma_2 = \frac{1}{2}+\frac{5f_1}{96\beta^2}\left[6\left(25-34v_0+22v_0^2\right)-\frac{36\alpha}{3\alpha+2\beta}\left(1-2v_0\right)\left(1+v_0\right)\right] \tag{3.32}$$

$$\alpha = 2\left(5v_0-1\right)+10\left(1-v_0\right)\left(\frac{K_0}{K_1-K_0}-\frac{\mu_0}{\mu_1-\mu_0}\right) \tag{3.33}$$

$$\beta = 2\left(4-5v_0\right)+15\left(1-v_0\right)\frac{\mu_0}{\mu_1-\mu_0} \tag{3.34}$$

Notice that these equations are only applied to two-phase composite, while our proposed asphalt mastic is a four-phase composite. In order to use the pairwise interacting solution, a multilevel homogenization procedure is established, as illustrated in Figure 3.6. Asphalt binder and p-DCPD are first mixed together, while the former is treated as the matrix and the latter as the inclusions, and we get an interim material M1. Then M1 is treated as the new matrix and fine aggregates are added in as inclusions, where we arrive at a stage of interim asphalt mastic. Finally, air voids are introduced into the mixture. It will be shown that different sequences of mixing the phases will affect the final stage effective moduli of the mixture, (refer to Figure 3.16), while the aforementioned sequence is the most suitable one in the case of this proposed asphalt mastic.

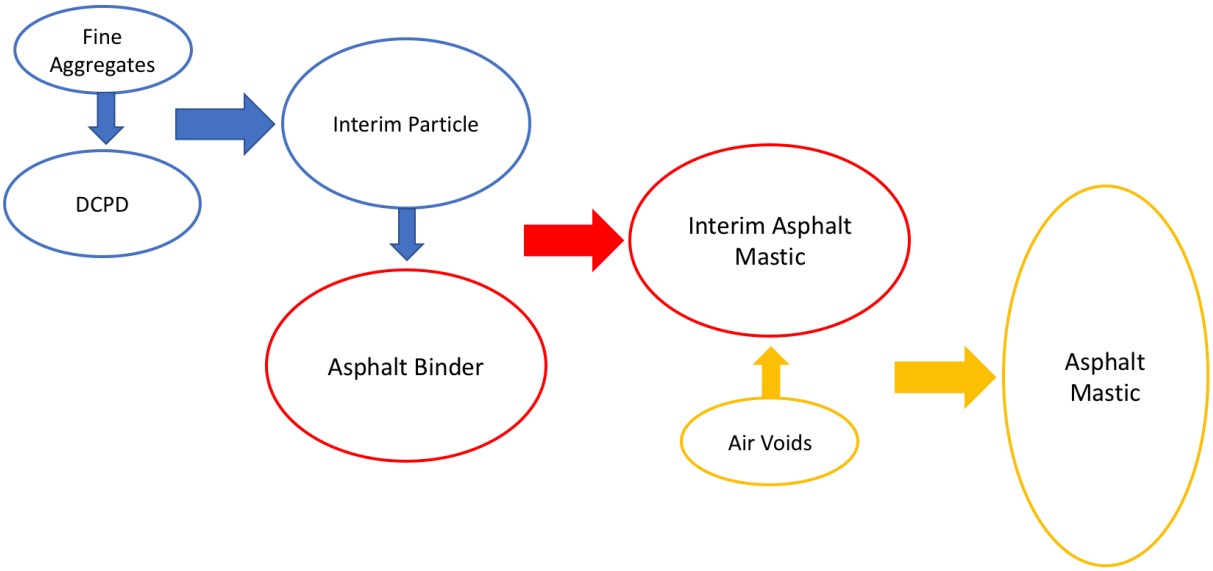

Figure 3.6 The illustration of applying the multilevel homogenization procedure with Ju and Chen's pairwise interacting solution to the proposed asphalt mastic

3.5 The Initial Elastic Strain Energy Based Isotropic Damage Framework

The continuum damage mechanics has been extensively introduced and employed for decades to describe the progressive degradation experienced by the mechanical properties of materials prior to the initiation of macro-cracks. Kachanov (Kachanov, 1958, 1999) was the first to introduce the effective stress concept to model creep rupture. Later, damage mechanics were widely used to model damage of fatigue and creep, ductile plastic damage and damage of brittle materials such as concrete and rocks.

Moreover, the continuum damage mechanics, developed based on the assumption that the damaged material is a macroscopically homogeneous one, leads to the possibility of globally modeling the nucleation and the propagation of micro-defects including their effect on the mechanical behavior. Physically, degradation of the material properties is the result of the initiation, growth and coalescence of micro-cracks or micro-voids. Within the context of continuum mechanics, one may model this process by introducing an internal damage variable which can be a scalar or a tensor quantity. We denote by **M** a fourth-order tensor which characterizes the state of damaged and transforms the homogenized stress tensor into the effective stress tensor, explicitly

$$\bar{\sigma} := \mathbf{M}^{-1} : \sigma \tag{3.35}$$

For isotropic damage case, the mechanical behavior of micro-cracks or micro-voids is independent of their orientation and depends only on a scalar variable *d*. Accordingly,

M will simply reduce to (1-*d*) **I**, where **I** is the rank four identity tensor and Eqn.(3.35) collapses to

$$\bar{\sigma}(t) \equiv \frac{\sigma(t)}{1-d(t)} \tag{3.36}$$

where $d(t)$ is the damage parameter, $\sigma(t)$ the Cauchy stress tensor, and $\bar{\sigma}(t)$ is the effective stress tensor. The value $d=0$ corresponds to the undamaged state whereas a value $d \in (0,1)$ corresponds to a damaged state. This damage parameter d may be interpreted physically as the ratio of damage surface area over total (nominal) surface area at a local material point, the ratio of air voids over total volume of material and damaged stiffness over original stiffness.

In addition, Lemaitre (Lemaitre, 1971) introduced a principle that "*Any strain constitutive equation for a damaged material may be derived in the same way as for a virgin material except that the usual stress is replaced by the effective stress*".

Lemaitre's principle was further translated by Simo and Ju, developed into the hypothesis of strain equivalence: "*The strain associate with a damaged state under the applied stress is equivalent to the strain associated with its undamaged state under the effective stress*"; and the hypothesis of stress equivalence: "*The stress associated with a damaged state under the applied strain is equivalent to the stress associated with its undamaged state under the effective strain*".

In the current chapter, the hypothesis of strain equivalence is employed to predict the damage evolution of the material under splitting tension test. A schematic illustration of

the hypothesis is exhibited in Figure 3.7.

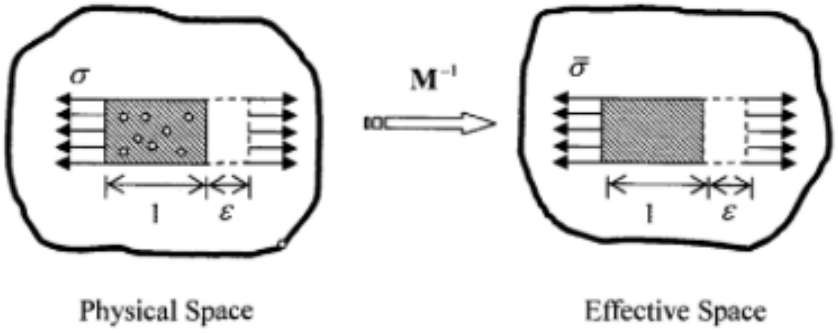

Figure 3.7 The schematic illustration of hypothesis of strain equivalence

3.5.1 The Damage Criterion

Experimental observations show that the non-linear behavior of concrete is due, basically, to the presence, growth, and coalescence of microcracks and/or microvoids depending on the loading path imposed. The development and propagation of macrocracks, leading to the rupture, are the final consequence of the microcrack mechanism (Polanco-Loria & Sǿrensen, 1995). To simulate some of these micro-mechanisms, the continuum damage mechanics has been applied by many researchers (Ju, 1990; Ju & Yuan, 2012; Lubliner et al., 1989; Malcher & Mamiya, 2014; Mazars, 1986; Mazars & Lemaitre, 1985; Oliver, 1990) by introducing an internal variable d which monitors the degradation of the elastic properties of the material. Among the different damage evolution criteria for

isotropic materials, the current research employs an initial elastic strain energy based damage criterion.

A characteristic energy norm ξ^+ of the tensile strain tensor based on the initial elastic strain energy (represented by the red triangle area in Figure 3.8) is proposed.

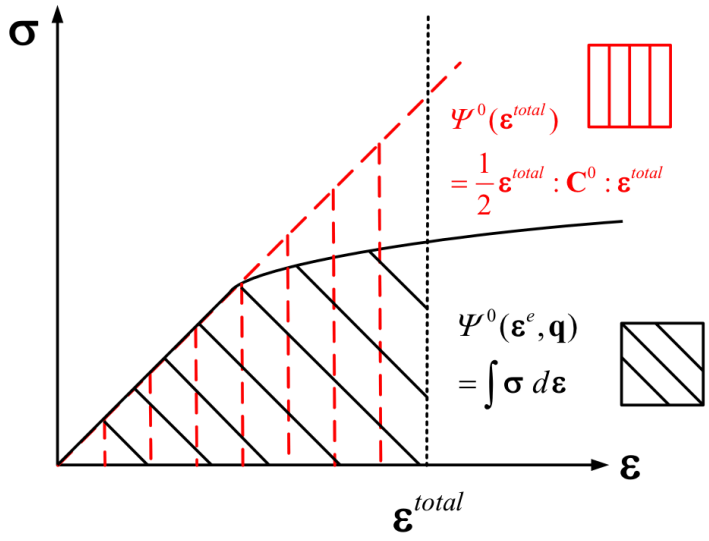

Figure 3.8 Initial elastic strain energy from a stress-strain curve

The energy norm ξ^+ can be calculated as follows:

(a) Rotate the original *total* strain tensor to its *principal* directions.

(b) Take the positive eigen-values only. Use the same eigenvectors to obtain the positive strain.

(c) Use this positive strain tensor to calculate the tensile strain energy ξ^+ .

The detailed equations can be summarized as follows:

$$\boldsymbol{\varepsilon}^{+} = \mathbf{Q}\,\boldsymbol{\Lambda}^{+}\mathbf{Q}^{T} \tag{3.37}$$

where

$$\mathbf{Q} = [\mathbf{q}_1, \mathbf{q}_2, \mathbf{q}_3]_{3x3} \quad \text{and} \quad \boldsymbol{\Lambda}^{+} = \begin{bmatrix} <\lambda_1> & 0 & 0 \\ 0 & <\lambda_2> & 0 \\ 0 & 0 & <\lambda_3> \end{bmatrix} \tag{3.38}$$

Here, λ_i are the eigenvalues, $\mathbf{q}_i$ denotes the corresponding eigenvectors, and $i = 1,2,3$. Further, the angular (McAuley) brackets are defined by $2 <\lambda_i> = \lambda_i + |\lambda_i|$.

Accordingly, we can obtain the tensile elastic strain energy norm as follows:

$$\xi^{+} = \sqrt{\frac{1}{2}\boldsymbol{\varepsilon}^{+} : \mathbf{C}^{\mathbf{0}} : \boldsymbol{\varepsilon}^{+}} \tag{3.39}$$

The projection tensors $\mathbf{P}^{+}$ can be derived by

$$\begin{aligned} \mathbf{P}^{+}_{ijkl} &= \mathbf{Q}_{im}\mathbf{Q}_{jn}\,\boldsymbol{\Lambda}^{+}_{mn}\,(\mathbf{Q}_{kx}\mathbf{Q}_{ly}\boldsymbol{\Lambda}_{xy})^{-1} \qquad or \\ \mathbf{P}^{+} &= (\mathbf{Q}\otimes\mathbf{Q} : \boldsymbol{\Lambda}^{+}) \otimes (\mathbf{Q}\otimes\mathbf{Q} : \boldsymbol{\Lambda})^{-1} \end{aligned} \tag{3.40}$$

See

Figure 3.9 for a schematic explanation.

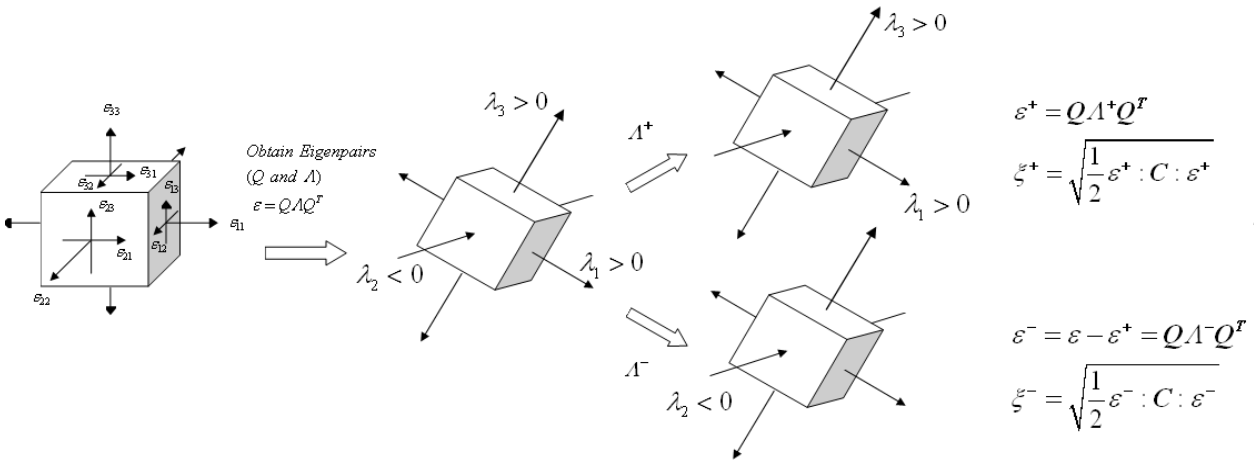

Figure 3.9 The procedure to obtain the tensile elastic strain energy norm ξ^+

3.5.2 The Damage Evolution Function

In order to build into the formulation of the notion of "irreversibility", the following Kuhn-Tucker conditions of damage evolution is required

$$\dot{\mu} \geq 0, \qquad \phi^d(\xi_t^+, g_t) \equiv \xi_t^+ - g_t \leq 0, \qquad \dot{\mu}\phi^d(\xi_t^+, g_t) = 0 \tag{3.41}$$

where g_t is an internal variable that function the "radius" of the damage surface ϕ^d at current time *t*. Figure 3.10 illustrates that damage surface is expended from step time at $t-1$ to t. Let g_0 denote the initial damage threshold before any loading is applied, we then have $g_t > g_0$. Here g_0 is considered as a characteristic material property. Eqn. (3.41) also states that damage is initiated when the energy norm of the tensile strain tensor ξ_t^+ exceeds the initial damage threshold g_0. For the isotropic damage case, we define the evolution of the damage variable d by a rate equation

$$\dot{d}_t = \dot{\mu}\mathrm{H}\left(\xi_t^+, d_t\right) \tag{3.42}$$

where $\mathrm{H}\left(\xi_t^+, d_t\right)$ is the damage hardening function which yields a unit scalar in the elastic-damage case. Hence the Kuhn-Tucker optimality conditions of a principle of maximum damage evolution become

$$\dot{d}_t \geq 0, \qquad \phi^d(\xi_t^+, g_t) \leq 0, \qquad \dot{d}_t\phi^d(\xi_t^+, g_t) = 0 \tag{3.43}$$

If $\phi^d\left(\xi_t^+, g_t\right) < 0$, the damage criterion (3.43) is not satisfied and $\dot{d} = 0$, i.e. no further damage takes place. If on the other hand, $\dot{d} > 0$, that implies further damage is happening, and according to the damage criterion, $\phi^d\left(\xi_t^+, g_t\right) = 0$.

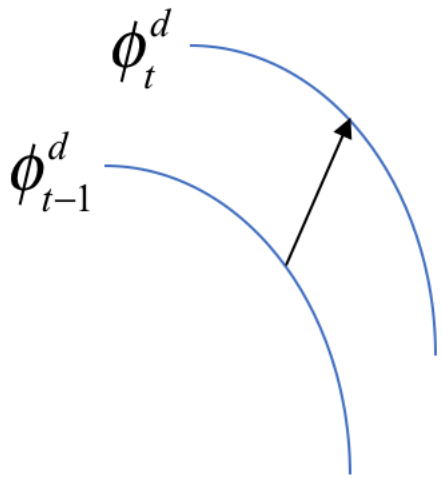

Figure 3.10 Damage surface expanding from step time t-1 to t

A damage evolution function is needed to describe the relationship between isotropic damage variable d_t and strain/strain energy norm. In the paper of Yuan et al. (K. Y. Yuan et al., 2014), Eqn. (26), a power law is used to describe the damage evolution. Despite a good performance, the power law is parameter sensitive and only valid under certain combinations of material parameters. Enlightened by previous works by Mazars, Simo and Ju, etc. (Lubliner et al., 1989; Mazars, 1986; Mazars & Pijaudier-Cabot, 1989; Polanco-

Loria & Sȼrensen, 1995; Simo & Ju, 1987), a new damage evolution function that employs exponential law is proposed

$$d_t = A \exp\left[B \left\langle \xi^+ \right\rangle \left(\xi^+ - g_0 \right) \right] \tag{3.44}$$

where g_0 is the initial tensile damage threshold and A, B are characteristic parameters of the material. Eqn. (3.44) is a general solution that can be applied to all possible material parameters combinations and provides improved performance over Eqn. (26) in Yuan et al.'s paper (K. Y. Yuan et al., 2014).

Table 3.1 Material parameters for damage evolution

Parameter	A	B	ε_0	g_0	*E(psi)*
Value	0.0020	0.0133	0.0196	4.7000	1.15e5

Figure 3.11 illustrates the evolution of damage variable d_t with a set of material parameters listed in Table 4.2, and Figure 3.12 is the corresponding stress-strain curve. Damage is not initiated until the equivalent tensile strain energy norm exceeds the initial tensile damage threshold, as emphasized by the red circles in Figure 3.11 and Figure 3.12. When $d = 0$, it means there is no damage, while with $d = 1$ the material is fully damaged. For numerical simulation, the damage variable range is set to be [0, 0.99] instead of [0, 1] to avoid numerical singularity.

The sensitivity of parameters A and B are paid additional attention by setting various values for one of them individually, the results are displayed in Figure 3.13 and Figure 3.14. We can tell that A and B both have strong influence on the damage evolution function, the smaller the values are, the slower the damage will evolve. When A is larger than a certain value, you may notice a jump when damage occurs, so we should keep A relatively small to avoid that.

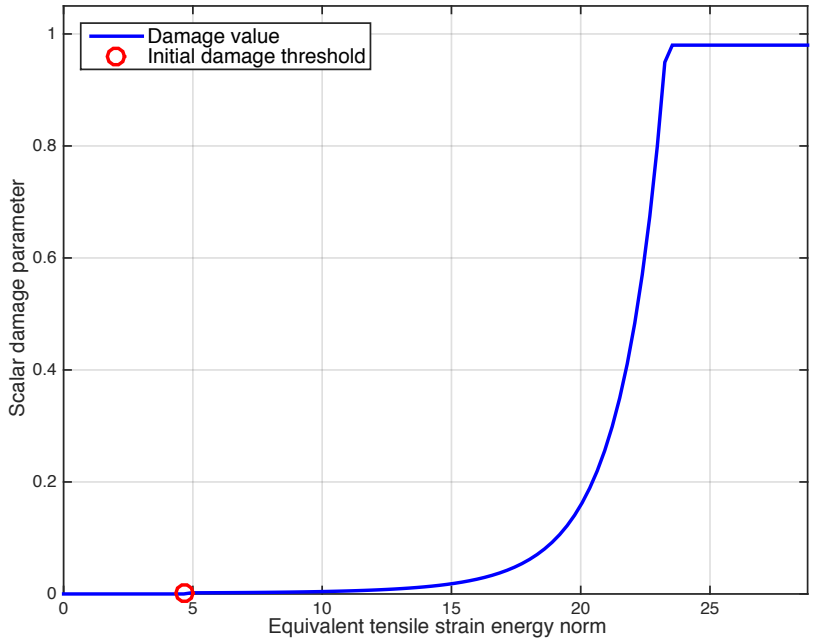

Figure 3.11 Evolution of damage variable with respect to equivalent tensile strain energy norm

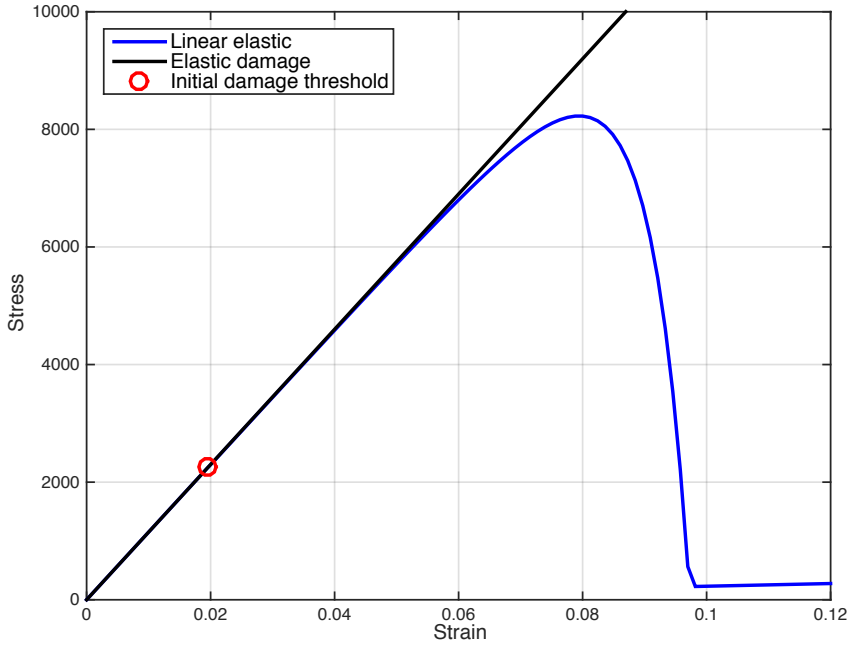

Figure 3.12 The stress-strain curve under isotropic elastic-damage

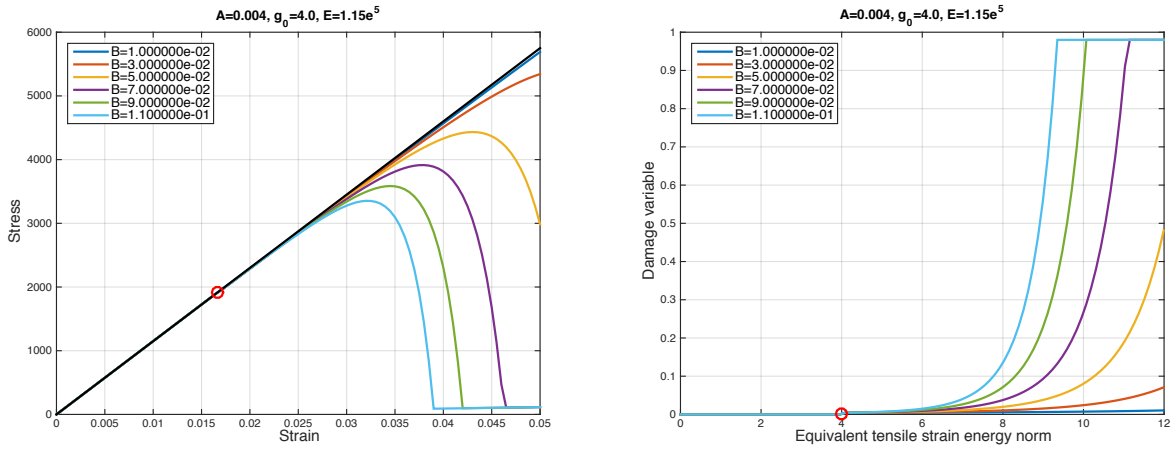

Figure 3.13 Parameter sensitivity of B with A remains constant

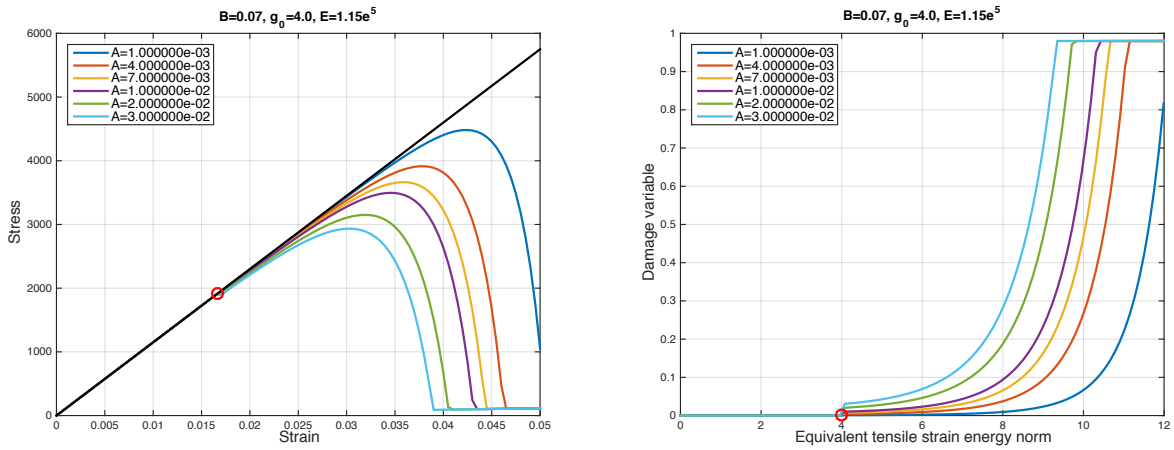

Figure 3.14 Parameter sensitivity of A with B remains constant

3.6 Experimental Data and Theoretical Results

Indirect tension tests of asphalt concrete cylinder specimens infiltrated DCPD were conducted by Yuan et al. (W. Yuan et al., 2011). D2 64-10 pothole mix was chosen as the base materials to cast the testing concrete cylinders. The D2 64-10 mix gradation is listed in Table 3.2. Based on this table, aggregates with size larger than No. 30 are considered coarse aggregates, while smaller than No.30 are considered as fine aggregates.

Table 3.2 Aggregates Designation and Percentage Passing (D2 Mix)

Designation	3/4”	1/2”	3/8”	No.4	No.8	No.30	No. 50	No. 200
Sieve size (*mm*)	19.0	12.5	9.5	4.75	2.36	0.60	0.30	0.075
Percentage passing (%)	100	100	99	71	55	24	14	5.2

The asphalt materials, whose aggregates are D2 mix and binder is PG 64-10 are heated at 160 ^{o}C for three hours into hot mixtures, which is then compacted into the SUPERPAVE standard cylindrical specimen by the PINE gyratory compactor with a size of 6 inch (diameter) by 4.75 inch (height). In order to facilitate DCPD resin infiltration into the compacted cylinder specimens, 12%-20% air void inside of specimens was specified and realized by only three times of gyrations. In order to obtain full DCPD infiltration, vacuum infiltration process is utilized. After the specimens cooled down to room temperature, they are placed into vacuum mold with a size of 152 mm (diameter) by 120 mm (height) and pumped for vacuum. By sealing one end of the mold, the low viscous DCPD resin containing inhibitor and catalyst was sucked into the mold from the other end and infiltrated into those porous specimens. Subsequently, the infiltrated DCPD resin is cured inside the cylindrical specimens.

Once the DCPD resin is fully cured, the indirect tension test is conducted. A 150 mm Lottman breaking head is used to split the specimens by an MTS machine at room temperature with a loading rate of 2 inches per minute, which ensures the viscous effects to be ignored in the post-analysis.

The elastic properties of each constituent in the asphalt concrete cylindrical specimens are listed in Table 3.3, values offered by the technician conducting the indirect tension test.

Table 3.3 Elastic Properties of Each Constituent

Constituent	Aggregates	Asphalt binder	p-DCPD
Young's modulus (*psi*)	7.250e6	1.770e4	2.784e5
Poisson's ratio	0.20	0.30	0.39

Based on the designation and percentage passing results in Table 3.2, a gradation curve is drawn, as shown in Figure 3.15. The diameters of the coarse aggregates are estimated based on the gradation curve, taking the gravity center of each segment. Diameters of three sizes of coarse aggregates are listed in Table 3.4.

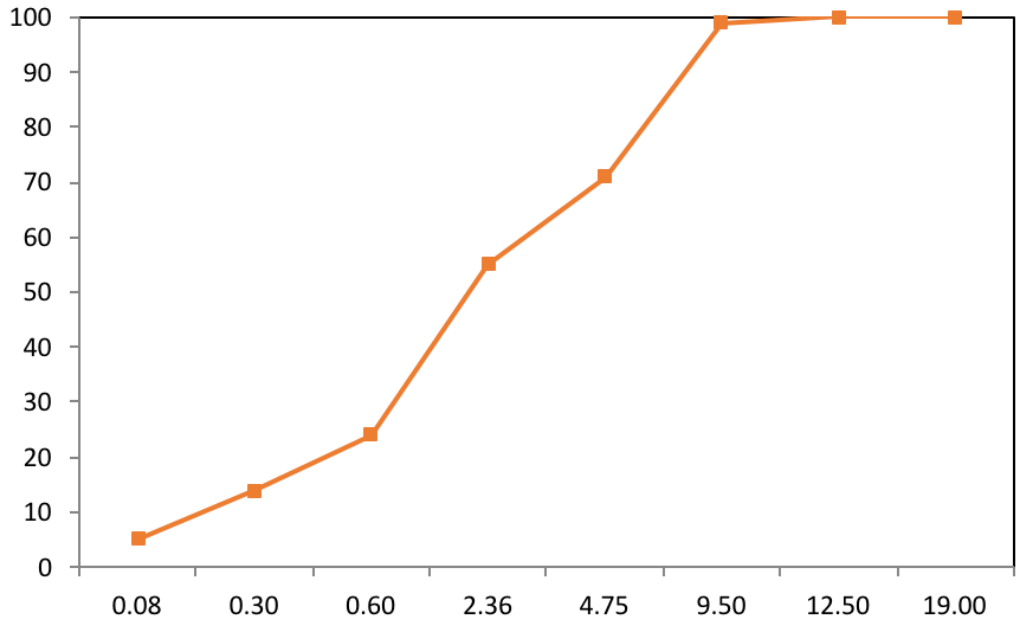

Figure 3.15 The gradation curve of aggregates

Table 3.4 Diameters of Coarse Aggregates

	Coarse Aggregate I	Coarse Aggregate II	Coarse Aggregate III
Diameter (*mm*)	11.000	5.300	3.556
Diameter (*inch*)	0.4331	0.2805	0.1400

Among various specimens conducting the indirect tension test, two specimens (named specimen #1 and specimen #2 in below) are chosen for comparison. The volume fractions of each ingredient in the two specimens corresponding to these two sets of data are listed in Table 3.5. Notice that volume fractions for coarse aggregates, fine aggregates and asphalt binder don't change in the two specimens, which is correct because both specimen are cast with the same superpave mixture. The only difference between the two specimens is the volume fraction of air voids, which can't be controlled precisely by the gyration procedures. Low viscosity DCPD resin is fully sucked into the specimens by vacuum infiltration and fills where there is an air void. Hence volume fractions of p-DCPD is related to air voids.

Table 3.5 Volume Fractions of the Innovative Asphalt Concrete Specimens, %

Specimen #1				
Coarse Aggregates	Fine Aggregates	Asphalt Binder	p-DCPD	Air Voids
33.565	41.023	13.312	8.800	3.3
Specimen #2				

Coarse Aggregates	Fine Aggregates	Asphalt Binder	p-DCPD	Air Voids
33.565	41.023	13.312	7.100	5.0

Based on the mixture gradations given in Table 3.2 and the global volume fractions of each specimen listed in Table 3.5, one can calculate the individual global volume fractions of all three sizes of coarse aggregates, which is listed in Table 3.6. Notice that the specimen number is not specified here. For two specimens with different air voids, the volume fractions of coarse aggregates stay the same. Again, this is because the two specimens are cast with the same superpave mixture.

Now that we have the elastic properties, particle sizes and volume fractions of the coarse aggregates, the elastic properties of the multilayer-coated particles can be calculated based on the equations in Section 3.2.1.

Table 3.6 Global Volume Fractions of Coarse Aggregates, %

Coarse Aggregate I	Coarse Aggregate II	Coarse Aggregate III
0.746	20.885	11.934

This work is almost unprocurable with hand calculation, so MATLAB is used to achieve the values. After gaining the results from MATLAB, Mathematica is used for verification. The elastic properties and particle sizes of the multilayer-coated particles are

presented in Table 3.7. An assumption is made that the contributions of asphalt binder and p-DCPD to the multilayer-coated particle won't affect their global volume fractions in the specimens and asphalt mastic.

Table 3.7 Material Properties of Multilayer-coated Coarse Aggregates

	Coarse Aggregate I	Coarse Aggregate II	Coarse Aggregate III
Global volume fraction (*%*)	0.746	20.885	11.934
Diameter (*in*)	0.4340	0.2814	0.1409
Specimen #1			
Young's modulus (*psi*)	3.3784e6	3.4149e6	2.2266e6
Poisson's ratio	0.2604	0.2032	0.2055
Specimen #2			
Young's modulus (*psi*)	3.4919e6	3.4215e6	2.2341e6
Poisson's ratio	0.2524	0.2026	0.2045

According to the concept of the interim asphalt mastic brought up in Section 3.2.2, the elastic properties of the interim asphalt mastic (fine aggregates, asphalt binder and p-DCPD) is first homogenized, air voids will then be considered as a degradation (or damage) factor. To homogenize the elastic properties of the interim asphalt mastic, volume fractions of each constituent need to be calculated. Based on the fact that proportion within each

constituent stays the same in both interim asphalt mastic and the specimen, the modified volume fraction of constituents in the interim asphalt mastic is calculated and listed in Table 3.8. Notice that now the volume fractions of the interim asphalt mastic of two specimens become different. This is because the air voids in the two specimens are different, so when the volume fractions for air voids are removed, even though the proportions of other constituents stay the same respectively, the volume fractions, seeing from the aspect of interim asphalt mastic, will change.

Table 3.8 Volume Fractions of the Interim Asphalt Mastic, %

Specimen #1, (Air Void=3.3%)		
Fine Aggregates	Asphalt Binder	p-DCPD
64.977	21.085	13.938
Specimen #2, (Air Void=5.0%)		
Fine Aggregates	Asphalt Binder	p-DCPD
66.775	21.668	11.557

To estimate the effective elastic properties of the four phase asphalt mastic, the three methods mentioned in Section 3.4 are employed. Among them, attention is required to apply Ju and Chen's pairwise interacting solutions. The proposed multilevel homogenization approach gives a sequence of how to treat each constituent (phase) as interim particles and matrices, while in general, there should be 12 possible combinations

to put the three phases, if air voids is considered last, in an order. which is shown in Table 3.9.

Table 3.9 Possible Combinations of 3-phase asphalt mastic without air voids

Sequence #		1	2	3	4	5	6
Particle		DCPD	Asph.	DCPD	Aggr.	Asph.	Aggr.
Matrix	Int. Par.	Aggr.	Aggr.	Asph.	Asph.	DCPD	DCPD
	Int. Mat.	Asph.	DCPD	Aggr.	DCPD	Aggr.	Asph.
Sequence #		7	8	9	10	11	12
Particle	Int. Par.	Aggr.	Aggr.	Asph.	Asph.	DCPD	DCPD
	Int. Mat.	Asph.	DCPD	Aggr.	DCPD	Aggr.	Asph.
Matrix		DCPD	Asph.	DCPD	Aggr.	Asph.	Aggr.

Following the sequence in Table 3.9, Ju and Chen's pairwise interacting solutions are applied, and the effective properties of the 12 combinations are shown in Figure 3.16 in black dots, while the red and blue dots represent the lower and upper bounds of the effective properties homogenized by Hashin-Shtrikman bounds. We can tell from the plots that results from sequence #4, 6, 8 and 11 lies within the bounds; however, sequence #4 overestimates the effective Young's modulus of the mixture while sequence #6 and 11 overestimates the Poisson's ratio. That being said, sequence #8 gives the best estimation of the effective moduli of the three phase asphalt mastic, i.e. fine aggregates are added as

interim particles to DCPD, and together contributes as particles in the asphalt binder matrix. This proves the multilevel homogenization approach we proposed in Section 3.4.3.

The effective properties of the interim asphalt mastic (without air voids) and the asphalt mastic (with air voids) by using the Hashin-Shtrikman bounds, Mori-Tanaka method and the multilevel homogenization approach with Ju and Chen's pairwise interacting solutions are listed in Table 3.10 and Table 3.11. Figure 3.17 and Figure 3.18 show the homogenization results of the three methods under different volume fractions of air voids. It can be noticed that the Mori-Tanaka method recovers Hashin-Shtrikman bounds results (upper or lower depending on the stiffness of matrix and particles) and the multilevel homogenization approach gives a close but more precise estimation on the effective properties of the homogenized composites. With the increasing of air voids volume fraction, both effective Young's modulus and Poisson's ratio are decreasing.

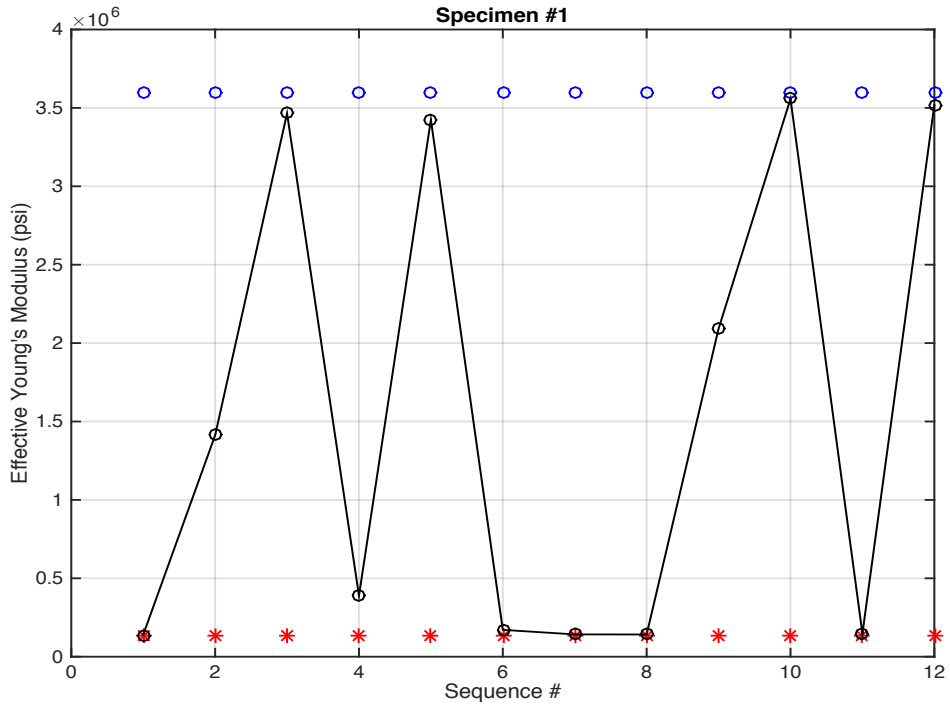
Specimen #1
×10^6
4
3.5
3
2.5
2
1.5
1
0.5
0
Effective Young's Modulus (psi)
0
2
4
6
8
10
12
Sequence #

(a)

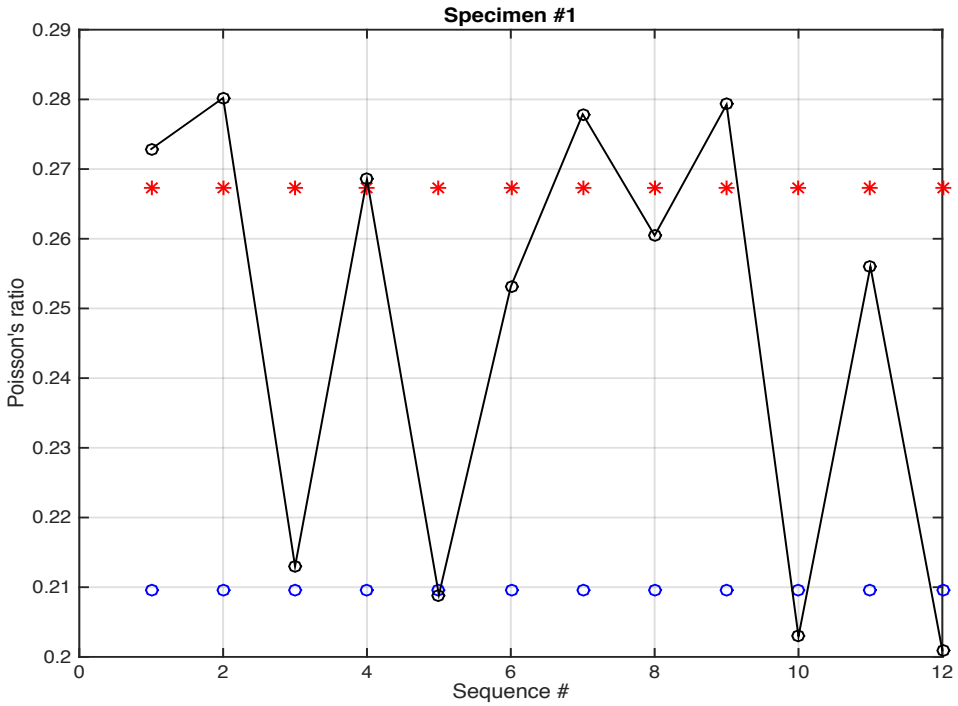
Specimen #1
0.29
0.28
0.27
0.26
0.25
0.24
0.23
0.22
0.21
0.2
Poisson's ratio
0
2
4
6
8
10
12
Sequence #

(b)

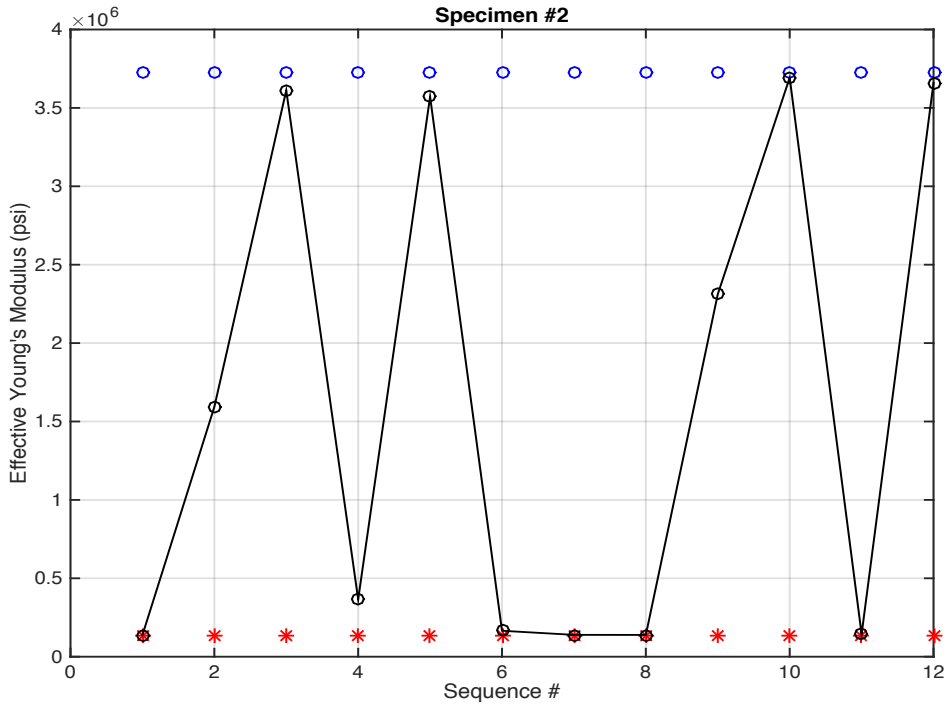
Specimen #2
×10^6
Effective Young's Modulus (psi)
Sequence #
0
0.5
1
1.5
2
2.5
3
3.5
4
0
2
4
6
8
10
12

(c)

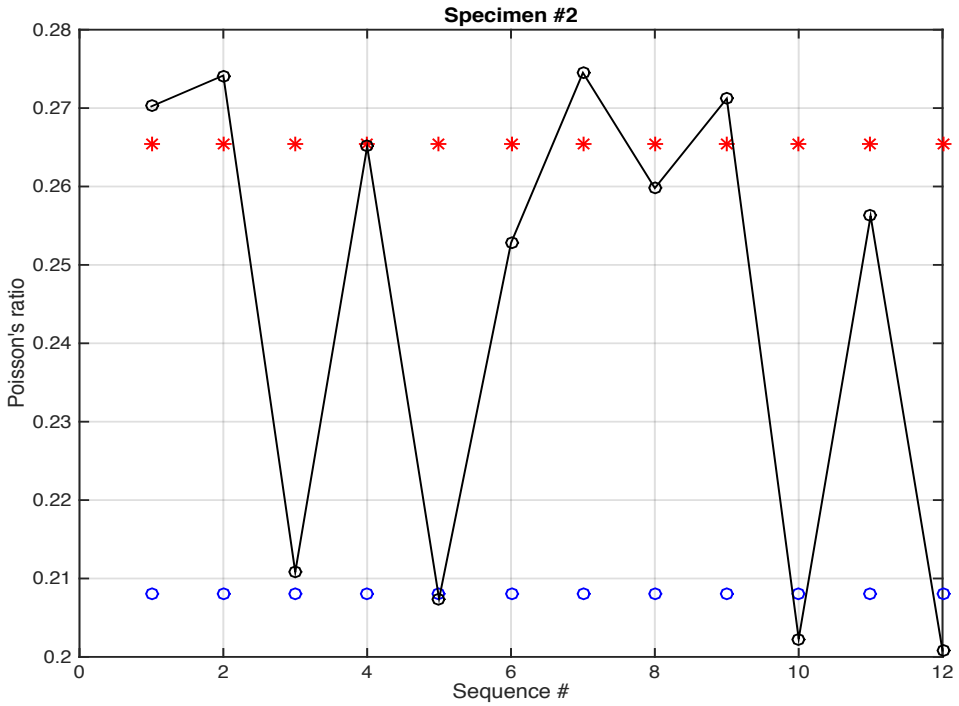
Specimen #2
Poisson's ratio
Sequence #
0.2
0.21
0.22
0.23
0.24
0.25
0.26
0.27
0.28
0
2
4
6
8
10
12

(d)

Figure 3.16 Homogenized elastic properties of the 3-phase asphalt mastic under 12 combinations using Ju-Chen's pairwise interacting solutions

Table 3.10 Effective Elastic Properties of the Interim Asphalt Mastic

	Homogenization Method	**Specimen #1**	**Specimen #2**
Young's modulus (*psi*)	H-S lower bound	1.3692e5	1.3490e5
	H-S upper bound	3.5968e6	3.7274e6
	M-T method	1.3692e5	1.3490e5
	Multilevel Homo	1.4175e5	1.3886e5
Poisson's ratio	H-S lower bound	0.2673	0.2655
	H-S upper bound	0.2096	0.2080
	M-T method	0.2673	0.2655
	Multilevel Homo	0.2605	0.2605

Table 3.11 Effective Elastic Properties of 4-Phase Asphalt Mastic

	Homogenization Method	**Specimen #1**	**Specimen #2**
Young's modulus (*psi*)	H-S upper bound	1.2393e5	1.1597e5
	M-T method	1.2392e5	1.1597e5
	Multilevel Homo	1.2827e5	1.1937e5
Poisson's ratio	H-S upper bound	0.2634	0.2599
	M-T method	0.2634	0.2599
	Multilevel Homo	0.2570	0.2547

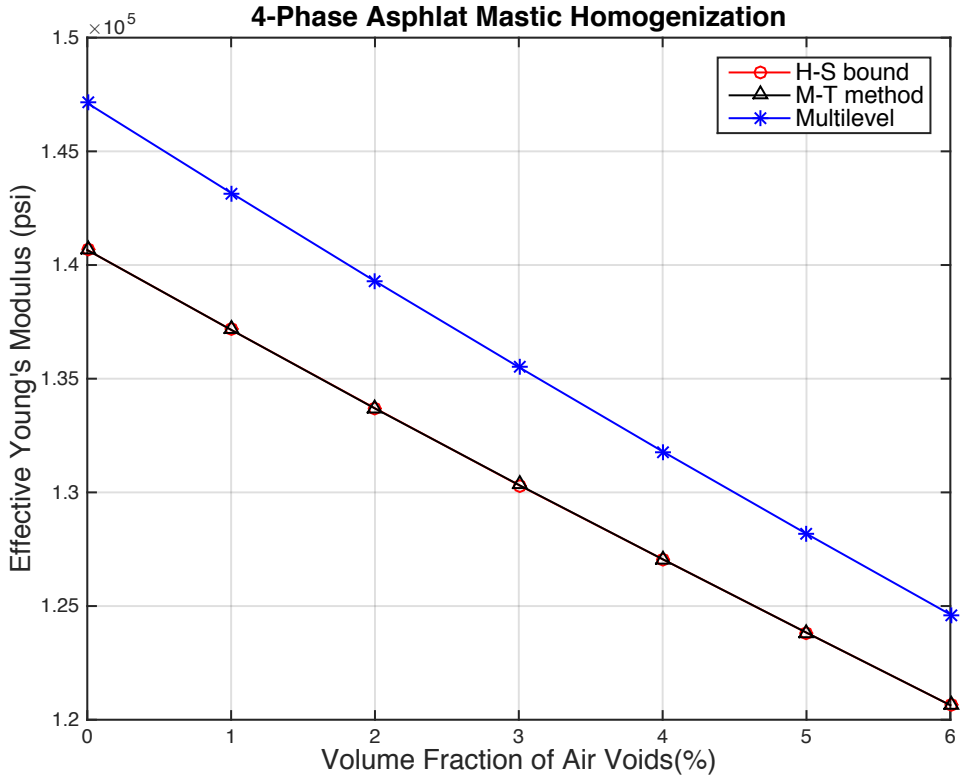

Figure 3.17 Effective Young's modulus of 4-phase asphalt mastic with different air voids volume fraction

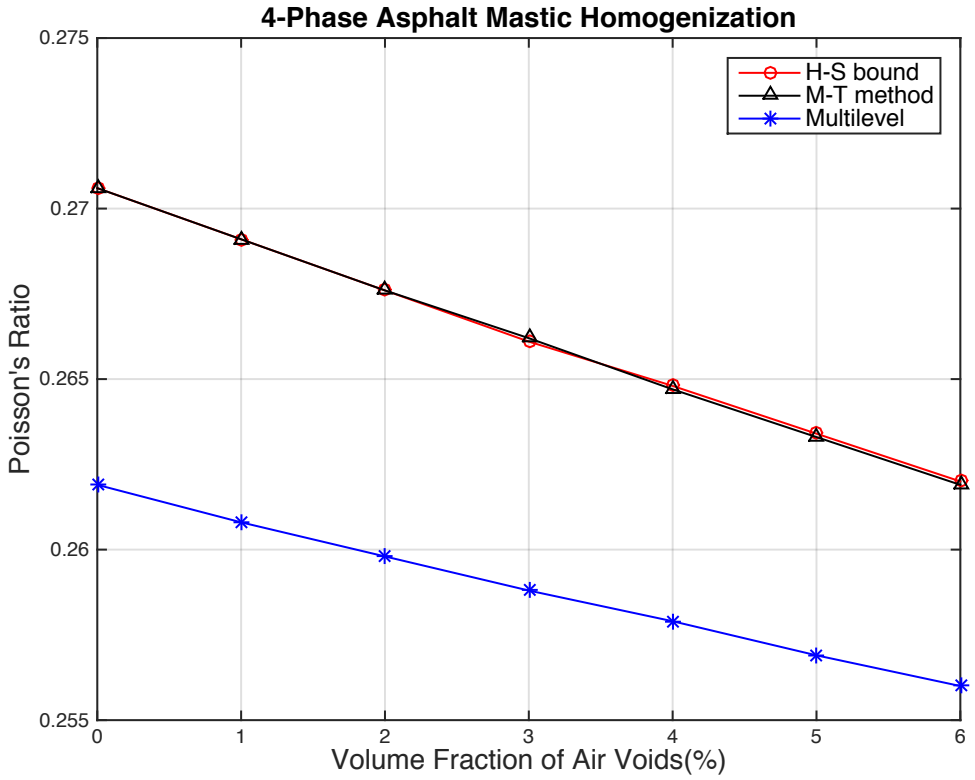

Figure 3.18 Effective Poisson's ratio of 4-phase asphalt mastic with different air voids volume fraction

3.7 Numerical Simulations

To validate the theoretical framework, a numerical simulation of splitting tension test is processed using finite element analysis software (such as ABAQUS). In the two-dimensional numerical simulations, various sizes of regular shapes, mostly circles and ellipsoids, are selected to represent the different size aggregates utilized in the asphalt concrete mixture. The majority of the existing literature follows the aforementioned two-dimensional framework, which either involves simple numerical procedure to select the center coordinate of each circle/ellipsoid with a specific aggregate size (Yin et al., 2015;

K. Y. Yuan et al., 2014) or obtains the cross-sectional microstructure by CT scanning and image processing (Bandyopadhyaya et al., 2008; Dai et al., 2006; H. Wang & Hao, 2011). By contrast, in a three-dimensional numerical simulation with random microstructures, an object-oriented programming language (such as Python) has to be employed to appropriately define the three-dimensional coordinate of the center of each spherical particle with specific aggregate size. Further, it needs to ensure that these randomly generated spheres do not overlap. The numerical complexity of constructing random three-dimensional spheres is substantially higher than that of the two-dimensional numerical simulation with random circles.

The limited previous studies which involved three-dimensional numerical simulation mostly remained obtaining the microstructure with two-dimensional CT scanning and three-dimensional converting technique (Dai, 2011; Vadood et al., 2015; Zhang et al., 2011). There exists one research group who employed a similar random aggregates generation approach in their three-dimensional simulation (Absi et al., 2016; Tehrani et al., 2013) but their emphasis was on the influence of different modeling techniques on dynamic moduli of bituminous materials. Therefore, an aforementioned three-dimensional model needs to be constructed to simulate the elastic-damage behavior of the innovative material.

Shown as in Figure 3.19, the numerical model is a 3×4.5 in. cylinder cast with homogenized asphalt mastic matrix, with equivalent multilayer-coated spherical particles of three representative sizes randomly dispersed in the matrix. Figure 3.20 is a cross section

cut along the plane direction, where the randomly dispersed coarse aggregates can be seen directly. The coarse aggregates are simulated as spherical particles for simplicity and three representative sizes (shown in white, maroon and deep blue) are chosen based on the degradation results of the D2 mix, as discussed previously.

To simulate the real splitting tension test, where a 150mm Lottman breaking head was used in the direct tensile test to split the specimens by an MTS machine at room temperature (25◦C ± 0.5 ◦C) , a displacement control compression along its vertical diameter direction is applied to the steel bar, which is then transmitted to the plywood, hence distributed onto the cylindrical specimen evenly. The loading rate was 2 in. per minute so that the viscous effect can be ignored.

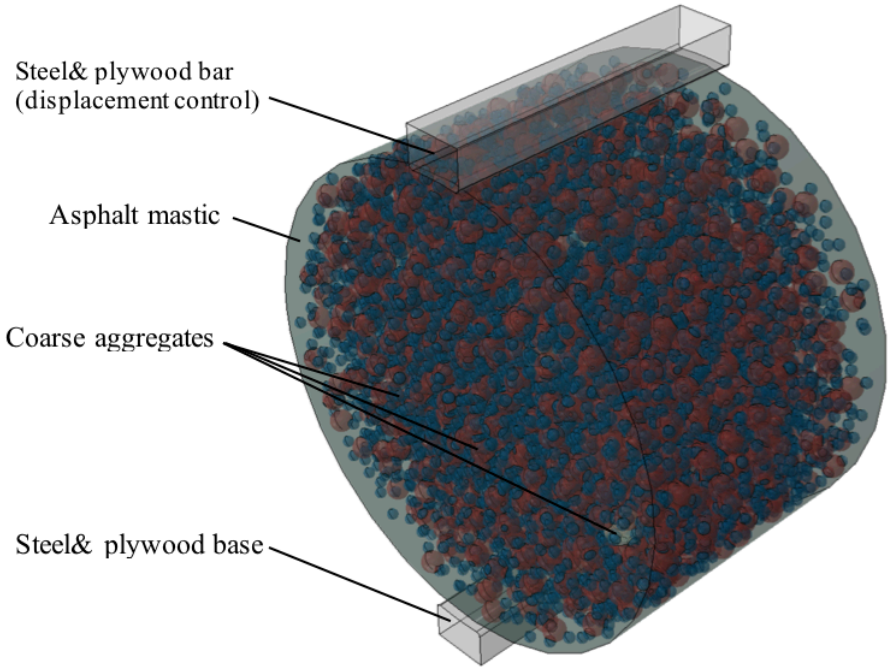

Figure 3.19 The numerical model of the cylindrical asphalt concrete specimen

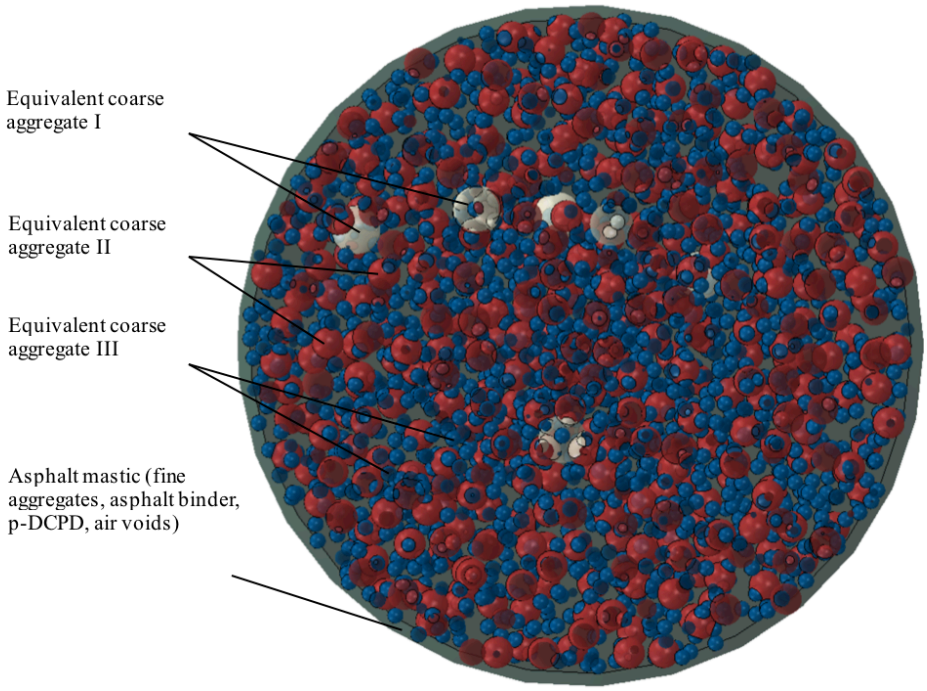

Figure 3.20 A cross section view of the numerical cylindrical model with spherical coarse aggregates of three representative sizes

The elastic properties and volume fraction of each constituent in the innovative asphalt concrete specimens are tabulated in Table 3.3 and Table 3.5. The material properties of the equivalent multilayer-coated coarse aggregates are listed in **Table 3.7** while Table 3.11 provides the effective elastic moduli of asphalt mastic using multilevel homogenization approach with Ju & Chen's pairwise interacting solution. The selection of representative volume element (RVE, i.e. the cylinder) size is in the order of 1000 times of

the largest aggregate size, therefore, this RVE is statically representative and satisfies the size effect consideration. Based on the volume fractions of the three representative coarse aggregate particles, the numbers of each spherical particles are calculated and rounded up. 19 particles with a diameter of 0.4340, 1898 particles with a diameter of 0.2814, and 8639 particles with a diameter of 0.1409 are generated. At the same time, we have to make sure the particles are randomly dispersed in the specimen, while do not collide with each other nor the surface of the cylinder. ABAQUS CAE alone cannot satisfy this demand. Hence Python scripting is employed to realize this goal. First the script randomly allocates a center origin to each particle with its (x,y,z) coordinates lie within the space of the cylinder. Then the center coordinate with a radius of the particle is calculated and compared with the center coordinates with the radii of all previous particles (and the surface of the cylinder), if the newly generated particle is judged as not colliding with all previous ones (nor the surface of the cylinder), the information of the new particle will be written down and passed on to ABAQUS to generate a new particle. Otherwise iteration will be done until a suitable location comes up. It is noted that the same algorithm can be applied to generate inclusions of more representative sizes with random, uniform or other forms of distributions with sizes and locations in principle.

Figure 3.21 are principle stress contours in xx-direction of the 3-D model under splitting tensile loading at the same cross section, we can see that when the number of mesh elements increases (i.e. mesh size decreases), the results gradually converge. In other words,

when the size of the element decreases to a certain value, the finite element model is mesh size dependent.

Figure 3.22 compares the load-displacement curves from the numerical modeling, whose elastic moduli and damage criterion are provided and supported by the theoretical framework, and the experimental data. Four asphalt concrete specimens were tested in the experiment, two with DCPD infiltrated and two without. It is clearly shown that the specimens with DCPD infiltrated in them can take almost two times larger the load comparing to the ones without DCPD. Also, the curves yielded from the numerical simulation meet reasonably well with the experimental observations. Thus, it is positive to say that our proposed framework has grasped the elastic-damage behavior of specimens and can fairly describe the mechanical behavior of the innovative asphalt concrete material within the elastic range. The deviation at the beginning is due to the gauge-specimen engagement, gradual closure of air voids, and interlocking among aggregates. The deviation in the second half of the curves mainly come from the neglection of taking into consideration of elastoplastic behavior of the material.

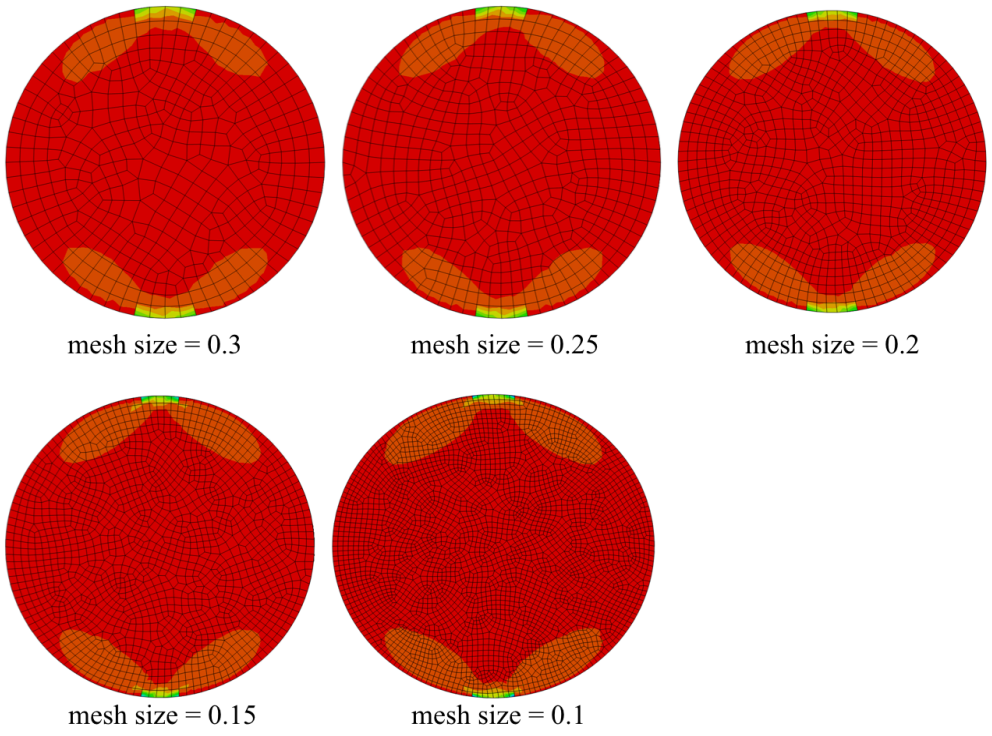

(a)

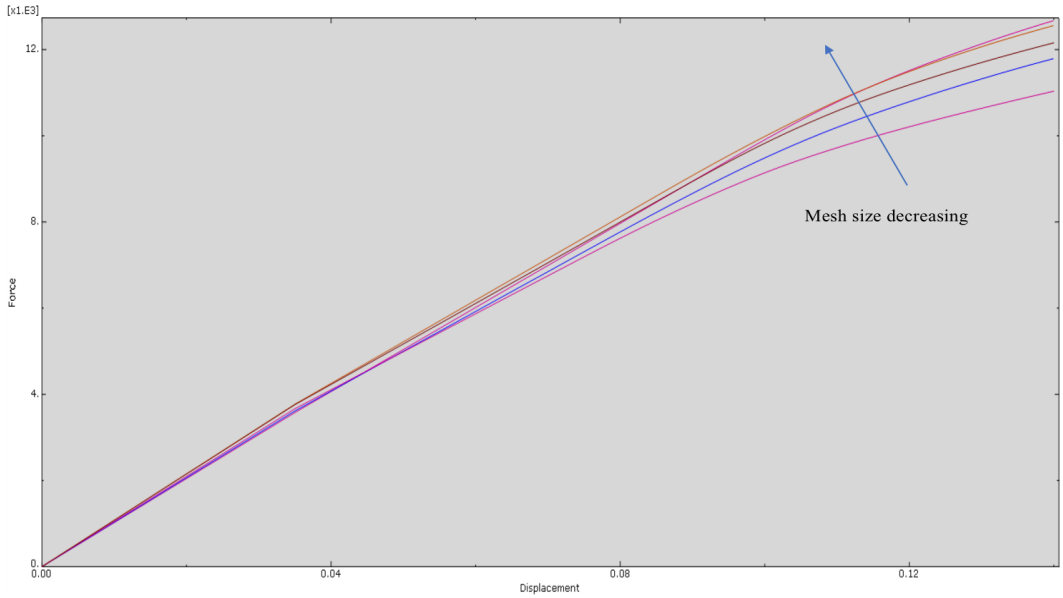

(b)

Figure 3.21 σ_{xx} Stress contours and load-displacement curves of model under splitting tension test with different mesh sizes

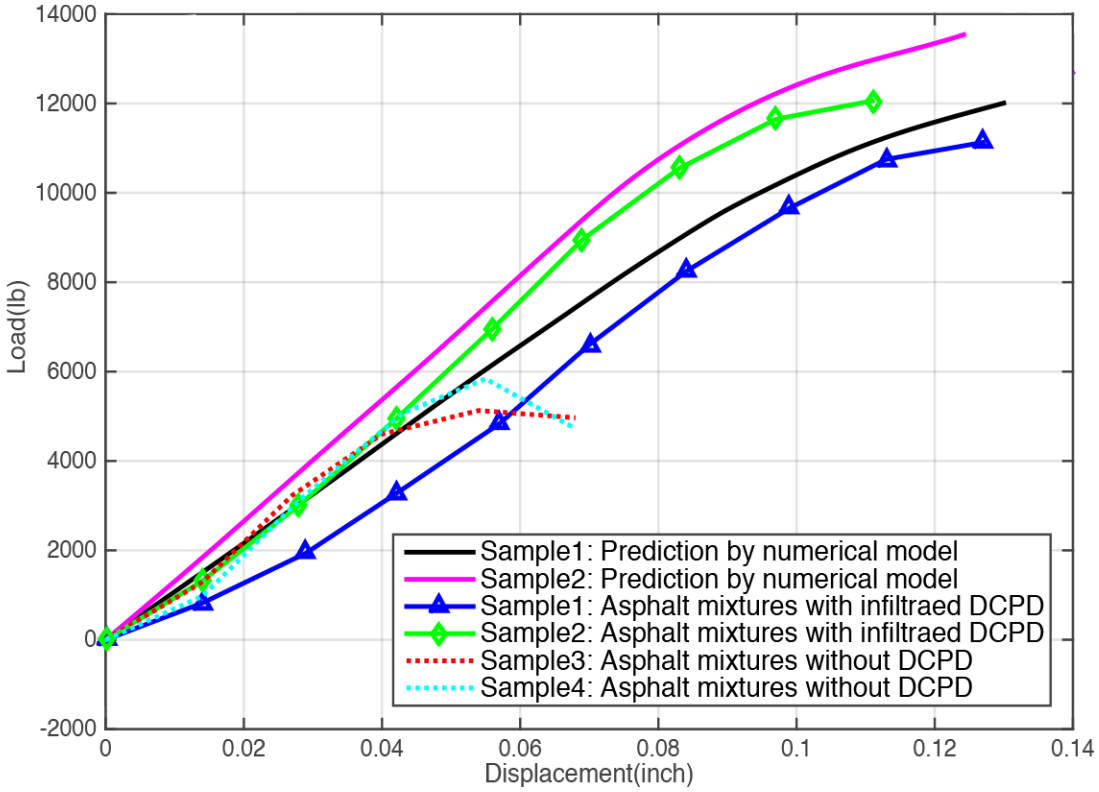

Figure 3.22 Load-displacement curves by experiments and numerical prediction (elastic-damage framework)

3.8 References

Absi, J., Tehrani, F. F., Courreges, F., & Petit, C. (2016). *Mechanical Behavior of Asphalt Mixture Based on X-ray Computed Tomography Images and Random Generation of Aggregates Skeleton.* Paper presented at the 8th RILEM International Conference on Mechanisms of Cracking and Debonding in Pavements.

Abu Al-Rub, R. K., Darabi, M. K., Little, D. N., & Masad, E. A. (2010). A micro-damage healing model that improves prediction of fatigue life in asphalt mixes. *International Journal of Engineering Science, 48*(11), 966-990.

Ahmed, S., & Jones, F. R. (1990). A review of particulate reinforcement theories for polymer composites. *Journal of Materials Science, 25*(12), 4933-4942.

Bandyopadhyaya, R., Das, A., & Basu, S. (2008). Numerical simulation of mechanical behaviour of asphalt mix. *Construction and Building Materials, 22*(5), 1051-1058.

Benveniste, Y. (1987). A new approach to the application of Mori-Tanaka's theory in composite materials. *Mechanics of Materials, 6*(2), 147-157.

Berryman, J. G. (1995). Mixture theories for rock properties. In T. J. Ahrens (Ed.), *Rock Physics & Phase Relations: A Handbook of Physical Constants* (Vol. 3, pp. 205-228). New York: American Geophysical Union.

Bower, A. F. (2009). *Applied Mechanics of Solids* (1st ed.). Boca Raton: CRC Press.

Chaboche, J. L. (1981). Continuous damage mechanics — A tool to describe phenomena before crack initiation. *Nuclear Engineering and Design, 64*(2), 233-247.

Chaboche, J. L., & Lesne, P. M. (1988). A non-linear continuous fatigue damage mode. *Fatigue & Fracture of Engineering Materials & Structures, 11*(1), 1-17.

Chow, C. L., & Wang, J. (1987). An anisotropic theory of continuum damage mechanics for ductile fracture. *Engineering Fracture Mechanics, 27*(5), 547-558.

Dai, Q. (2011). Two- and three-dimensional micromechanical viscoelastic finite element modeling of stone-based materials with X-ray computed tomography images. *Construction and Building Materials, 25*(2), 1102-1114.

Dai, Q., Sadd, M. H., & You, Z. (2006). A micromechanical finite element model for linearand damage-coupled viscoelastic behaviour of asphalt mixture. *International Journal for Numerical and Analytical Methods in Geomechanics, 30*(11), 1135-1158.

Hashin, Z. (1962). The elastic moduli of heterogeneous materials. *Journal of Applied Mechanics, 29*(2), 143-150.

Hashin, Z., & Shtrikman, S. (1961). Note on a variational approach to the theory of composite elastic materials. *Journal of the Franklin Institute, 274*(4), 336-341.

Hashin, Z., & Shtrikman, S. (1963). A variational approach to the theory of the elastic behaviour of multiphase materials. *Journal of the Mechanics and Physics of Solids, 11*(2), 127-140.

Ju, J. W. (1990). Isotropic and anisotropic damage variables. *Journal of Engineering Mechanics, ASCE, 116*(12), 2764-2770.

Ju, J. W., & Chen, T. M. (1994a). Effective elastic moduli of two-phase composites containing randomly dispersed spherical inhomogeneities. *Acta Mechanica, 103*(1-4), 123-144.

Ju, J. W., & Chen, T. M. (1994b). Micromechanics and effective moduli of elastic composites containing randomly dispersed ellipsoidal inhomogeneities. *Acta Mechanica, 103*(1-4), 103-121.

Ju, J. W., & Yuan, K. Y. (2012). New strain-energy based coupled elastoplastic two-parameter damage and healing models for earth moving processes. *International Journal of Damage Mechanics, 21*(7), 989-1019.

Kachanov, L. M. (1958). Time of the rupture process under creep conditions. [English Translation 1999]. *Izvestiia Akademii Nauk SSSR, 8*, 26-31.

Kachanov, L. M. (1999). Rupture time under creep conditions. *International Journal of Fracture, 97*(1-4), 11-18.

Kao, W. H., Carlson, L., Yang, J. M., & Ju, J. W. (2011). US9348024B2.

Kiefer, B., Waffenschmidt, T., Sprave, L., & Menzel, A. (2018). A gradient-enhanced damage model coupled to plasticity—multi-surface formulation and algorithmic concepts. *International Journal of Damage Mechanics, 27*(2), 253-295.

Krajcinovic, D. (1983). Creep of structures - a continuous damage mechanics approach. *Journal of Structural Mechanics, 11*(1), 1-11.

Krajcinovic, D., & Fonseka, G. U. (1981). The continuous damage theory of brittle materials: Part 1: General theory. *Journal of Applied Mechanics, 48*(4), 809-815.

Ladeveze, P., & Lemaitre, J. (1984). *Damage effective stress in quasi-unilateral conditions.* Paper presented at the 16th International congress of theoretical and applied mechanics, Lyngby, Denmark.

Lemaitre, J. (1971). *Evaluation of dissipation and damage in metals submitted to dynamic loading.* Paper presented at the Proceedings of International Congress of Methametics, Kyoto, Japan.

Li, G. Q., Li, Y. Q., Metcalf, J. B., & Pang, S. S. (1999). Elastic modulus prediction of asphalt concrete. *Journal of Materials in Civil Engineering, 11*(3), 236-241.

Lipinski, P., Barhdadi, E. H., & Cherkaoui, M. (2006). Micromechanical modeling of an arbitrary ellipsoidal multi-coated inclusion. *Philosophical Magazine, 86*(10), 1305-1326.

Lubarda, V. A., & Krajcinovic, D. (1994). Tensorial representation of the effective elastic properties of the damaged material. *International Journal of Damage Mechanics, 3*(1), 38-56.

Lubliner, J., Oliver, J., Oller, S., & Oñate, E. (1989). A plastic-damage model for concrete. *International Journal of Solids and Structures, 25*(3), 299-326.

Malcher, L., & Mamiya, E. N. (2014). An improved damage evolution law based on continuum damage mechanics and its dependence on both stress triaxiality and the third invariant. *International Journal of Plasticity, 56*, 232-261.

Martínez, E., Romero, J., Lousa, A., & Esteve, J. (2003). Nanoindentation stress–strain curves as a method for thin-film complete mechanical characterization: application to nanometric CrN/Cr multilayer coatings. *Applied Physics A-Materials Science & Processing, 7*(3-4), 419-426.

Mazars, J. (1986). A description of micro- and macroscale damage of concrete structures. *Engineering Fracture Mechanics, 25*(5-6), 729-737.

Mazars, J., & Lemaitre, J. (1985). Application of Continuous Damage Mechanics to Strain and Fracture Behavior of Concrete. In S. S.P. (Ed.), *Application of Fracture Mechanics to Cementitious Composites. NATO ASI Series (Series E: Applied Sciences)* (Vol. 94, pp. 507-520): Springer, Dordrecht.

Mazars, J., & Pijaudier-Cabot, G. (1989). Continumm damage theory: application to concrete. *Journal of Engineering Mechanics, ASCE, 115*(2), 55-64.

Mori, T., & Tanaka, T. (1973). Average stress in matrix and average elastic energy of materials with misfitting inclusions. *Acta Metallurgica, 21*(5), 571-574.

Mould, J. C. J., Levine, H. S., & Tennant, D. (1994). *Evaluation of a rate-dependent three invariant softening model for concrete.* Paper presented at the Fracture and Damage in Quasibrittle Structures, Chapman and Hall, London.

Mura, T. (1987). *Micromechanics of defects in solids* (2nd ed.): Springer Netherlands.

Murakami, S., & Ohno, N. (1981). *A continuum theory of creep and creep damage*. Paper presented at the IUTAM Symposium on Creep in Structures Berlin, Heidelberg.

Norris, A. N. (1989). An examination of the Mori-Tanaka effective medium approximation for multiphase composites. *Journal of Applied Mechanics, ASME, 56*, 83-88.

Oliver, J. (1990). IOn the discrete constitutive models induced by strong discontinuity kinematics and continuum constitutive equations. *International Journal of Solids and Structures, 37*, 7207-7229.

Ortiz, M. (1987). A method of homogenization of elastic media. *International Journal of Engineering Science, 25*(7), 923-934.

Pandey, V. B., Singh, I. V., Mishra, B. K., Ahmad, S., Rao, A. V., & Kumar, V. (2019). Creep crack simulations using continuum damage mechanics and extended finite element method. *International Journal of Damage Mechanics, 28*(1), 3-34.

Polanco-Loria, M., & Sǿrensen, S. I. (1995). Damage evolution laws for concrete - a comparative study. *Fracture Mechanics of Concrete Structures, Proceedings FRAMCOS-2*, 1027-1036.

Puissant, S., Demay, Y., Vergnes, B., & Agassant, J. F. (1994). Two-dimensional multilayer coextrusion flow in a flat coat-hanger die. Part I: Modeling. *Polymer Engineering and Science, 34*(3), 201-208.

Qu, J., & Cherkaoui, M. (2006). *Fundamentals of Micromechanics of Solids*: Wiley.

Rabotnov, Y. N. (1963). On the Equation of State of Creep. *Proceedings of the Institution of Mechanical Engineers, 178*(1), 2-117-112-122.

Sermage, J. P., Lemaitre, J., & Desmorat, R. (2000). Multiaxial creep fatigue under anisothermal conditions. *Fatigue & Fracture of Engineering Materials & Structures, 23*(2), 241-252.

Simo, J. C., & Ju, J. W. (1987). Strain- and stress-based continuum damage model - I. Formulation. *International Journal of Solids and Structures, 23*(7), 821-840.

Taya, M., & Mura, T. (1981). On stiffness and strength of an aligned short-fiber reinforced composite containing fiber-end cracks under uniaxial applied stress. *Journal of Applied Mechanics, 48*(2), 361-347.

Tehrani, F. F., Allou, F., Absi, J., & Petit, C. (2013). *Investigation on Mechanical Properties of Bituminous Materials through 2D/3D Finite Element Numerical*

Simulations. Paper presented at the Multi-Scale Modeling and Characterization of Infrastructure Materials.

Vadood, M., Johari, M. S., & Rahai, A. R. (2015). A new approach for simulation of hot mix asphalt; numerical and experimental. *Journal of Mechanics, 31*(6), 701-711.

Wang, H., & Hao, P. (2011). Numerical simulation of indirect tensile test based on the microstructure of asphalt mixture. *Journal of Materials in Civil Engineering, 23*(1), 21-29.

Weng, G. J. (1984). Some elastic properties of reinforced solids, with special reference to isotropic ones containing spherical inclusions. *International Journal of Engineering Science, 22*, 845-856.

Weng, G. J. (1990). The theoretical connection between Mori-Tanaka's theory and the Hashin-Shtrikman-Walpole bounds. *International Journal of Engineering Science, 28*, 1111-1120.

Wu, Y., & Ju, J. W. (2017). Elastoplastic damage micromechanics for continuous fiber-reinforced ductile matrix composites with progressive fiber breakage. *International Journal of Damage Mechanics, 26*(1), 4-28.

Yan, Z. G., Zhang, Y., Ju, J. W., Chen, Q., & Zhu, H. H. (2019). An equivalent elastoplastic damage model based on micromechanics for hybrid fiber-reinforced composites under uniaxial tension. *International Journal of Damage Mechanics, 28*(1), 79-117.

Yang, R. B., & Mal, A. K. (1995). The effective transverse moduli of a composite with degraded fiber-matrix interfaces. *International Journal of Engineering Science, 33*(11), 1623-1632.

Yin, A. Y., Yang, X. H., Zeng, G. W., & Gao, H. (2015). Experimental and numerical investigation of fracture behavior of asphalt mixture under direct shear loading. *Construction and Building Materials, 86*, 1.

Yuan, K. Y., Ju, J. W., Yuan, W., & Yang, J. M. (2014). Numerical predictions of mechanical behavior of innovative pothole patching materials featuring high toughness, low-viscosity nano-molecular resins. *Acta Mechanica, 225*(4-5), 1141-1151.

Yuan, W., Yuan, K. Y., Zou, L., Yang, J. M., Ju, J. W., Kao, W., . . . Stephen, T. (2012). *DCPD resin catalyzed with Grubbs catalysts for reinforcing pothole patching materials.* Paper presented at the SPIE 8347, Nondestructive Characterization for Composite Materials, Aerospace Engineering, Civil Infrastructure, and Homeland Security 2012, San Diego, California.

Yuan, W., Yuan, K. Y., Zou, L., Yang, J. M., Ju, J. W., Kao, W., . . . Aktan, A. E. (2013). *Two layer structure for reinforcing pothole repair*. Paper presented at the Nondestructive Characterization for Composite Materials, Aerospace Engineering, Civil Infrastructure, and Homeland Security 2013.

Yuan, W., Yuan, M., Zou, L., Yang, J. M., Ju, W., Kao, W., . . . Solamon, R. (2011). *Development of high-toughness low-viscosity nano-molecular resins for reinforcing pothole patching materials.* Paper presented at the SPIE 7983, Nondestructive Characterization for Composite Materials, Aerospace Engineering, Civil Infrastructure, and Homeland Security 2011, San Diego, California.

Zhang, X., Wan, C., Wang, D., & He, L. (2011). Numerical simulation of asphalt mixture based on three-dimensional heterogeneous specimen. *Journal of Central South University of Technology, 18*(6), 2201-2206.

CHAPTER 4 : MICROMECHANICS-BASED ISOTROPIC ELASTO-PLASTIC-DAMAGE FRAMEWORK OF ASPHALT CONCRETE MATERIALS FEATURING HIGH TOUGHNESS, LOW VISCOSITY NANO-MOLECULAR RESINS

4.1 Introduction

In the previous chapter, a three-dimensional isotropic elastic micromechanical framework is developed to predict the elastic-damage behavior of the innovative pothole patching material. The proposed isotropic elastic framework has shown reasonably good performance in predicting the mechanical behavior, however neglecting the plastic deformation of the innovative asphalt composites beyond the elastic limit.

The discipline of setting up the continuum damage mechanics on a more rigorous basis using thermodynamics and micromechanics and bringing it to engineering applications to modeling of elasticity coupled damage, elastoplastic damage, creep damage, fatigue damage, etc. In particular, a lot of researches have been done in elastoplastic damage in concrete (Ju, 1989; Ju et al., 2009; Ju & Yanase, 2009; Ju & Yuan, 2012; Kiefer et al., 2018; Ko & Ju, 2008; Lubarda, 1994; Lubliner et al., 1989; Voyiadjis et al., 2008; Y. Wu & Ju, 2017), asphalt concrete (K. Chen et al., 2010; Jefferson, 1998; S. M. Kim & Abu Al-Rub, 2011; H. Zhu & Sun, 2013) and other composite materials (Edlund &

Klarbring, 1993; Oller et al., 1996; Shen et al., 2015; Tham et al., 2005) in the past couple decades.

A class of elastoplastic-damage model based on a continuum thermodynamic framework is proposed in the current chapter within an initial elastic strain energy-based formulation to predict the behavior of the innovative material with an improved precision. Specifically, the governing damage evolution is characterized through the effective stress concept in conjunction with the hypothesis of strain equivalence; the plastic flow is introduced by means of an additive split of the stress tensor. A two-step operator splitting computational algorithms of the elastic-damage part and the plastic part are implemented into the existing numerical model to present a more precise prediction of the suitably designed splitting tension test results.

4.2 Equivalent Multilayer-coated Particles

In Chapter 3, the irregular coarse aggregates in the innovative asphalt concrete materials are characterized by spherical multilayer-coated particles whose core is spherical aggregate of certain representative sizes wrapped by thin layers of asphalt binder and p-DCPD. This simplified characterization has been proven to be not only efficient in describing the mechanical properties of irregular coarse aggregates but also taking the caging effect of p-DCPD networks into consideration. Given the fact that p-DCPD is a comparatively brittle and rigid material (Kovačič et al., 2013; Vallons et al., 2015; Y. Wang

et al., 2017), and it's wrapped at the outer layer of the particle, it is reasonable for us to assume that the multilayer-coated particles behave mainly their elasticity not plasticity. However, if we want to be more accurate, we can definitely take the plastic deformation into consideration, which is discussed in below.

4.2.1 Deformation of Elastic-Perfectly Plastic Spherical Shell

In order to understand to what extent has the plastic deformation taken place, we need to know the analytical solution of the multilayer-coated particle under monotonically increasing external pressure. Similar to my previous chapter, we take one representative layer into consideration at first. Assume that an elastic-perfectly plastic spherical shell is under internal and external pressure. This pressurized shell first reaches yield at the outer surface, i.e., $r = b$. If effective pressure goes beyond the yield criterion, we anticipate that a region $x < r \leq b$ will deform plastically, while the region $a \leq r \leq x$ remains elastic, as illustrated in Figure 4.1.

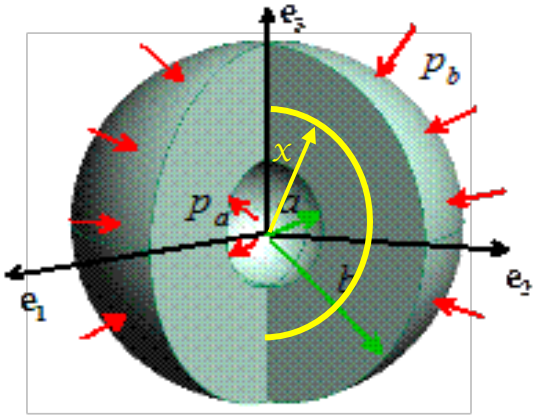

Figure 4.1 A 3-D hollow spherical shell under both internal and external pressures, with elastic-plastic interface at $r = x$

For a spherically symmetric problem with no external body force, the equilibrium equation is

$$\frac{d\sigma_{rr}}{dr} + 2\frac{\sigma_{rr} - \sigma_{\theta\theta}}{r} = 0 \tag{4.1}$$

where the principal stresses are given by

$$\begin{aligned} \sigma_{rr} &= \frac{E}{(1+\upsilon)(1-2\upsilon)}\left[(1-\upsilon)\left(\varepsilon_{rr} - \varepsilon_{rr}^{p}\right) + 2\upsilon\left(\varepsilon_{\theta\theta} - \varepsilon_{\theta\theta}^{p}\right)\right] \\ \sigma_{\theta\theta} &= \frac{E}{(1+\upsilon)(1-2\upsilon)}\left[\left(\varepsilon_{\theta\theta} - \varepsilon_{\theta\theta}^{p}\right) + \upsilon\left(\varepsilon_{rr} - \varepsilon_{rr}^{p}\right)\right] \end{aligned} \tag{4.2}$$

and the volumetric strain is

$$\varepsilon = \left(\varepsilon_{rr}^{e} + \varepsilon_{rr}^{p}\right) + 2\left(\varepsilon_{\theta\theta}^{e} + \varepsilon_{\theta\theta}^{p}\right) = \frac{du}{dr} + 2\frac{u}{r} \tag{4.3}$$

Substituting Eqn. (4.3) into Eqn. (4.2), which in turn, is substituted into Eqn. (4.1), we obtain

$$\left(\frac{\upsilon}{1-2\upsilon}\right)\frac{d}{dr}\left(\frac{du}{dr}+2\frac{u}{r}\right)+\frac{d^2u}{dr^2}+\frac{2}{r}\left(\frac{du}{dr}-\frac{u}{r}\right)=\left(\frac{\upsilon}{1-2\upsilon}\right)\frac{d\varepsilon^p}{dr}+\frac{d\varepsilon_{rr}^p}{dr}+2\frac{\varepsilon_{rr}^p-\varepsilon_{\theta\theta}^p}{r} \quad (4.4)$$

Solving this governing equation, we get

$$\begin{aligned} u=&\left(\frac{\upsilon}{1-\upsilon}\right)\frac{1}{r^2}\int_a^r r^2\varepsilon^p\,dr+\frac{1-2\upsilon}{1-\upsilon}\frac{1}{r^2}\int_a^r r^2\varepsilon_{rr}^p\,dr+\frac{1-2\upsilon}{1-\upsilon}\frac{2}{r^2}\int_a^r r^2\int_a^r\frac{\varepsilon_{rr}^p-\varepsilon_{\theta\theta}^p}{r}dr\,dr \\ &+C_1r+\frac{C_2}{r^2} \end{aligned} \quad (4.5)$$

By substituting Eqn. (4.5) back into Eqn. (4.2), we get the principle stresses

$$\begin{aligned} \sigma_{rr}=&-\frac{2E\upsilon}{(1-\upsilon)(1+\upsilon)}\frac{1}{r^3}\int_a^r r^2\varepsilon^p\,dr-\frac{2E(1-2\upsilon)}{(1-\upsilon)(1+\upsilon)}\frac{1}{r^3}\int_a^r r^2\varepsilon_{rr}^p\,dr \\ &+\frac{2E}{1+\upsilon}\int_a^r\frac{\varepsilon_{rr}^p-\varepsilon_{\theta\theta}^p}{r}dr-\frac{4E(1-2\upsilon)}{(1-\upsilon)(1+\upsilon)}\frac{1}{r^3}\int_a^r r^2\int_a^r\frac{\varepsilon_{rr}^p-\varepsilon_{\theta\theta}^p}{r}dr\,dr \\ &+\frac{E}{1-2\upsilon}C_1-\frac{2(1-2\upsilon)}{1-\upsilon}\frac{C_2}{r^3} \\ \sigma_{\theta\theta}=&\frac{E\upsilon}{(1-\upsilon)(1+\upsilon)}\frac{1}{r^3}\int_a^r r^2\varepsilon^p\,dr+\frac{E(1-2\upsilon)}{(1-\upsilon)(1+\upsilon)}\frac{1}{r^3}\int_a^r r^2\varepsilon_{rr}^p\,dr \\ &+\frac{2E\upsilon}{(1-\upsilon)(1+\upsilon)}\int_a^r\frac{\varepsilon_{rr}^p-\varepsilon_{\theta\theta}^p}{r}dr+\frac{2E(1-2\upsilon)}{(1-\upsilon)(1+\upsilon)}\frac{1}{r^3}\int_a^r r^2\int_a^r\frac{\varepsilon_{rr}^p-\varepsilon_{\theta\theta}^p}{r}dr\,dr \\ &-\frac{E^2}{2(1-2\upsilon)(1+\upsilon)}\varepsilon_{\theta\theta}^p+\frac{E}{1-2\upsilon}C_1+\frac{1-2\upsilon}{1-\upsilon}\frac{C_2}{r^3} \end{aligned} \quad (4.6)$$

where C_1 and C_2 are identical to the ones in Eqn. (4.5).

Within the elastic region, all plastic strain terms in Eqn. (4.5) and (4.6) vanish, i.e., $\varepsilon^p=\varepsilon_{rr}^p=\varepsilon_{\theta\theta}^p=0$.

In order to obtain the limiting pressure that triggers the plastic deformation of the shell, we need to know the solutions of principle stresses while the entire shell remains in elastic range, which can be easily derived based on the boundary conditions

$$\begin{aligned}\sigma_{rr} &= -p_a \quad \text{at} \quad r = a \\ \sigma_{rr} &= -p_b \quad \text{at} \quad r = b\end{aligned} \tag{4.7}$$

The principle stresses in elastic range are

$$\begin{aligned}\sigma_{rr} &= \frac{a^3 b^3 \left(p_b - p_a\right) - \left(b^3 p_b - a^3 p_a\right) r^3}{\left(b^3 - a^3\right) r^3} \\ \sigma_{\theta\theta} &= -\frac{2a^3 b^3 \left(p_b - p_a\right) + \left(b^3 p_b - a^3 p_a\right) r^3}{2\left(b^3 - a^3\right) r^3}\end{aligned} \tag{4.8}$$

According to the result of Eqn. (4.8), we anticipate that $\sigma_{rr} > \sigma_{\theta\theta}$ in both elastic and plastic ranges. Therefore, the yield criterion is defined as

$$\left|\sigma_{\theta\theta} - \sigma_{rr}\right| = \sigma_{rr} - \sigma_{\theta\theta} = Y \tag{4.9}$$

Based on Eqn. (4.7), (4.8) and the assumption that the plastic behavior, if ever occurs, initiates from the outer surface, the limiting pressure for plastic deformation then gives

$$p^* = p_b - p_a = \frac{2Y}{3}\frac{b^3 - a^3}{a^3} \tag{4.10}$$

When the difference in outer and inner pressures increases beyond the limiting pressure p^*, plastic deformation spreads from the outer surface to inner surface.

Assume at a certain p^*, plastic deformation reaches a radius of $r = x$ where $a \le x \le b$. In this case, $x < r \le b$ is the plastic region while $a \le r \le x$ remains in elastic.

Knowing that boundary conditions for elastic region ($a \le r \le x$) are

$$\begin{aligned}\sigma_{rr} &= -p_a \quad \text{at} \quad r = a \\ \sigma_{rr} - \sigma_{\theta\theta} &= Y \quad \text{at} \quad r = x\end{aligned} \tag{4.11}$$

C_1 and C_2 can be solved by combining Eqn. (4.6) and (4.11)

$$C_1 = -\frac{\left(1-2\upsilon\right)\left(2Yx^3+3P_a a^3\right)}{3Ea^3}$$
$$C_2 = -\frac{\left(1+\upsilon\right)Yx^3}{3E} \tag{4.12}$$

Therefore, displacement of shell within the elastic region ($a \le r \le x$) is

$$\begin{aligned} u_{(r)} &= -\frac{\left(1-2\upsilon\right)\left(2Yx^3+3P_a a^3\right)}{3Ea^3}r - \frac{\left(1+\upsilon\right)Yx^3}{3Er^2} \\ &= -\frac{1}{Er^2}\left\{\left(1-2\upsilon\right)\left[\frac{2}{3}Y\left(\frac{x}{a}\right)^3 + p_a\right]r^3 + \frac{1}{3}\left(1+\upsilon\right)Yx^3\right\} \end{aligned} \tag{4.13}$$

And the stresses are

$$\sigma_{rr} = -\frac{2Yx^3}{3a^3}\left(1-\frac{a^3}{r^3}\right) - p_a$$
$$\sigma_{\theta\theta} = -\frac{2Yx^3}{3a^3}\left(1+\frac{a^3}{2r^3}\right) - p_a \tag{4.14}$$

When $x < r \le b$, i.e., in the plastic region, based on Eqn. (4.1) and (4.9), we have

$$\frac{d\sigma_{rr}}{dr} + 2\frac{Y}{r} = 0$$
$$\sigma_{rr} = -2Y\ln r + C_3 \tag{4.15}$$
$$\sigma_{\theta\theta} = \sigma_{rr} - Y = -2Y\ln r - Y + C_3$$

Based on the boundary condition

$$\sigma_{rr} = -p_b \quad \text{at} \quad r = b \tag{4.16}$$

We obtain

$$C_3 = 2Y\ln b - p_b \tag{4.17}$$

Then the stresses in the plastic region become

$$\sigma_{rr} = 2Y\ln\left(\frac{b}{r}\right) - p_b$$
$$\sigma_{\theta\theta} = 2Y\ln\left(\frac{b}{r}\right) - Y - p_b \tag{4.18}$$

According to Eqn. (4.2) and (4.3), we may have

$$\frac{du}{dr} + 2\frac{u}{r} = \frac{1-2\upsilon}{E}\left(\sigma_{rr} + 2\sigma_{\theta\theta}\right) \tag{4.19}$$

from which the displacement of shell within the plastic region ($x < r \le b$) can be derived as

$$u_{(r)} = \frac{1-2\upsilon}{E} r\left[2Y\ln\left(\frac{b}{r}\right) - p_b\right] + \frac{C_4}{r^2} \tag{4.20}$$

The continuity condition must hold at the interface of elastic and plastic regions, i.e. $r = x$.

$$u_{(x,e)} = u_{(x,p)} \tag{4.21}$$

$$\sigma_{rr}^{\ x,e} = \sigma_{rr}^{\ x,p} \tag{4.22}$$

From Eqn. (4.21), we obtain

$$C_4 = -\frac{1-\upsilon}{E} Y x^3 \tag{4.23}$$

Eqn. (4.20) now becomes

$$\begin{aligned} u_{(r)} &= \frac{1-2\upsilon}{E} r\left[2Y\ln\left(\frac{b}{r}\right) - p_b\right] - \frac{1-\upsilon}{E} Y\frac{x^3}{r^2} \\ &= -\frac{1}{Er^2}\left\{\left(1-2\upsilon\right)\left[p_b - 2Y\ln\left(\frac{b}{r}\right)\right]r^3 + \left(1-\upsilon\right)Yx^3\right\} \end{aligned} \tag{4.24}$$

And Eqn. (4.22) provides the location of x, which satisfies

$$\frac{2Y}{3}\left[\frac{x^3}{a^3}-1+3\ln\left(\frac{b}{x}\right)\right]=p_b-p_a \tag{4.25}$$

It is noticed that when $x=b$, i.e. the outer surface of the shell is reaching the critical point of elastic to plastic deformation, both Eqn. (4.13) and (4.24) become identical to Eqn. (3,1), which is the displacement solution of this shell under pure elastic deformation. This validates our derivation of displacement field under elastic-plastic deformation.

4.2.2 Effective Young's Modulus of Multilayer-coated Particles

It is impossible to derive a general analytical solution for the effective (overall) Young's modulus of a layered spherical shell composites that have plastic behavior considering a different yield stress of each constituent. In order to take advantage of the aforementioned deformation solutions for spherical shell, it is not harmful to make an assumption that asphalt binder and p-DCPD behave like elastic-perfect plastic materials, and when both reach their yield points, the core (coarse) aggregates hasn't reached its ultimate stress yet (i.e., remains elastic), considering the differences in magnitudes of the ultimate stress of these materials (scale of ten each).

According to these assumptions, the stress-strain curve of a multilayer-coated particle should look like Figure 4.2 where $\overline{E}$ is the effective (secant) modulus.

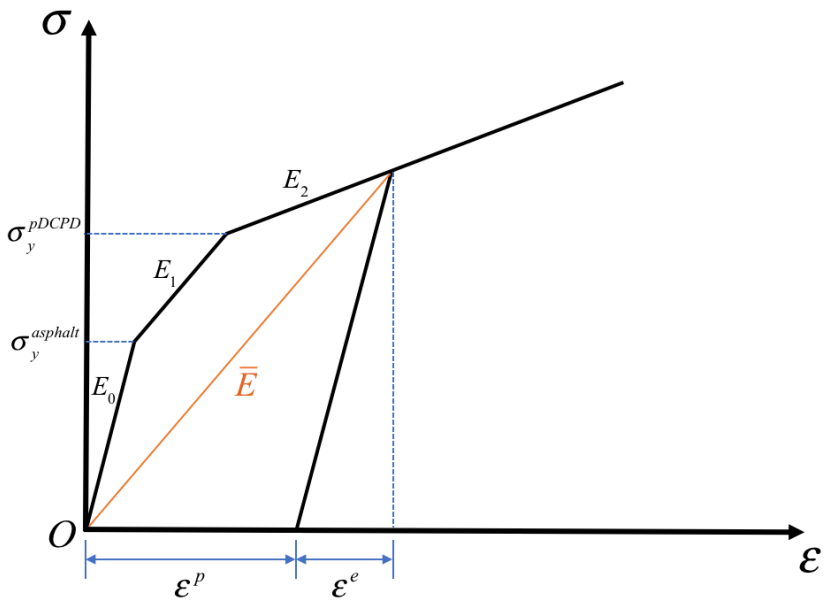

Figure 4.2 The illustration of secant method in estimating the effective Young's modulus of the multilayer-coated particle

The effective (secant) Young's modulus of the multilayer-coated particle can be derived as follows (notations may vary from the ones in Figure 4.2): According to Figure 4.3, the continuity of interfaces of each layer should be

$$\begin{aligned} u_{3a} &= u_{2a} \\ u_{2b} &= u_{1b} \\ u_{1c} &= u_{0c} \end{aligned} \tag{4.26}$$

where the elastic-plastic interface between aggregate and asphalt binder should be at $x = a$ and $x = b$ between apshalt binder and p-DCPD.

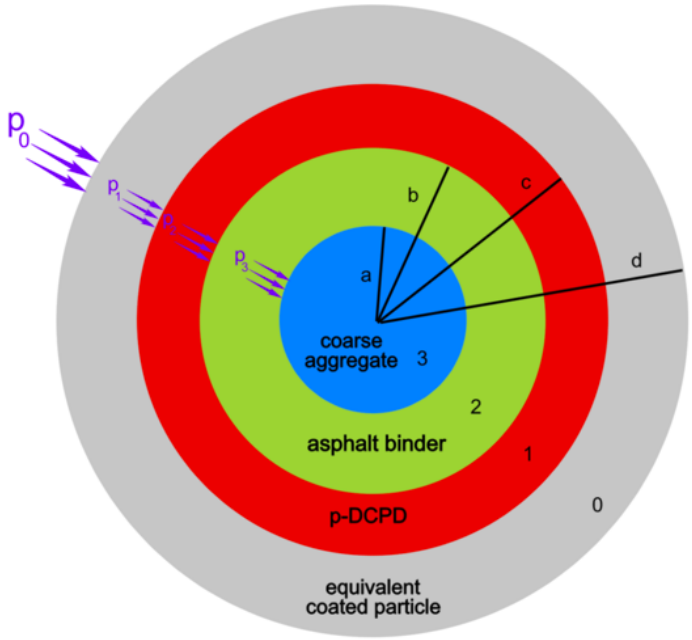

Figure 4.3 Boundary conditions for the multilayer-coated particle (cross section cutting through center of particle)

The displacement expressions are

$$u_{3a} = -\frac{a(1-2\upsilon_3)}{E_3} p_3 \tag{4.27}$$

$$u_{2a} = -\frac{1}{E_2 a^2}\left[a^3(1-2\upsilon_2)p_3 + \frac{a^3(1-\upsilon_2)(p_2-p_3)}{2\ln\left(\frac{b}{a}\right)} \right] \tag{4.28}$$

$$u_{2b} = -\frac{1}{E_2 b^2}\left[b^3(1-2\upsilon_2)p_2 + \frac{b^3(1-\upsilon_2)(p_2-p_3)}{2\ln\left(\frac{b}{a}\right)} \right] \tag{4.29}$$

$$u_{1b} = -\frac{1}{E_1 b^2}\left[b^3(1-2\upsilon_1)p_2 + \frac{b^3(1-\upsilon_1)(p_1-p_2)}{2\ln\left(\frac{c}{b}\right)} \right] \tag{4.30}$$

$$u_{1c} = -\frac{1}{E_1 c^2}\left[c^3(1-2\upsilon_1)p_1 + \frac{c^3(1-\upsilon_1)(p_1-p_2)}{2\ln\left(\frac{c}{b}\right)} \right] \tag{4.31}$$

$$u_{0c} = -\frac{1}{E_0 c^2}\left[c^3(1-2\upsilon_0)p_3 + \frac{a^3(1-\upsilon_0)(p_1-p_3)}{2\ln\left(\frac{c}{a}\right)} \right] \tag{4.32}$$

By applying these displacements to the continuity boundary conditions, we obtain

$$E_0 = E_1 \frac{\left[2A_{23}A_{12} - E_2(1-\upsilon_2)A_{13}\right]B + \left[A_{23}B - E_3(1-\upsilon_2)(1-2\upsilon_0)\right](1-\upsilon_1)E_2}{\left[2A_{23}A_{12} - E_2(1-\upsilon_2)A_{13}\right]C + \left[2A_{23} - E_3(1-\upsilon_2)\right](1-2\upsilon_1)E_2} \tag{4.33}$$

where

$$A_{12} = \left[E_1(1-2\upsilon_2) - E_2(1-2\upsilon_1)\right]\ln\left(\frac{c}{b}\right) \tag{4.34}$$

$$A_{23} = \left[E_3(1-2\upsilon_2) - E_2(1-\upsilon_3)\right]\ln\left(\frac{b}{a}\right) \tag{4.35}$$

$$A_{13} = \left[E_1(1-\upsilon_3) - E_3(1-2\upsilon_1)\right]\ln\left(\frac{c}{b}\right) \tag{4.36}$$

$$B = (1-\upsilon_0)/\ln\left(\frac{c}{a}\right) + 2(1-2\upsilon_0) \tag{4.37}$$

$$C = (1-\upsilon_1)/\ln\left(\frac{c}{b}\right) + 2(1-2\upsilon_1) \tag{4.38}$$

From Eqn. (4.33), we can tell that the effective Young's modulus of the multilayer-coated particle is a function of Young's moduli and the Poisson's ratios of p-DCPD, asphalt

binder and coarse aggregate and the radius (size) of the coarse aggregate, E_1, E_2, E_3, υ_1, υ_2, υ_3, a, thickness of the asphalt binder and p-DCPD layers, b, c and its own effective Poisson's ratio υ_0.

The effective Poisson's ratio, υ_0, can be solved by the empirical formula given by Ahmed and Jones (Ahmed & Jones, 1990)

$$\upsilon_0 = \frac{\upsilon_1 f_1 E_1 + \upsilon_2 f_2 E_2 + \upsilon_3 f_3 E_3}{f_1 E_1 + f_2 E_2 + f_3 E_3} \tag{4.39}$$

where f_1, f_2 and f_3 denote the volume fraction of p-DCPD, asphalt binder and coarse aggregate respectively. Notice that for different sizes of coarse aggregates, the volume fractions are different. The value of b and c can be derived from the thicknesses of p-DCPD layer and asphalt binder layer. As mentioned before, coarse aggregates are categorized into several different sizes. Yet we assume the multilayer-coated particles, whatever sizes of coarse aggregates they contain, share the same thicknesses of p-DCPD layer and asphalt binder layer. The thicknesses of p-DCPD layer and asphalt binder layer are defines as

$$t_1 = c - b; \qquad t_2 = b - a \tag{4.40}$$

which can be solved by the following formulas

$$\sum_{i=1}^{n} f_{3i} \frac{(a_i + t_1 + t_2)^3 - a_i^3}{(a_i + t_1 + t_2)^3} = \frac{f_1}{f_1 + f_2 + f_{3i}} \tag{4.41}$$

$$\sum_{i=1}^{n} f_{3i} \frac{(a_i + t_2)^3 - a_i^3}{(a_i + t_2)^3} = \frac{f_2}{f_2 + f_{3i}} \tag{4.42}$$

Based on Eqn. (4.33)-(4.42), the effective Young's modulus and Poisson's ratio of the multilayer-coated particle can be estimated.

Given the fact that p-DCPD is a comparatively brittle and rigid material (Kovačič et al., 2013; Vallons et al., 2015; Y. Wang et al., 2017), and it's wrapped at the outer layer of the particle, it is reasonable for us to assume that the multilayer-coated particles behave mainly their elasticity not plasticity.

4.3 Effective Elastic Moduli of Asphalt Mastic

Asphalt mastic, which can be treated as the matrix for the spherical multilayer-coated particles to randomly dispersed in it, is a multi-phase composite composed of fine aggregates, asphalt binder, p-DCPD and air voids. To simplify the analysis, the heterogeneous asphalt mastic matrix can be represented by equivalent homogeneous continuum media with appropriately defined effective properties.

In the previous chapters, various approaches such as Hashin-Shtrikman bounds (Hashin, 1962; Hashin & Shtrikman, 1961, 1963), Mori-Tanaka method (Benveniste, 1987; Mori & Tanaka, 1973), and Ju and Chen's solutions (Ju & Chen, 1994a, 1994b) have been employed to estimate the effective elastic properties of the multi-phase composites. Based on the comparisons made in Chapter 3 among these different approaches, it is trustworthy to pick Ju and Chen's pairwise interacting solution to predict the effective elastic moduli of the asphalt mastic matrix. In particular, the pairwise interacting solution may lead to an

accurate higher-order formulation for the prediction of elastic particulate composites at moderately high particle concentrations.

The results from the pairwise interacting solution are summarized as follows

$$\bar{K} = K_0\left[1+\frac{30\left(1-v_0\right)f_1\left(3\gamma_1+2\gamma_2\right)}{3\alpha+2\beta-10\left(1+v_0\right)f_1\left(3\gamma_1+2\gamma_2\right)}\right] \tag{4.43}$$

$$\bar{\mu} = \mu_0\left[1+\frac{30\left(1-v_0\right)f_1\gamma_2}{\beta-4\left(4-5v_0\right)f_1\gamma_2}\right] \tag{4.44}$$

where K_0, μ_0 , v_0 are the bulk modulus, shear modulus and Poisson's ratio of the matrix respectively, f_1 is the volume fraction of inclusions, and

$$\gamma_1 = \frac{5f_1}{96\beta^2}\left[12v_0\left(13-14v_0\right)-\frac{96\alpha}{3\alpha+2\beta}\left(1-2v_0\right)\left(1+v_0\right)\right] \tag{4.45}$$

$$\gamma_2 = \frac{1}{2}+\frac{5f_1}{96\beta^2}\left[6\left(25-34v_0+22v_0^2\right)-\frac{36\alpha}{3\alpha+2\beta}\left(1-2v_0\right)\left(1+v_0\right)\right] \tag{4.46}$$

$$\alpha = 2\left(5v_0-1\right)+10\left(1-v_0\right)\left(\frac{K_0}{K_1-K_0}-\frac{\mu_0}{\mu_1-\mu_0}\right) \tag{4.47}$$

$$\beta = 2\left(4-5v_0\right)+15\left(1-v_0\right)\frac{\mu_0}{\mu_1-\mu_0} \tag{4.48}$$

K_1 and μ_1 are the bulk and shear moduli of the inclusions.

Eqn. (4.43) and (4.44) are valid for any arbitrary radial distribution function, whereas γ_1 and γ_2 are explicitly given for the case where uniform distribution is considered for simplicity. A general expression for γ_1 and γ_2 can be found in Eqn. (44)-(49) in Ju and Chen(Ju & Chen, 1994a) and for a real particulate composite, if the radial distribution function may be measured via nondestructive characterization (e.g., three-dimensional X-

ray computerized tomography) of a series of specimens produced from the same material processing procedure, a certain expression for γ_1 and γ_2 can be derived.

Eqn. (4.43)-(4.48) are valid for two-phase composites yet the proposed asphalt mastic is a four-phase composite. In order to use the pairwise interacting solution, a multilevel homogenization procedure is established, illustrated as in Figure 4.4. A comparison of effective elastic moduli of an interim asphalt mastic (neglecting air voids) and final state asphalt mastic (with air voids) calculated based on this proposed multilevel homogenization procedure has been proven to be slightly more accurate than that of Hashin-Shtrikman bounds and Mori-Tanaka method in the previous Chapter.

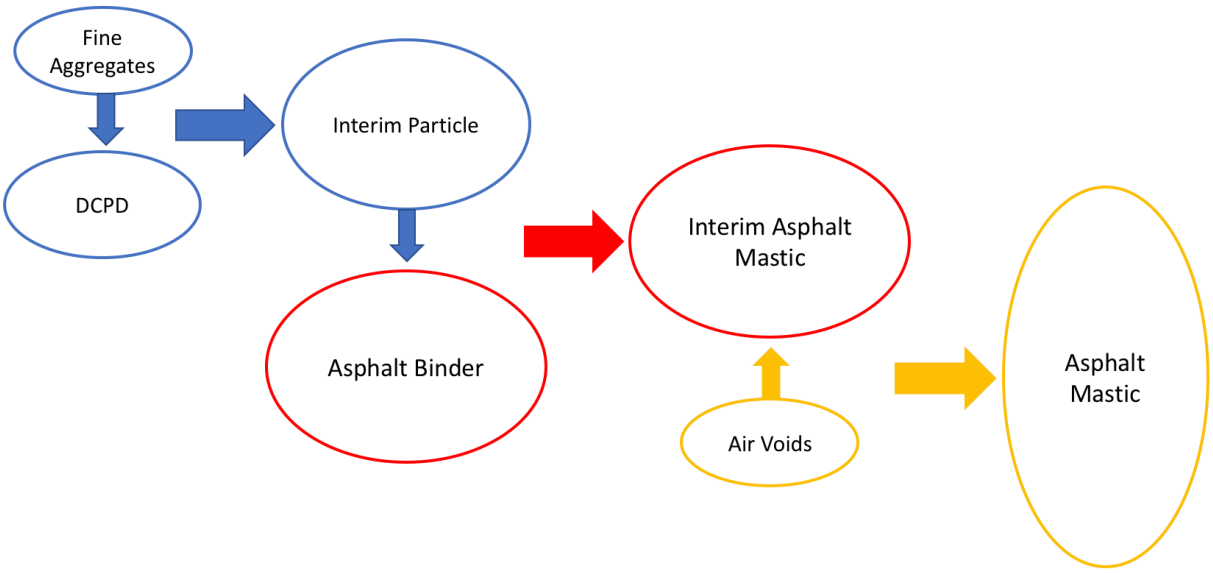

Figure 4.4 The multilevel homogenization procedure to apply Ju and Chen's pairwise interacting solution

4.4 The Initial Elastic Strain Energy Based Isotropic Damage Evolution

As stated in Chapter 2 and 3, the definition of damage in our approach can be described as the separation of portions of materials due to the breaking of bonding or cohesion between portions by local tension which leads to the partial or complete loss of elastic stiffness. A class of damage evolution criterion, based on a continuum damage mechanics framework, is proposed within an initial elastic strain energy based formulation.

General form to satisfy Kuhn-Tucker condition

$$\begin{cases} \dot{d}_t = \dot{\mu}\mathrm{H}\left(\xi_t^+, d_t\right) \\ \dot{g}_t = \dot{\mu} \\ \dot{\mu} \geq 0, \;\; \phi^d(\xi_t^+, g_t) \equiv \xi_t^+ - g_t \leq 0, \;\; \dot{\mu}\phi^d(\xi_t^+, g_t) = 0 \end{cases} \tag{4.49}$$

where $\dot{\mu}$ is the damage consistency parameter that defines the damage loading/unloading conditions according to the Kuhn-Tucker relations; ϕ^d describes the current damage criterion, or in other words, the damage surface; g_t is the damage threshold at the current time *t*; $\mathrm{H}\left(\xi_t^+, d_t\right)$ is the damage hardening function which yields a unit scalar in the elastic-damage case; and ξ_t^+ is the equivalent tensile strain energy norm which is defined as (Lemaitre, 1985; Mazars & Lemaitre, 1985)

$$\xi^+ \equiv \sqrt{\frac{1}{2}\boldsymbol{\varepsilon}^+ : \mathbf{C}^0 : \boldsymbol{\varepsilon}^+} \tag{4.50}$$

The tensile strain tensor $\boldsymbol{\varepsilon}^+ = \mathbf{P}^+ : \boldsymbol{\varepsilon}$ and $\mathbf{P}^+$ is the Mode I tensile projection tensor which can be calculated by following equations

$$\mathbf{P}^{+}_{ijkl}(\boldsymbol{\varepsilon}) \equiv \frac{1}{2}\left(\mathbf{Q}^{+}_{ik}\mathbf{Q}^{+}_{jl} + \mathbf{Q}^{+}_{il}\mathbf{Q}^{+}_{jk}\right) \tag{4.51}$$

$$\mathbf{Q}^{+} \equiv \sum_{i=1}^{3}\left\langle \lambda^{i} \right\rangle \left(\mathbf{p}_{i} \otimes \mathbf{p}_{i}\right) \tag{4.52}$$

$$\boldsymbol{\varepsilon} = \sum_{i=1}^{3}\lambda^{i}\left(\mathbf{p}_{i} \otimes \mathbf{p}_{i}\right) \tag{4.53}$$

where $\left|\mathbf{p}_{i}\right| = 1$ and $2\langle\lambda^{i}\rangle = \left(\lambda^{i} + \left|\lambda^{i}\right|\right)$.

An isotropic elastic-damage evolution function is proposed in Chapter 3.

$$d_{t} = A\ \exp\left[\ B\ \xi_{t}^{+}\left(\xi_{t}^{+} - g_{0}\right)\right] \tag{4.54}$$

where g_0 is the initial tensile damage threshold (g_t at t=0) and A, B are characteristic parameters of the material.

4.5 The Effective Elastoplastic Behavior of the Innovative Material

4.5.1 The Coupled Isotropic Formulation

The governing incremental damage evolutions are characterized through the effective stress concept in conjunction with the hypothesis of strain equivalence; plastic flow is introduced by means of an additive split of the stress tensor. In this innovative formulation, a characteristic energy norm of the tensile strain tensor is introduced for the for the damage mechanics.

A new computational algorithm is systematically developed based on the two-step operator splitting methodology. The elastic-damage predictor and the plastic corrector are implemented within ABAQUS user routine (Fortran).

A crucial idea underling the initial elastic strain energy based isotropic damage model presented in this chapter is the hypothesis that incremental damage history is directly linked to the history of total strains. The notion of effective stress along with the hypothesis of strain equivalence then follows from the assumed form of free energy. Attention is focused on the proposed isotropic damage variable.

4.5.2 The Additive Stress Split

Within the present strain space framework, the plastic flow is introduced by means of an additive split of the stress tensor into initial and inelastic parts (Simo & Ju, 1987), i.e.

$$\bar{\boldsymbol{\sigma}} = \frac{\partial \Psi^0(\boldsymbol{\varepsilon})}{\partial \boldsymbol{\varepsilon}} - \bar{\boldsymbol{\sigma}}^p \tag{4.55}$$

where $\bar{\boldsymbol{\sigma}}$ is the effective stress, $\boldsymbol{\varepsilon}$ is the total strain, $\Psi^0(\boldsymbol{\varepsilon})$ is the initial elastic stored energy function of the undamaged material, and $\bar{\boldsymbol{\sigma}}^p$ denotes the effective plastic relaxation stress. For linear elasticity, we write

$$\Psi^0(\boldsymbol{\varepsilon}) = \frac{1}{2}\boldsymbol{\varepsilon} : \mathbf{C}^0 : \boldsymbol{\varepsilon} \tag{4.56}$$

where $\mathbf{C}^0$ denotes the linear elasticity tensor. Eqn. (4.55) then can be written as the following

$$\bar{\boldsymbol{\sigma}} = \mathbf{C}^0 : \boldsymbol{\varepsilon} - \bar{\boldsymbol{\sigma}}^p \tag{4.57}$$

4.5.3 The Thermodynamic Basis

In order to introduce the damage effect and plastic flow processes, a free energy potential of the following form is proposed

$$\Psi\left(\boldsymbol{\varepsilon}, \boldsymbol{\sigma}^p, \mathbf{q}, d\right) \equiv \left(1-d\right)\Psi^0\left(\boldsymbol{\varepsilon}\right) - \boldsymbol{\varepsilon} : \boldsymbol{\sigma}^p + \Xi\left(\mathbf{q}, \boldsymbol{\sigma}^p\right) \tag{4.58}$$

where $\boldsymbol{\varepsilon}$ denotes the total strain tensor, $\boldsymbol{\sigma}^p$ is the plastic relaxation stress tensor, $\mathbf{q}$ is a suitable set of internal (plastic) variables. Further, d defines the isotropic scalar damage variable between 0 and 1 (or a maximum damage threshold less than 1) whose function has been discussed in Section 4.4. $\Psi^0\left(\boldsymbol{\varepsilon}\right)$ is the initial elastic stored energy function of the undamaged material, and $\Xi\left(\mathbf{q}, \sigma^p\right)$ is the plastic potential function.

Confining our attention to the purely mechanical theory, the Clausius-Duhem reduced dissipation inequality for purely mechanical isothermal theory takes the form for any admissible process (Milan & Zdenek, 2001)

$$-\dot{\Psi} + \boldsymbol{\sigma} : \dot{\boldsymbol{\varepsilon}} \geq 0 \tag{4.59}$$

By taking the time derivative of Eqn. (4.58), substituting it into Eqn. (4.59), and making use of the classical Coleman-Noll argument (Coleman & Noll, 1963) and its variation, the Coleman-Gurtin theory (Coleman & Gurtin, 1967) along with the additional

assumption that the damage effect and plastic unloading are elastic processes, we can obtain the stress-strain constitutive law

$$\boldsymbol{\sigma} = \frac{\partial \Psi(\boldsymbol{\varepsilon})}{\partial \boldsymbol{\varepsilon}} = (1-d)\frac{\partial \Psi^0(\boldsymbol{\varepsilon})}{\partial \boldsymbol{\varepsilon}} - \boldsymbol{\sigma}^p = (1-d)\bar{\boldsymbol{\sigma}} \tag{4.60}$$

and the dissipative inequalities

$$-\frac{\partial \Xi}{\partial \mathbf{q}} \bullet \dot{\mathbf{q}} - \left(\frac{\partial \Xi}{\partial \boldsymbol{\sigma}^p} - \boldsymbol{\varepsilon} \right) : \dot{\boldsymbol{\sigma}}^p \geq 0 \tag{4.61}$$

$$\Psi^0(\boldsymbol{\varepsilon})\dot{d} - \frac{\partial \Xi}{\partial \mathbf{q}} \bullet \dot{\mathbf{q}} - \left(\frac{\partial \Xi}{\partial \boldsymbol{\sigma}^p} - \boldsymbol{\varepsilon} \right) : \dot{\boldsymbol{\sigma}}^p \geq 0 \tag{4.62}$$

It follows from Eqn. (4.60) that within the present strain space formulation, the stress tensor is split into the elastic-damage part and the plastic relaxation part. From Eqn. (4.61) and (4.62), we observe that the dissipative energy by plasticity itself is positive; if damage effect is involved, the sum of damage and plasticity effect is also positive. It is also noted from Eqn. (4.60)-(4.62) that the present framework is capable of accommodating general (nonlinear) elastic response and general plastic response.

The potential $\Xi\left(\mathbf{q}, \boldsymbol{\sigma}^p\right)$ is linked to plastic dissipation. Its role is such that inequality (4.62) is satisfied for arbitrary processes. Note that we have assumed that the potential $\Xi\left(\mathbf{q}, \boldsymbol{\sigma}^p\right)$ is independent of damage variable d. From Eqn. (4.58), it then follows that

$$-Y \equiv -\frac{\partial \Psi\left(\boldsymbol{\varepsilon}, \boldsymbol{\sigma}^p, \mathbf{q}, d\right)}{\partial d} = \Psi^0(\boldsymbol{\varepsilon}) \tag{4.63}$$

Hence, the initial (undamaged) elastic strain energy $\Psi^0(\boldsymbol{\varepsilon})$ is the thermodynamic force Y conjugate to the damage variable d.

4.5.4 Characterization of Effective Plastic Response and Tangent Moduli

In accordance with the notion of effective stress, the characterization of the plastic response should be formulated in effective stress space in terms of effective stress $\bar{\boldsymbol{\sigma}}$ and $\bar{\boldsymbol{\sigma}}^p$. Therefore, for the classical situation in which the yield function is postulated in the stress space, we replace the homogenized Cauchy stress tensor $\boldsymbol{\sigma}$ by the effective stress tensor $\bar{\boldsymbol{\sigma}}$, so that the elastic-damage domain is characterized by $f\left(\bar{\boldsymbol{\sigma}},\mathbf{q}\right)\leq 0$. Here, $\mathbf{q}$ represents the internal plastic variables and the evolution of which is defined below. With the assumption of an associative flow rule, rate-independent plastic response is characterized in the strain space by the flowing constitutive equations (Simo & Ju, 1987)

$$\dot{\bar{\boldsymbol{\sigma}}}^p = \dot{\lambda}\frac{\partial f}{\partial \boldsymbol{\varepsilon}}\left(\frac{\partial \Psi^0(\boldsymbol{\varepsilon})}{\partial \boldsymbol{\varepsilon}} - \bar{\boldsymbol{\sigma}}^p, \mathbf{q}\right) \quad \textit{(associative flow rule)} \tag{4.64}$$

$$\dot{\mathbf{q}} = \dot{\lambda}\mathbf{h}\left(\frac{\partial \Psi^0(\boldsymbol{\varepsilon})}{\partial \boldsymbol{\varepsilon}} - \bar{\boldsymbol{\sigma}}^p, \mathbf{q}\right) \quad \textit{(plastic hardening law)} \tag{4.65}$$

$$f\left(\frac{\partial \Psi^0(\boldsymbol{\varepsilon})}{\partial \boldsymbol{\varepsilon}} - \bar{\boldsymbol{\sigma}}^p, \mathbf{q}\right) \leq 0 \quad \textit{(yield condition)} \tag{4.66}$$

where $\dot{\bar{\boldsymbol{\sigma}}}^p$ denotes the plastic relaxation effective stress rate tensor, $\dot{\lambda}$ denotes the plastic consistency parameter, and $\mathbf{h}$ signifies the hardening law. Eqn. (4.64)-(4.66) provide a characterization of plasticity in the strain space. Loading/unloading conditions may be expressed in a compact form by requiring that

$$f\left(\frac{\partial \Psi^0(\boldsymbol{\varepsilon})}{\partial \boldsymbol{\varepsilon}} - \bar{\boldsymbol{\sigma}}^p, \mathbf{q}\right) \leq 0, \quad \dot{\lambda} \geq 0, \quad \dot{\lambda} f\left(\frac{\partial \Psi^0(\boldsymbol{\varepsilon})}{\partial \boldsymbol{\varepsilon}} - \bar{\boldsymbol{\sigma}}^p, \mathbf{q}\right) = 0 \tag{4.67}$$

Note that if $f < 0$, then $\dot{\lambda} = 0$ and the process is elastic-damage. On the other hand, for plastic loading, $\dot{\lambda} > 0$ and $f = 0$. In the latter case, $\dot{\lambda}$ is determined by requiring that $\dot{f} = 0$, which is considered as the so-called plastic consistency condition. Making use of Eqn. (4.55) during loading, one has

$$\frac{\partial f}{\partial \bar{\boldsymbol{\sigma}}} : \dot{\bar{\boldsymbol{\sigma}}} + \frac{\partial f}{\partial \mathbf{q}} \bullet \dot{\mathbf{q}} = 0 \tag{4.68}$$

where $\dfrac{\partial f}{\partial \bar{\boldsymbol{\sigma}}}$ denotes the partial derivative of $f\left(\dfrac{\partial \Psi^0(\boldsymbol{\varepsilon})}{\partial \boldsymbol{\varepsilon}} - \bar{\boldsymbol{\sigma}}^p, \mathbf{q} \right)$ with respect to the first argument. From Eqn. (4.60) we obtain

$$\dot{\bar{\boldsymbol{\sigma}}} = \frac{\partial^2 \Psi^0(\boldsymbol{\varepsilon})}{\partial \boldsymbol{\varepsilon}^2} : \dot{\boldsymbol{\varepsilon}} - \dot{\bar{\boldsymbol{\sigma}}}^p = \frac{\partial^2 \Psi^0(\boldsymbol{\varepsilon})}{\partial \boldsymbol{\varepsilon}^2} : \left(\dot{\boldsymbol{\varepsilon}} - \dot{\lambda} \frac{\partial f}{\partial \bar{\boldsymbol{\sigma}}} \right) \tag{4.69}$$

where the flow rule (4.64) has been applied. Therefore, $\dot{\lambda}$ can be determined from Eqn. (4.68), (4.69) and the hardening law (4.65) as

$$\dot{\lambda} = \frac{\dfrac{\partial f}{\partial \bar{\boldsymbol{\sigma}}} : \dfrac{\partial^2 \Psi^0(\boldsymbol{\varepsilon})}{\partial \boldsymbol{\varepsilon}^2} : \dot{\boldsymbol{\varepsilon}}}{\dfrac{\partial f}{\partial \bar{\boldsymbol{\sigma}}} : \dfrac{\partial^2 \Psi^0(\boldsymbol{\varepsilon})}{\partial \boldsymbol{\varepsilon}^2} : \dfrac{\partial f}{\partial \bar{\boldsymbol{\sigma}}} - \dfrac{\partial f}{\partial \mathbf{q}} \bullet \mathbf{h}} \tag{4.70}$$

Substitution of Eqn. (4.70) into Eqn. (4.69) then yields $\dot{\bar{\boldsymbol{\sigma}}} = \bar{\mathbf{C}}^{ep} : \dot{\boldsymbol{\varepsilon}}$, where $\bar{\mathbf{C}}^{ep}$ is the effective elastoplastic tangent moduli given by

$$\begin{aligned}\bar{\mathbf{C}}^{ep} &= \frac{\partial^2 \Psi^0(\boldsymbol{\varepsilon})}{\partial \boldsymbol{\varepsilon}^2} - \frac{\left[\dfrac{\partial^2 \Psi^0(\boldsymbol{\varepsilon})}{\partial \boldsymbol{\varepsilon}^2} : \dfrac{\partial f}{\partial \bar{\boldsymbol{\sigma}}}\right] \otimes \left[\dfrac{\partial^2 \Psi^0(\boldsymbol{\varepsilon})}{\partial \boldsymbol{\varepsilon}^2} : \dfrac{\partial f}{\partial \bar{\boldsymbol{\sigma}}}\right]}{\dfrac{\partial f}{\partial \bar{\boldsymbol{\sigma}}} : \dfrac{\partial^2 \Psi^0(\boldsymbol{\varepsilon})}{\partial \boldsymbol{\varepsilon}^2} : \dfrac{\partial f}{\partial \bar{\boldsymbol{\sigma}}} - \dfrac{\partial f}{\partial \mathbf{q}} \bullet \mathbf{h}} \\ &= \mathbf{C}^0 - \frac{\left(\mathbf{C}^0 : \dfrac{\partial f}{\partial \bar{\boldsymbol{\sigma}}}\right) \otimes \left(\mathbf{C}^0 : \dfrac{\partial f}{\partial \bar{\boldsymbol{\sigma}}}\right)}{\dfrac{\partial f}{\partial \bar{\boldsymbol{\sigma}}} : \mathbf{C}^0 : \dfrac{\partial f}{\partial \bar{\boldsymbol{\sigma}}} - \dfrac{\partial f}{\partial \mathbf{q}} \bullet \mathbf{h}}\end{aligned} \tag{4.71}$$

4.6 Computational Algorithms

In Section 4.4 and 4.5., an initial elastic strain energy based isotropic elastoplastic damage model with the concept of additive stress split in the effective stress space. To use the proposed model within the context of numerical method, a two-step operator splitting methodology (Simo & Hughes, 1998) is introduced. In particular, the resulting procedure takes the form of an elastic-damage part and an effective plastic return mapping part, as follows:

Elastic-Damage Part

$$\dot{\boldsymbol{\varepsilon}} = \nabla^s \dot{\mathbf{u}}(t)$$

$$\dot{d} = \begin{cases} \mathrm{H}\left(\xi^+\right)\dot{\xi}^+ & \text{iff} \quad \phi^d = \dot{\phi}^d = 0 \\ 0 & \text{otherwise} \end{cases}$$

$$\dot{g} = \begin{cases} \dot{\xi}^+ & \text{iff} \quad \phi^d = \dot{\phi}^d = 0 \\ 0 & \text{otherwise} \end{cases}$$

$$\dot{\bar{\boldsymbol{\sigma}}} = \frac{d}{dt}\left[\frac{\partial \Psi^0(\boldsymbol{\varepsilon})}{\partial \boldsymbol{\varepsilon}}\right]$$

$$\dot{\bar{\boldsymbol{\sigma}}}^p = 0$$

$$\dot{\mathbf{q}} = 0$$

Plastic Part

$$\dot{\boldsymbol{\varepsilon}} = 0$$
$$\dot{d} = 0$$
$$\dot{\bar{\boldsymbol{\sigma}}} = -\dot{\bar{\boldsymbol{\sigma}}}^{p}$$
$$\dot{\bar{\boldsymbol{\sigma}}}^{p} = \dot{\lambda}\frac{\partial f}{\partial \boldsymbol{\varepsilon}}\left(\frac{\partial \Psi^{0}(\boldsymbol{\varepsilon})}{\partial \boldsymbol{\varepsilon}} - \bar{\boldsymbol{\sigma}}^{p}, \mathbf{q}\right)$$
$$\dot{\mathbf{q}} = \dot{\lambda}\mathbf{h}\left(\frac{\partial \Psi^{0}(\boldsymbol{\varepsilon})}{\partial \boldsymbol{\varepsilon}} - \bar{\boldsymbol{\sigma}}^{p}, \mathbf{q}\right)$$

A following step-by-step procedure is developed to solve the two parts of the elastoplastic damage problem:

Step 1: Update the total strain. Given the incremental displacement field $\mathbf{u}_{n+1}$, the total strain tensor is updated as

$$\boldsymbol{\varepsilon}_{n+1} = \boldsymbol{\varepsilon}_{n} + \nabla^{s}\mathbf{u}_{n+1} \tag{4.72}$$

Step 2: Compute the tensile strain tensor

$$\boldsymbol{\varepsilon}^{+}_{n+1} = \mathbf{Q}\boldsymbol{\Lambda}^{+}\mathbf{Q}^{T} \tag{4.73}$$

where $\mathbf{Q} = \left[\mathbf{q}_1\ \mathbf{q}_2\ \mathbf{q}_3\right]_{3\times 3}$ and $\boldsymbol{\Lambda}^{+} = \begin{bmatrix} \langle\lambda_1\rangle & 0 & 0 \\ 0 & \langle\lambda_2\rangle & 0 \\ 0 & 0 & \langle\lambda_3\rangle \end{bmatrix}$; $\mathbf{q}_i$ and λ_i (i=1~3) denote the corresponding eigenvectors and eigenvalues of the total strain tensor $\boldsymbol{\varepsilon}_{n+1}$ respectively; the angular McAuley brackets are defined by $2\langle\lambda_i\rangle = \lambda_i + |\lambda_i|$.

Step 3: Compute the initial (undamaged) elastic tensile strain energy

$$\xi^{+}_{n+1} = \sqrt{\Psi^{0}\left(\boldsymbol{\varepsilon}^{+}_{n+1}\right)} = \sqrt{\frac{1}{2}\boldsymbol{\varepsilon}^{+}_{n+1} : \mathbf{C}^{0} : \boldsymbol{\varepsilon}^{+}_{n+1}} \tag{4.74}$$

Step 4: Compute the scalar damage parameter

$$\text{if} \quad \xi_{n+1}^{+} \begin{cases} \leq g_0 & d_{n+1} = 0 \quad \text{(no damage)} \\ > g_0 & d_{n+1} = A\exp\left[B\xi_{n+1}^{+}\left(\xi_{n+1}^{+} - g_0\right)\right] \end{cases} \tag{4.75}$$

Step 5: Obtain trial (predictor) stress tensor and internal plastic variable

$$\begin{aligned} \boldsymbol{\sigma}_{n+1}^{0} &= \frac{\partial \Psi^{0}}{\partial \boldsymbol{\varepsilon}}\left(\boldsymbol{\varepsilon}_{n+1}\right) = \mathbf{C}^{0} : \boldsymbol{\varepsilon}_{n+1} \\ \bar{\boldsymbol{\sigma}}_{n+1}^{trial} &= \boldsymbol{\sigma}_{n+1}^{0} - \bar{\boldsymbol{\sigma}}_{n}^{p} \\ \mathbf{q}_{n+1}^{trial} &= \mathbf{q}_{n} \end{aligned} \tag{4.76}$$

Step 6: Check for yielding

$$\text{if} \quad f\left(\bar{\boldsymbol{\sigma}}_{n+1}^{trial}, \mathbf{q}_{n+1}^{trial}\right) \begin{cases} \leq 0 & \bar{\boldsymbol{\sigma}}_{n+1} = \bar{\boldsymbol{\sigma}}_{n+1}^{trial} \;;\; \mathbf{q}_{n+1} = \mathbf{q}_{n+1}^{trial} \;; \text{skip step 7} \\ > 0 & \text{plastic; go to step 7} \end{cases} \tag{4.77}$$

Step 7: Cutting plane return mapping

In the case of plastic loading, the trial (predictor) stresses and internal variables need to be returned back to the yield surface along the algorithmic counterpart of the flow generated to satisfy the Kuhn-Tucker conditions. There exist many return mapping algorithms, whereas the cutting plane algorithm developed by Simo and Ortiz (Ortiz & Simo, 1986; Simo & Ortiz, 1985) is employed here. The cutting plane algorithmic construction was inspired by a form of the convex cutting plane method (Kelley, 1960) with its basic structure inherited from Newton's iteration method. Two advantages of this cutting plane return mapping algorithm are the quadratic rate of convergence towards the yield surface and the need for computing the gradient of the flow rule and hardening law are entirely bypassed. The procedures (iterations) are as follows:

(i) Initialize: $K = 0, \quad \bar{\boldsymbol{\sigma}}_{n+1}^{K} = \bar{\boldsymbol{\sigma}}_{n+1}^{trial}, \quad \mathbf{q}_{n+1}^{K} = \mathbf{q}_{n+1}^{trial}$

(ii) Compute the hardening moduli and yield function:

$$h_{n+1}^{K} = h\left(\bar{\boldsymbol{\sigma}}_{n+1}^{K}, \mathbf{q}_{n+1}^{K}\right)$$
$$f_{n+1}^{K} = f\left(\bar{\boldsymbol{\sigma}}_{n+1}^{K}, \mathbf{q}_{n+1}^{K}\right)$$
IF $f_{n+1}^{K} \le 0$ (TOL) EXIT
ELSE GOTO (iii)

(iii) Linearize the plastic consistency condition:

$$\Delta\lambda_{n+1}^{K} = \frac{f_{n+1}^{K}}{\frac{\partial f_{n+1}^{K}}{\partial \bar{\boldsymbol{\sigma}}_{n+1}^{K}} : \mathbf{C}_{n+1}^{K} : \frac{\partial f_{n+1}^{K}}{\partial \bar{\boldsymbol{\sigma}}_{n+1}^{K}} - \frac{\partial f_{n+1}^{K}}{\partial \mathbf{q}_{n+1}^{K}} \bullet \mathbf{h}_{n+1}^{K}}$$

(iv) Update the state variables and consistency parameter:

$$\bar{\boldsymbol{\sigma}}_{n+1}^{K+1} = \bar{\boldsymbol{\sigma}}_{n+1}^{K+1} - \Delta\lambda_{n+1}^{K} \mathbf{C}_{n+1}^{K} : \frac{\partial f_{n+1}^{K}}{\partial \bar{\boldsymbol{\sigma}}_{n+1}^{K}}$$
$$\mathbf{q}_{n+1}^{K+1} = \mathbf{q}_{n+1}^{K} + \Delta\lambda_{n+1}^{K} h_{n+1}^{K}$$
SET $K \leftarrow K+1$; GOTO (ii)

Step 8: Update the homogenized stress

$$\boldsymbol{\sigma}_{n+1} = \left(1 - d_{n+1}\right)\bar{\boldsymbol{\sigma}}_{n+1} \tag{4.78}$$

4.7 Numerical Simulations

4.7.1 A 1-D Driven Problem

To test the proposed elastoplastic-damage framework, a 1-D strain driven problem is tested by MATLAB. One cycle strain loading (compressive loading of strain in 11-direction, unloading, tensile loading of strain in 11-direction and unloading) is applied, as shown in Figure 4.5. In particular, the Drucker-Prager yield function (Drucker & Prager,

1952) is used for loading function. The Drucker-Prager yield function is a simple modification of the Von Mises criterion whereby the hydrostatic-dependent first invariant $\mathbf{I}_1$ is introduced to the original Von Mises yield function and becomes suitable for the modeling of plasticity of materials where there is a strong dependence on the hydrostatic pressure such as rocks, soil and concrete.

It is defined as

$$f\left(\mathbf{I}_1, J_2\right) \equiv \sqrt{J_2} - \alpha \mathbf{I}_1 - k = 0 \tag{4.79}$$

where α is a material constant related to the theoretical cohesive strength of the material and k is the modified yield strength in absence of mean stress.

Figure 4.6-Figure 4.10 demonstrate the stress-strain relationships between effective stress $\bar{\sigma}_{11}$ and strain ε_{11}, and homogenized stress σ_{11} and strain ε_{11}; the history of plastic strain ε_{11}^{p}, plastic stress σ_{11}^{p} and the evolution of the scalar damage variable, respectively. The stress-strain relationship in the effective space appears to be linear in each segment, while in the homogenized (true) space, it becomes nonlinear under tension loading segment. This consequence meets the expectation of the hypothesis of strain equivalence. The effective stress $\bar{\sigma}_{11}$ didn't not go back to origin after a full cylce, due to the fact of irriversibility of the plastic deformation, the residual stress is about 1000 psi, which is the amount of plastic stress σ_{11}^{p} at the end of the cycle. Also, we notice in Figure 4.10 that damage didn't occur until around 200 time steps, i.e. only within the segment of tensile loading, which agrees with our definition of the damage evolution function (tensile

strain and tensile strain energy norm). Damage history remains flat during the tensile unloading segment due to the fact that no further energy is introduced to precipitate further damage while no healing effect exists in the material at the same time. The outputs from the 1-D strain driven problem are reasonable, and the proposed elastoplastic-damage framework will be implemented by Fortran code in ABAQUS UMAT to simulate the elastoplastic behavior of the specimen infiltrated with DCPD under splitting tension test.

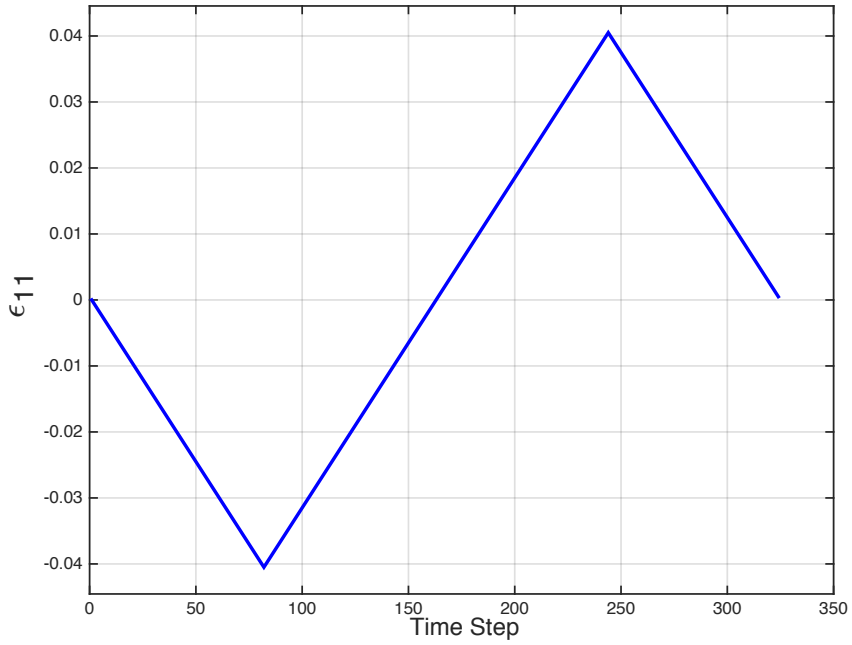

Figure 4.5 The history of (total) strain input ε_{11}

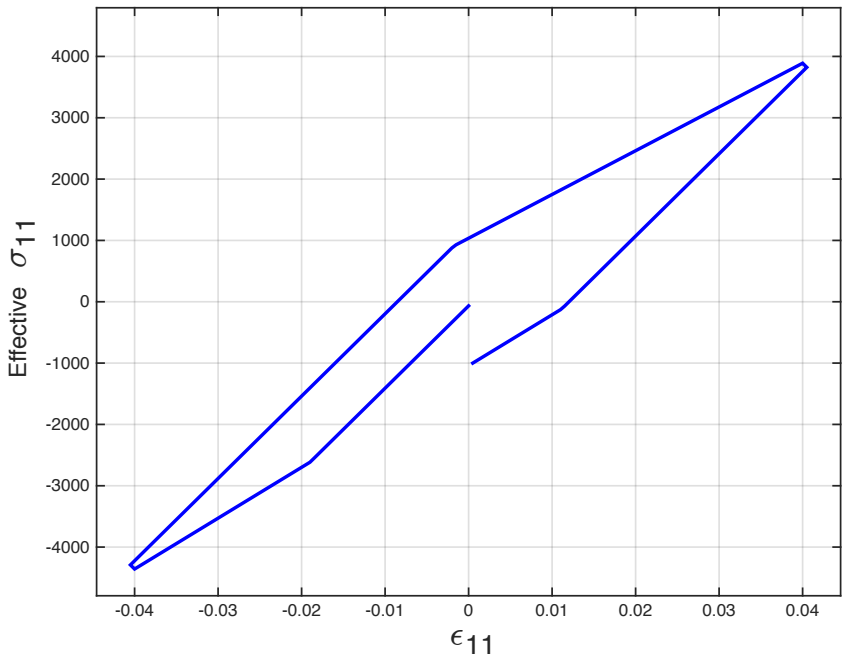

Figure 4.6 The stress-strain relationship of $\bar{\sigma}_{11}$ vs. ε_{11}

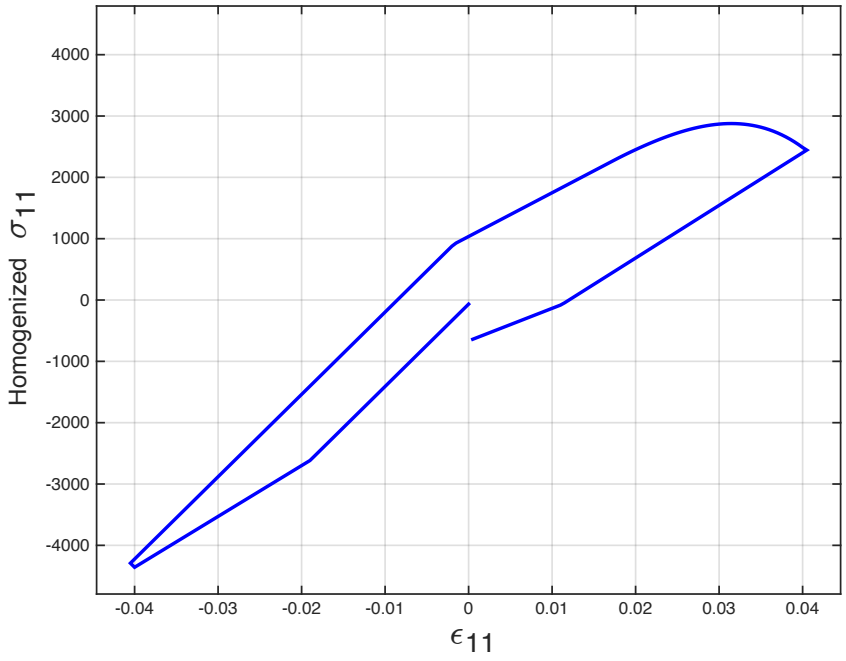

Figure 4.7 The stress-strain relationship of σ_{11} vs. ε_{11}

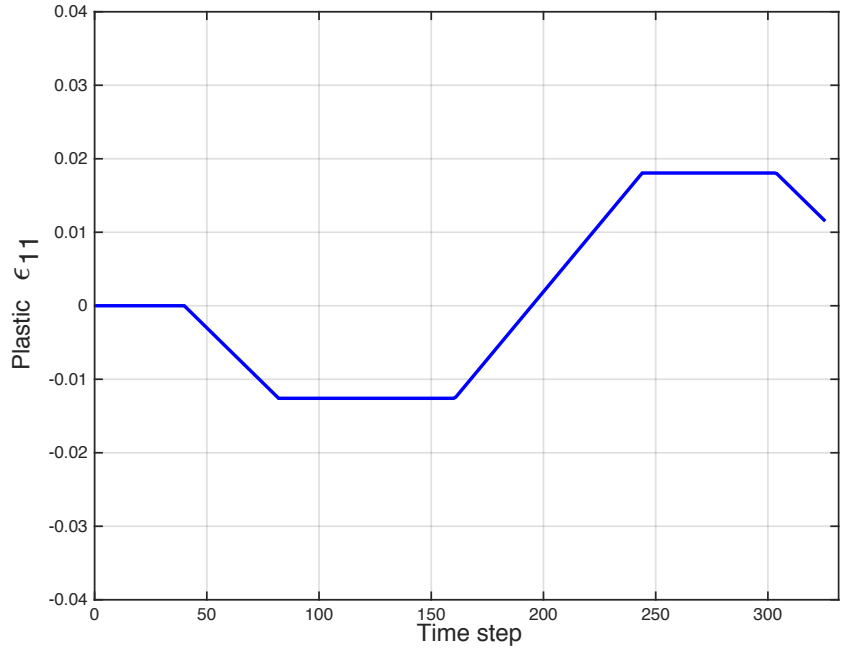

Figure 4.8 The history of plastic strain ε_{11}^{p}

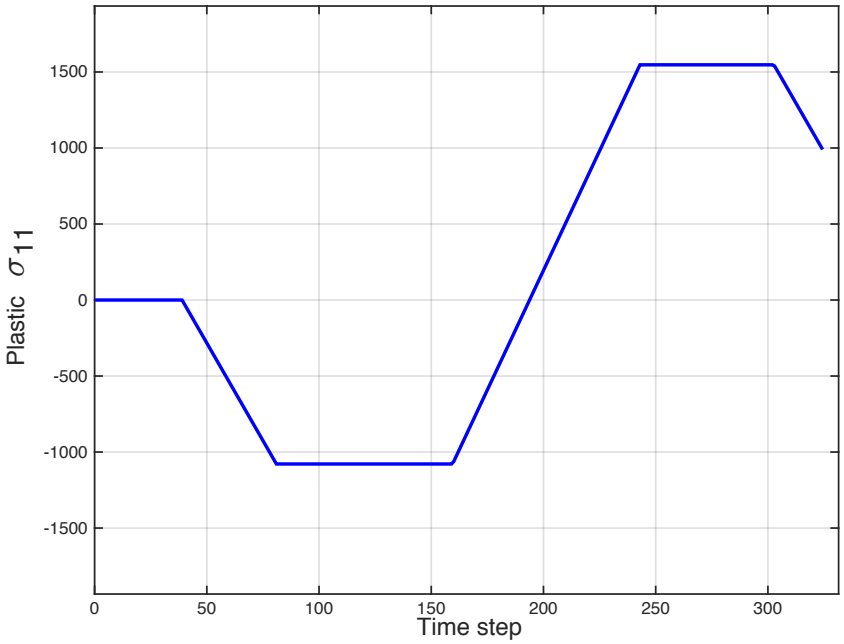

Figure 4.9 The history of plastic stress σ_{11}^{p}

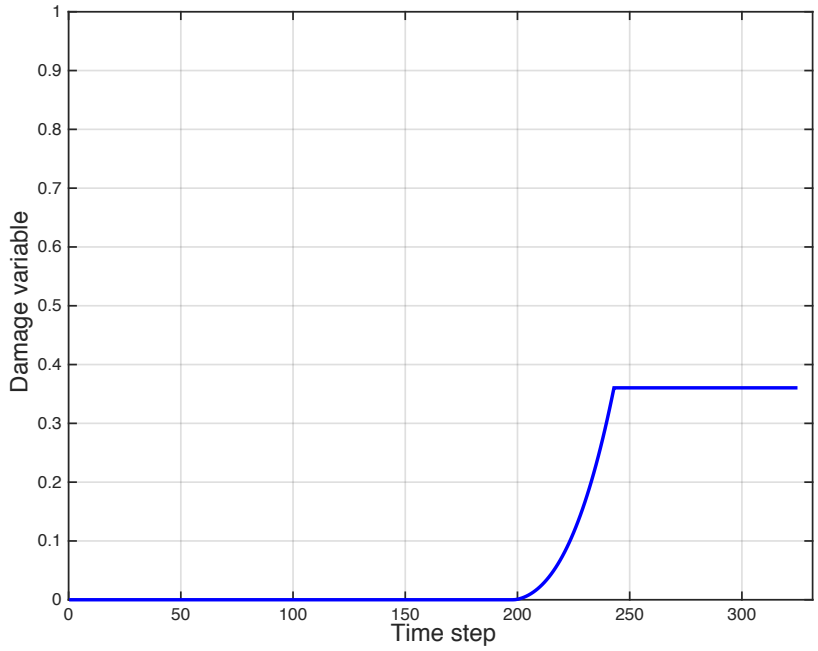

Figure 4.10 The history of damage evolution

4.7.2 The Splitting Tension Test

To validate the theoretical framework, a numerical simulation of splitting tension test is processed using finite element analysis software (ABAQUS). In the two-dimensional numerical simulations, various sizes of regular shapes, mostly circles and ellipsoids, are selected to represent the different size aggregates utilized in the asphalt concrete mixture. The majority of the existing literature follows the aforementioned two-dimensional framework, which either involves simple numerical procedure to select the center coordinate of each circle/ellipsoid with a specific aggregate size (Yin et al., 2015; K. Y. Yuan et al., 2014) or obtains the cross-sectional microstructure by CT scanning and image

processing (Bandyopadhyaya et al., 2008; Dai et al., 2006; H. Wang & Hao, 2011). By contrast, in a three-dimensional numerical simulation with random microstructures, an object-oriented programming language (such as Python and Fortran) has to be employed to appropriately define the three-dimensional coordinate of the center of each spherical particle with specific aggregate size. Further, it needs to ensure that these randomly generated spheres do not overlap. The numerical complexity of constructing random three-dimensional spheres is substantially higher than that of the two-dimensional numerical simulation with random circles.

The limited previous studies which involved three-dimensional numerical simulation mostly remained obtaining the microstructure with two-dimensional CT scanning and three-dimensional converting technique (Dai, 2011; Vadood et al., 2015; Zhang et al., 2011). There exists one research group who employed a similar random aggregates generation approach in their three-dimensional simulation (Absi et al., 2016; Tehrani et al., 2013) but their emphasis was on the influence of different modeling techniques on dynamic moduli of bituminous materials. Therefore, an aforementioned three-dimensional model needs to be constructed to simulate the elastic-damage behavior of the innovative material.

To simulate the real splitting tension test, where a 150mm Lottman breaking head was used in the direct tensile test to split the specimens by an MTS machine at room temperature ($25^{\circ}C \pm 0.5^{\circ}C$) , a displacement control compression along its vertical diameter direction is applied to the steel bar, which is then transmitted to the plywood, hence distributed onto

the cylindrical specimen evenly. The loading rate was 2 in. per minute so that the viscous effect can be ignored.

Shown as in Figure 4.11, the numerical model is a 3×4.5 in. cylinder cast with homogenized asphalt mastic matrix, with equivalent multilayer-coated spherical particles of three representative sizes randomly dispersed in the matrix. Figure 4.12 is a cross section cut along the plane direction, where the randomly dispersed coarse aggregates can be seen directly. The coarse aggregates are simulated as spherical particles for simplicity and three representative sizes (shown in white, maroon and deep blue) are chosen based on the degradation results of the D2 mix.

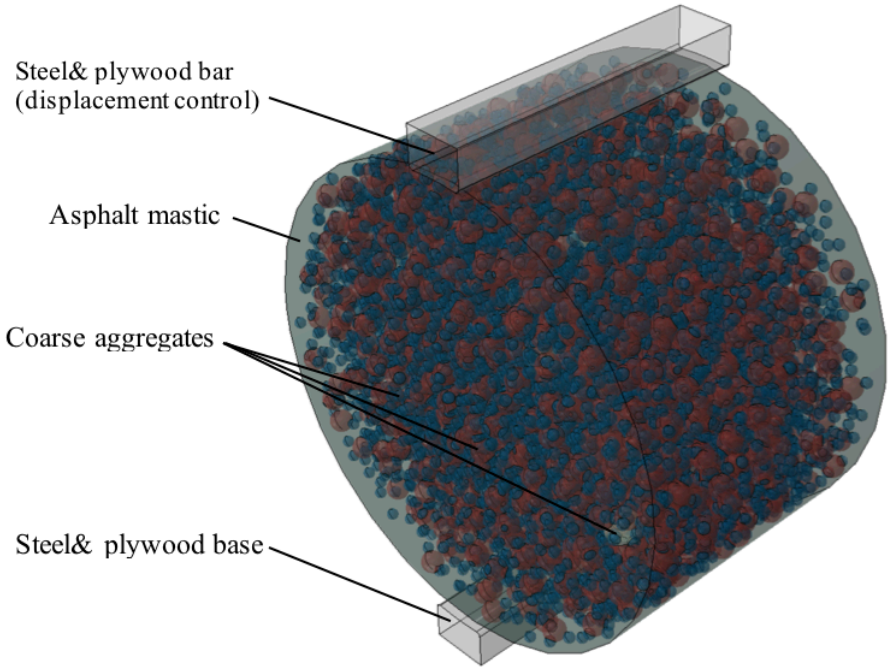

Figure 4.11 The numerical model of the cylindrical asphalt concrete specimen

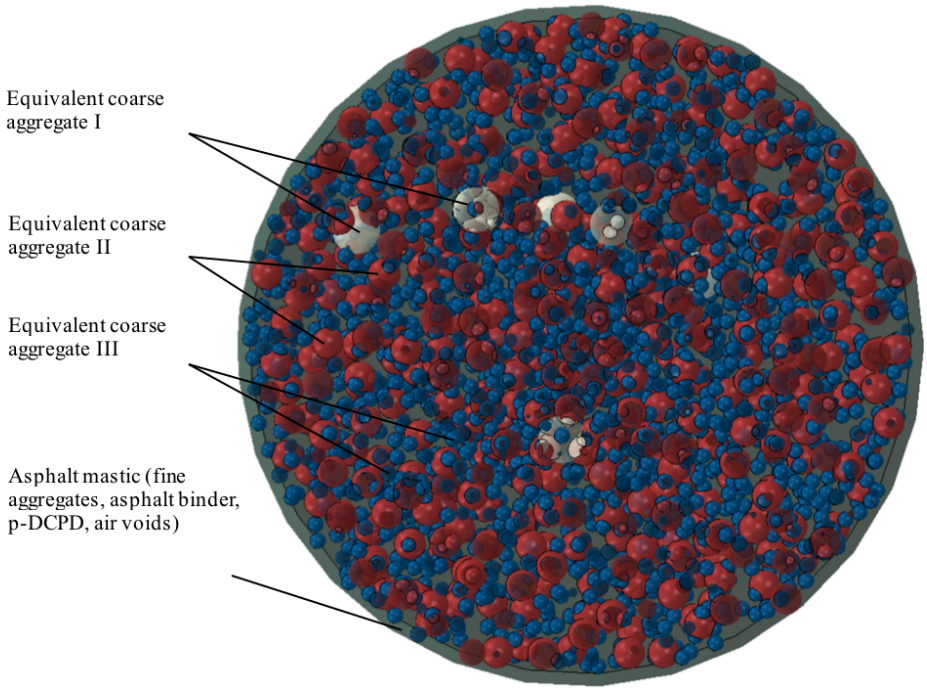

Figure 4.12 A cross section view of the numerical cylindrical model with spherical coarse aggregates of three representative sizes

The elastic properties and volume fraction of coarse aggregates and asphalt mastic in the innovative asphalt concrete specimens are tabulated in Table 4.1. The selection of representative volume element (RVE, i.e. the cylinder) size is in the order of 1000 times of the largest aggregate size, therefore, this RVE is statically representative and satisfies the size effect consideration.

Based on the volume fractions of the three representative aggregate particles, the numbers of each spherical particles are calculated and rounded up. 19 particles with a diameter of 0.4340, 1898 particles with a diameter of 0.2814, and 8639 particles with a diameter of 0.1409 are generated.

At the same time, we have to make sure the particles are randomly dispersed in the specimen, while do not collide with each other nor the surface of the cylinder. ABAQUS CAE alone cannot satisfy this demand. Hence Python scripting is employed to realize this goal. First the script randomly allocates a center origin to each particle with its (x,y,z) coordinates lie within the space of the cylinder. Then the center coordinate with a radius of the particle is calculated and compared with the center coordinates with the radii of all previous particles (and the surface of the cylinder), if the newly generated particle is judged as not colliding with all previous ones (nor the surface of the cylinder), the information of the new particle will be written down and passed on to ABAQUS to generate a new particle. Otherwise iteration will be done until a suitable location comes up.

The initial elastic strain energy based damage criterion is introduced to predict the progressive degradation experienced by the mechanical properties of materials prior to the increasing strain thus accumulated stress. Another phenomenon with increasing strain would be that material reaches yield point and performs its plastic behavior. Specifically, the Drucker-Prager yield criterion is picked for plasticity estimation. Table 2 listed the

material parameters that are used in the numerical simulation. The computational algorithm in Section 4.5.5 is realized with the assistant of Fortran UMAT interacting with ABAQUS.

Table 4.1 Material properties of constituents in the model

	Coarse Aggregate I	Coarse Aggregate II	Coarse Aggregate III	Asphalt Mastic
Global volume fraction (%)	0.746	20.885	11.934	
Diameter (*in*)	0.4340	0.2814	0.1409	
Specimen #1				
Young's modulus (*psi*)	3.3784e6	3.4149e6	2.2266e6	1.2827e5
Poisson's ratio	0.2604	0.2032	0.2055	0.2570
Specimen #2				
Young's modulus (*psi*)	3.4919e6	3.4215e6	2.2341e6	1.1937e5
Poisson's ratio	0.2524	0.2026	0.2045	0.2547

Table 4.2 Material parameters for damage evolution and yield function

Parameter	A	B	g_0	α	k
Value	0.0020	0.0133	4.7000	0.05	2000

Figure 4.13 compares the load-displacement curves from the numerical modeling and the experimental data. Four asphalt concrete specimens were tested in the experiment, two

with DCPD infiltrated and two without. It is clearly shown that the specimens with DCPD infiltrated in them can take almost two times larger the load comparing to the ones without DCPD. The predicted load-displacement responses show visible improvements over the elastic-damage framework in Chapter 3, where plasticity was not taken into consideration. The numerical simulations can fairly describe the experimental output from splitting tension tests.

While the elastoplastic mechanical behavior of the innovative material are discussed in this paper, the proposed framework cannot be directly applied to study the fatigue endurance of the innovative material, where loading is assumed to be dynamic and viscous behavior of asphalt should be considered. To fulfill this need, an isotropic elasto-viscoplastic-damage micromechanical framework will be discussed in the following chapter.

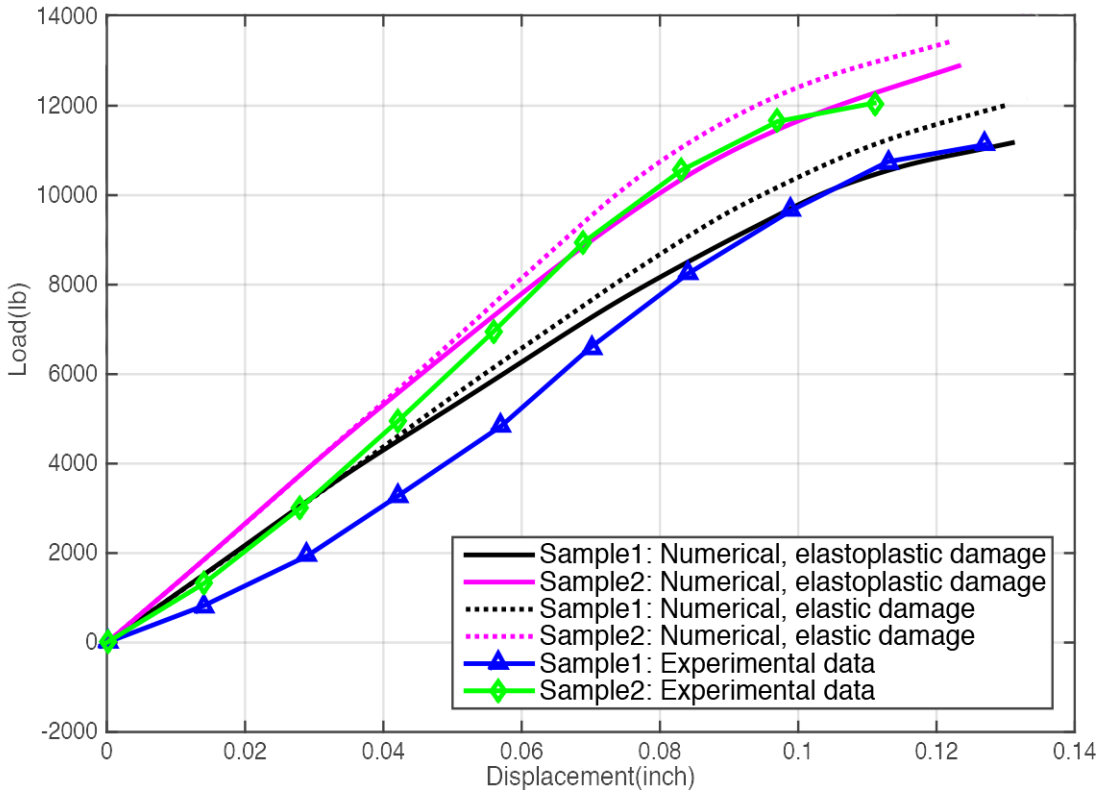

Figure 4.13 Load-displacement curves by experiments and numerical predictions (elastic-damage vs elastoplastic-damage framework)

4.8 References

Absi, J., Tehrani, F. F., Courreges, F., & Petit, C. (2016). *Mechanical Behavior of Asphalt Mixture Based on X-ray Computed Tomography Images and Random Generation of Aggregates Skeleton.* Paper presented at the 8th RILEM International Conference on Mechanisms of Cracking and Debonding in Pavements.

Ahmed, S., & Jones, F. R. (1990). A review of particulate reinforcement theories for polymer composites. *Journal of Materials Science, 25*(12), 4933-4942.

Bandyopadhyaya, R., Das, A., & Basu, S. (2008). Numerical simulation of mechanical behaviour of asphalt mix. *Construction and Building Materials, 22*(5), 1051-1058.

Benveniste, Y. (1987). A new approach to the application of Mori-Tanaka's theory in composite materials. *Mechanics of Materials, 6*(2), 147-157.

Chen, K., Yu, J., & Zhang, X. (2010). Micromechanical analysis of damage evolution in splitting test of asphalt mixtures. *Journal of Central South University of Technology, 17*(3), 628-634.

Coleman, B. D., & Gurtin, M. E. (1967). Thermodynamics with internal state variables. *Journal of Chemical Physics, 47*(2), 597-613.

Coleman, B. D., & Noll, W. (1963). The thermodynamics of elastic materials with heat conduction and viscosity. *Archive for Rational Mechanics and Analysis, 13*(1), 167-178.

Dai, Q. (2011). Two- and three-dimensional micromechanical viscoelastic finite element modeling of stone-based materials with X-ray computed tomography images. *Construction and Building Materials, 25*(2), 1102-1114.

Dai, Q., Sadd, M. H., & You, Z. (2006). A micromechanical finite element model for linearand damage-coupled viscoelastic behaviour of asphalt mixture. *International Journal for Numerical and Analytical Methods in Geomechanics, 30*(11), 1135-1158.

Drucker, D. C., & Prager, W. (1952). Soil Mechanics and Plastic Analysis or Limite Design. *Quarterly of Applied Mathematics, 10*, 157-175.

Edlund, U., & Klarbring, A. (1993). A coupled elastic-plastic damage model for rubber-modified epoxy adhesives. *International Journal of Solids and Structures, 30*(19), 2693-2708.

Hashin, Z. (1962). The elastic moduli of heterogeneous materials. *Journal of Applied Mechanics, 29*(2), 143-150.

Hashin, Z., & Shtrikman, S. (1961). Note on a variational approach to the theory of composite elastic materials. *Journal of the Franklin Institute, 274*(4), 336-341.

Hashin, Z., & Shtrikman, S. (1963). A variational approach to the theory of the elastic behaviour of multiphase materials. *Journal of the Mechanics and Physics of Solids, 11*(2), 127-140.

Jefferson, A. D. (1998). Plastic-Damage Model for Interfaces in Cementitious Materials. *Journal of Engineering Mechanics, ASCE, 124*(7), 775-782

Ju, J. W. (1989). On energy-based coupled elastoplastic damage theories-constitutive modeling and computational aspects. *International Journal of Solids and Structures, 25*(7), 803-833.

Ju, J. W., & Chen, T. M. (1994a). Effective elastic moduli of two-phase composites containing randomly dispersed spherical inhomogeneities. *Acta Mechanica, 103*(1-4), 123-144.

Ju, J. W., & Chen, T. M. (1994b). Micromechanics and effective moduli of elastic composites containing randomly dispersed ellipsoidal inhomogeneities. *Acta Mechanica, 103*(1-4), 103-121.

Ju, J. W., Ko, Y. F., & Zhang, X. D. (2009). Multi-level elastoplastic damage mechanics for elliptical fiber reinforced composites with evolutionary fiber debonding. *International Journal of Damage Mechanics, 18*(5), 419-460.

Ju, J. W., & Yanase, K. (2009). Micromechanical elastoplastic damage mechanics for elliptical fiber reinforced composites with progressive partial fiber debonding. *Journal of Damage Mechanics, 18*(7), 639-668.

Ju, J. W., & Yuan, K. Y. (2012). New strain-energy based coupled elastoplastic two-parameter damage and healing models for earth moving processes. *International Journal of Damage Mechanics, 21*(7), 989-1019.

Kelley, J. E., Jr. (1960). The cutting-plane method for solving convex programs. *Journal of the Society for Industrial & Applied Mathematics, 8*(4), 703–712.

Kiefer, B., Waffenschmidt, T., Sprave, L., & Menzel, A. (2018). A gradient-enhanced damage model coupled to plasticity—multi-surface formulation and algorithmic concepts. *International Journal of Damage Mechanics, 27*(2), 253-295.

Kim, S. M., & Abu Al-Rub, R. K. (2011). Meso-scale computational modeling of the plastic-damage response of cementitious composites. *Cement and Concrete Research, 41*(3), 339-358.

Ko, Y., & Ju, J. W. (2008). Micromechanical Elastoplastic Damage Modeling of Evolutionary Interfacial Arc Debonding for Fiber Reinforced Composites. *International Journal of Damage Mechanics, 14*(4), 307-356.

Kovačič, S., Matskob, N. B., Ferkc, G., & Slugovc, C. (2013). Macroporous poly(dicyclopentadiene) γFe2O3/Fe3O4 nanocomposite foams by high internal phase emulsion templating. *Journal of Materials Chemistry A, 1*, 7971-7978.

Lemaitre, J. (1985). A Continuous Damage Mechanics Model for Ductile Fracture. *Journal of Engineering Materials and Technology, 107*(1), 83-89.

Lubarda, V. A. (1994). An analysis of large-strain damage elastoplasticity. *International Journal of Solids and Structures, 31*(21), 2951-2964.

Lubliner, J., Oliver, J., Oller, S., & Oñate, E. (1989). A plastic-damage model for concrete. *International Journal of Solids and Structures, 25*(3), 299-326.

Mazars, J., & Lemaitre, J. (1985). Application of Continuous Damage Mechanics to Strain and Fracture Behavior of Concrete. In S. S.P. (Ed.), *Application of Fracture Mechanics to Cementitious Composites. NATO ASI Series (Series E: Applied Sciences)* (Vol. 94, pp. 507-520): Springer, Dordrecht.

Milan, J., & Zdenek, P. B. (2001). *Inelastic Analysis of Structures*: John Wiley& Sons.

Mori, T., & Tanaka, T. (1973). Average stress in matrix and average elastic energy of materials with misfitting inclusions. *Acta Metallurgica, 21*(5), 571-574.

Oller, S., Oñate, E., Miquel, J., & Botello, S. (1996). A plastic damage constitutive model for composite materials. *International Journal of Solids and Structures, 33*(17), 2501-2518.

Ortiz, M., & Simo, J. C. (1986). An analysis of a new class of integration algorithms for elastoplastic constitutive relations. *International Journal for Numerical Methods in Engineering, 23*(3), 353-366.

Shen, F., Hu, W., & Meng, Q. (2015). A damage mechanics approach to fretting fatigue life prediction with consideration of elastic–plastic damage model and wear. *Tribology International, 82*(A), 176-190.

Simo, J. C., & Hughes, T. J. R. (1998). *Computational Inelasticity*: Springer New York.

Simo, J. C., & Ju, J. W. (1987). Strain- and stress-based continuum damage model - I. Formulation. *International Journal of Solids and Structures, 23*(7), 821-840.

Simo, J. C., & Ortiz, M. (1985). A unified approach to finite deformation elastoplastic analysis based on the use of hyperelastic constitutive equations. *Computer Methods in Applied Mechanics and Engineering, 49*(2), 221-245.

Tehrani, F. F., Allou, F., Absi, J., & Petit, C. (2013). *Investigation on Mechanical Properties of Bituminous Materials through 2D/3D Finite Element Numerical Simulations.* Paper presented at the Multi-Scale Modeling and Characterization of Infrastructure Materials.

Tham, C. L., Zhang, Z., & Masud, A. (2005). An elasto-plastic damage model cast in a co-rotational kinematic framework for large deformation analysis of laminated composite shells. *Computer Methods in Applied Mechanics and Engineering, 194*(21-24), 2641-2660.

Vadood, M., Johari, M. S., & Rahai, A. R. (2015). A new approach for simulation of hot mix asphalt; numerical and experimental. *Journal of Mechanics, 31*(6), 701-711.

Vallons, K., Drozdzak, R., Charret, M., & Lomov, S. (2015). *Damage development in woven glass fibre composites with tough thermoset matrix*. Paper presented at the TexComp-12, Raleigh, NC.

Voyiadjis, G. Z., Taqieddin, Z. N., & Kattan, P. (2008). Theoretical Formulation of a Coupled Elastic—Plastic Anisotropic Damage Model for Concrete using the Strain Energy Equivalence Concept. *International Journal of Damage Mechanics, 18*(7), 603-638.

Wang, H., & Hao, P. (2011). Numerical simulation of indirect tensile test based on the microstructure of asphalt mixture. *Journal of Materials in Civil Engineering, 23*(1), 21-29.

Wang, Y., Zhang, L., Sun, J., Bao, J. B., Wang, Z., & Ni, L. (2017). Dramatic Toughness Enhancement of Polydicyclopentadiene Composites by Incorporating Low Amounts of Vinyl-Functionalized SiO2. *Industrial & Engineering Chemistry Research, 56*(16), 4750-4757.

Wu, Y., & Ju, J. W. (2017). Elastoplastic damage micromechanics for continuous fiber-reinforced ductile matrix composites with progressive fiber breakage. *International Journal of Damage Mechanics, 26*(1), 4-28.

Yin, A. Y., Yang, X. H., Zeng, G. W., & Gao, H. (2015). Experimental and numerical investigation of fracture behavior of asphalt mixture under direct shear loading. *Construction and Building Materials, 86*, 1.

Yuan, K. Y., Ju, J. W., Yuan, W., & Yang, J. M. (2014). Numerical predictions of mechanical behavior of innovative pothole patching materials featuring high

toughness, low-viscosity nano-molecular resins. *Acta Mechanica, 225*(4-5), 1141-1151.

Zhang, X., Wan, C., Wang, D., & He, L. (2011). Numerical simulation of asphalt mixture based on three-dimensional heterogeneous specimen. *Journal of Central South University of Technology, 18*(6), 2201-2206.

Zhu, H., & Sun, L. (2013). A viscoelastic–viscoplastic damage constitutive model for asphalt mixtures based on thermodynamics. *International Journal of Plasticity, 40*, 81-100.

CHAPTER 5 : MICROMECHANICS-BASED ISOTROPIC THERMO-ELASTO-VISCOPLASTIC-DAMAGE FRAMEWORK OF ASPHALT CONCRETE MATERIALS FEATURING HIGH TOUGHNESS, LOW VISCOSITY NANO-MOLECULAR RESINS

5.1 Introduction

Asphalt concrete materials have been widely used in pavement construction since the beginning of the twentieth century. In the meanwhile, a lot of investigations have been done to characterize the structural and mechanical behavior of the asphalt concrete. Various models were proposed to estimate the modulus of asphalt concrete (Christensen Jr et al., 2003; Khazanovich, 2008; Y. R. Kim & Little, 1990, 2004; H. J. Lee & Kim, 1998; Roque & Buttlar, 1992; Tashman et al., 2005). Continuum damage mechanics were introduced to viscoelastic and viscoplastic models to predict the fatigue characterizations (Chehab et al., 2003; Y. R. Kim et al., 1997; H. J. Lee et al., 2000; Park et al., 1996). Numerical models were established to characterize the behavior of the asphalt concrete mixtures under different loading conditions (Buttlar & You, 2001; Dai et al., 2006; H. W. Kim & Buttlar, 2009; Scarpas et al., 1997; You & Buttlar, 2004). Other aspects such as temperature effect, induction healing and influence of aggregates are also broadly studied (Abu Al-Rub et al.,

2010; Button et al., 1990; Chehab et al., 2002; García et al., 2013; Hong et al., 2017; Q. Liu et al., 2011; Si et al., 2002).

The current chapter proposed an isotropic thermo- elasto-viscoplastic model to evaluate the time-dependent mechanical behavior of an innovative asphalt concrete material featuring high toughness, low viscosity nano-molecular resins. By taking advantage of the proposed isotropic elastic/elastoplastic damage frameworks in Chapter 3 and 4, and considering the viscosity behavior of asphalt mastic, a class of temperature sensitive viscoplastic damage model is proposed within an initial elastic strain energy-based continuum thermodynamic framework.

Same concept of breaking down the asphalt concrete composites into an effective asphalt mastic matrix and spherical inhomogeneities are applied in the beginning of setting up the model. The Laplace domain is introduced to apply the multilevel homogenization approach to evaluate the viscoelastic mechanical properties of the 4-phase asphalt mastic. The governing damage evolution is characterized through the effective stress concept in conjunction with the hypothesis of strain equivalence; the viscoplastic flow is introduced by means of an additive split of the stress tensor. An Arrhenius-type temperature term, which is uncoupled with the Helmholtz free energy potential, is proposed to account for the effect of temperature. Corresponding computational algorithms are implemented to numerical simulations.

5.2 Micromechanical Frameworks for Coarse Aggregates and Asphalt Mastic

The innovative asphalt concrete materials can be decomposed into two parts: matrix and inhomogeneities, respectively: 1). asphalt mastic containing fine aggregates, asphalt binder (PG 64-10), polymerized DCPD and air voids, 2). coarse aggregates, as illustrated in Figure 5.1. The overall viscoelastic properties of four-phase asphalt mastic composites are appropriately transformed into the Laplace domain based on the correspondence principle, making it possible to homogenize the transformed elastic moduli by the multilevel homogenization approach proposed and validated in Chapter 3 and 4. The homogenized asphalt mastic is then treated as an isotropic matrix, while the equivalent multilayer-coated spherical inclusions are randomly dispersed in the matrix. The coarse aggregates are represented by spherical multilayer-coated particles in three sizes and randomly disposed in the matrix.

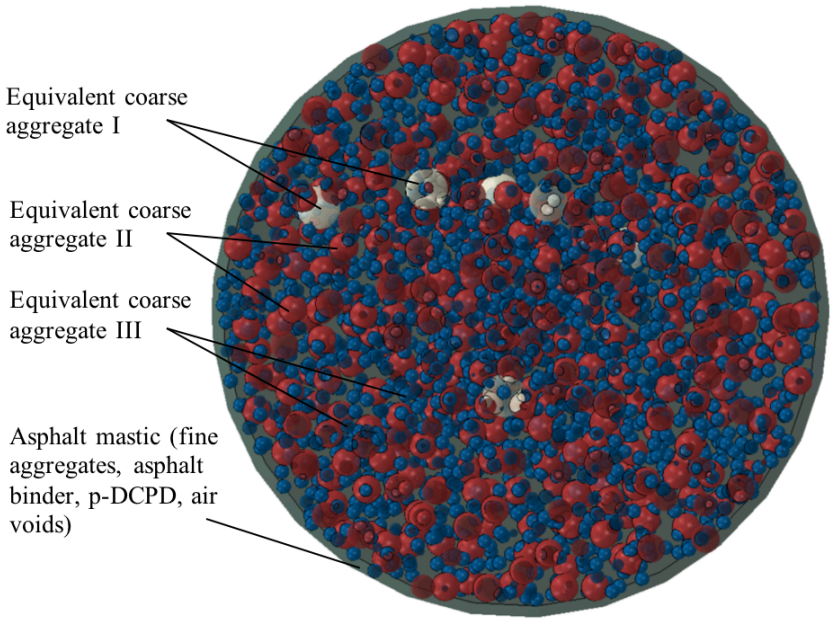

Figure 5.1 The illustration of the proposed micromechanical framework concept (cross sectional view)

5.2.1 Equivalent Multilayer-coated Spherical Particles

To simplify the simulation and also take into consideration of the caging effect of the p-DCPD network, the irregular coarse aggregates are replaced and simulated by multilayer-coated spherical particles of three representative sizes, as demonstrated in Figure 5.2. Given the fact that p-DCPD is a comparatively brittle and rigid material (Kovačič et al., 2013; Vallons et al., 2015; Y. Wang et al., 2017), and it's wrapped at the outer layer of the particle, it is reasonable for us to assume that the multilayer-coated particles behave mainly their elasticity not plasticity nor viscosity.

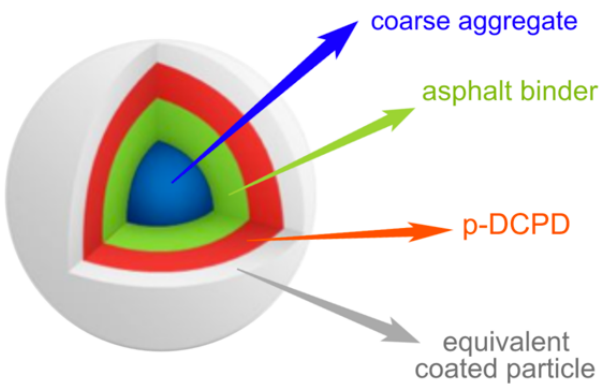

Figure 5.2 The schematic illustration of an equivalent multilayer-coated spherical particle

The analytical solution of elastic properties for the multilayer-coated spherical particle can be derived starting from the elastic problem of a 3-D spherical shell under both internal and external pressures and the concept of continuity conditions at interfaces between layers. The effective Young's modulus E_0 and Poisson's ratio υ_0 of an equivalent multilayer-coated particle of a certain size are given as Eqn. (5.1) and (5.2) whereas the detailed derivation can be found in Chapter 3.

$$E_0 = E_1 \frac{1-2\upsilon_0}{1-2\upsilon_1} \frac{Ca^3\left(2Ab^3+2Bc^3\right)+Nb^3\left(Dc^3+2Mb^3\right)}{Ca^3\left(\Lambda Ab^3+2Bc^3\right)+Nb^3\left(Dc^3+\Lambda Mb^3\right)} \tag{5.1}$$

$$\upsilon_0 = \frac{\upsilon_1 f_1 E_1 + \upsilon_2 f_2 E_2 + \upsilon_3 f_3 E_3}{f_1 E_1 + f_2 E_2 + f_3 E_3} \tag{5.2}$$

where

$$
\begin{aligned}
A &= E_1\left(1+\upsilon_2\right)+2E_2\left(1-2\upsilon_1\right)\\
B &= E_2\left(1+\upsilon_1\right)-E_1\left(1+\upsilon_2\right)\\
C &= E_3\left(1-2\upsilon_2\right)-E_2\left(1-2\upsilon_3\right)\\
D &= E_2\left(1+\upsilon_1\right)+2E_1\left(1-2\upsilon_2\right)\\
M &= E_2\left(1-2\upsilon_1\right)-E_1\left(1-2\upsilon_2\right)\\
N &= E_3\left(1+\upsilon_2\right)+2E_2\left(1-2\upsilon_3\right)\\
\Lambda &= -\frac{1+\upsilon_1}{1-2\upsilon_1}
\end{aligned}
$$

E_1, E_2, E_3, υ_1, υ_2, υ_3, f_1, f_2 and f_3 denote the Young's moduli, Poisson's ratios and local volume fractions of p-DCPD, asphalt binder and coarse aggregate, respectively; a is the radius (size) of the coarse aggregate. b and c are radii related to the thicknesses of p-DCPD layer and asphalt binder layer whose values can be calculated by the following formulas

$$
\begin{aligned}
\frac{\sum_{i=1}^{n} f_{3i}\left[\left(a_i+t_2\right)^3-a_i^3\right]}{\sum_{i=1}^{n} f_{3i}\left(a_i+t_2\right)^3} &= \frac{f_2}{f_2+f_3}\\
\frac{\sum_{i=1}^{n} f_{3i}\left[\left(a_i+t_1+t_2\right)^3-\left(a_i+t_2\right)^3\right]}{\sum_{i=1}^{n} f_{3i}\left(a_i+t_1+t_2\right)^3} &= \frac{f_1}{f_1+f_2+f_3}
\end{aligned}
\tag{5.3}
$$

$$
\begin{aligned}
b_i &= t_2+a_i\\
c_i &= t_1+b_i
\end{aligned}
\tag{5.4}
$$

Notice that for different sizes of coarse aggregates, the thicknesses of asphalt binder and p-DCPD layers are assumed to remain the same, while radii b and c vary based on sizes of coarse aggregate. Three representative sizes of coarse aggregates are picked in this simulation based on the aggregates gradation result of the proposed D2 mix.

5.2.2 The Multilevel Homogenization Approach in Laplace Domain

Asphalt mastic, composed by fine aggregates, asphalt binder, p-DCPD and air voids, is a composite material. To simplify the analysis, the heterogeneous asphalt mastic whose viscoelastic properties are functions with respect to time can be reduced (transformed) into elastic moduli in Laplace domain, and represented by an equivalent homogeneous continuum media with appropriately defined effective properties.

Based on the comparisons made in Chapter 3 among these different approaches, it is trustworthy to pick Ju and Chen's pairwise interacting solution (Ju & Chen, 1994a, 1994b) to predict the effective transformed elastic moduli of the asphalt mastic matrix. In particular, the pairwise interacting solution may lead to an accurate higher-order formulation for the prediction of elastic particulate composites at moderately high particle concentrations. Ju and Chen's elastic formulation for a two-phase (inclusions and matrix) composite states that, if the inclusions (particles) are assumed to be identical and spherical in an elastic matrix, the effective bulk modulus K^* and effective shear modulus μ^* of this composite can be explicitly evaluated as

$$K^* = K_0\left[1+\frac{30\left(1-\upsilon_0\right)f_1\left(3\gamma_1+2\gamma_2\right)}{3\alpha+2\beta-10\left(1+\upsilon_0\right)f_1\left(3\gamma_1+2\gamma_2\right)}\right] \tag{5.5}$$

$$\mu^* = \mu_0\left[1+\frac{30\left(1-\upsilon_0\right)f_1\gamma_2}{\beta-4\left(4-5\upsilon_0\right)f_1\gamma_2}\right] \tag{5.6}$$

where

$$\gamma_1 = \frac{5f_1}{96\beta^2}\left\{12\upsilon_0\left(13-14\upsilon_0\right)-\frac{96\alpha}{3\alpha+2\beta}\left(1-2\upsilon_0\right)\left(1+\upsilon_0\right)\right\}$$

$$\gamma_2 = \frac{1}{2}+\frac{5f_1}{96\beta^2}\left\{6\left(25-34\upsilon_0+22\upsilon_0{}^2\right)-\frac{36\alpha}{3\alpha+2\beta}\left(1-2\upsilon_0\right)\left(1+\upsilon_0\right)\right\}$$

and

$$\alpha = 2\left(5\upsilon_0-1\right)+10\left(1-\upsilon_0\right)\left(\frac{K_0}{K_1-K_0}-\frac{\mu_0}{\mu_1-\mu_0}\right)$$

$$\beta = 2\left(4-5\upsilon_0\right)+15\left(1-\upsilon_0\right)\frac{\mu_0}{\mu_1-\mu_0}$$

Subscript 0 denotes the matrix and 1 denotes the particles, υ_0 is Poisson's ratio of the matrix and f_1 is the volume fraction of the particles.

Something about Laplace transform, domain.

Corresponding to these elastic expressions, and with the assumptions that particles remain elastic while the matrix is viscoelastic in shear but elastic in volume, we would have the effective bulk and shear moduli in the transformed domain are:

$$K^*\left(s\right) = K_0\left[1+\frac{30\left(1-\upsilon_0\right)f_1\left(3\gamma_1^s+2\gamma_2^s\right)}{3\bar{\alpha}\left(s\right)+2\bar{\beta}\left(s\right)-10\left(1+\upsilon_0\right)f_1\left(3\gamma_1^s+2\gamma_2^s\right)}\right] \tag{5.7}$$

$$\mu^*\left(s\right) = \bar{\mu}_0\left(s\right)\left[1+\frac{30\left(1-\upsilon_0\right)f_1\gamma_2^s}{\bar{\beta}\left(s\right)-4\left(4-5\upsilon_0\right)f_1\gamma_2^s}\right] \tag{5.8}$$

where

$$\gamma_1^s = \frac{5f_1}{96\bar{\beta}\left(s\right)^2}\left\{12\upsilon_0\left(13-14\upsilon_0\right)-\frac{96\bar{\alpha}\left(s\right)}{3\bar{\alpha}\left(s\right)+2\bar{\beta}\left(s\right)}\left(1-2\upsilon_0\right)\left(1+\upsilon_0\right)\right\}$$

$$\gamma_2^s = \frac{1}{2}+\frac{5f_1}{96\bar{\beta}\left(s\right)^2}\left\{6\left(25-34\upsilon_0+22\upsilon_0{}^2\right)-\frac{36\bar{\alpha}\left(s\right)}{3\bar{\alpha}\left(s\right)+2\bar{\beta}\left(s\right)}\left(1-2\upsilon_0\right)\left(1+\upsilon_0\right)\right\}$$

and

$$\bar{\alpha}(s) = 2(5\upsilon_0 - 1) + 10(1-\upsilon_0)\left(\frac{K_0}{K_1 - K_0} - \frac{\bar{\mu}_0(s)}{\mu_1 - \bar{\mu}_0(s)}\right)$$

$$\bar{\beta}(s) = 2(4 - 5\upsilon_0) + 15(1-\upsilon_0)\frac{\bar{\mu}_0(s)}{\mu_1 - \bar{\mu}_0(s)}$$

Notice that $\bar{\mu}_0(s)$ is the shear modulus of the matrix in Laplace domain with reference to μ_0 in elasticity and the expression of $\bar{\mu}_0(s)$ depends on the viscoelastic model one used.

Eqn. (5.7) and (5.8) are valid for two-phase composites yet the proposed asphalt mastic is a four-phase composite. In order to use the pairwise interacting solution, a multilevel homogenization procedure is established, illustrated in Figure 5.3. A comparison of effective elastic moduli of an interim asphalt mastic (neglecting air voids) and final state asphalt mastic (with air voids) calculated by Eqn. (5.5) and (5.6) based on the aforementioned multilevel homogenization procedure and those by Hashin-Shtrikman bounds have proved the multilevel homogenization to be reasonable (Figure 3.16, Table 3.10, 3.11).

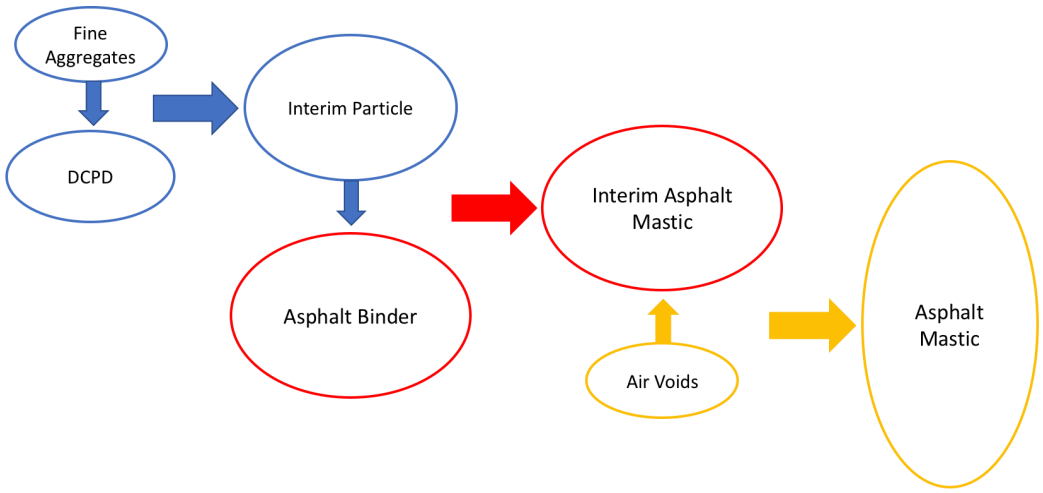

Figure 5.3 The multilevel homogenization procedure to apply Ju and Chen's pairwise interacting solution

5.3 The Initial Elastic Strain Energy Based Isotropic Damage Evolution

As stated in previous chapters, the definition of damage in our approach can be described as the separation of portions of materials due to the breaking of bonding or cohesion between portions by local tension which leads to the partial or complete loss of elastic stiffness. A class of damage evolution criterion, based on a continuum damage mechanics framework, is proposed within an initial elastic strain energy based formulation.

General form to satisfy Kuhn-Tucker condition:

$$\begin{cases} \dot{d}_t = \dot{\mu}\mathrm{H}\left(\xi_t^+, d_t\right) \\ \dot{g}_t = \dot{\mu} \\ \dot{\mu} \geq 0, \;\; \phi^d(\xi_t^+, g_t) \equiv \xi_t^+ - g_t \leq 0, \;\; \dot{\mu}\phi^d(\xi_t^+, g_t) = 0 \end{cases} \tag{5.9}$$

where $\dot{\mu}$ is the damage consistency parameter that defines the damage loading/unloading conditions according to the Kuhn-Tucker relations; ϕ^d describes the current damage criterion, or in other words, the damage surface; g_t is the damage threshold at the current time t; $\mathrm{H}\left(\xi_t^+, d_t\right)$ is the damage hardening function which yields a unit scalar in the elastic-damage case; and ξ_t^+ is the equivalent tensile strain energy norm which is defined as (Lemaitre, 1985; Mazars & Lemaitre, 1985):

$$\xi^+ \equiv \sqrt{\frac{1}{2}\boldsymbol{\varepsilon}^+ : \mathbf{C}^0 : \boldsymbol{\varepsilon}^+} \tag{5.10}$$

The tensile strain tensor $\boldsymbol{\varepsilon}^+ = \mathbf{P}^+ : \boldsymbol{\varepsilon}$ and $\mathbf{P}^+$ is the Mode I tensile projection tensor which can be calculated by following equations:

$$\mathbf{P}^+_{ijkl}(\boldsymbol{\varepsilon}) \equiv \frac{1}{2}\left(\mathbf{Q}^+_{ik}\mathbf{Q}^+_{jl} + \mathbf{Q}^+_{il}\mathbf{Q}^+_{jk}\right) \tag{5.11}$$

$$\mathbf{Q}^+ \equiv \sum_{i=1}^{3}\left\langle \lambda^i \right\rangle\left(\mathbf{p}_i \otimes \mathbf{p}_i\right) \tag{5.12}$$

$$\boldsymbol{\varepsilon} = \sum_{i=1}^{3}\lambda^i\left(\mathbf{p}_i \otimes \mathbf{p}_i\right) \tag{5.13}$$

where $\left|\mathbf{p}_i\right| = 1$ and $2\langle\lambda^i\rangle = \left(\lambda^i + \left|\lambda^i\right|\right)$.

An isotropic elastic-damage evolution function is proposed in Chapter 3.

$$d_t = A\ \exp\left[B\ \xi_t^+\left(\xi_t^+ - g_0\right)\right] \tag{5.14}$$

where g_0 is the initial tensile damage threshold (g_t at t=0) and A, B are characteristic parameters of the material.

5.4 The Effective Elasto-viscoplastic Behavior of the Innovative Material

5.4.1 The Additive Stress Split

Within the present strain space framework, the viscoplastic flow is introduced by means of an additive split of the stress tensor into initial and inelastic parts by following the same concept within the effective space of plasticity (Simo & Ju, 1987), i.e.

$$\bar{\boldsymbol{\sigma}} = \frac{\partial \Psi^0(\boldsymbol{\varepsilon})}{\partial \boldsymbol{\varepsilon}} - \bar{\boldsymbol{\sigma}}^{vp} \tag{5.15}$$

where $\bar{\boldsymbol{\sigma}}$ is the effective stress, $\boldsymbol{\varepsilon}$ is the total strain, $\Psi^0(\boldsymbol{\varepsilon})$ is the initial elastic stored energy function of the undamaged material, and $\bar{\boldsymbol{\sigma}}^{vp}$ denotes the effective viscoplastic relaxation stress. For linear elasticity, we write

$$\Psi^0(\boldsymbol{\varepsilon}) = \frac{1}{2}\boldsymbol{\varepsilon} : \mathbf{C}^0 : \boldsymbol{\varepsilon} \tag{5.16}$$

where $\mathbf{C}^0$ denotes the linear elasticity tensor. Eqn. (4.55) then can be written as the following equation

$$\bar{\boldsymbol{\sigma}} = \mathbf{C}^0 : \boldsymbol{\varepsilon} - \bar{\boldsymbol{\sigma}}^{vp} \tag{5.17}$$

5.4.2 The Thermodynamic Basis

In order to introduce the damage effect and viscoplastic flow processes, a free energy potential of the following form is proposed

$$\Psi(\boldsymbol{\varepsilon}, \boldsymbol{\sigma}^p, \mathbf{q}, d, T) \equiv \kappa(T)\left\{(1-d)\Psi^0(\boldsymbol{\varepsilon}) - \boldsymbol{\varepsilon} : \boldsymbol{\sigma}^{vp} + \Xi(\mathbf{q}, \boldsymbol{\sigma}^{vp})\right\} \tag{5.18}$$

where $\boldsymbol{\varepsilon}$ denotes the total strain tensor, $\boldsymbol{\sigma}^{vp}$ is the viscoplastic relaxation stress tensor, $\mathbf{q}$ is a suitable set of internal (viscoplastic) variables. Further, d defines the isotropic scalar damage variable between 0 and 1 (or a maximum damage threshold less than 1) whose function has been discussed in (Section 5.3). $\Psi^0\left(\boldsymbol{\varepsilon}\right)$ is the initial elastic stored energy function of the undamaged material, and $\Xi\left(\mathbf{q},\sigma^{vp}\right)$ is the viscoplastic potential function. Furthermore, $\kappa\left(T\right)$ is a modified Arrhenius-type temperature dependent factor that accounts for the temperature effect to the viscosity of materials. The factor is properly defined as follows so that it is uncoupled with the Helmholtz free energy potential

$$\kappa\left(T\right)=\alpha\exp\left\{-\left(\frac{T_0}{T}\right)^{\beta}\right\} \tag{5.19}$$

where α is a positive pre-exponential factor, which can be treated as a material constant; β is a dimensionless correction factor in the order of 1; T is the current temperature while T_0 is the reference temperature.

Confining our attention to the purely mechanical theory, the Clausius-Plank reduced dissipation inequality for purely mechanical isothermal theory takes the form for any admissible process

$$-s\dot{T}-\dot{\Psi}+\boldsymbol{\sigma}:\dot{\boldsymbol{\varepsilon}}\geq 0 \tag{5.20}$$

By taking the time derivative of Eqn. (4.58), substituting it into Eqn. (4.59), and making use of the classical Coleman-Noll argument (Coleman & Noll, 1963) and its variation, the Coleman-Gurtin theory (Coleman & Gurtin, 1967) along with the additional

assumption that the damage effect and viscoplastic unloading are elastic processes, we can obtain the stress-strain constitutive law

$$\boldsymbol{\sigma} = \frac{\partial \Psi(\boldsymbol{\varepsilon})}{\partial \boldsymbol{\varepsilon}} = \kappa(T)\left\{(1-d)\frac{\partial \Psi^0(\boldsymbol{\varepsilon})}{\partial \boldsymbol{\varepsilon}} - \boldsymbol{\sigma}^{vp}\right\} = \kappa(T)(1-d)\bar{\boldsymbol{\sigma}} \tag{5.21}$$

and the dissipative inequalities

$$\kappa(T)\left\{-\frac{\partial \Xi}{\partial \mathbf{q}} \bullet \dot{\mathbf{q}} - \left(\frac{\partial \Xi}{\partial \boldsymbol{\sigma}^{p}} - \boldsymbol{\varepsilon}\right) : \dot{\boldsymbol{\sigma}}^{vp}\right\} \geq 0 \tag{5.22}$$

$$\kappa(T)\left\{\Psi^0(\boldsymbol{\varepsilon})\dot{d} - \frac{\partial \Xi}{\partial \mathbf{q}} \bullet \dot{\mathbf{q}} - \left(\frac{\partial \Xi}{\partial \boldsymbol{\sigma}^{vp}} - \boldsymbol{\varepsilon}\right) : \dot{\boldsymbol{\sigma}}^{vp}\right\} \geq 0 \tag{5.23}$$

and the entropy

$$s = -\frac{\partial \boldsymbol{\Psi}(\boldsymbol{\varepsilon}, \boldsymbol{\sigma}^{vp}, \mathbf{q}, d, T)}{\partial T} = -\frac{\partial \kappa(T)}{\partial T}\boldsymbol{\Psi}(\boldsymbol{\varepsilon}, \boldsymbol{\sigma}^{vp}, \mathbf{q}, d) \tag{5.24}$$

It follows from Eqn. (4.60) that within the present strain space formulation, the stress tensor is split into the elastic-damage part and the viscoplastic relaxation part. From Eqn. (4.61) and (4.62), we observe that the dissipative energy by viscoplasticity itself is positive (since the temperature dependent factor is always positive); if damage effect is involved, the sum of damage and viscoplasticity effect is also positive. It is also noted from Eqn. (4.60)-(4.62) that the present framework is capable of accommodating general (nonlinear) elastic response and general viscoplastic response.

The potential $\Xi(\mathbf{q}, \boldsymbol{\sigma}^{vp})$ is linked to viscoplastic dissipation. Its role is such that inequality (4.62) is satisfied for arbitrary processes. Note that we have assumed that the

potential $\Xi\left(\mathbf{q},\boldsymbol{\sigma}^{vp}\right)$ is independent of damage variable d. From Eqn. (4.58), it then follows that

$$-Y \equiv -\frac{\partial \Psi\left(\boldsymbol{\varepsilon},\boldsymbol{\sigma}^{vp},\mathbf{q},d,T\right)}{\partial d} = \kappa\left(T\right)\Psi^{0}\left(\boldsymbol{\varepsilon}\right) \tag{5.25}$$

Hence, the initial (undamaged) elastic strain energy $\Psi^{0}\left(\boldsymbol{\varepsilon}\right)$ is the thermodynamic force Y conjugate to the damage variable d.

5.4.3 Characterization of Effective Plastic Response and Tangent Moduli

In accordance with the notion of effective stress, the characterization of the viscoplastic response should be formulated in effective stress space in terms of effective stresses $\bar{\boldsymbol{\sigma}}$ and $\bar{\boldsymbol{\sigma}}^{vp}$. Therefore, for the classical situation in which the yield function is postulated in the stress space, we replace the homogenized Cauchy stress tensor $\boldsymbol{\sigma}$ by the effective stress tensor $\bar{\boldsymbol{\sigma}}$, so that the elastic-damage domain is characterized by $f\left(\bar{\boldsymbol{\sigma}},\mathbf{q}\right)\leq 0$, where $\mathbf{q}$ represents the internal viscoplastic variables whose evolution will be defined below. A general Perzyna type viscoplasticity assumed that the flow function is a function of loading function in the form of $g\left(f\right)=f^{m}$ (Perzyna, 1966). With the assumption of a general non-associative flow rule, rate-dependent viscoplastic response is characterized in the strain space by the flowing constitutive equations (Simo & Ju, 1987)

$$\dot{\bar{\boldsymbol{\sigma}}}^{vp} = \dot{\lambda}\frac{\partial g_P}{\partial \boldsymbol{\varepsilon}}\left(\frac{\partial \Psi^0(\boldsymbol{\varepsilon})}{\partial \boldsymbol{\varepsilon}} - \bar{\boldsymbol{\sigma}}^{vp}, \mathbf{q}\right) \quad \textit{(non-associative flow rule)} \tag{5.26}$$

$$\dot{\mathbf{q}} = \dot{\lambda}\mathbf{h}\left(\frac{\partial \Psi^0(\boldsymbol{\varepsilon})}{\partial \boldsymbol{\varepsilon}} - \bar{\boldsymbol{\sigma}}^{vp}, \mathbf{q}\right) \quad \textit{(viscoplastic hardening law)} \tag{5.27}$$

$$f\left(\frac{\partial \Psi^0(\boldsymbol{\varepsilon})}{\partial \boldsymbol{\varepsilon}} - \bar{\boldsymbol{\sigma}}^{vp}, \mathbf{q}\right) \le 0 \quad \textit{(loading function)} \tag{5.28}$$

where $\dot{\bar{\boldsymbol{\sigma}}}^{vp}$ denotes the viscoplastic relaxation effective stress rate tensor, g_P signifies the viscoplastic potential function, $\mathbf{h}$ signifies the hardening law, and $\dot{\lambda}$ denotes the viscoplastic consistency parameter which is defined as

$$\dot{\lambda} = \frac{1}{\eta}\left\langle g\left(f\left(\frac{\partial \Psi^0(\boldsymbol{\varepsilon})}{\partial \boldsymbol{\varepsilon}} - \bar{\boldsymbol{\sigma}}^{vp}, \mathbf{q}\right)\right)\right\rangle \tag{5.29}$$

where $\eta \in (0,\infty)$ is the viscosity parameter or fluidity parameter, $g(f)$ is the flow function mentioned previously, $\langle\ \rangle$ is the McAuley bracket. If $\eta \to 0$ (no viscosity), we recover the rate-independent plasticity, i.e., as $\eta \to 0$, $f \to 0$ such that $\frac{1}{\eta}\langle g(f)\rangle \to \dot{\lambda}$ is finite. If $\eta \to \infty$ (huge viscosity), then $\dot{\lambda} = \frac{1}{\eta}\langle g(f)\rangle \to 0$, i.e., $\bar{\boldsymbol{\sigma}}^{vp} = 0$ and $\mathbf{q} = 0$, which yields instantaneous elasticity.

Eqn. (4.64)-(5.29) provide a characterization of viscoplasticity in the strain space. Loading/unloading conditions may be expressed in a compact form by requiring that

$$f\left(\frac{\partial \Psi^0(\boldsymbol{\varepsilon})}{\partial \boldsymbol{\varepsilon}} - \bar{\boldsymbol{\sigma}}^{vp}, \mathbf{q}\right) \le 0, \quad \dot{\lambda} \ge 0, \quad \dot{\lambda} f\left(\frac{\partial \Psi^0(\boldsymbol{\varepsilon})}{\partial \boldsymbol{\varepsilon}} - \bar{\boldsymbol{\sigma}}^{vp}, \mathbf{q}\right) = 0 \tag{5.30}$$

Note that if $f<0$, then $\dot{\lambda}=0$ and the process is elastic-damage. On the other hand, for viscoplastic loading, $\dot{\lambda}>0$ and $f=0$. In the latter case, $\dot{\lambda}$ is determined by requiring that $\dot{f}=0$. Making use of Eqn. (4.55) during loading, one has

$$\frac{\partial f}{\partial \bar{\boldsymbol{\sigma}}}:\dot{\bar{\boldsymbol{\sigma}}}+\frac{\partial f}{\partial \mathbf{q}}\bullet\dot{\mathbf{q}}=0 \tag{5.31}$$

where $\dfrac{\partial f}{\partial \bar{\boldsymbol{\sigma}}}$ denotes the partial derivative of $f\left(\dfrac{\partial \Psi^0(\boldsymbol{\varepsilon})}{\partial \boldsymbol{\varepsilon}}-\bar{\boldsymbol{\sigma}}^{vp},\mathbf{q}\right)$ with respect to the first argument. From Eqn. (4.60) we obtain

$$\dot{\bar{\boldsymbol{\sigma}}}=\frac{\partial^2\Psi^0(\boldsymbol{\varepsilon})}{\partial \boldsymbol{\varepsilon}^2}:\dot{\boldsymbol{\varepsilon}}-\dot{\bar{\boldsymbol{\sigma}}}^{vp}=\frac{\partial^2\Psi^0(\boldsymbol{\varepsilon})}{\partial \boldsymbol{\varepsilon}^2}:\left(\dot{\boldsymbol{\varepsilon}}-\dot{\lambda}\frac{\partial g_P}{\partial \bar{\boldsymbol{\sigma}}}\right) \tag{5.32}$$

where the non-associative flow rule (4.64) has been applied. Therefore, $\dot{\lambda}$ can be determined from Eqn. (4.68), (4.69) and the viscoplastic hardening law (4.65) as

$$\dot{\lambda}=\frac{\dfrac{\partial f}{\partial \bar{\boldsymbol{\sigma}}}:\dfrac{\partial^2\Psi^0(\boldsymbol{\varepsilon})}{\partial \boldsymbol{\varepsilon}^2}:\dot{\boldsymbol{\varepsilon}}}{\dfrac{\partial f}{\partial \bar{\boldsymbol{\sigma}}}:\dfrac{\partial^2\Psi^0(\boldsymbol{\varepsilon})}{\partial \boldsymbol{\varepsilon}^2}:\dfrac{\partial g_P}{\partial \bar{\boldsymbol{\sigma}}}-\dfrac{\partial f}{\partial \mathbf{q}}\bullet\mathbf{h}} \tag{5.33}$$

Substitution of Eqn. (4.70) into Eqn. (4.69) then yields $\dot{\bar{\boldsymbol{\sigma}}}=\bar{\mathbf{C}}^{evp}:\dot{\boldsymbol{\varepsilon}}$, where $\bar{\mathbf{C}}^{evp}$ is the effective elasto-viscoplastic tangent moduli given by

$$\bar{\mathbf{C}}^{evp}=\frac{\partial^2\Psi^0(\boldsymbol{\varepsilon})}{\partial \boldsymbol{\varepsilon}^2}-\frac{\left[\dfrac{\partial^2\Psi^0(\boldsymbol{\varepsilon})}{\partial \boldsymbol{\varepsilon}^2}:\dfrac{\partial f}{\partial \bar{\boldsymbol{\sigma}}}\right]\otimes\left[\dfrac{\partial^2\Psi^0(\boldsymbol{\varepsilon})}{\partial \boldsymbol{\varepsilon}^2}:\dfrac{\partial g_P}{\partial \bar{\boldsymbol{\sigma}}}\right]}{\dfrac{\partial f}{\partial \bar{\boldsymbol{\sigma}}}:\dfrac{\partial^2\Psi^0(\boldsymbol{\varepsilon})}{\partial \boldsymbol{\varepsilon}^2}:\dfrac{\partial g_P}{\partial \bar{\boldsymbol{\sigma}}}-\dfrac{\partial f}{\partial \mathbf{q}}\bullet\mathbf{h}} \tag{5.34}$$

It is easily to recognize that the effective elasto-viscoplastic tangent moduli derived under the general non-associative flow rule is nonsymmetric, and to simplify the estimation procedure, we consider a special case of Perzyna type viscoplasticity, where the flow

function equals to the loading function, i.e. $g(f) = f$. Under such assumption, the non-associative flow rule becomes associative flow rule and Eqn. (5.34) takes the form of

$$\bar{\mathbf{C}}^{evp} = \frac{\partial^2 \Psi^0(\boldsymbol{\varepsilon})}{\partial \boldsymbol{\varepsilon}^2} - \frac{\left[\dfrac{\partial^2 \Psi^0(\boldsymbol{\varepsilon})}{\partial \boldsymbol{\varepsilon}^2} : \dfrac{\partial f}{\partial \bar{\boldsymbol{\sigma}}}\right] \otimes \left[\dfrac{\partial^2 \Psi^0(\boldsymbol{\varepsilon})}{\partial \boldsymbol{\varepsilon}^2} : \dfrac{\partial f}{\partial \bar{\boldsymbol{\sigma}}}\right]}{\dfrac{\partial f}{\partial \bar{\boldsymbol{\sigma}}} : \dfrac{\partial^2 \Psi^0(\boldsymbol{\varepsilon})}{\partial \boldsymbol{\varepsilon}^2} : \dfrac{\partial f}{\partial \bar{\boldsymbol{\sigma}}} - \dfrac{\partial f}{\partial \mathbf{q}} \bullet \mathbf{h}} \tag{5.35}$$

5.5 Computational Algorithms

In Section 5.3 and 5.4., an initial elastic strain energy based isotropic thermo-elasto-viscoplastic-damage model with the concept of additive stress split in the effective stress space. To use the proposed model within the context of numerical method, a two-step operator splitting methodology (Simo & Hughes, 1998) is introduced. Similar to the procedures we talked about in Chapter 4, the additive decomposition of the isotropic elasto-viscoplastic-damage problem takes the form of an elastic-damage part and an effective plastic return mapping part, as follows:

Elastic-Damage Part

$$\dot{\boldsymbol{\varepsilon}} = \nabla^s \dot{\mathbf{u}}(t)$$

$$\dot{d} = \begin{cases} \mathrm{H}\left(\xi^+\right)\dot{\xi}^+ & \text{iff} \quad \phi^d = \dot{\phi}^d = 0 \\ 0 & \text{otherwise} \end{cases}$$

$$\dot{g} = \begin{cases} \dot{\xi}^+ & \text{iff} \quad \phi^d = \dot{\phi}^d = 0 \\ 0 & \text{otherwise} \end{cases}$$

$$\dot{\bar{\boldsymbol{\sigma}}} = \frac{d}{dt}\left[\frac{\partial \Psi^0(\boldsymbol{\varepsilon})}{\partial \boldsymbol{\varepsilon}}\right]$$

$$\dot{\bar{\boldsymbol{\sigma}}}^{vp} = 0$$

$$\dot{\mathbf{q}} = 0$$

Viscoplastic Part

$$\dot{\boldsymbol{\varepsilon}} = 0$$

$$\dot{d} = 0$$

$$\dot{\bar{\boldsymbol{\sigma}}} = -\dot{\bar{\boldsymbol{\sigma}}}^{vp}$$

$$\dot{\bar{\boldsymbol{\sigma}}}^{vp} = \dot{\lambda}\frac{\partial f}{\partial \boldsymbol{\varepsilon}}\left(\frac{\partial \Psi^0(\boldsymbol{\varepsilon})}{\partial \boldsymbol{\varepsilon}} - \bar{\boldsymbol{\sigma}}^{vp}, \mathbf{q}\right)$$

$$\dot{\mathbf{q}} = \dot{\lambda}\mathbf{h}\left(\frac{\partial \Psi^0(\boldsymbol{\varepsilon})}{\partial \boldsymbol{\varepsilon}} - \bar{\boldsymbol{\sigma}}^{vp}, \mathbf{q}\right)$$

A following step-by-step procedure is developed to solve the two parts of the thermo-elasto-viscoplastic-damage problem:

Step 1: Update the total strain. Given the incremental displacement field $\mathbf{u}_{n+1}$, the total strain tensor is updated as

$$\boldsymbol{\varepsilon}_{n+1} = \boldsymbol{\varepsilon}_n + \nabla^s \mathbf{u}_{n+1} \tag{5.36}$$

Step 2: Compute the tensile strain tensor

$$\boldsymbol{\varepsilon}^+_{n+1} = \mathbf{Q}\boldsymbol{\Lambda}^+\mathbf{Q}^T \tag{5.37}$$

where $\mathbf{Q}=\left[\mathbf{q}_1\ \mathbf{q}_2\ \mathbf{q}_3\right]_{3\times3}$ and $\boldsymbol{\Lambda}^{+}=\begin{bmatrix}\langle\lambda_1\rangle & 0 & 0\\ 0 & \langle\lambda_2\rangle & 0\\ 0 & 0 & \langle\lambda_3\rangle\end{bmatrix}$; $\mathbf{q}_i$ and λ_i (i=1~3) denote the corresponding eigenvectors and eigenvalues of the total strain tensor $\boldsymbol{\varepsilon}_{n+1}$ respectively; the angular McAuley brackets are defined by $2\langle\lambda_i\rangle=\lambda_i+|\lambda_i|$.

Step 3: Compute the initial (undamaged) elastic tensile strain energy

$$\xi^{+}_{n+1}=\sqrt{\Psi^0\left(\boldsymbol{\varepsilon}^{+}_{n+1}\right)}=\sqrt{\frac{1}{2}\boldsymbol{\varepsilon}^{+}_{n+1}:\mathbf{C}^0:\boldsymbol{\varepsilon}^{+}_{n+1}} \tag{5.38}$$

Step 4: Compute the scalar damage parameter

$$\text{if}\quad \xi^{+}_{n+1}\begin{cases}\le g_0 & d_{n+1}=0\quad\text{(no damage)}\\ > g_0 & d_{n+1}=A\exp\left[B\xi^{+}_{n+1}\left(\xi^{+}_{n+1}-g_0\right)\right]\end{cases} \tag{5.39}$$

Step 5: Obtain trial (predictor) stress tensor and internal viscoplastic variable

$$\begin{aligned}\boldsymbol{\sigma}^0_{n+1}&=\frac{\partial\Psi^0}{\partial\boldsymbol{\varepsilon}}\left(\boldsymbol{\varepsilon}_{n+1}\right)=\mathbf{C}^0:\boldsymbol{\varepsilon}_{n+1}\\ \bar{\boldsymbol{\sigma}}^{trial}_{n+1}&=\boldsymbol{\sigma}^0_{n+1}-\bar{\boldsymbol{\sigma}}^{vp}_{n}\\ \mathbf{q}^{trial}_{n+1}&=\mathbf{q}_n\end{aligned} \tag{5.40}$$

Step 6: Check for yielding

$$\text{if}\quad f\left(\bar{\boldsymbol{\sigma}}^{trial}_{n+1},\mathbf{q}^{trial}_{n+1}\right)\begin{cases}\le 0 & \bar{\boldsymbol{\sigma}}_{n+1}=\bar{\boldsymbol{\sigma}}^{trial}_{n+1}\ ;\ \mathbf{q}_{n+1}=\mathbf{q}^{trial}_{n+1}\ ;\ \text{skip step 7}\\ > 0 & \text{viscoplastic; go to step 7}\end{cases} \tag{5.41}$$

Step 7: Cutting plane return mapping

In the case of viscoplastic loading, the trial (predictor) stresses and internal variables need to be returned back to the yield surface along the algorithmic counterpart of the flow generated to satisfy the Kuhn-Tucker conditions. There exist many return mapping algorithms, whereas the cutting plane algorithm developed by Simo and Ortiz (Ortiz &

Simo, 1986; Simo & Ortiz, 1985) is employed here. The cutting plane algorithmic construction was inspired by a form of the convex cutting plane method (Kelley, 1960) with its basic structure inherited from Newton's iteration method. Two advantages of this cutting plane return mapping algorithm are the quadratic rate of convergence towards the yield surface and the need for computing the gradient of the flow rule and hardening law are entirely bypassed. The procedures (iterations) are as follows:

(v) Initialize: $K = 0, \quad \bar{\boldsymbol{\sigma}}_{n+1}^{K} = \bar{\boldsymbol{\sigma}}_{n+1}^{trial}, \quad \mathbf{q}_{n+1}^{K} = \mathbf{q}_{n+1}^{trial}$

(vi) Compute the hardening moduli and yield function:

$$h_{n+1}^{K} = h\left(\bar{\boldsymbol{\sigma}}_{n+1}^{K}, \mathbf{q}_{n+1}^{K}\right)$$
$$f_{n+1}^{K} = f\left(\bar{\boldsymbol{\sigma}}_{n+1}^{K}, \mathbf{q}_{n+1}^{K}\right)$$
IF $f_{n+1}^{K} \le 0$ (TOL) EXIT
ELSE GOTO (iii)

(vii) Linearize the viscoplastic consistency condition:

$$\Delta\lambda_{n+1}^{K} = \frac{f_{n+1}^{K}}{\dfrac{\partial f_{n+1}^{K}}{\partial \bar{\boldsymbol{\sigma}}_{n+1}^{K}} : \mathbf{C}_{n+1}^{K} : \dfrac{\partial f_{n+1}^{K}}{\partial \bar{\boldsymbol{\sigma}}_{n+1}^{K}} - \dfrac{\partial f_{n+1}^{K}}{\partial \mathbf{q}_{n+1}^{K}} \bullet \mathbf{h}_{n+1}^{K}}$$

(viii) Update the state variables and consistency parameter:

$$\bar{\boldsymbol{\sigma}}_{n+1}^{K+1} = \bar{\boldsymbol{\sigma}}_{n+1}^{K+1} - \Delta\lambda_{n+1}^{K} \mathbf{C}_{n+1}^{K} : \frac{\partial f_{n+1}^{K}}{\partial \bar{\boldsymbol{\sigma}}_{n+1}^{K}}$$
$$\mathbf{q}_{n+1}^{K+1} = \mathbf{q}_{n+1}^{K} + \Delta\lambda_{n+1}^{K} h_{n+1}^{K}$$
SET $K \leftarrow K + 1;$ GOTO (ii)

Step 8: Update the homogenized stress

$$\boldsymbol{\sigma}_{n+1} = \kappa\left(T\right)\left(1 - d_{n+1}\right)\bar{\boldsymbol{\sigma}}_{n+1} \tag{5.42}$$

5.6 A 1-D Driven Problem

To test the proposed elasto-viscoplastic-damage framework, a 1-D strain driven problem is tested by MATLAB. One cycle strain loading (compressive loading of strain in 11-direction, unloading, tensile loading of strain in 11-direction and unloading) is applied, as shown in Figure 5.4. In particular, the Drucker-Prager yield function (Drucker & Prager, 1952) is used for loading function. The Drucker-Prager yield function is a simple modification of the Von Mises criterion whereby the hydrostatic-dependent first invariant I_1 is introduced to the original Von Mises yield function and becomes suitable for the modeling of plasticity of materials where there is a strong dependence on the hydrostatic pressure such as rocks, soil and concrete.

Figure 5.5-Figure 5.9 demonstrate the stress-strain relationships between effective stress $\bar{\sigma}_{11}$ and strain ε_{11}, and homogenized stress σ_{11} and strain ε_{11}; the history of viscoplastic strain ε_{11}^{vp}, viscoplastic stress σ_{11}^{vp} and the evolution of the scalar damage variable, respectively.

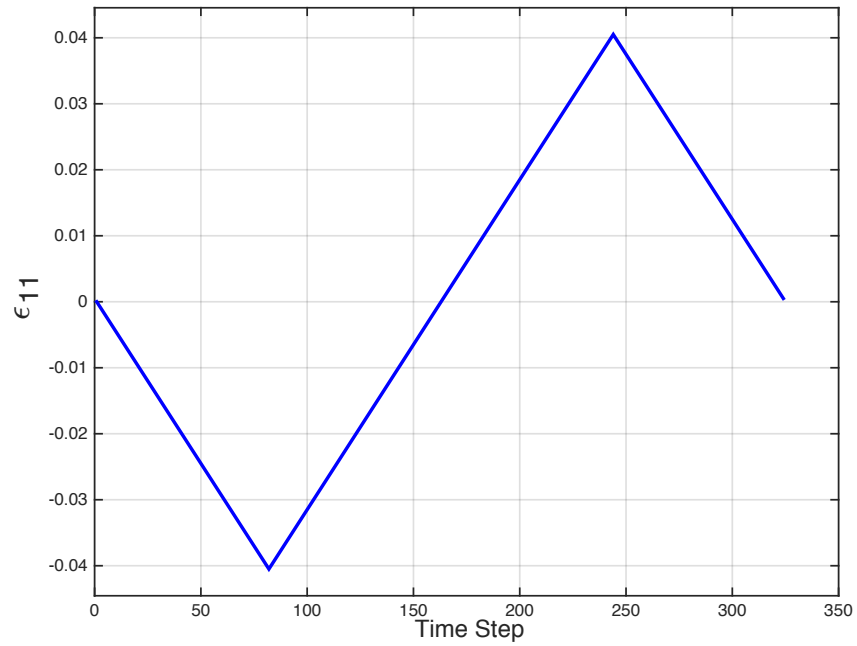

Figure 5.4 The history of (total) strain input ε_{11}

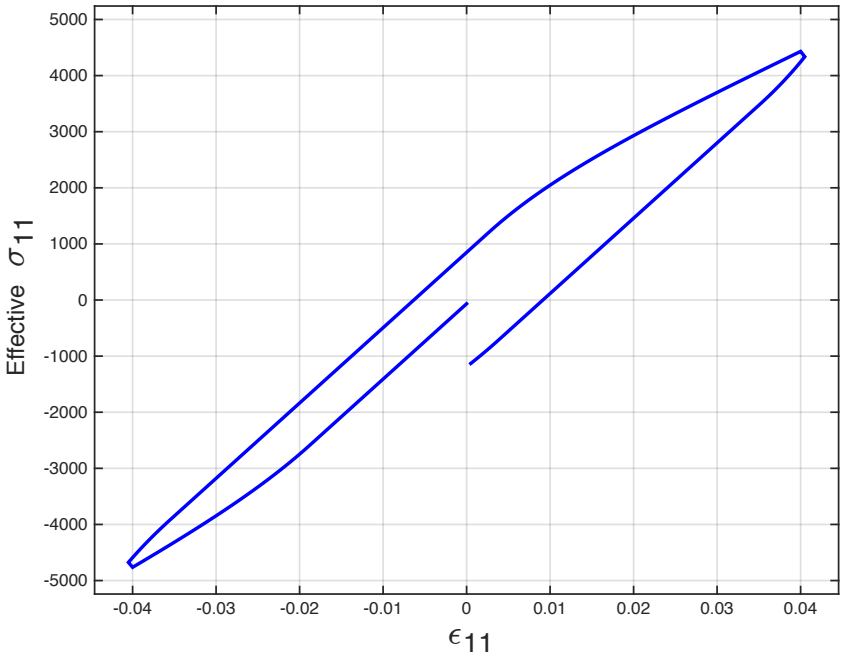

Figure 5.5 The stress-strain relationship of $\bar{\sigma}_{11}$ vs. ε_{11}

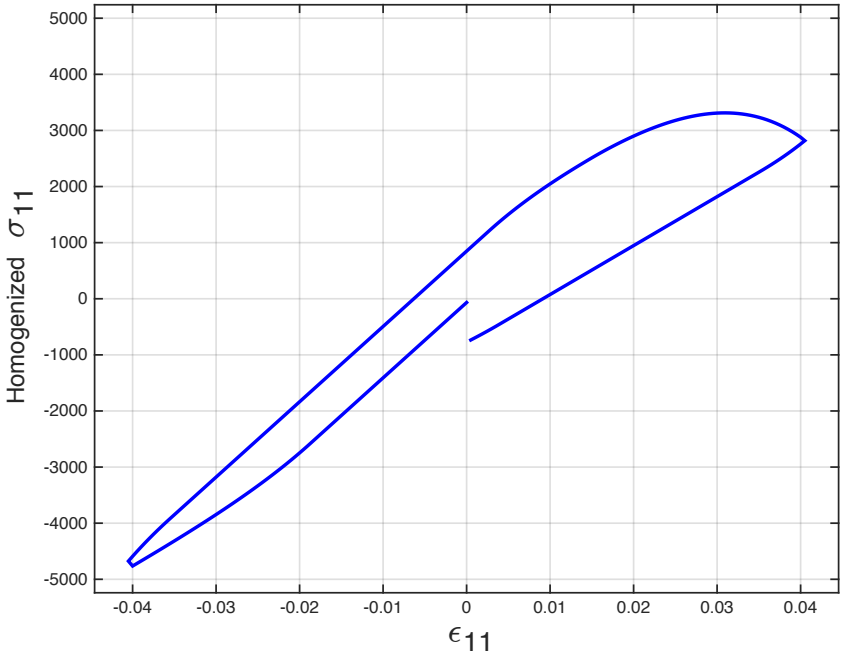

Figure 5.6 The stress-strain relationship of σ_{11} vs. ε_{11}

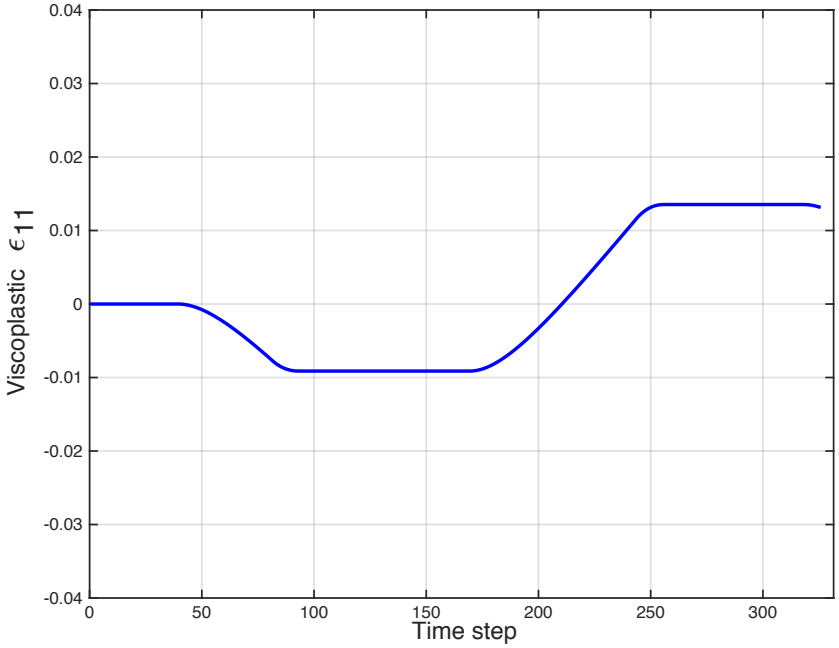

Figure 5.7 The history of viscoplastic strain ε_{11}^{vp}

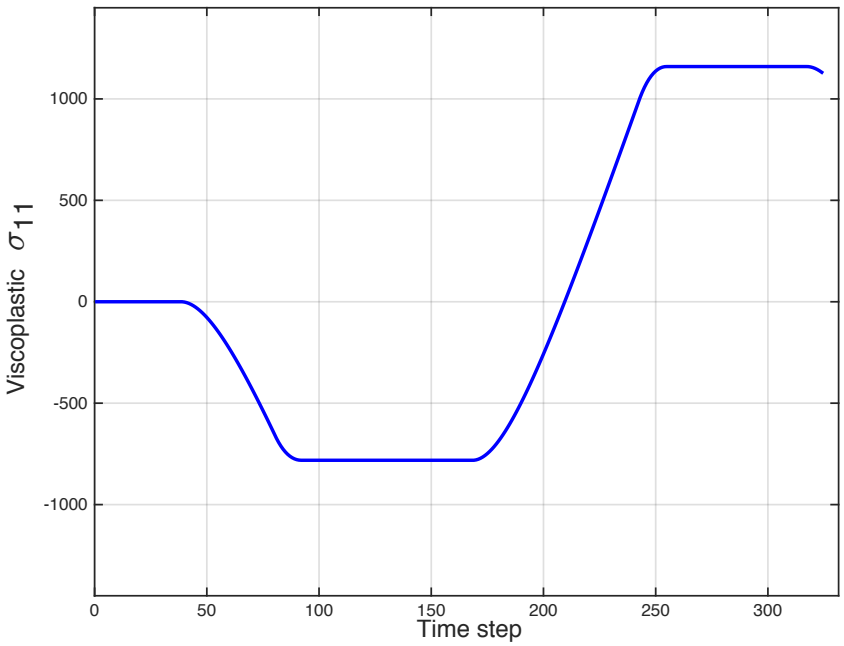

Figure 5.8 The history of viscoplastic stress σ_{11}^{vp}

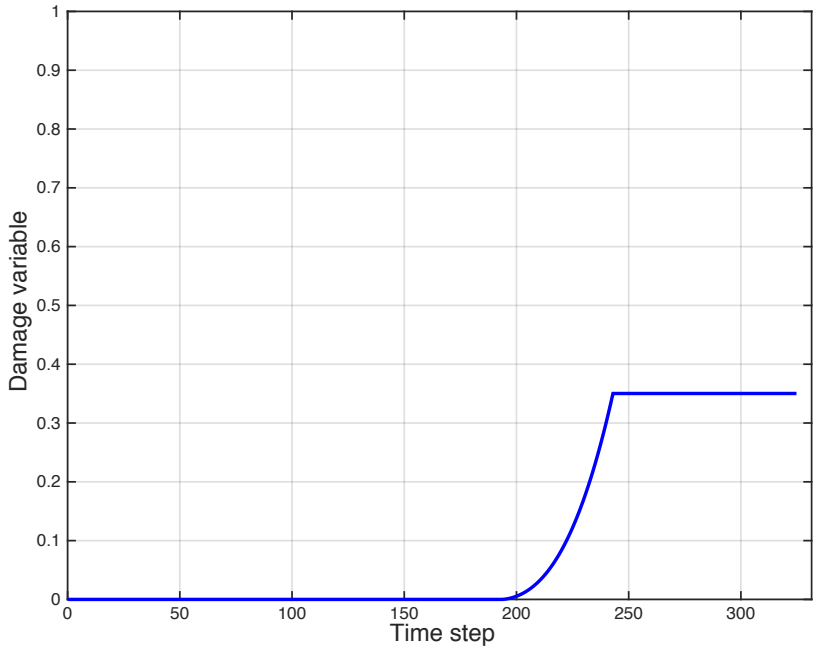

Figure 5.9 The history of damage evolution

When viscosity approaches zero, the viscoplastic model should recover to rate-independent plasticity (Drucker-Prager model). Figure 5.10 shows (a) stress-strain curve in the effective space, (b) stress-strain curve in the homogenized space, (c) history of viscoplastic strain in the 11-direction and (d) history of viscoplastic stress in the 11-direction. The plots agree with Figure 4.6-4.9 in Chapter 4.

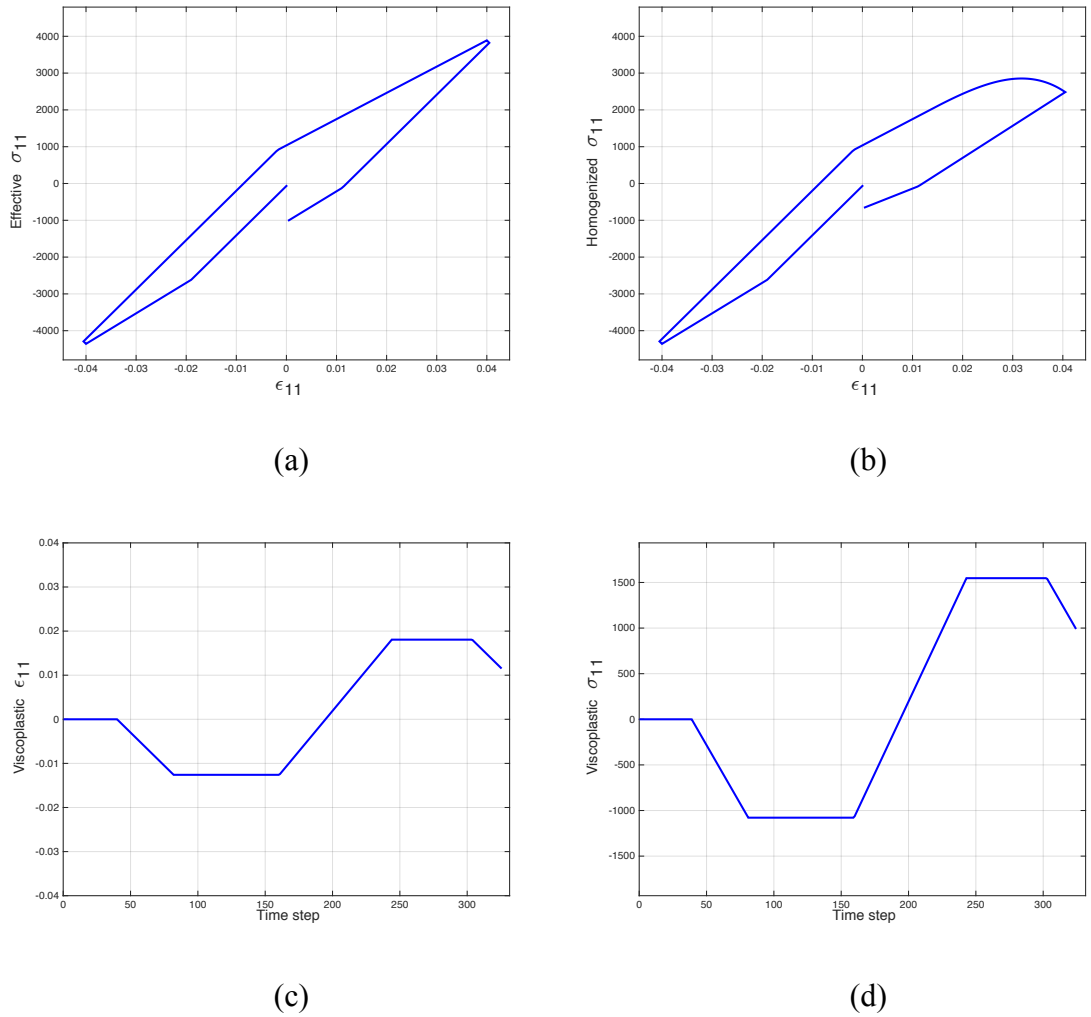

Figure 5.10 Responses of the proposed model when viscosity approaches zero

When viscosity goes to infinity, the viscoplastic model should behavior instantaneously elastic. Figure shows (a) stress-strain curve in the effective space, (b) stress-strain curve in the homogenized space, (c) history of viscoplastic strain in the 11-direction and (d) history of viscoplastic stress in the 11-direction.

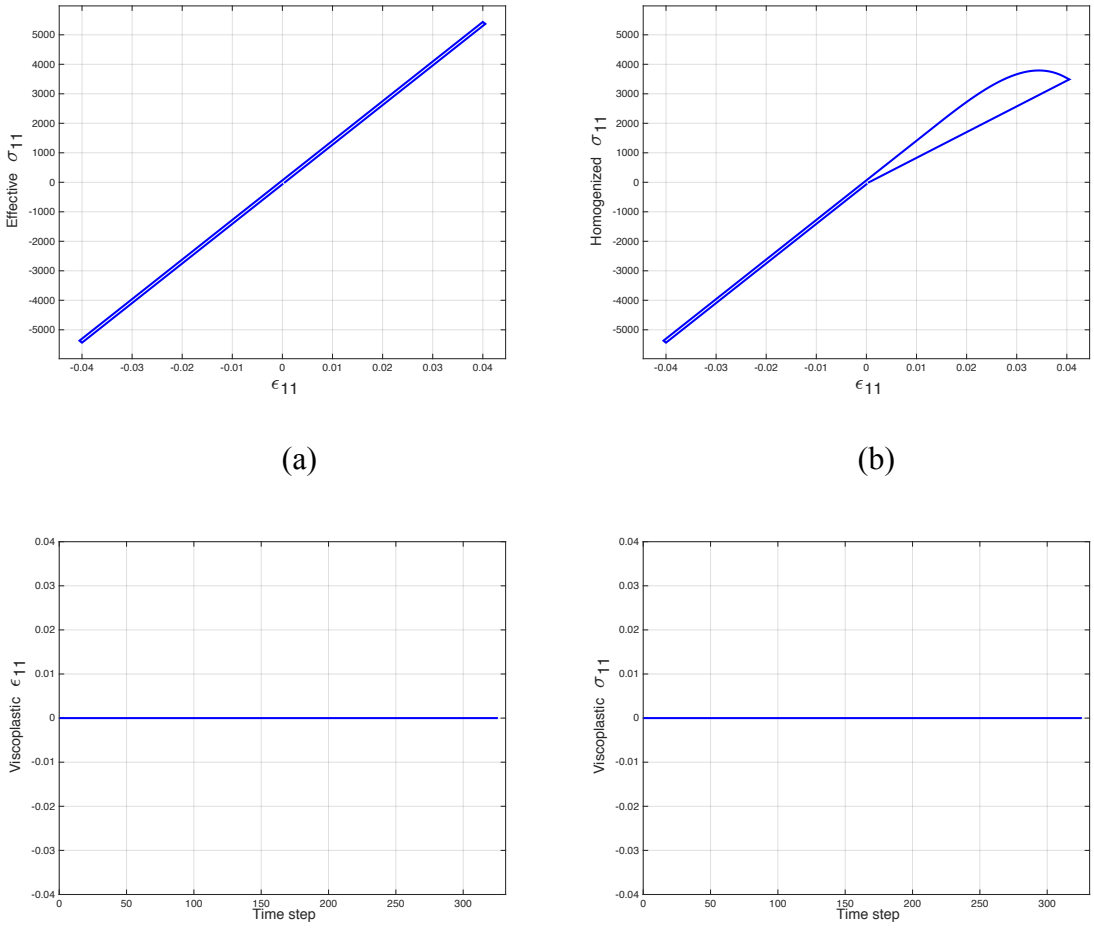

(a) (b)

(c) (d)

Figure 5.11 Responses of the proposed model when viscosity goes to infinity

5.7 References

Abu Al-Rub, R. K., Darabi, M. K., Little, D. N., & Masad, E. A. (2010). A micro-damage healing model that improves prediction of fatigue life in asphalt mixes. *International Journal of Engineering Science, 48*(11), 966-990.

Buttlar, W. G., & You, Z. (2001). Discrete Element Modeling of Asphalt Concrete: Microfabric Approach. *Transportation Research Record: Journal of the Transportation Research Board, 1757*(1), 111-118.

Button, J. W., Perdomo, D., & Lytton, R. L. (1990). Influence of aggregate on rutting in asphalt concrete pavements. *Transportation Research Record: Chip seals, friction courses, and asphalt pavement rutting 1990*(1259), 141-152.

Chehab, G. R., Kim, Y. R., Schapery, R. A., Witczak, M. W., & Bonaquist, R. F. (2002). *Time-temperature superposition principle for asphalt concrete with growing damage in tension state*. Paper presented at the Asphalt Paving Technology 2002, Colorado Springs, Colorado.

Chehab, G. R., Kim, Y. R., Schapery, R. A., Witczak, M. W., & Bonaquist, R. F. (2003). Characterization of asphalt concrete in uniaxial tension using a viscoelastoplastic continuum damage model. *Asphalt paving technology 2003: Journal of the Association of Asphalt Paving Technologists from the proceedings of the technical sessions, 72*, 315-355.

Christensen Jr, D. W., Pellinen, T. K., & Bonaquist, R. F. (2003). Hirsch model for estimating the modulus of asphalt concrete. *Journal of the Association of Asphalt Paving Technologists, 72*, 97-121.

Coleman, B. D., & Gurtin, M. E. (1967). Thermodynamics with internal state variables. *Journal of Chemical Physics, 47*(2), 597-613.

Coleman, B. D., & Noll, W. (1963). The thermodynamics of elastic materials with heat conduction and viscosity. *Archive for Rational Mechanics and Analysis, 13*(1), 167-178.

Dai, Q., Sadd, M. H., & You, Z. (2006). A micromechanical finite element model for linearand damage-coupled viscoelastic behaviour of asphalt mixture. *International Journal for Numerical and Analytical Methods in Geomechanics, 30*(11), 1135-1158.

Drucker, D. C., & Prager, W. (1952). Soil Mechanics and Plastic Analysis or Limite Design. *Quarterly of Applied Mathematics, 10*, 157-175.

García, A., Bueno, M., Norambuena-Contreras, J., & Partla, M. N. (2013). Induction healing of dense asphalt concrete. *Construction and Building Materials, 49*, 1-7.

Hong, S., Yuan, K. Y., & Ju, J. W. (2017). New strain energy-based thermo-elastoviscoplastic isotropic damage–self-healing model for bituminous composites—Part I: Formulations. *International Journal of Damage Mechanics, 26*(5), 651-671.

Ju, J. W., & Chen, T. M. (1994a). Effective elastic moduli of two-phase composites containing randomly dispersed spherical inhomogeneities. *Acta Mechanica, 103*(1-4), 123-144.

Ju, J. W., & Chen, T. M. (1994b). Micromechanics and effective moduli of elastic composites containing randomly dispersed ellipsoidal inhomogeneities. *Acta Mechanica, 103*(1-4), 103-121.

Kelley, J. E., Jr. (1960). The cutting-plane method for solving convex programs. *Journal of the Society for Industrial & Applied Mathematics, 8*(4), 703–712.

Khazanovich, L. (2008). The elastic–viscoelastic correspondence principle for non-homogeneous materials with time translation non-invariant properties. *International Journal of Solids and Structures, 45*(17), 4739-4747.

Kim, H. W., & Buttlar, W. G. (2009). Discrete fracture modeling of asphalt concrete. *International Journal of Solids and Structures, 46*(13), 2593-2604.

Kim, Y. R., LEE, H. J., & Little, D. N. (1997). Fatigue characterization of asphalt concrete using viscoelasticity and continuum damage theory. *Journal of the Association of Asphalt Paving Technologists, 66*, 520-569.

Kim, Y. R., & Little, D. N. (1990). One-Dimensional Constitutive Modeling of Asphalt Concrete. *Journal of Engineering Mechanics, ASCE, 116*(4), 751-772.

Kim, Y. R., & Little, D. N. (2004). Linear viscoelastic analysis of asphalt mastics. *Journal of Materials in Civil Engineering, 16*(2), 122-132.

Kovačič, S., Matskob, N. B., Ferkc, G., & Slugovc, C. (2013). Macroporous poly(dicyclopentadiene) γFe2O3/Fe3O4 nanocomposite foams by high internal phase emulsion templating. *Journal of Materials Chemistry A, 1*, 7971-7978.

Lee, H. J., Daniel, J. S., & Kim, Y. R. (2000). Continuum damage mechanics-based fatigue model of asphalt concrete. *Journal of Material in Civil Engineering, 12*(2), 105-112.

Lee, H. J., & Kim, Y. R. (1998). Viscoelastic constitutive model for asphalt concrete under cyclic loading. *Journal of Engineering Mechanics, ASCE, 11*(3), 236-241.

Lemaitre, J. (1985). A Continuous Damage Mechanics Model for Ductile Fracture. *Journal of Engineering Materials and Technology, 107*(1), 83-89.

Liu, Q., García, A., Schlangen, E., & Ven, M. (2011). Induction healing of asphalt mastic and porous asphalt concrete. *Construction and Building Materials, 25*(9), 3746-3752.

Mazars, J., & Lemaitre, J. (1985). Application of Continuous Damage Mechanics to Strain and Fracture Behavior of Concrete. In S. S.P. (Ed.), *Application of Fracture Mechanics to Cementitious Composites. NATO ASI Series (Series E: Applied Sciences)* (Vol. 94, pp. 507-520): Springer, Dordrecht.

Ortiz, M., & Simo, J. C. (1986). An analysis of a new class of integration algorithms for elastoplastic constitutive relations. *International Journal for Numerical Methods in Engineering, 23*(3), 353-366.

Park, S. W., Kim, Y. R., & Schapery, R. A. (1996). A viscoelastic continuum damage model and its application to uniaxial behavior of asphalt concrete. *Mechanics of Materials, 24*(4), 241-255.

Perzyna, P. (1966). Fundamental problems in viscoplasticity. *Advances in Applied Mechanics, 9*(2), 243-377.

Roque, R., & Buttlar, W. G. (1992). Development of a measurement and analysis system to accurately determine asphalt concrete properties using the indirect tensile mode. *Asphalt Paving Technology: Association of Asphalt Paving Technologists-Proceedings of the Technical Sessions, 61*, 304-333.

Scarpas, A., Al-Khoury, R., Van Gurp, C., & Erkens, S. M. J. G. (1997). *Finite element simulation of damage development in asphalt concrete pavements*. Paper presented at the Eighth International Conference on Asphalt Pavements, Seattle, Washington.

Si, Z., Little, D. N., & Lytton, R. L. (2002). Characterization of Microdamage and Healing of Asphalt Concrete Mixtures. *Journal of Materials in Civil Engineering, 14*(6), 461-470.

Simo, J. C., & Hughes, T. J. R. (1998). *Computational Inelasticity*: Springer New York.

Simo, J. C., & Ju, J. W. (1987). Strain- and stress-based continuum damage model - I. Formulation. *International Journal of Solids and Structures, 23*(7), 821-840.

Simo, J. C., & Ortiz, M. (1985). A unified approach to finite deformation elastoplastic analysis based on the use of hyperelastic constitutive equations. *Computer Methods in Applied Mechanics and Engineering, 49*(2), 221-245.

Tashman, L., Masad, E., Little, D. N., & Zbib, H. (2005). A microstructure-based viscoplastic model for asphalt concrete. *International Journal of Plasticity, 21*(9), 1659-1685.

Vallons, K., Drozdzak, R., Charret, M., & Lomov, S. (2015). *Damage development in woven glass fibre composites with tough thermoset matrix*. Paper presented at the TexComp-12, Raleigh, NC.

Wang, Y., Zhang, L., Sun, J., Bao, J. B., Wang, Z., & Ni, L. (2017). Dramatic Toughness Enhancement of Polydicyclopentadiene Composites by Incorporating Low Amounts of Vinyl-Functionalized SiO2. *Industrial & Engineering Chemistry Research, 56*(16), 4750-4757.

You, Z., & Buttlar, W. G. (2004). Discrete Element Modeling to Predict the Modulus of Asphalt Concrete Mixtures. *Journal of Materials in Civil Engineering, 16*(2), 140-146.

CHAPTER 6 : MICROMECHANICAL FIELD APPLICATION OF BURGERS MODEL ON PREDICTING THE VISCOELASTIC PROPERTIES OF INNOVATIVE ASPHALT MASTIC COMPOSITES FEATURING HIGH TOUGHNESS, LOW VISCOSITY NANO-MOLECULAR RESINS

6.1 Introduction

The mechanical behavior of the innovative asphalt concrete materials has been studied from the continuum damage mechanics aspect in the previous chapters, whereas in this chapter, focus is situated on the rheology behavior of asphalt mastic materials.

As one of the most commonly used materials for road construction, the systematical assessment of rheology behavior of asphalt materials can be dated back to the nineteenth century. Since then, various researches have been done to characterize the phenomena from analytical aspect (Christensen, 1982; Hopkins & Hamming, 1957; Y. R. Kim, 2008; Málek et al., 2018; Masad et al., 2009; Tschoegl, 1989, 1997), experimental aspect (Daniel et al., 2007; Goh & You, 2009; Goodrich, 1991; Khodaii & Mehrara, 2009; Y. R. Kim et al., 2004; Monismith et al., 1966; Monismith et al., 1965; Xiao et al., 2007; X. Y. Zhu et al., 2014) and numerical aspect (Dai & You, 2007; Y. Liu & You, 2011; Park & Schapery, 1999; Tarefder & Faisal, 2013; You et al., 2011).

Experimental observations have shown clearly that asphalt exhibits more than one relaxation mechanism that can be identified by the different relaxation times which cannot be described by some classical models such as Maxwell model (Maxwell, 1867). Under such circumstance, Burgers (Burgers, 1939) proposed a higher order model that is capable of describing two different relaxation times, and the so-called Burgers model has been widely applied in the case of geomaterials (Monismith & Secor, 1962; Narayan et al., 2012) and biomaterials (Málek et al., 2015; Sharif-Kashani et al., 2011).

This chapter propose an analytical approach to predict the viscoelastic properties of the innovative asphalt mastic composites composed of asphalt binder, fine aggregates, polymerized DCPD and air voids. Some common mechanical models of viscoelasticity and their constitutive laws are discussed in Section 6.2. Section 6.3 introduced the correspondence principle along with the Laplace transform to solve linear viscoelastic problems. In Section 6.5 an ensemble-volume averaged micromechanical field based multilevel homogenization approach is proposed to evaluate the effective modulus of the heterogenous asphalt mastic composites. Finally, the theoretical solutions are compared with numerical simulation results. A methodology flowchart is shown in Figure 6.1.

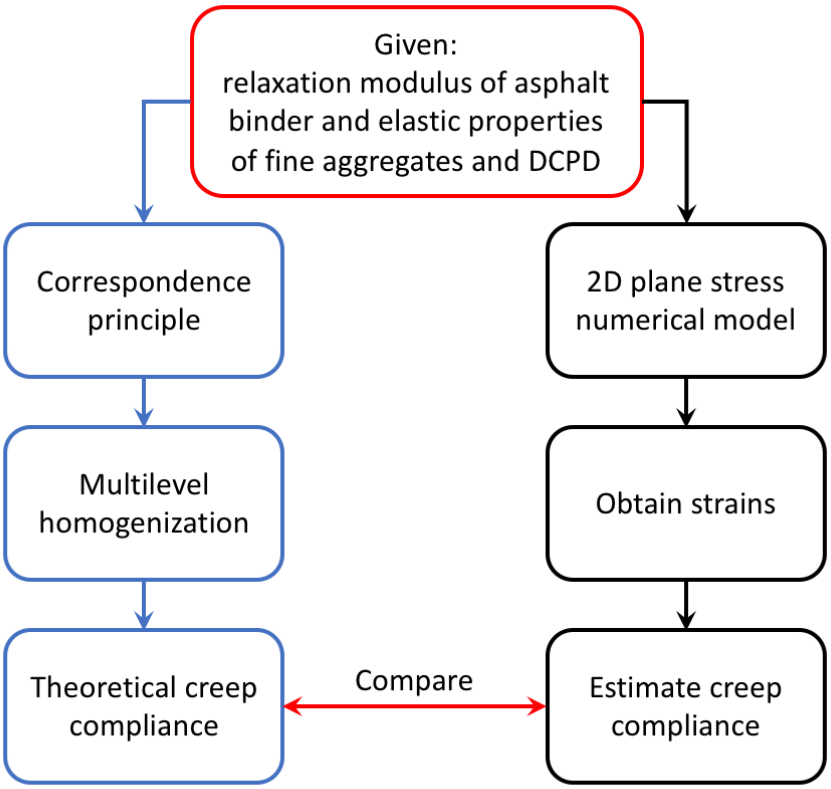

Figure 6.1 The methodology flowchart for the procedures of theoretical evaluation and numerical simulation comparison

6.2 The Correspondence Principle

The classical method of solving boundary value problems in the linear quasi-static theory of viscoelasticity is to apply an integral transform (with respect to time) to the time-dependent field equations and boundary conditions. The transformed field equations then have the same form as the field equations of elasticity theory and if a solution to these, which is compatible with the transformed boundary conditions, can be found then the solution to the original problem is reduced to transform inversion. This method of solving

viscoelastic stress analysis problems is referred to as the "correspondence principle" (Graham, 1968; Read, 1950) and has been extensively applied to linear and nonlinear viscoelastic problems (Khazanovich, 2008; E. H. Lee, 1965; Mukherjee & Paulino, 2003; Rajagopal & Srinivasa, 2005; Rizzo & Shippy, 1971). The correspondence principle is valid in general whenever the viscoelastic relaxation functions in deviatoric (shear) and in volumetric (bulk) have the forms $\mu(\mathbf{x},t)=\mu(\mathbf{x})g(t)$, $K(\mathbf{x},t)=K(\mathbf{x})f(t)$, respectively, where $g(t)$ and $f(t)$ are sufficiently well behaved but otherwise arbitrary functions of time. In other words, the stresses, strains and relaxation functions have to be separable.

A general class of viscoelastic boundary value problems for which the principle is applied via the Laplace transform is developed in the current section. The purpose is to describe and demonstrate an approximate solution procedure capable of efficiently and accurately treating viscoelastic problems.

Traditionally, the general form of an elastic boundary value problem can be described as follows

$$
\begin{aligned}
&\varepsilon_{ij}=\frac{1}{2}\left(u_{i,j}+u_{j,i}\right)\\
&s_{ij}=2\mu e_{ij}\\
&\sigma_{kk}=3k\varepsilon_{kk}\\
&\sigma_{ij,j}+F_i=0\\
&\varepsilon_{ij,kl}+\varepsilon_{kl,ij}=\varepsilon_{ik,jl}+\varepsilon_{jl,ik}\\
&\textbf{B.C.s}\\
&\qquad \sigma_{ij}n_j=S_i \ \ on \ \ B_\sigma\\
&\qquad u_i=\Delta_i \ \ on \ \ B_u
\end{aligned}
\tag{6.1}
$$

On the other hand, for a viscoelastic boundary value problem, the governing equations in time domain are

$$
\begin{aligned}
&\varepsilon_{ij}(t)=\frac{1}{2}\left(u_{i,j}+u_{j,i}\right)\\
&s_{ij}(t)=2\int_{-\infty}^{t}\mu(t-\tau)\frac{\partial e_{ij}(\tau)}{\partial\tau}d\tau\\
&\sigma_{kk}(t)=3\int_{-\infty}^{t}k(t-\tau)\frac{\partial \varepsilon_{ij}(\tau)}{\partial\tau}d\tau\\
&\sigma_{ij,j}(t)+F_i(t)=0\\
&\varepsilon_{ij,kl}(t)+\varepsilon_{kl,ij}(t)=\varepsilon_{ik,jl}(t)+\varepsilon_{jl,ik}(t)\\
&\textbf{B.C.s}\\
&\qquad\sigma_{ij}(t)n_j=S_i(t)\ \ on\ \ B_\sigma\\
&\qquad u_i(t)=\Delta_i(t)\ \ on\ \ B_u
\end{aligned}
\tag{6.2}
$$

If all the equations in Eqn. (6.2) can be transformed to Laplace domain, the governing equations in Laplace domain can then be expressed by

$$
\begin{aligned}
&\overline{\varepsilon}_{ij}(s)=\frac{1}{2}\left(\overline{u}_{i,j}+\overline{u}_{j,i}\right)\\
&\overline{s}_{ij}(s)=2s\overline{\mu}\overline{e}_{ij}\\
&\overline{\sigma}_{kk}(s)=3s\overline{k}\,\overline{\varepsilon}_{kk}\\
&\overline{\sigma}_{ij,j}(s)+\overline{F}_i(s)=0\\
&\overline{\varepsilon}_{ij,kl}(s)+\overline{\varepsilon}_{kl,ij}(s)=\overline{\varepsilon}_{ik,jl}(s)+\overline{\varepsilon}_{jl,ik}(s)\\
&\textbf{B.C.s}\\
&\qquad\overline{\sigma}_{ij}(s)n_j=\overline{S}_i(s)\ \ on\ \ B_\sigma\\
&\qquad\overline{u}_i(s)=\overline{\Delta}_i(s)\ \ on\ \ B_u
\end{aligned}
\tag{6.3}
$$

By comparing Eqn. (6.3) and Eqn. (6.1), it can be observed that both governing equations are almost identical except the representations of shear and bulk moduli. Upon the concept of correspondence principle, $s\overline{\mu}$ and $s\overline{k}$ in Eqn. (6.3) can be considered as the elastic moduli in Laplace domain and the solution to this viscoelastic problem can be

obtained through an identical elastic problem by replacing the elastic moduli in the elastic solution with transformed moduli. In other words, correspondence principle states that theory of viscoelasticity allows one to take an appropriate transformation of the governing field and boundary equations of viscoelastic problems with respect to time and reduce them so that they are mathematically equivalent to those for elasticity problem with transformed elastic moduli.

6.3 The Response of Viscoelastic Materials

Viscoelasticity is the study of materials which have a time-dependence. Vicat, a French engineer from the Department of Road Construction, noticed in the 1830s that bridge cables continued to elongate over time even though under constant load, a viscoelastic phenomenon known as creep. Many other investigators, such as Weber and Boltzmann, studied viscoelasticity throughout the nineteenth century, but the real driving force for its study came later – the increased demand for power and the associated demand for materials which would stand up to temperatures and pressures that went beyond previous experience. By then it had been recognized that significant creep occurred in metals at high temperatures. The theory developed further with the emergence of synthetic polymer plastics, which exhibit strong viscoelastic properties. The study of viscoelasticity is also important in biomechanics, since many biomaterials respond viscoelastically, for example, heart tissue, muscle tissue and cartilage.

6.3.1Comparison Between the Elastic and Viscous Materials

Elastic materials are those for which stress is proportional to strain. A typical example of elastic behavior is provided by an ideal spring for which force (stress) is proportional to displacement (strain). The ideal spring as shown in Figure 6.2 can be used to model the general behavior of elastic materials. Specifically, for an isotropic elastic material, the stress-strain relation can be described as in Figure 6.2 (a)

$$\sigma = E\varepsilon \tag{6.4}$$

Another way to describe the stress-strain relation is to split them in deviatoric and volumetric parts, respectively, by the following equations:

$$\sigma_D = 2\mu\varepsilon_D \quad , \quad \sigma_V = K\varepsilon_V \tag{6.5}$$

where σ_D is the deviatoric stress, μ is the shear modulus, ε_D is the deviatoric strain, σ_V is the volumetric stress, K is the bulk modulus, and ε_V is the volumetric strain.

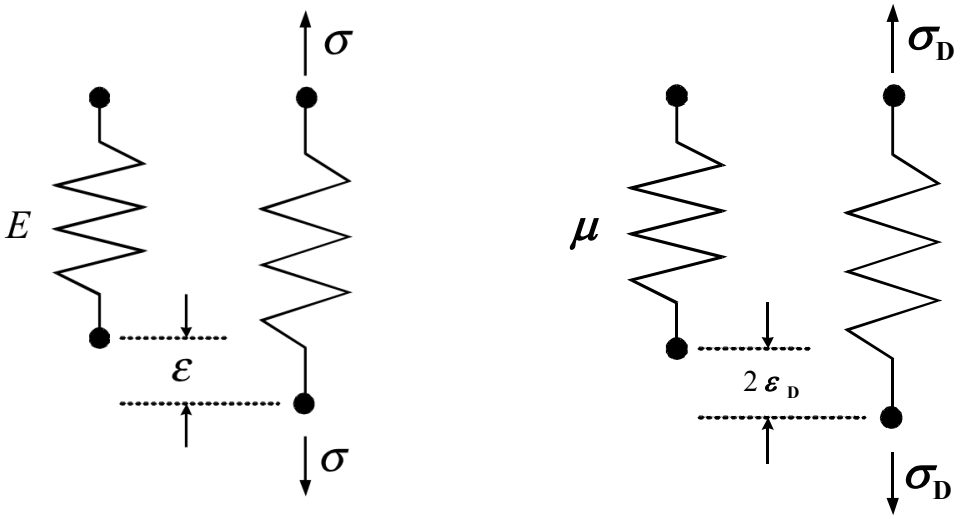

(a) (b)

Figure 6.2 A linear Hookean elastic spring model

Viscous fluids, on the other hand, have a part of the stress that is proportional to the rate of strain. A typical example of the mechanism that exhibits such behavior is the shock absorber or dashpot as shown in Figure 6.3. The stress-strain relation can be expressed, for instance, as follows

$$\sigma = \eta\dot{\varepsilon} \tag{6.6}$$

Or for deviatoric part:

$$\sigma_D = 2\eta\dot{\varepsilon}_D \tag{6.7}$$

in which η is the viscosity and $\dot{\varepsilon}_D$ is the deviatoric strain rate.

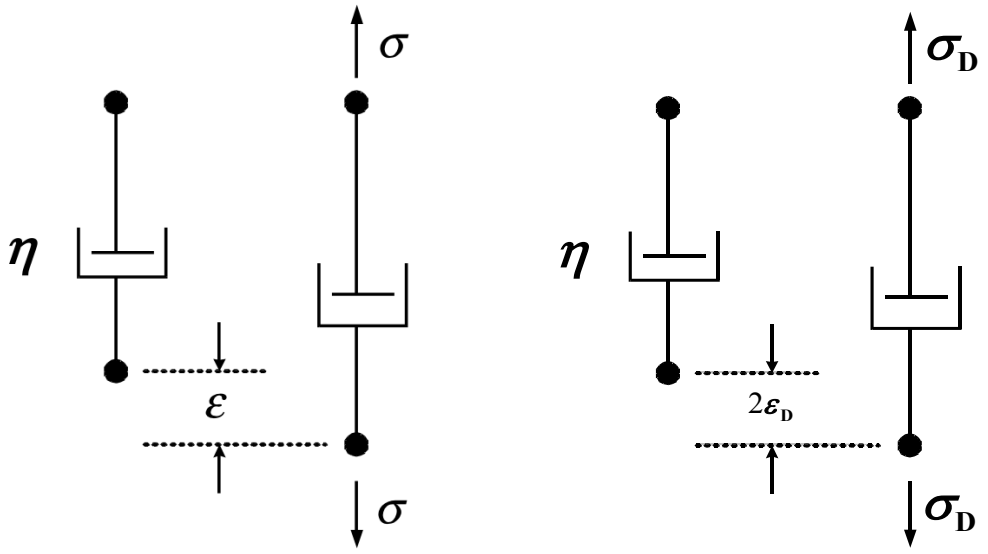

Figure 6.3 A linear Newtonian dashpot model

From the viewpoint of energy, elastic materials have a capacity to store mechanical energy with no dissipation of the energy. On the other hand, a Newton viscous fluid in a non-hydrostatic stress state implies a capacity for dissipating energy, but none of them for storing it.

Further, when elastic materials are subjected to a suddenly applied load, response (or deformation) will be generated instantaneously with a state of deformation which remains constant. However, a Newton viscous fluid responds to a suddenly applied load (shear stress) by a steady flow process which means instantaneous deformation is not allowed. Instead, the fluid will undergo time-dependent straining.

For some materials such as asphalt and polymers that possess a capacity to both store and dissipate mechanical energy are called viscoelastic materials. Theory of viscoelasticity is used to describe the mechanical behavior of viscoelastic materials.

6.3.2 Constitutive Models for Linear Viscoelasticity

Viscoelastic materials, such as amorphous polymers, semi-crystalline polymers, biopolymers and even the living tissue and cells can be modeled in order to determine their stress and strain or force and displacement interactions as well as their temporal dependencies. These models, which can be divided into two groups: simple models and generalized models, are used to predict a material's response under different loading conditions. Simple models are models that have up to four elements, which include

the Maxwell model, the Kelvin–Voigt model, the standard linear solid (SLS) model, and the Burgers model. Generalized models can be established in two ways, the first one is a Hooke model (spring) connected with a chain of several Maxwell models in parallel (referred as the Maxwell chain or the Wiechert model); the second generalized model is a Maxwell model connected with a chain of several Kelvin models in series (referred as Kelvin chain). Viscoelastic behavior has elastic and viscous components modeled as linear combinations of springs that store the energy and dashpots that dissipate the energy, respectively. Each model differs in the arrangement of these elements (notice all of these viscoelastic models can be equivalently modeled as electrical circuits). Among them, Burgers model is the most general yet simple form for linear viscoelasticity. It takes into account that the relaxation does not occur at a single time, but at a distribution of times.

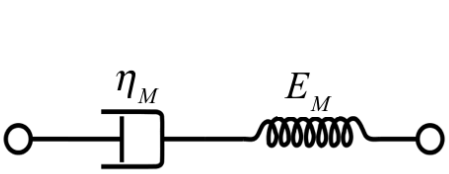

(a) Maxwell model

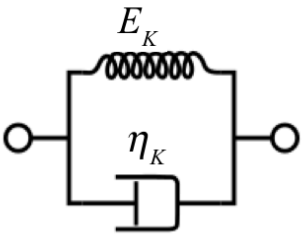

(b) Kelvin model

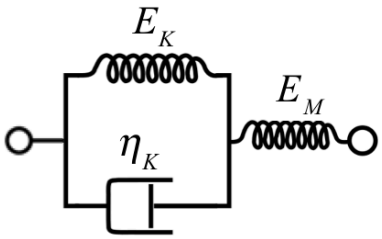

(c) SLS model (Thomson type)

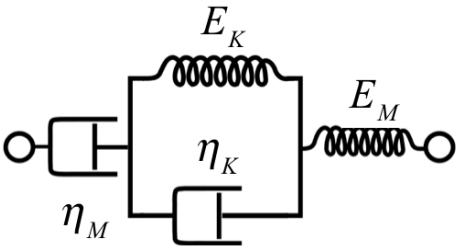

(d) Burgers model

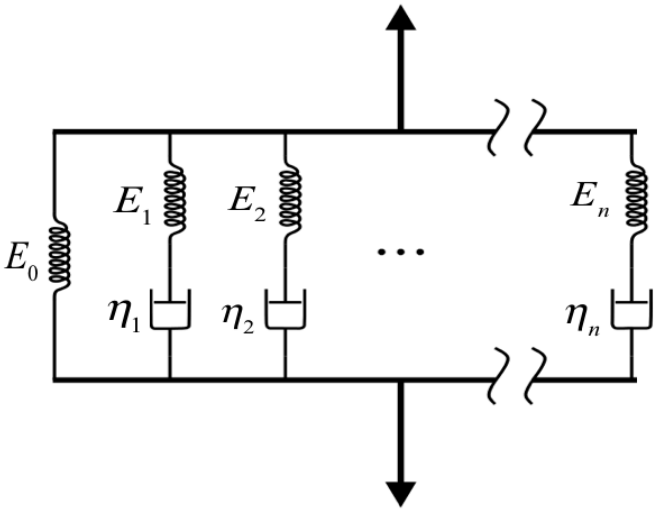

(e) Maxwell chain (Wiechert model)

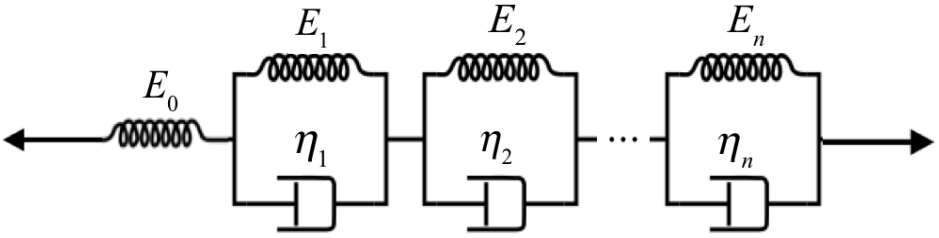

(f) Kelvin chain

Figure 6.4 Some constitutive models for linear viscoelasticity

6.3.3 The Analogy Young's Modulus of Simple Viscoelastic Models

The analogy Young's modulus of a viscoelastic material is defined as

$$E^A(s) \equiv \frac{\sigma^{TD}(s)}{\varepsilon^{TD}(s)} \tag{6.8}$$

where $\sigma^{TD}(s)$ is the transformed stress in the Laplace domain and $\varepsilon^{TD}(s)$ is the transformed strain in the Laplace domain. The superscript index *TD* denotes the transformed domain.

According to this definition, the analogy Young's modulus of a certain viscoelastic model can be derived from the corresponding stress-strain relations. For example, the analogy Young's modulus of the linear Newton dashpot in Figure 6.3, whose stress-strain relation can be described by Eqn. (6.6), can be expressed as

$$E^A = \eta s, \qquad \sigma^{TD} = E^A \varepsilon^{TD} \tag{6.9}$$

Analytical expressions (closed forms) for stress-strain relation and analogy Young's modulus of some aforementioned simple viscoelastic models are listed in Table 6.1.

Table 6.1 Closed form stress-strain relations and analogy Young's moduli of some simple viscoelastic models

Model	Stress-Strain Relation	Analogy Young's modulus
Maxwell	$\frac{d\sigma}{dt} + \frac{\sigma}{\tau_M} = E_M \frac{d\varepsilon}{dt}$	$E_M \frac{s}{s + 1/\tau_M}$

Kelvin	$\sigma = E_K\left(\tau_K \dfrac{d\varepsilon}{dt} + \varepsilon\right)$	$E_K \tau_K \left(s + 1/\tau_K\right)$
Thomson	$\tau_K \dfrac{d\sigma}{dt} + m_T \sigma = E_M\left(\tau_K \dfrac{d\varepsilon}{dt} + \varepsilon\right)$	$E_M \dfrac{s + 1/\tau_K}{s + m_T/\tau_K}$
Burgers	$\tau_K^2 \dfrac{d^2\sigma}{dt^2} + \left(m_{B1} + m_{B2}\right)\tau_K \dfrac{d\sigma}{dt} + m_{B1} m_{B2}\sigma = E_M\left(\tau_K^2 \dfrac{d^2\varepsilon}{dt^2} + \tau_K \dfrac{d\varepsilon}{dt}\right)$	$E_M \dfrac{s\left(s + 1/\tau_K\right)}{\left(s + m_{B1}/\tau_K\right)\left(s + m_{B2}/\tau_K\right)}$

τ_M, τ_K are the relaxation times for Maxwell and Kelvin model defined as the ratio of viscosity to stiffness

$$\tau_M = \frac{\eta_M}{E_M}, \qquad \tau_K = \frac{\eta_K}{E_K} \tag{6.10}$$

and m_T, m_{B1}, m_{B2} are the pertinent elastic moduli of Thomson and Burgers models respectively, which are defined as

$$m_T = 1 + \frac{E_M}{E_K} \tag{6.11}$$

$$\begin{matrix} m_{B1} \\ m_{B2} \end{matrix} = \frac{1}{2}\left(m_T + \frac{\tau_K}{\tau_M} \pm \sqrt{\left(m_T + \frac{\tau_K}{\tau_M}\right)^2 - 4\frac{\tau_K}{\tau_M}}\right) \tag{6.12}$$

Contrasting to simple models, the stress-strain relation of generalized models can be expressed in a differential form as follows in deviatoric and volumetric parts, respectively:

$$\begin{aligned} R(D)\sigma_D(t) &= S(D)\varepsilon_D(t) \\ P(D)\sigma_V(t) &= Q(D)\varepsilon_V(t) \end{aligned} \tag{6.13}$$

where *R, S, P* and *Q* are differential operators and *D* represents the time derivative.

More specifically, Eqn. (6.13) can be extended and expressed by the following equations:

$$\begin{aligned}\sum_{n=1}^{N}\alpha_n\frac{d^n\sigma_D}{dt^n}+\alpha_0\sigma_D&=\sum_{n=1}^{N}2\beta_n\frac{d^n\varepsilon_D}{dt^n}+2\beta_0\varepsilon_D\\ \sum_{n=1}^{N}\bar{\alpha}_n\frac{d^n\sigma_V}{dt^n}+\bar{\alpha}_0\sigma_V&=\sum_{n=1}^{N}2\bar{\beta}_n\frac{d^n\varepsilon_V}{dt^n}+2\beta_0\bar{\varepsilon}_V\end{aligned} \tag{6.14}$$

where $\alpha_n,\beta_n,\bar{\alpha}_n$ *and* $\bar{\beta}_n\left(n=1\sim N\right)$ are constants from *N* connected elements.

Therefore, the analogy Young's modulus of generalized models can be written as follows:

For Maxwell chain in Figure 6.4

$$E^A=E_0+\int_0^\infty\frac{sH(\tau)}{1+\tau s}d\tau \tag{6.15}$$

For Kevin chain in Figure 6.4

$$E^A=\left[\frac{1}{E_0}+\frac{1}{\eta_0 s}+\int_0^\infty\frac{L(\tau)}{\tau(1+\tau s)}d\tau\right]^{-1} \tag{6.16}$$

where $L(\tau)$ is the retardation spectrum and $H(\tau)$ is the relaxation spectrum (Dziugys & Peters, 2001).

6.3.4 The Creep Compliance and Relaxation Modulus

Creep is defined as a time-dependent deformation that occurs when a material is subjected to loading over time. In a creep test a static load is applied to a specimen and the deformation over time is measured. The creep compliance is then computed using

$$C(t) = \frac{\varepsilon(t)}{\sigma_0} \tag{6.17}$$

where σ_0 is the constant stress.

The creep strain usually increases with an ever decreasing strain rate so that eventually a more-or-less constant-strain steady state is reached, but many materials often do not reach such a noticeable steady-state, even after a very long time.

On the other hand, if the instant strain is fixed and remains constant, the stress required to hold the viscoelastic material at the constant strain will be found to decrease over time. This phenomenon is called stress relaxation; it is due to a re-arrangement of the material on the molecular or micro-scale. The relaxation modulus $E(t)$ is computed using

$$E(t) = \frac{\sigma(t)}{\varepsilon_0} \tag{6.18}$$

where ε_0 is the constant strain.

For general viscoelastic models, the solutions to Eqn. (6.13) and (6.14) can be represented in an integral form. For any smooth strain history $\boldsymbol{\varepsilon}(t)$ with $\boldsymbol{\varepsilon}(0) = 0$, the general solution of the stress-strain relation is given by the well-known Boltzmann superposition integral representation (Christensen, 1982)

$$\sigma(t) = \int_0^t E(t-\tau)\dot{\varepsilon}(t)\,d\tau \tag{6.19}$$

For any smooth stress history $\boldsymbol{\sigma}(t)$ with $\boldsymbol{\sigma}(0) = 0$, the general solution of the stress-strain relation can be obtained by

$$\varepsilon(t) = \int_0^t C(t-\tau)\,\dot{\sigma}(\tau)\,d\tau \tag{6.20}$$

The creep function and relaxation function are related by an integral equation so that if one function is determined, the other function can be obtained by solving the following equation

$$E^{TD}(s)C^{TD}(s)=\frac{1}{s^2} \tag{6.21}$$

where $E^{TD}(s)$ is the transformed relaxation function in Laplace domain and $C^{TD}(s)$ is the transformed creep function in Laplace domain (Ferry, 1980; Leaderman, 1958).

Specifically, for a four-parameter Burgers model, the creep and the relaxation functions can be expressed by the following forms (Burgers, 1939)

$$\begin{aligned} C(t)&=\frac{1}{E_M}\left[1+\frac{t}{\tau_M}+\alpha\left(1-\exp\left(-\frac{t}{\tau_K}\right)\right)\right] \\ E(t)&=\frac{E_M}{m_{B1}-m_{B2}}\left[\left(m_{B1}-1\right)\exp\left(-m_{B1}\frac{t}{\tau_K}\right)-\left(m_{B2}-1\right)\exp\left(-m_{B2}\frac{t}{\tau_K}\right)\right] \end{aligned} \tag{6.22}$$

When considering the viscoelastic behavior of asphalt materials, it is often more advantageous to use the creep compliance than to use the modulus because the compliance can allow separation of its response over time into time-dependent and time independent components (Witczak et al., 2002).

6.3.5 The Complex Modulus

The complex modulus is another important viscoelastic property used for characterizing the relations between the oscillating stress and strain. It can be determined

in the lab by applying steady-state sinusoidal loading to asphalt specimens at different frequencies. The applied stress and corresponding strain response are measured, and the axial complex modulus is defined/calculated by

$$E^* = \left|E^*\right| e^{i\varphi} = \frac{\sigma^*}{\varepsilon^*} = \frac{\sigma_0 e^{iwt}}{\varepsilon_0 e^{i(wt-\varphi)}} = E^*_{real} + iE^*_{imag} \tag{6.23}$$

where σ_0 is the stress amplitude, ε_0 is the strain amplitude, w is the frequency and φ is the phase lag or phase angle. In the complex plane, the real part of the complex modulus is called the storage or elastic modulus E^*_{real} while the imaginary part is the loss or viscous modulus E^*_{imag} shown in Figure 6.5.The phase angle gives an indication of how viscous the material is; the material becomes more viscous as the phase angle increases. For example, if the phase angle is zero, the material behaves as purely elastic. A phase angle of 90 degree means that the material behaves as purely viscous.

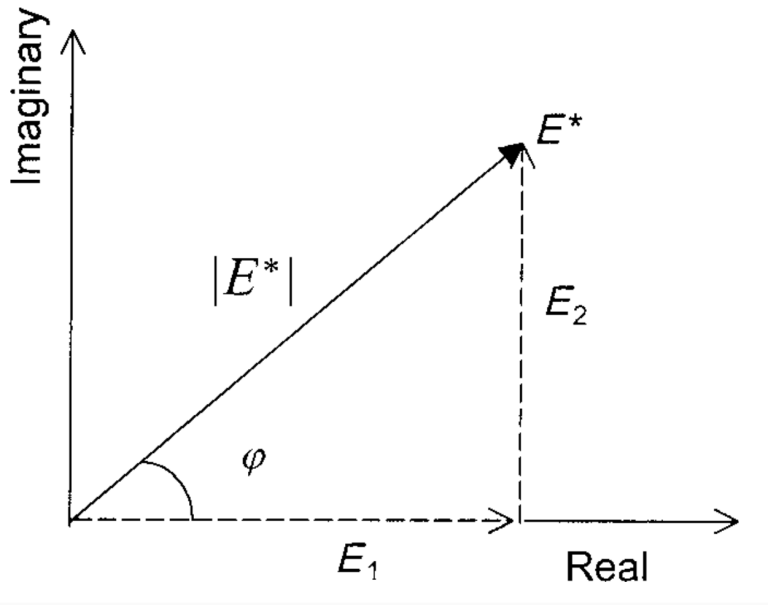

Figure 6.5 The storage and loss moduli in complex plane (Y. R. Kim, 2008)

For simple models such as Burgers model, the complex modulus can be derived by employing the correspondence principle to the analogy Young's modulus. The theoretical expression of complex modulus for Burgers model is proposed below as

$$E^*\left(iw\right)=\frac{E_M\eta_M\left(E_K+\eta_K iw\right)iw}{E_M E_K+\left(E_M\eta_M+E_M\eta_K+E_K\eta_M\right)iw+E_M E_K\left(iw\right)^2} \tag{6.24}$$

$$\varphi\left(w\right)=\tan^{-1}\left(\frac{E^*_{imag}\left(w\right)}{E^*_{real}\left(w\right)}\right) \tag{6.25}$$

6.4 Evaluating Viscoelastic Properties of Asphalt Mastic Composite

Asphalt mastic, composed by fine aggregates, asphalt binder, p-DCPD and air voids, is a composite material. To simplify the analysis, the heterogeneous asphalt mastic whose viscoelastic properties are functions with respect to time can be reduced (transformed) into elastic moduli in Laplace domain, and represented by an equivalent homogeneous continuum media with appropriately defined effective properties.

From Table 6.1, the analogy Young's modulus of Burgers model can be simplified as

$$E^A=E_M\frac{s\left(s+n_1\right)}{\left(s+n_2\right)\left(s+n_3\right)} \tag{6.26}$$

where $n_1=1/\boldsymbol{\tau}_K$, $n_2=m_{B1}/\boldsymbol{\tau}_K$, $n_3=m_{B2}/\boldsymbol{\tau}_K$.

Therefore, for a constituent simulated by Burgers model, the bulk and shear moduli in transformed domain are

$$K^{TD} = K_M \frac{s\left(s+n_1\right)}{\left(s+n_2\right)\left(s+n_3\right)}$$
$$\mu^{TD} = \mu_M \frac{s\left(s+n_1\right)}{\left(s+n_2\right)\left(s+n_3\right)} \tag{6.27}$$

Hashin-Shtrikman bounds of bulk and shear moduli in transformed domain of two-phase composite materials with spherical inclusion by Li and Weng (J. Li & Weng, 1994) are used

$$K^{TD}\left(s\right) = K_0^{TD} + \frac{f_1\left(K_1^{TD} - K_0^{TD}\right)}{f_0\alpha_0^{TD}\left(K_1^{TD} - K_0^{TD}\right) + K_0^{TD}} K_0^{TD}$$
$$\mu^{TD}\left(s\right) = \mu_0^{TD} + \frac{f_1\left(\mu_1^{TD} - \mu_0^{TD}\right)}{f_0\beta_0^{TD}\left(\mu_1^{TD} - \mu_0^{TD}\right) + \mu_0^{TD}} \mu_0^{TD} \tag{6.28}$$

where

$$\alpha_0^{TD} = \frac{1}{3}\frac{1+v_0^{TD}}{1-v_0^{TD}} = \frac{3K_0^{TD}}{3K_0^{TD}+4\mu_0^{TD}}$$
$$\beta_0^{TD} = \frac{2}{15}\frac{4-5v_0^{TD}}{1-v_0^{TD}} = \frac{6}{5}\frac{K_0^{TD}+2\mu_0^{TD}}{3K_0^{TD}+4\mu_0^{TD}} \tag{6.29}$$

and 0 and 1 denote the matrix and particles, respectively.

The stress-strain relation of the isotropic composite in transformed domain can be expressed as follow

$$\bar{\sigma}_{kk}^{TD} = 3K^{TD}\left(s\right)\bar{\varepsilon}_{kk}^{TD}, \qquad \bar{\sigma}_{ij}^{TD} = 2\mu^{TD}\left(s\right)\bar{\varepsilon}_{ij}^{TD} \tag{6.30}$$

6.4.1 The Effective Bulk and Shear Moduli

Under a constant strain rate, if the initial conditions are assumed to be zero, one has $\bar{\varepsilon}_{ij}^{TD}(s)=\dot{\bar{\varepsilon}}_{ij}/s^2$. With the given K^{TD} and μ^{TD} in Eqn. (6.28) , the growth of $\bar{\sigma}_{kk}(t)$ and $\bar{\sigma}_{ij}(t)$ in time domain can be determined by Laplace inverse on Eqn. (6.30) . Here, inclusions are assumed to be elastic. Furthermore, Poisson's ratio is assumed to be a constant when the asphalt is under viscoelastic deformation which implies $v_0^{TD}=v_0$. With the above two assumptions, the effective bulk and shear moduli in transformed domain for two-phase asphalt matrix can be expressed by

$$\begin{aligned} K^{TD}(s)&=\left[1+\frac{f_1\left(K_1-K_0^{TD}\right)}{f_0\alpha_0\left(K_1-K_0^{TD}\right)+K_0^{TD}}\right]K_0^{TD}\\ \mu^{TD}(s)&=\left[1+\frac{f_1\left(\mu_1-\mu_0^{TD}\right)}{f_0\beta_0\left(\mu_1-\mu_0^{TD}\right)+\mu_0^{TD}}\right]\mu_0^{TD} \end{aligned} \tag{6.31}$$

Take volumetric part for demonstration. Plug bulk modulus equation in Eqn. (6.31) into Eqn. (6.30), one can have

$$\bar{\sigma}_{kk}^{TD}=3K^{TD}(s)\dot{\bar{\varepsilon}}_{kk}/s^2=\left[(1)+(2)+(3)+(4)\right]3\dot{\bar{\varepsilon}}_{kk} \tag{6.32}$$

where

$$(1)=K_M\frac{s+n_1}{s\left(s+n_2\right)\left(s+n_3\right)}$$

$$(2)=\frac{f_1K_M\left(K_1-K_M\right)}{f_0\alpha_0\left(K_1-K_M\right)+K_M}\frac{s\left(s+n_1\right)}{\left(s+n_2\right)\left(s+n_3\right)\left(s^2+2n_4s+n_5\right)}$$

$$(3)=\frac{f_1K_M\left[K_1\left(n_2+n_3\right)-K_Mn_1\right]}{f_0\alpha_0\left(K_1-K_M\right)+K_M}\frac{s+n_1}{\left(s+n_2\right)\left(s+n_3\right)\left(s^2+2n_4s+n_5\right)}$$

$$(4)=\frac{f_1K_1K_M n_2 n_3}{f_0\alpha_0\left(K_1-K_M\right)+K_M}\frac{s+n_1}{s\left(s+n_2\right)\left(s+n_3\right)\left(s^2+2n_4 s+n_5\right)}$$

in which $2n_4=\dfrac{f_0\alpha_0\left[K_1\left(n_2+n_3\right)-K_M n_1\right]}{f_0\alpha_0\left(K_1-K_M\right)+K_M}$, $n_5=\dfrac{f_0\alpha_0 K_1 n_2 n_3}{f_0\alpha_0\left(K_1-K_M\right)+K_M}$.

To obtain the effective bulk modulus in time domain, Laplace inverse is performed on Eqn. (6.32) and renders

$$K\left(t\right)=Laplace\ inverse\left[(1)+(2)+(3)+(4)\right]=(5)+(6)+(7)+(8) \tag{6.33}$$

where

$$(5)=K_M\left[\frac{n_1}{n_2 n_3}+\frac{n_1-n_2}{n_2\left(n_2-n_3\right)}e^{-n_2 t}+\frac{n_3-n_1}{n_3\left(n_2-n_3\right)}e^{-n_3 t}\right]$$

$$(6)=\frac{f_1K_M\left(K_1-K_M\right)}{f_0\alpha_0\left(K_1-K_M\right)+K_M}\left[A_1e^{-n_2 t}+B_1e^{-n_3 t}+C_1e^{-\left(n_4+m\right)t}+D_1e^{-\left(n_4-m\right)t}\right]$$

$$(7)=\frac{f_1K_M\left[K_1\left(n_2+n_3\right)-K_M n_1\right]}{f_0\alpha_0\left(K_1-K_M\right)+K_M}\left[A_2e^{-n_2 t}+B_2e^{-n_3 t}+C_2e^{-\left(n_4+m\right)t}+D_2e^{-\left(n_4-m\right)t}\right]$$

$$(8)=\frac{f_1K_1K_M n_2 n_3}{f_0\alpha_0\left(K_1-K_M\right)+K_M}\left[A_3+B_3e^{-n_2 t}+C_3e^{-n_3 t}+D_3e^{-\left(n_4+m\right)t}+E_3e^{-\left(n_4-m\right)t}\right]$$

in which $m=\sqrt{n_4^2-n_5}>0$, $A_1=\dfrac{n_2\left(n_1-n_2\right)}{\left(n_2-n_3\right)\left(-m+n_2-n_4\right)\left(m+n_2-n_4\right)}$,

$B_1=\dfrac{n_3\left(n_3-n_1\right)}{\left(n_2-n_3\right)\left(-m+n_3-n_4\right)\left(m+n_3-n_4\right)}$, $C_1=-\dfrac{\left(m+n_4\right)\left(m-n_1+n_4\right)}{2m\left(m-n_2+n_4\right)\left(m-n_3+n_4\right)}$,

$D_1=\dfrac{\left(m-n_4\right)\left(m+n_1-n_4\right)}{2m\left(m+n_2-n_4\right)\left(m+n_3-n_4\right)}$, $A_2=\dfrac{n_2-n_1}{\left(n_2-n_3\right)\left(-m+n_2-n_4\right)\left(m+n_2-n_4\right)}$,

$B_2=\dfrac{n_3-n_1}{\left(n_3-n_2\right)\left(-m+n_3-n_4\right)\left(m+n_3-n_4\right)}$, $C_2=\dfrac{m-n_1+n_4}{2m\left(m-n_2+n_4\right)\left(m-n_3+n_4\right)}$,

$D_2=\dfrac{m+n_1-n_4}{2m\left(m+n_2-n_4\right)\left(m+n_3-n_4\right)}$, $A_3=\dfrac{n_1}{-m^2n_2n_3+n_2n_3n_4^2}$,

$$B_3=\frac{n_1-n_2}{n_2\left(n_2-n_3\right)\left(-m+n_2-n_4\right)\left(m+n_2-n_4\right)},\ C_3=\frac{n_3-n_1}{n_3\left(n_2-n_3\right)\left(-m+n_3-n_4\right)\left(m+n_3-n_4\right)},$$

$$D_3=-\frac{m-n_1+n_4}{2m\left(m+n_4\right)\left(m-n_2+n_4\right)\left(m-n_3+n_4\right)},\ E_3=\frac{m+n_1-n_4}{2m\left(m-n_4\right)\left(m+n_2-n_4\right)\left(m+n_3-n_4\right)}.$$

Effective shear modulus in time domain can be obtained by following the same procedures demonstrated above.

6.4.2 The Effective Relaxation Function

The effective relaxation behavior can be examined as well by means of Eqn. (6.30) with a constant strain. It follows that

$$\bar{\sigma}_{kk}^{TD}=\left[(9)+(10)+(11)+(12)\right]3\bar{\varepsilon}_{kk} \tag{6.34}$$

where

$$(9)=K_M\frac{s+n_1}{\left(s+n_2\right)\left(s+n_3\right)}$$

$$(10)=\frac{f_1K_M\left(K_1-K_M\right)}{f_0\alpha_0\left(K_1-K_M\right)+K_M}\frac{s^2\left(s+n_1\right)}{\left(s+n_2\right)\left(s+n_3\right)\left(s^2+2n_4s+n_5\right)}$$

$$(11)=\frac{f_1K_M\left[K_1\left(n_2+n_3\right)-K_Mn_1\right]}{f_0\alpha_0\left(K_1-K_M\right)+K_M}\frac{s\left(s+n_1\right)}{\left(s+n_2\right)\left(s+n_3\right)\left(s^2+2n_4s+n_5\right)}$$

$$(12)=\frac{f_1K_1n_2n_3}{f_0\alpha_0\left(K_1-K_M\right)+K_M}\frac{s+n_1}{\left(s+n_2\right)\left(s+n_3\right)\left(s^2+2n_4s+n_5\right)}$$

To obtain the effective volumetric relaxation function, Laplace inverse is performed on Eqn. (6.34)

$$E_K\left(t\right)=Laplace\ inverse\left[(9)+(10)+(11)+(12)\right]=(13)+(14)+(15)+(16) \tag{6.35}$$

where

$$(13) = K_M\left[\frac{n_2-n_1}{n_2-n_3}e^{-n_2 t}+\frac{n_1-n_3}{n_2-n_3}e^{-n_3 t}\right]$$

$$(14) = \frac{f_1 K_M\left(K_1-K_M\right)}{f_0\alpha_0\left(K_1-K_M\right)+K_M}\left[A_4 e^{-n_2 t}+B_4 e^{-n_3 t}+C_4 e^{-\left(n_4+m\right)t}+D_4 e^{-\left(n_4-m\right)t}\right]$$

$$(15) = \frac{f_1 K_M\left[K_1\left(n_2+n_3\right)-K_M n_1\right]}{f_0\alpha_0\left(K_1-K_M\right)+K_M}\left[A_5 e^{-n_2 t}+B_5 e^{-n_3 t}+C_5 e^{-\left(n_4+m\right)t}+D_5 e^{-\left(n_4-m\right)t}\right]$$

$$(16) = \frac{f_1 K_1 K_M n_2 n_3}{f_0\alpha_0\left(K_1-K_M\right)+K_M}\left[A_6 e^{-n_2 t}+B_6 e^{-n_3 t}+C_6 e^{-\left(n_4+m\right)t}+D_6 e^{-\left(n_4-m\right)t}\right]$$

in which $A_4 = \frac{n_2^2\left(n_2-n_1\right)}{\left(n_2-n_3\right)\left(-m+n_2-n_4\right)\left(m+n_2-n_4\right)}$,

$B_4 = \frac{n_3^2\left(n_1-n_3\right)}{\left(n_2-n_3\right)\left(-m+n_3-n_4\right)\left(m+n_3-n_4\right)}$, $C_4 = \frac{\left(m+n_4\right)^2\left(m-n_1+n_4\right)}{2m\left(m-n_2+n_4\right)\left(m-n_3+n_4\right)}$,

$D_4 = \frac{\left(m-n_4\right)^2\left(m+n_1-n_4\right)}{2m\left(m+n_2-n_4\right)\left(m+n_3-n_4\right)}$, $A_5 = A_1$, $B_5 = B_1$, $C_5 = C_1$, $D_5 = D_1$, $A_6 = A_2$,

$B_6 = B_2$, $C_6 = C_2$, $D_6 = D_2$.

Effective deviatoric relaxation function in time domain can be obtained by following the same procedures demonstrated above. The effective creep function can be calculated by following Eqn. (6.21).

6.4.3 The Effective Complex Modulus

The effective complex bulk modulus can be expressed as

$$K^* = K_0^* + \frac{f_1\left(K_1-K_o^*\right)}{f_0\alpha_0\left(K_1-K_0^*\right)+K_0^*}K_0^* \tag{6.36}$$

where

$$K_0^* = K_0^R + iK_0^I \tag{6.37}$$

in which

$$K_0^R = K_M \frac{w^4 + \left[n_1\left(n_2+n_3\right) - n_2 n_3 \right] w^2}{\left(n_2 n_3 - w^2\right)^2 + w^2\left(n_2+n_3\right)^2}$$

$$K_0^I = K_M \frac{w\left[n_1\left(n_2 n_3 - w^2\right) + \left(n_2+n_3\right) w^2 \right]}{\left(n_2 n_3 - w^2\right)^2 + w^2\left(n_2+n_3\right)^2}$$

Then, the real part and the imaginary part of the effective complex bulk modulus can be written as

$$\begin{aligned} K^R &= K_0^R + \frac{\xi_1}{1+\xi_3^2}\left[K_0^R\left(1-\xi_2\xi_3\right) + K_0^I\left(\xi_2+\xi_3\right) \right] \\ K^I &= K_0^I + \frac{\xi_1}{1+\xi_3^2}\left[K_0^I\left(1-\xi_2\xi_3\right) - K_0^R\left(\xi_2+\xi_3\right) \right] \end{aligned} \tag{6.38}$$

where $\xi_1 = \dfrac{f_1\left(K_1 - K_0^R\right)}{f_0\alpha_0\left(K_1 - K_0^R\right) + K_0^R}$, $\xi_2 = \dfrac{K_0^I}{K_1 - K_0^R}$, $\xi_3 = \dfrac{\left(1-f_0\alpha_0\right)K_0^I}{f_0\alpha_0\left(K_1 - K_0^R\right) + K_0^R}$.

By following the same procedure, the real part and the imaginary part of the effective complex shear modulus can be obtained

$$\begin{aligned} \mu^R &= \mu_0^R + \frac{\xi_4}{1+\xi_6^2}\left[\mu_0^R\left(1-\xi_5\xi_6\right) + \mu_0^I\left(\xi_5+\xi_6\right) \right] \\ \mu^I &= \mu_0^I + \frac{\xi_4}{1+\xi_6^2}\left[\mu_0^I\left(1-\xi_5\xi_6\right) - \mu_0^R\left(\xi_5+\xi_6\right) \right] \end{aligned} \tag{6.39}$$

where $\xi_4 = \dfrac{f_1\left(\mu_1 - \mu_0^R\right)}{f_0\beta_0\left(\mu_1 - \mu_0^R\right) + \mu_0^R}$, $\xi_5 = \dfrac{\mu_0^I}{\mu_1 - \mu_0^R}$, $\xi_6 = \dfrac{\left(1-f_0\beta_0\right)\mu_0^I}{f_0\beta_0\left(\mu_1 - \mu_0^R\right) + \mu_0^R}$.

The above derivations (starting Eqn. (6.28)) are valid for two-phase composites yet the proposed asphalt mastic is a four-phase composite. In order to evaluate the viscoelastic

properties of the 4-phase asphalt mastic, a multilevel homogenization procedure is established, illustrated in Figure 6.6.

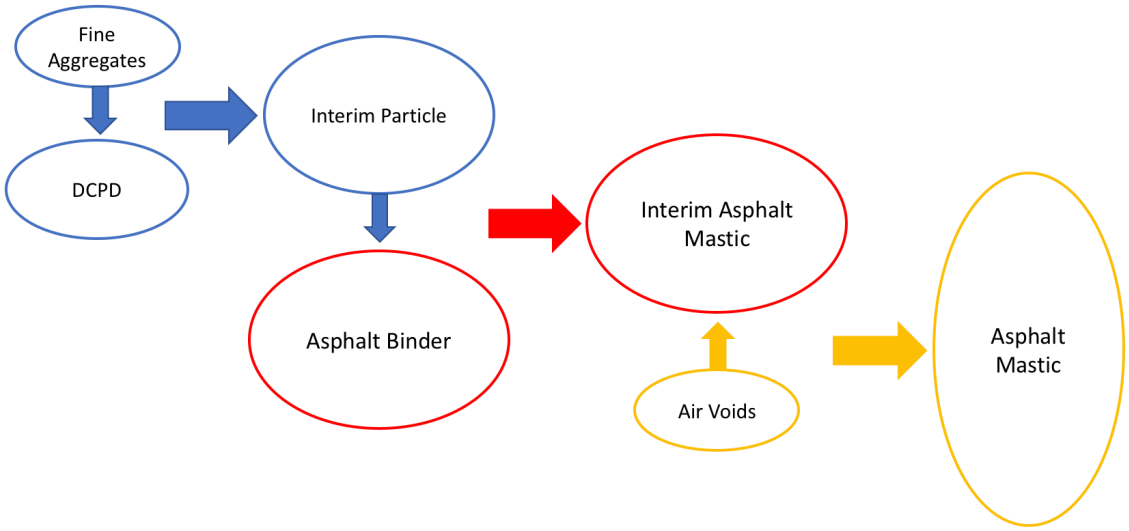

Figure 6.6 The multilevel homogenization procedure to apply Ju and Chen's pairwise interacting solution

A relatively more precise evaluation of effective bulk and shear moduli is to employ Ju and Chen's pairwise interacting solution (Ju & Chen, 1994a, 1994b) comparing to Hashin-Shtrikman bounds. In particular, the pairwise interacting solution may lead to an accurate higher-order formulation for the prediction of elastic particulate composites at moderately high particle concentrations. Ju and Chen's elastic formulation for a two-phase (inclusions and matrix) composite states that, if the inclusions (particles) are assumed to

be identical and spherical in an elastic matrix, the effective bulk modulus $\overline{K}$ and effective shear modulus $\overline{\mu}$ of this composite can be explicitly evaluated as

$$\begin{aligned}\overline{K} &= K_0\left[1+\frac{30\left(1-\upsilon_0\right)f_1\left(3\gamma_1+2\gamma_2\right)}{3\alpha+2\beta-10\left(1+\upsilon_0\right)f_1\left(3\gamma_1+2\gamma_2\right)}\right]\\ \overline{\mu} &= \mu_0\left[1+\frac{30\left(1-\upsilon_0\right)f_1\gamma_2}{\beta-4\left(4-5\upsilon_0\right)f_1\gamma_2}\right]\end{aligned} \tag{6.40}$$

where

$$\begin{aligned}\gamma_1 &= \frac{5f_1}{96\beta^2}\left\{12\upsilon_0\left(13-14\upsilon_0\right)-\frac{96\alpha}{3\alpha+2\beta}\left(1-2\upsilon_0\right)\left(1+\upsilon_0\right)\right\}\\ \gamma_2 &= \frac{1}{2}+\frac{5f_1}{96\beta^2}\left\{6\left(25-34\upsilon_0+22\upsilon_0^{\,2}\right)-\frac{36\alpha}{3\alpha+2\beta}\left(1-2\upsilon_0\right)\left(1+\upsilon_0\right)\right\}\end{aligned}$$

and

$$\begin{aligned}\alpha &= 2\left(5\upsilon_0-1\right)+10\left(1-\upsilon_0\right)\left(\frac{K_0}{K_1-K_0}-\frac{\mu_0}{\mu_1-\mu_0}\right)\\ \beta &= 2\left(4-5\upsilon_0\right)+15\left(1-\upsilon_0\right)\frac{\mu_0}{\mu_1-\mu_0}\end{aligned}$$

Corresponding to these elastic expressions, and with the same assumptions that particles remain elastic while the matrix is viscoelastic, and that Poisson's ratio of asphalt is a constant during viscoelastic deformation, we would have the effective bulk and shear moduli in the transformed domain are:

$$\begin{aligned}\overline{K}^{TD}\left(s\right) &= K_0^{TD}\left(s\right)\left[1+\frac{30\left(1-\upsilon_0\right)f_1\left(3\gamma_1^s+2\gamma_2^s\right)}{3\overline{\alpha}\left(s\right)+2\overline{\beta}\left(s\right)-10\left(1+\upsilon_0\right)f_1\left(3\gamma_1^s+2\gamma_2^s\right)}\right]\\ \overline{\mu}^{TD}\left(s\right) &= \mu_0^{TD}\left(s\right)\left[1+\frac{30\left(1-\upsilon_0\right)f_1\gamma_2^s}{\overline{\beta}\left(s\right)-4\left(4-5\upsilon_0\right)f_1\gamma_2^s}\right]\end{aligned} \tag{6.41}$$

where

$$\gamma_1^s = \frac{5f_1}{96\bar{\beta}(s)^2}\left\{12\upsilon_0(13-14\upsilon_0) - \frac{96\bar{\alpha}(s)}{3\bar{\alpha}(s)+2\bar{\beta}(s)}(1-2\upsilon_0)(1+\upsilon_0)\right\}$$

$$\gamma_2^s = \frac{1}{2} + \frac{5f_1}{96\bar{\beta}(s)^2}\left\{6(25-34\upsilon_0+22\upsilon_0^{\,2}) - \frac{36\bar{\alpha}(s)}{3\bar{\alpha}(s)+2\bar{\beta}(s)}(1-2\upsilon_0)(1+\upsilon_0)\right\}$$

and

$$\bar{\alpha}(s) = 2(5\upsilon_0-1) + 10(1-\upsilon_0)\left(\frac{K_0^{TD}(s)}{K_1 - K_0^{TD}(s)} - \frac{\mu_0^{TD}(s)}{\mu_1 - \mu_0^{TD}(s)}\right)$$

$$\bar{\beta}(s) = 2(4-5\upsilon_0) + 15(1-\upsilon_0)\frac{\mu_0^{TD}(s)}{\mu_1 - \mu_0^{TD}(s)}$$

The effective bulk and shear moduli, relaxation and creep functions, and complex modulus can be derived with the same procedures as illustrated above using Hashin-Shtrikman bounds. The expressions would be quite lengthy due to the fact that formulations of Ju and Chen's pairwise interacting solution is one order higher than those of Hashin-Shtrikman bounds.

Complex modulus can also be numerically evaluated based on the relaxation or creep functions, or the vice versa, based on the transformation methodology developed by Schapery and Park (Schapery & Park, 1999).

6.4.4 Results and Comparison

The effective bulk modulus, relaxation functions and complex modulus of various phases of asphalt mastic composites are calculated following the aforementioned procedures in Mathematica, while some results shown in Figure 6.7-Figure 6.10. To be

specific, the 2-phase composite includes asphalt binder and fine aggregates; the 3-phase composite includes asphalt binder, fine aggregates and DCPD; and the 4-phase composite includes asphalt binder, fine aggregates, DCPD and air voids. Among all these composites, asphalt binder is always considered as the matrix. The strain rate is constant. The elastic properties of the fine aggregates and DCPD, and viscoelastic properties of asphalt binder are listed in Table 6.2.

Table 6.2 Elastic and viscoelastic properties for the asphalt mastic composite

	Fine aggregates		**DCPD**	
Young's modulus	7.25e6 (*psi*)		2.784e5 (*psi*)	
Poisson's ratio	0.2		0.39	
Asphalt binder (Burgers model)				
E_M	η_M	E_K	η_K	Poisson's ratio
1.45e4 (*psi*)	1.0e5 (*psi.s*)	1.0e4 (*psi*)	2.3e5 (*psi.s*)	0.3

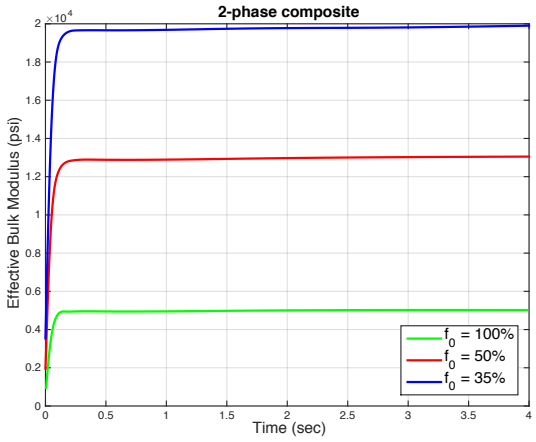

(a)

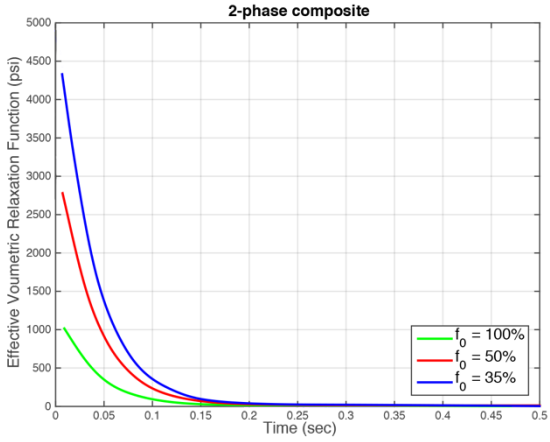

(b)

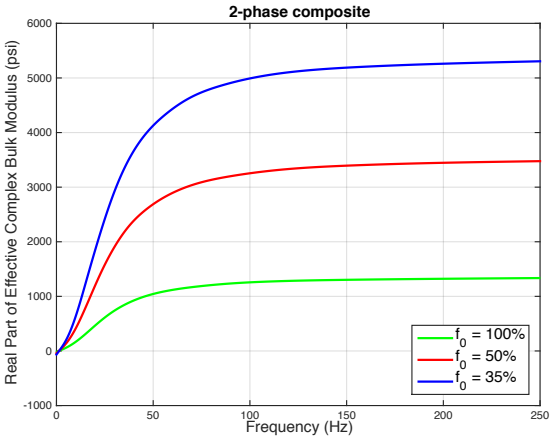

(c)

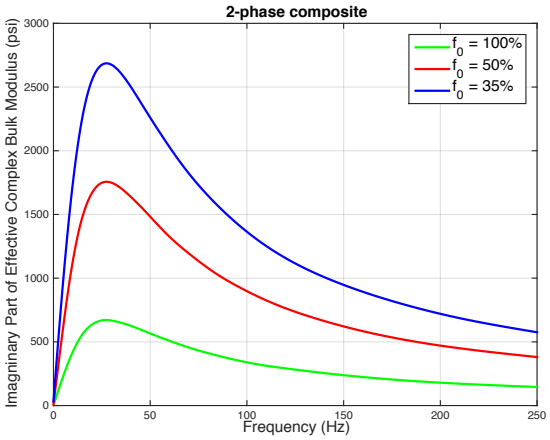

(d)

Figure 6.7 Results for 2-Phase Composite: (a) Effective bulk modulus under constant strain rate; (b) Effective bulk relaxation function under constant strain; (c) Real part of effective complex bulk modulus; (d) Imaginary part of effective complex bulk modulus

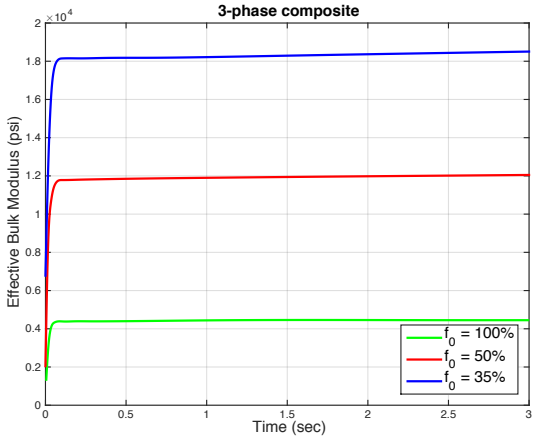

(a)

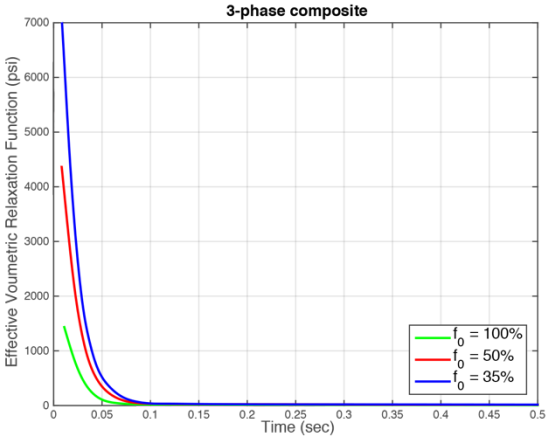

(b)

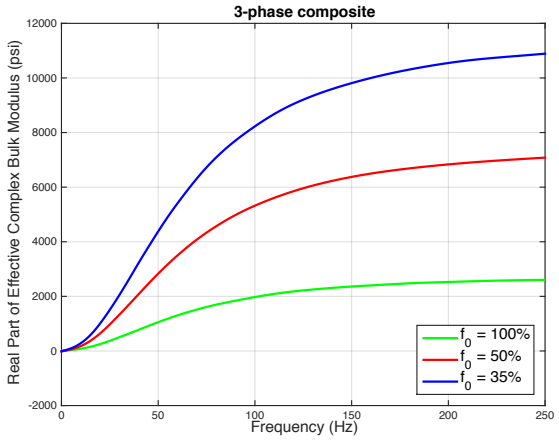

(c)

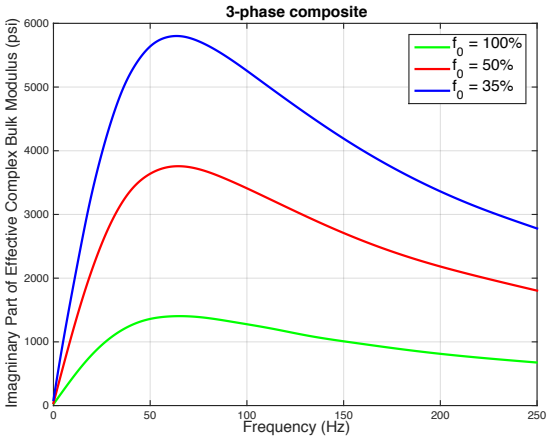

(d)

Figure 6.8 Results for 3-Phase Composite: (a) Effective bulk modulus under constant strain rate; (b) Effective bulk relaxation function under constant strain; (c) Real part of effective complex bulk modulus; (d) Imaginary part of effective complex bulk modulus

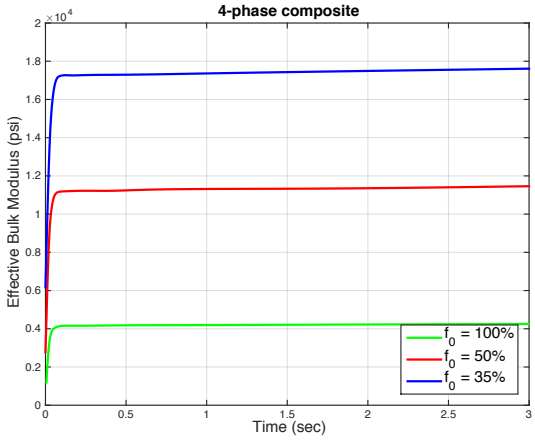

(a)

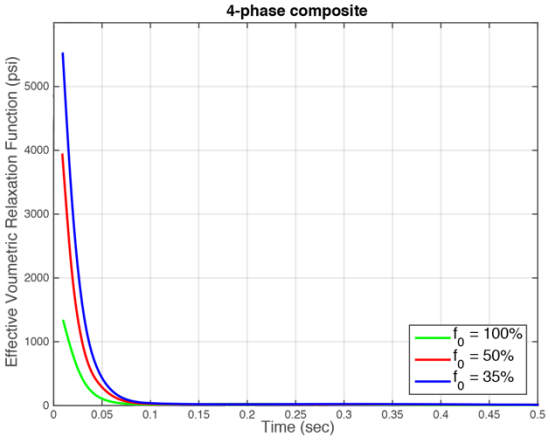

(b)

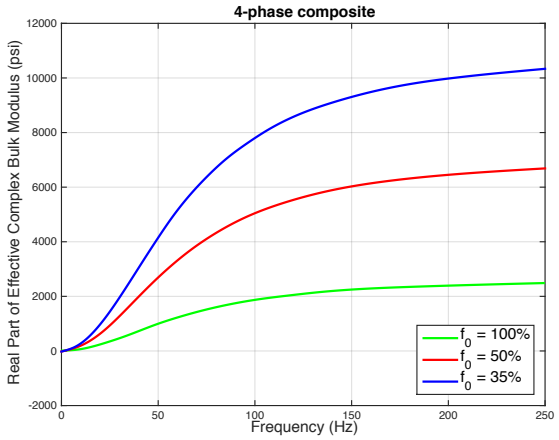

(c)

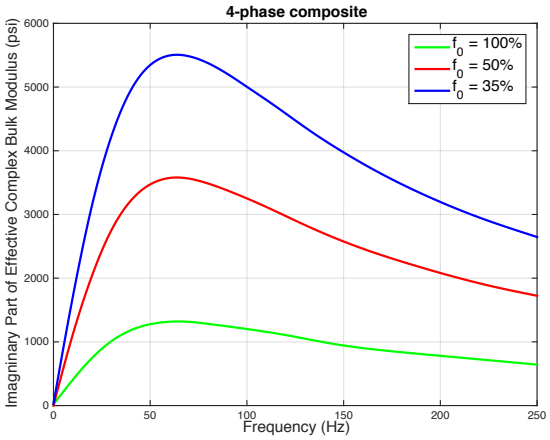

(d)

Figure 6.9 Results for 4-Phase Composite: (a) Effective bulk modulus under constant strain rate; (b) Effective bulk relaxation function under constant strain; (c) Real part of effective complex bulk modulus; (d) Imaginary part of effective complex bulk modulus

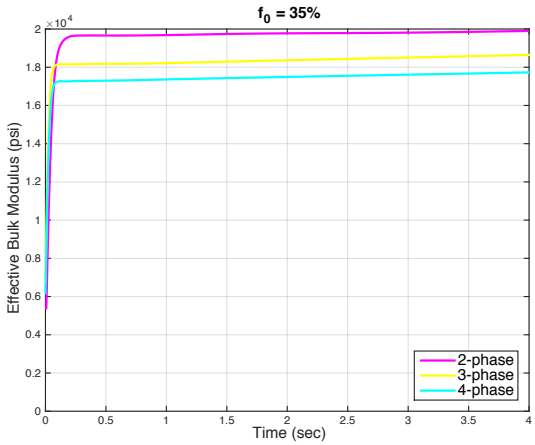

(a)

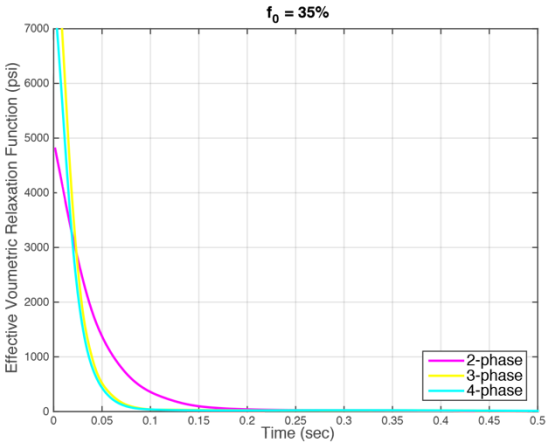

(b)

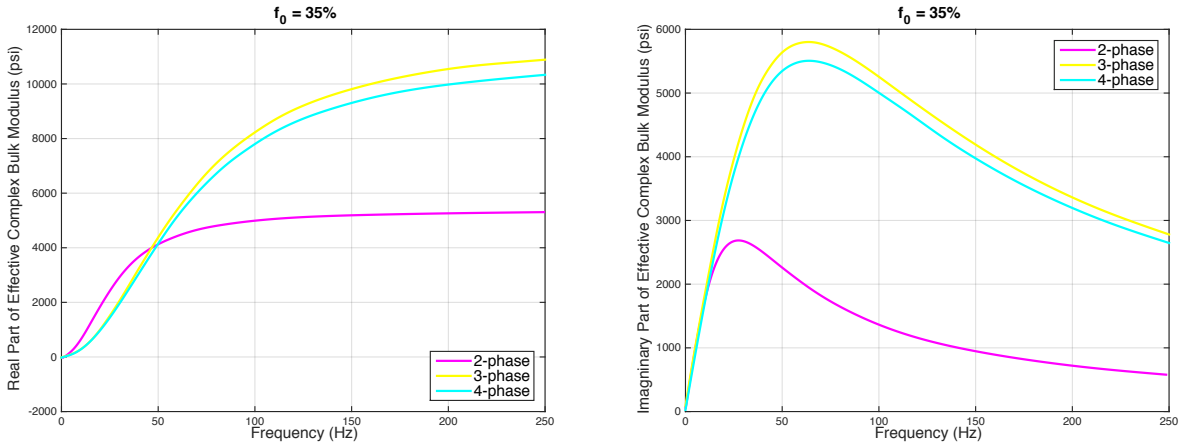

(c) (d)

Figure 6.10 Comparison of Results from 2-Phase, 3-Phase and 4-Phase Composite (volume fraction for asphalt binder =35%): (a) Effective bulk modulus under constant strain rate; (b) Effective bulk relaxation function under constant strain; (c) Real part of effective complex bulk modulus; (d) Imaginary part of effective complex bulk modulus

6.5 Viscoelastic Solutions of Indirect Tensile Creep Tests

To evaluate the creep compliance of materials from indirect tensile creep test, it is necessary to have the elastic solutions of indirect tension test. In 1959, Hondros (Hondros, 1959) presented the analysis of a 2-D circular specimen loaded to conform to the accepted practical recommendation for the Brazilian test. The equations of stress distribution on horizontal and vertical diameter under the assumptions of plane-stress condition were derived. As shown in Hondros' work, if the boundary and loading conditions of a 2-D circular specimen are applied as illustrated in Figure 6.11, the stresses along the horizontal/vertical diameters take the form

$$\sigma_x(x)=\frac{2P}{\pi ad}\left[f(x)-g(x)\right],\qquad \sigma_y(x)=-\frac{2P}{\pi ad}\left[f(x)+g(x)\right]$$
$$\sigma_x(y)=\frac{2P}{\pi ad}\left[m(y)-n(y)\right],\qquad \sigma_y(y)=-\frac{2P}{\pi ad}\left[m(y)+n(y)\right] \tag{6.42}$$

where

$$f(x)=\frac{\left(1-\frac{x^2}{R^2}\right)\sin 2\alpha}{1+\frac{2x^2}{R^2}\cos 2\alpha+\frac{x^4}{R^4}},\qquad g(x)=\tan^{-1}\left(\frac{1-\frac{x^2}{R^2}}{1+\frac{x^2}{R^2}}\tan\alpha\right)$$
$$m(y)=\frac{\left(1-\frac{y^2}{R^2}\right)\sin 2\alpha}{1-\frac{2y^2}{R^2}\cos 2\alpha+\frac{y^4}{R^4}},\qquad n(y)=\tan^{-1}\left(\frac{1+\frac{y^2}{R^2}}{1-\frac{y^2}{R^2}}\tan\alpha\right) \tag{6.43}$$

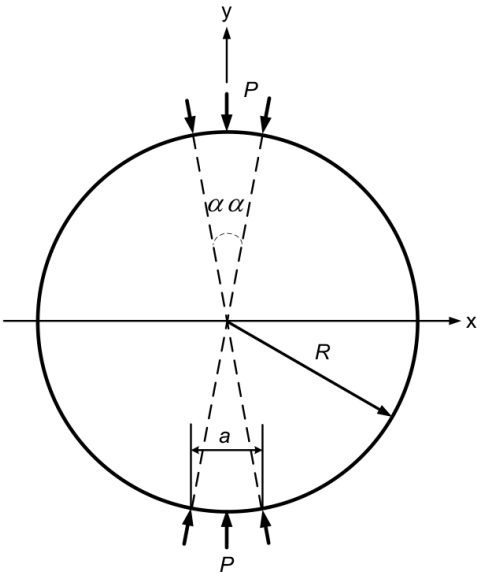

Figure 6.11 Boundary and loading conditions of 2-D circular specimen

Under the assumption of the plane stress condition, the elastic constitutive law can be described as

$$\varepsilon_x = \frac{1}{E}\left(\sigma_x - v\sigma_y\right)$$
$$\varepsilon_y = \frac{1}{E}\left(\sigma_y - v\sigma_x\right) \tag{6.44}$$

To obtain the viscoelastic solutions, the correspondence principle is applied as follows

$$\bar{\varepsilon}_x(s) = \frac{1}{E^{TD}(s)}\left[\bar{\sigma}_x(s) - v\bar{\sigma}_y(s)\right] = C^{TD}(s)\left[\bar{\sigma}_x(s) - v\bar{\sigma}_y(s)\right]$$
$$\bar{\varepsilon}_y(s) = \frac{1}{E^{TD}(s)}\left[\bar{\sigma}_y(s) - v\bar{\sigma}_x(s)\right] = C^{TD}(s)\left[\bar{\sigma}_y(s) - v\bar{\sigma}_x(s)\right] \tag{6.45}$$

Take the stress distribution on horizontal diameter for example, the stress distribution along the horizontal diameter takes the form of

$$\bar{\varepsilon}_x(s) = C^{TD}(s)\left[\bar{\sigma}_x(s) - \frac{\bar{\varepsilon}_x(s) - \bar{\varepsilon}_y(s)/\beta}{\bar{\varepsilon}_x(s) - \beta\bar{\varepsilon}_y(s)}\beta\bar{\sigma}_y(s)\right] \tag{6.46}$$

where $\beta = \dfrac{\bar{\sigma}_y}{\bar{\sigma}_x} = -\dfrac{f(x)+g(x)}{f(x)-g(x)}$.

We can solve for $\bar{\varepsilon}_x(x,0,s)$ from Eqn. (6.46)

$$\bar{\varepsilon}_x(x,0,s) = \beta\bar{\varepsilon}_y(x,0,s) + C^{TD}(s)\bar{\sigma}_x(x,0,s) - \beta C^{TD}(s)\bar{\sigma}_y(x,0,s) \tag{6.47}$$

If the external strip load is set as $P = P(t) = P_0 H(t)$, $H(t)$ is the Heaviside step function, the creep compliance along the horizontal diameter can be obtained and expressed by

$$C(x,0,t) = \frac{\pi ad}{2P_0 A(x,0)}\left[\varepsilon_x(x,0,t) - \beta\varepsilon_y(x,0,t)\right] \tag{6.48}$$

where $A(x,0) = (1+\beta)f(x,0) - (1-\beta)g(x,0)$.

Similarly, the creep compliance can also be obtained from the measurement of strains along the vertical diameter following the same procedures

$$C(0,y,t)=\frac{\pi ad}{2P_0B(0,y)}\left[\varepsilon_x(0,y,t)-\beta\varepsilon_y(0,y,t)\right] \tag{6.49}$$

where $B(0,y)=(1+\beta)m(0,y)-(1-\beta)n(0,y)$.

6.6 Numerical Simulations

6.6.1 Simulation Background

In order to validate the homogenization approach proposed in the previous section with asphalt binder evaluated as a 4-parameter Burgers model, 2-D plane stress numerical simulation for creep test is conducted. Three cases are modeled in this section, with two sub-conditions for Case 2 and Case 3. More specific information is listed in Table 6.3. The material properties of each constituent are listed in Table 6.4. Figure 6.12 illustrates a few significant models.

Table 6.3 Case Description

Case 1		100% asphalt binder
Case 2	Case 2-1	94% asphalt binder, 5% fine aggregates, 1%DCPD
	Case 2-2	64% asphalt binder, 30% fine aggregates, 6%DCPD
Case 3	Case 3-1	90% asphalt binder, 5% fine aggregates, 1%DCPD, 4% air voids
	Case 3-2	60% asphalt binder, 30% fine aggregates, 6%DCPD, 4% air voids

Table 6.4 Material properties for constituents in asphalt mastic composites

	Young's modulus (*psi*)	Poisson's ratio	Drucker Prager Creep model
Fine aggregates	7.25e6	0.2	
DCPD	2.784e5	0.39	
Asphalt binder	1.77e4	0.3	A=2.95e-5 n=0.8, m=-0.5

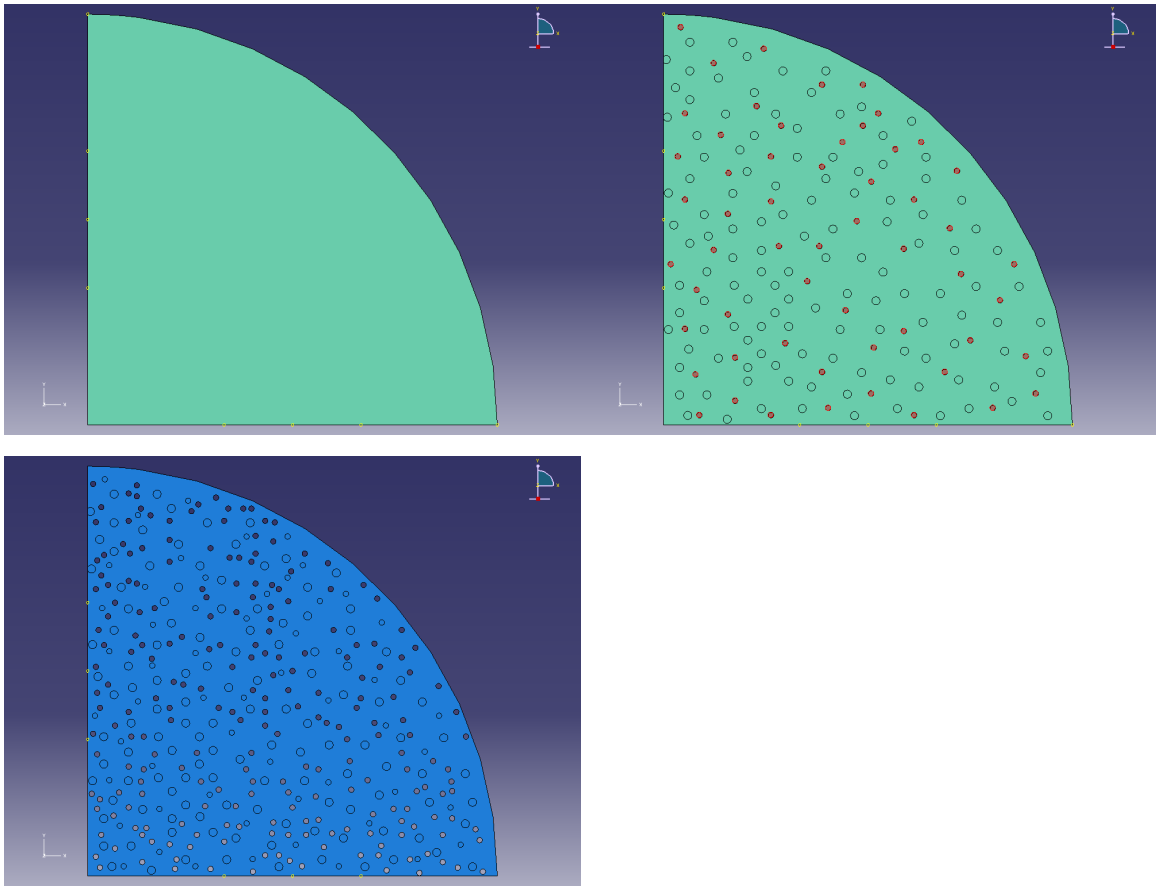

Figure 6.12 The numerical models of Case 1, Case 2-1, Case 3-1 (from left to right, top to bottom, respectively)

Local deformation and stress distribution of Case 1, Case 2-1, Case 3-1 at the final step of the simulations of indirect tensile creep test are demonstrated in Figure 6.13.

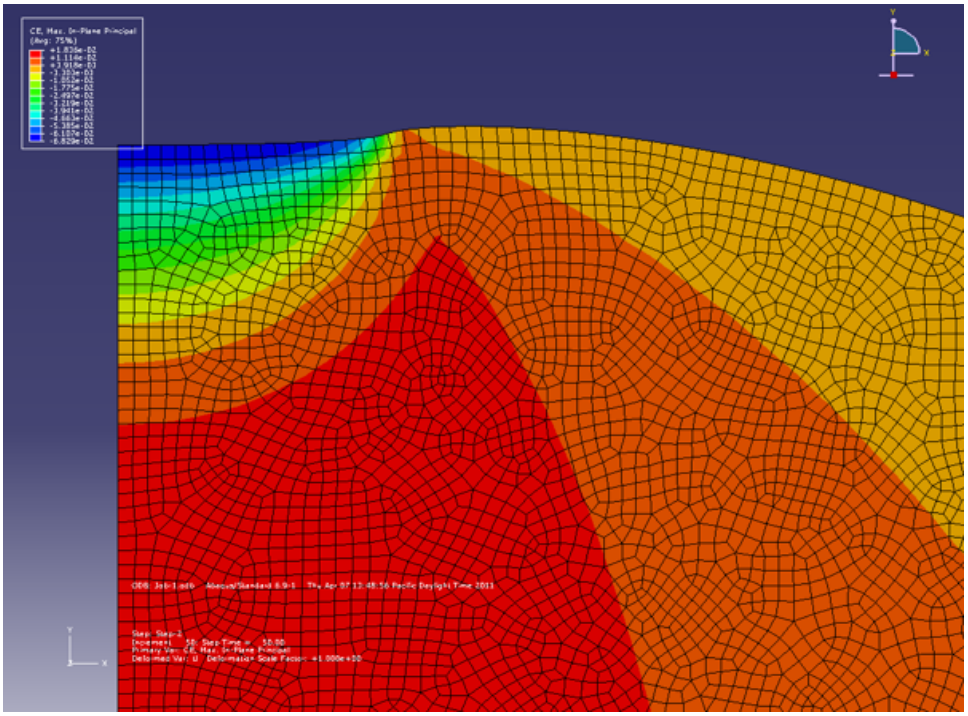

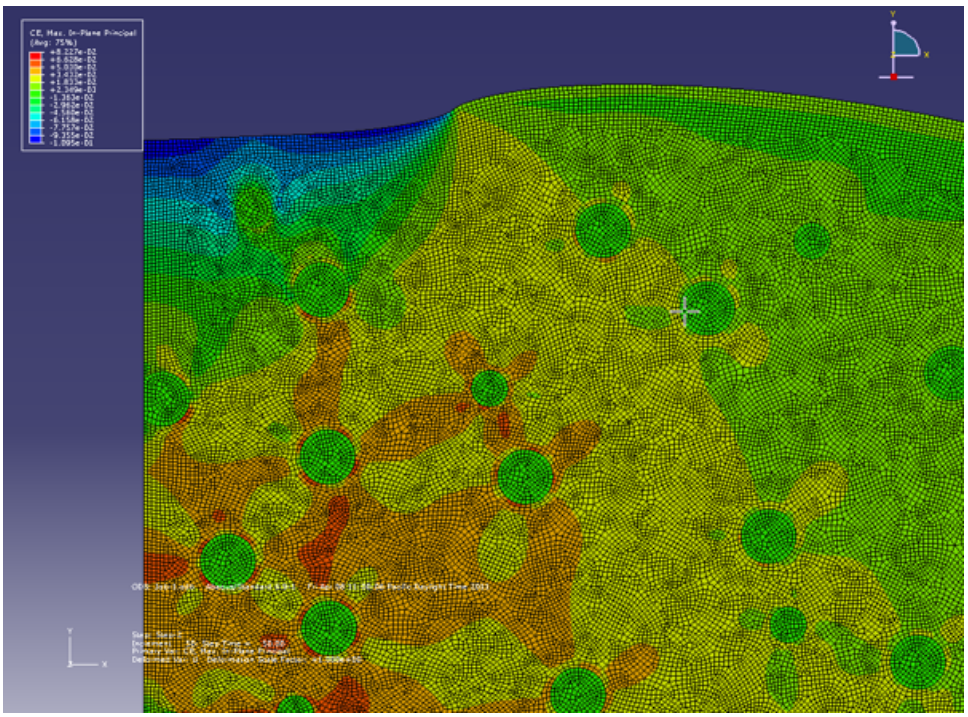

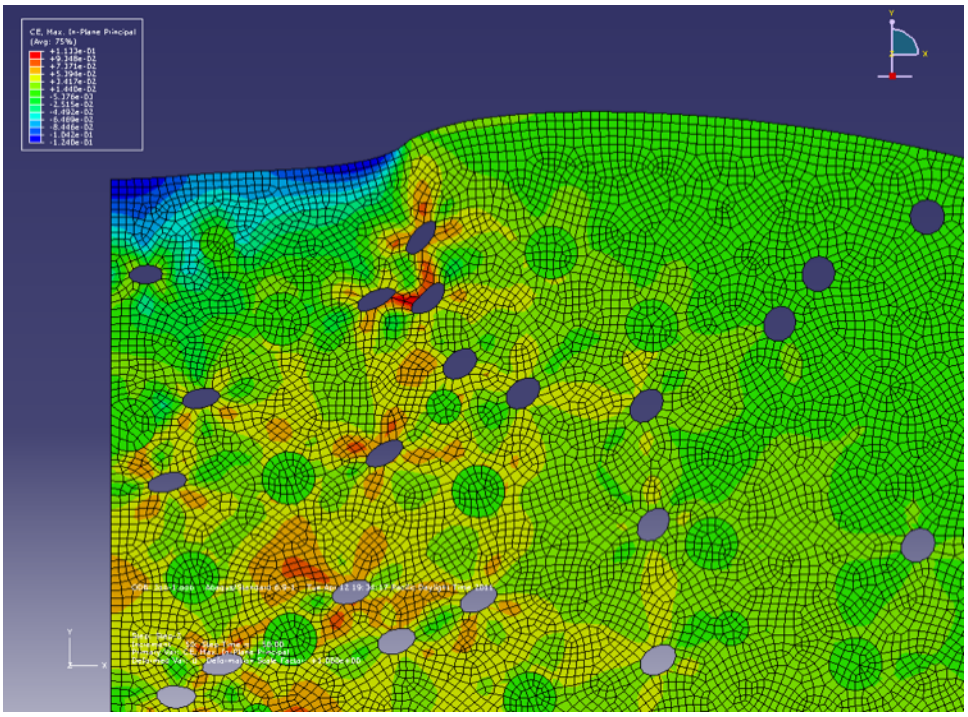

Figure 6.13 Deformations and stress distributions of Case 1, Case 2-1 and Case 3-1 (from top to bottom, respectively)

6.6.2 Results and Comparison

Figure 6.14 compares the creep compliance directly given by theoretical derivation and that calculated from the numerical strain output for Case 1. Specifically, the strain output from ABAQUS (radius = 1.0 inch, 1.5 inch and 2.0 inch) on the horizontal diameter (the x-axis) and the vertical diameter (the y-axis). Good agreement is expected, and the calculated creep compliance is closest to the theoretical values when the strain is output at 1.0 inch both on the horizontal and vertical axes.

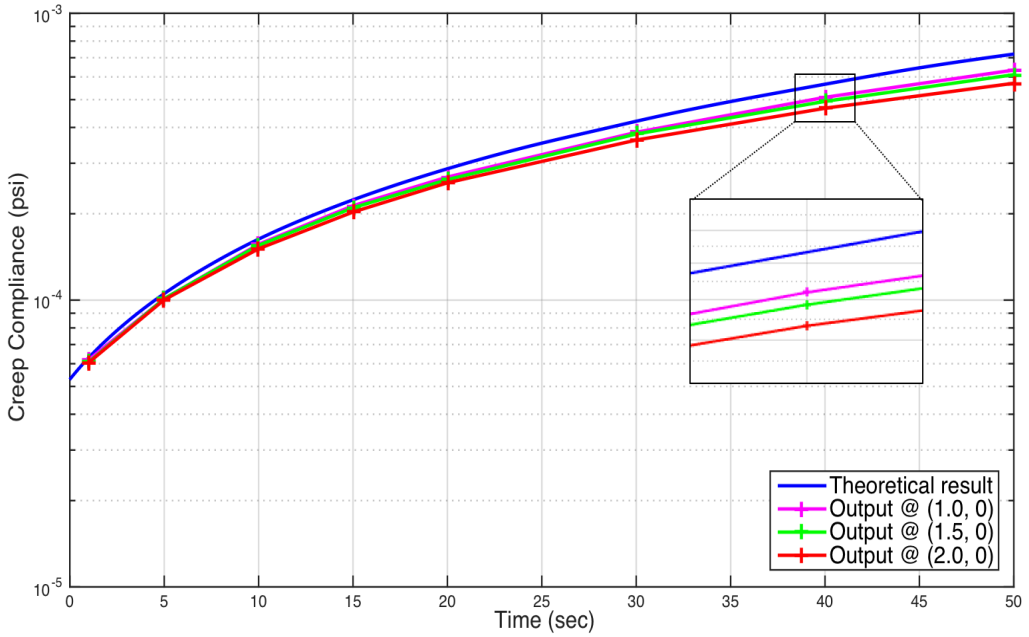

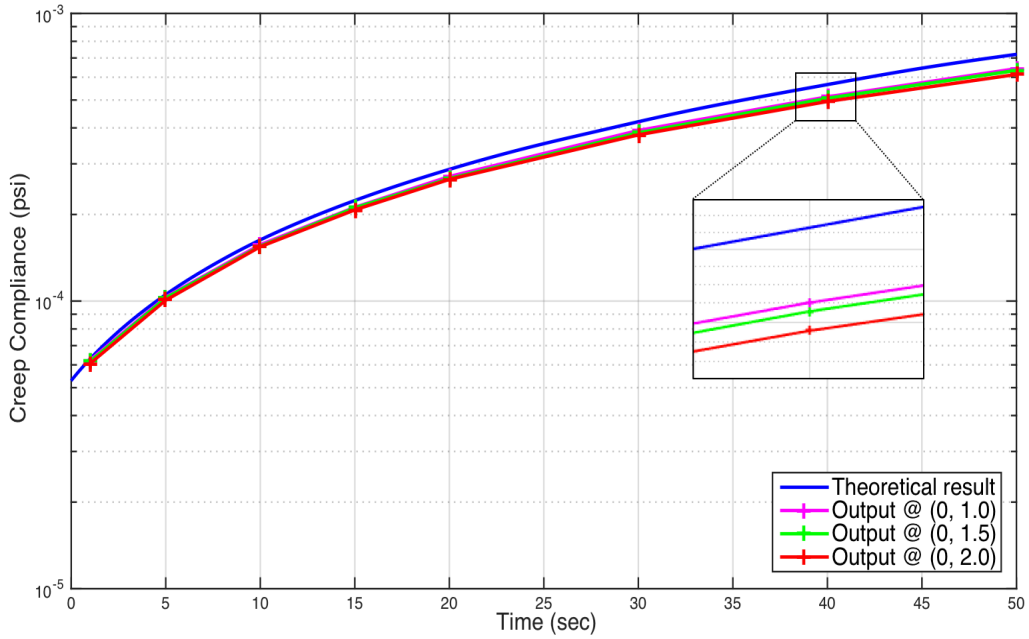

Figure 6.14 The creep compliances of Case 1 vs. the theoretical curve

Figure 6.15 shows the theoretical and numerical curves of creep compliance for Case 2-1 and Case 2-2, while Case 3-1 and Case 3-2 (with theoretical curve of Case 1 as reference) are demonstrated in Figure 6.16. It is seen that the theoretical curves capture the tendency of numerical results reasonably well. It is shown that when the fine aggregates and DCPD are added to the asphalt matrix, the asphalt mastic has more creep resistance. The theoretical formulation tends to overestimate the effective creep compliance when the volume fraction of fine aggregates is low (5%) and underestimate when the volume fraction is high (30%).

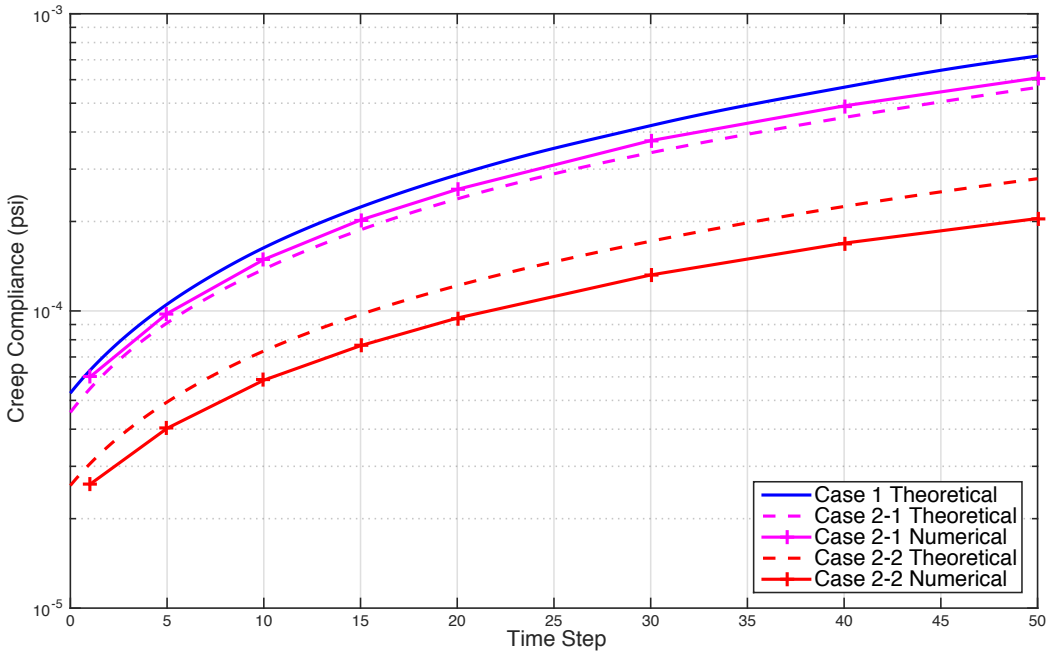

Figure 6.15 The creep compliances of Case 2-1, Case 2-2 vs. the theoretical estimations

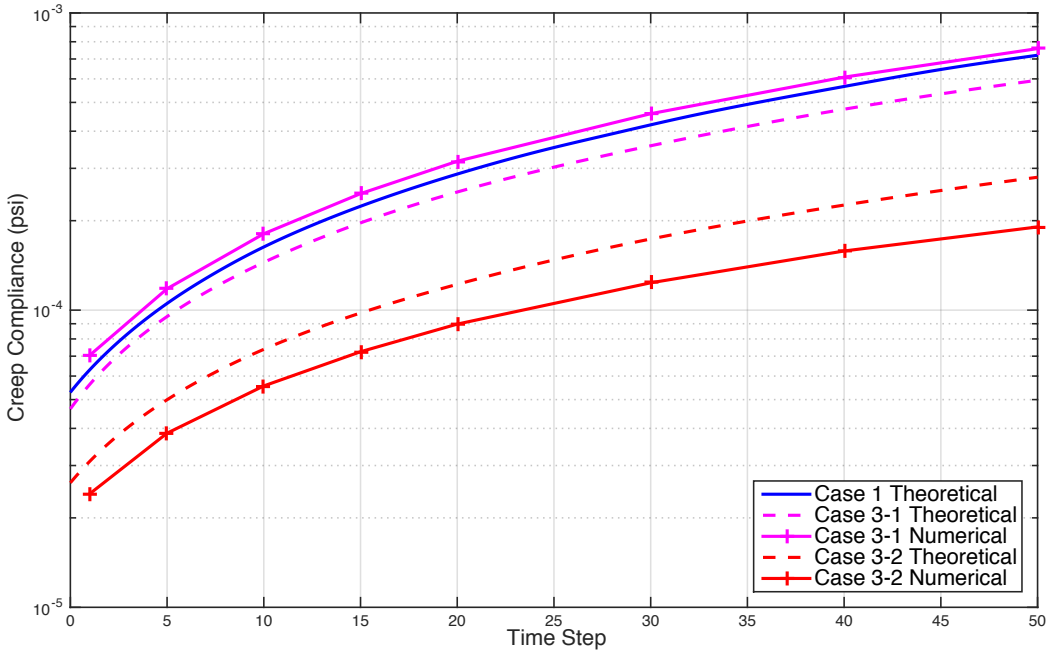

Figure 6.16 The creep compliances of Case 3-1, Case 3-2 vs. the theoretical estimations

Additionally, comparison of theoretical estimations among all five cases under 50 seconds and 1,000,000 seconds are demonstrated in Figure 6.17. It is noticed that the differences are more obvious at the beginning of creep. Also, it is clear that air voids will slightly increase the creep compliance. It is also observed that when the volume fraction of fine aggregates is low (5%), the air voids increase the creep compliance of asphalt mastic more significantly. while air voids have less influence on the creep compliance of asphalt mastic when the volume fraction of fine aggregates is high (30%).

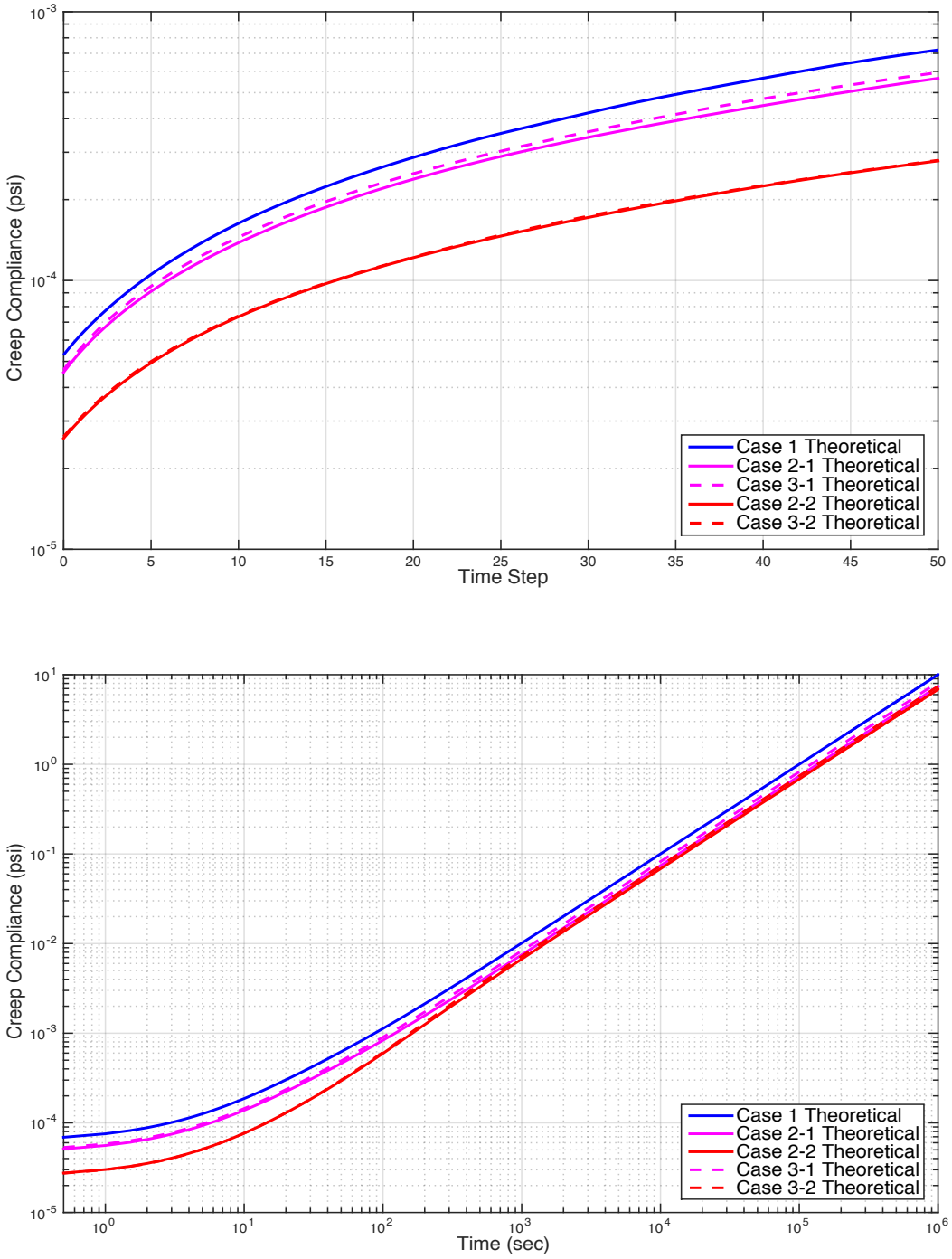

Figure 6.17 The theoretical estimations of creep compliances of Case 2-1 vs. Case 3-1 and Case 2-2 vs. Case 3-2

6.7 References

Absi, J., Tehrani, F. F., Courreges, F., & Petit, C. (2016). *Mechanical Behavior of Asphalt Mixture Based on X-ray Computed Tomography Images and Random Generation of Aggregates Skeleton.* Paper presented at the 8th RILEM International Conference on Mechanisms of Cracking and Debonding in Pavements.

Abu Al-Rub, R. K., Darabi, M. K., Little, D. N., & Masad, E. A. (2010). A micro-damage healing model that improves prediction of fatigue life in asphalt mixes. *International Journal of Engineering Science, 48*(11), 966-990.

Ahmed, S., & Jones, F. R. (1990). A review of particulate reinforcement theories for polymer composites. *Journal of Materials Science, 25*(12), 4933-4942.

Astarita, G. (1989). *Thermodynamics: an advanced textbook for chemical engineers*. New York and London: Plenum Press.

Bandyopadhyaya, R., Das, A., & Basu, S. (2008). Numerical simulation of mechanical behaviour of asphalt mix. *Construction and Building Materials, 22*(5), 1051-1058.

Benveniste, Y. (1987). A new approach to the application of Mori-Tanaka's theory in composite materials. *Mechanics of Materials, 6*(2), 147-157.

Beremin, F. M. (1981). *Experimental and numerical study of the different stages in ductile rupture: application to crack initiation and stable crack growth*. North Holland.

Berryman, J. G. (1995). Mixture theories for rock properties. In T. J. Ahrens (Ed.), *Rock Physics & Phase Relations: A Handbook of Physical Constants* (Vol. 3, pp. 205-228). New York: American Geophysical Union.

Berveiller, M., & Zaoui, A. (1979). An Extension of the Self-consistent Scheme to Plastically Flowing Polycrystals. *Journal of the Mechanics and Physics of Solids, 26*, 325-344.

Bower, A. F. (2009). *Applied Mechanics of Solids* (1st ed.). Boca Raton: CRC Press.

Budiansky, B., & Wu, T. T. (1962). Theoretical prediction of plastic strains of polycrystals. *Proceedings of the 4th U.S. National Congress of Applied Mechanics*, 1175.

Burgers, J. M. (1939). Mechanical considerations—Model systems—Phenomenological theories of relaxation and viscosity *First Report on Viscosity and Plasticity* (pp. 5-67). New York, NY, USA: Nordemann Publishing.

Buttlar, W. G., & You, Z. (2001). Discrete Element Modeling of Asphalt Concrete: Microfabric Approach. *Transportation Research Record: Journal of the Transportation Research Board, 1757*(1), 111-118.

Button, J. W., Perdomo, D., & Lytton, R. L. (1990). Influence of aggregate on rutting in asphalt concrete pavements. *Transportation Research Record: Chip seals, friction courses, and asphalt pavement rutting 1990*(1259), 141-152.

Castaneda, P. P. (1991). The effective mechanical properties of nonlinear isotropic composites. *Journal of the Mechanics and Physics of Solids, 39*, 45-71.

Castaneda, P. P., & Willis, J. R. (1988). On the overall properties of nonlinearly viscous composites. *Proceedings of the Royal Society of London, Series A, 416*, 217-244.

Chaboche, J. L. (1981). Continuous damage mechanics — A tool to describe phenomena before crack initiation. *Nuclear Engineering and Design, 64*(2), 233-247.

Chaboche, J. L., & Lesne, P. M. (1988). A non-linear continuous fatigue damage mode. *Fatigue & Fracture of Engineering Materials & Structures, 11*(1), 1-17.

Chehab, G. R., Kim, Y. R., Schapery, R. A., Witczak, M. W., & Bonaquist, R. F. (2002). *Time-temperature superposition principle for asphalt concrete with growing damage in tension state*. Paper presented at the Asphalt Paving Technology 2002, Colorado Springs, Colorado.

Chehab, G. R., Kim, Y. R., Schapery, R. A., Witczak, M. W., & Bonaquist, R. F. (2003). Characterization of asphalt concrete in uniaxial tension using a viscoelastoplastic continuum damage model. *Asphalt paving technology 2003: Journal of the Association of Asphalt Paving Technologists from the proceedings of the technical sessions, 72*, 315-355.

Chen, K., Yu, J., & Zhang, X. (2010). Micromechanical analysis of damage evolution in splitting test of asphalt mixtures. *Journal of Central South University of Technology, 17*(3), 628-634.

Chen, X., Wudl, F., Mal, A. K., Shen, H., & Nutt, S. R. (2003). New Thermally Remendable Highly Cross-Linked Polymeric Materials. *Macromolecules, 36*(6), 1802-1807.

Chow, C. L., & Wang, J. (1987). An anisotropic theory of continuum damage mechanics for ductile fracture. *Engineering Fracture Mechanics, 27*(5), 547-558.

Christensen Jr, D. W., Pellinen, T. K., & Bonaquist, R. F. (2003). Hirsch model for estimating the modulus of asphalt concrete. *Journal of the Association of Asphalt Paving Technologists, 72*, 97-121.

Christensen, R. M. (1982). *Theory of Viscoelasticity: An Introduction, 2nd Edition*: Academic Press, New York.

Coleman, B. D., & Gurtin, M. E. (1967). Thermodynamics with internal state variables. *Journal of Chemical Physics, 47*(2), 597-613.

Coleman, B. D., & Noll, W. (1963). The thermodynamics of elastic materials with heat conduction and viscosity. *Archive for Rational Mechanics and Analysis, 13*(1), 167-178.

Colorado, H. A., Yuan, W., Guo, Z., Juanri, J., & Yang, J. M. (2014). Poly-dicyclopentadiene-wollastonite composites toward structural applications. *Journal of Composite Materials, 48*(16), 2023-2031.

Dai, Q. (2011). Two- and three-dimensional micromechanical viscoelastic finite element modeling of stone-based materials with X-ray computed tomography images. *Construction and Building Materials, 25*(2), 1102-1114.

Dai, Q., Sadd, M. H., & You, Z. (2006). A micromechanical finite element model for linearand damage-coupled viscoelastic behaviour of asphalt mixture. *International Journal for Numerical and Analytical Methods in Geomechanics, 30*(11), 1135-1158.

Dai, Q., & You, Z. (2007). Prediction of Creep Stiffness of Asphalt Mixture with Micromechanical Finite-Element and Discrete-Element Models. *Journal of Engineering Mechanics, ASCE, 133*(2), 163-173.

Daniel, J. S., Kim, Y. R., & Lee, H. (2007). Effects of Aging on Viscoelastic Properties of Asphalt-Aggregate Mixture. *Transportation Research Record: Journal of theTransportation Research Board, 1630*, 21-27.

Dewey, J. M. (1947). The elastic constants of materials loaded with non-rigid fillers. *Journal of Applied Mechanics, 18*, 578-581.

Drucker, D. C., & Prager, W. (1952). Soil Mechanics and Plastic Analysis or Limite Design. *Quarterly of Applied Mathematics, 10*, 157-175.

Duenas, T., Enke, A., Chai, K., Castellucci, M., Sundaresan, V. B., Wudl, F., . . . Ooi, T. K. (2010). Smart Self-Healing Material Systems Using Inductive and Resistive Heating. *Smart Coatings III, 1050*, 45-60.

Dziugys, A., & Peters, B. (2001). A new approach to detect the contact of two-dimensional elliptical particles. *International Journal for Numerical and Analytical Methods in Geomechanics, 25*, 1487-1500.

Edlund, U., & Klarbring, A. (1993). A coupled elastic-plastic damage model for rubber-modified epoxy adhesives. *International Journal of Solids and Structures, 30*(19), 2693-2708.

Eshelby, J. D. (1957). The determination of the elastic field of an ellipsoidal inclusion, and related problems. *Proceedings of the Royal Society of London, Series A, 241*(1226), 376–396.

Ferry, J. D. (1980). *Viscoleastic Properties of Polymers, 3rd Edition*: John Wiley & Sons.

FHWA. (2014). *Highway Statistics, Table HM-63, Miles by Measured Pavement Roughness / Present Serviceability Rating*.Federal Highway Administration.

FHWA. (2017). *U.S. Department of Transportation, 2015 Conditions and Performance Report to Congress: Status of the Nation's Highways, Bridges, and Transit: Conditions & Performance*.Federal Highway Administration.

García, A., Bueno, M., Norambuena-Contreras, J., & Partla, M. N. (2013). Induction healing of dense asphalt concrete. *Construction and Building Materials, 49*, 1-7.

Germain, P., Nguyen, Q. S., & Suquet, P. (1983). Continuum thermodynamics. *Journal of Applied Mechanics, ASME, 50*(4B), 1010-1020.

Goh, S. W., & You, Z. (2009). A simple stepwise method to determine and evaluate the initiation of tertiary flow for asphalt mixtures under dynamic creep test. *Construction and Building Materials, 23*(11), 3398-3405.

Goodrich, J. L. (1991). Asphaltic binder rheology, asphalt concrete rheology and asphalt concrete mix properties. *Journal of the Association of Asphalt Paving Technologists, 60*, 80-120.

Graham, G. A. C. (1968). The correspondence principle of linear viscoelasticity theory for mixed boundary value problems involving time-dependent boundary regions. *Quarterly of Applied Mathematics, 26*(2), 167-174.

Hashin, Z. (1959). *The moduli of an elastic solid, containing spherical particles of another elastic material*. Paper presented at the IUTAM Non-homogeneity in elasticity and plasticity symposium, Warsaw.

Hashin, Z. (1962). The elastic moduli of heterogeneous materials. *Journal of Applied Mechanics, 29*(2), 143-150.

Hashin, Z. (1988). The differential scheme and its applications to cracked materials. *Journal of the Mechanics and Physics of Solids, 36*(6), 719-734.

Hashin, Z., & Shtrikman, S. (1961). Note on a variational approach to the theory of composite elastic materials. *Journal of the Franklin Institute, 274*(4), 336-341.

Hashin, Z., & Shtrikman, S. (1963). A variational approach to the theory of the elastic behaviour of multiphase materials. *Journal of the Mechanics and Physics of Solids, 11*(2), 127-140.

Hill, R. (1965a). Continuum micro-mechanics of elastoplastic polycrystals. *Journal of the Mechanics and Physics of Solids, 13*, 89-101.

Hill, R. (1965b). A Self-Consistent Mechanics of Composite Materials. *Journal of the Mechanics and Physics of Solids, 13*(4), 213-222.

Hill, R., & Rice, J. R. (1973). Elastic potentials and structure of inelastic constitutive laws. *Siam Journal on Applied Mathematics, 25*(3), 448-461.

Hondros, G. (1959). The Evaluation of Poisson's Ratio and the Modulus of Materials of a Low Tensile Resistance by the Brazilian (Indirect Tensile) Test with Particular Reference to Concrete. *Australian Journal of Applied Science, 10*(243-268).

Hong, S., Yuan, K. Y., & Ju, J. W. (2017). New strain energy-based thermo-elastoviscoplastic isotropic damage–self-healing model for bituminous composites—Part I: Formulations. *International Journal of Damage Mechanics, 26*(5), 651-671.

Hopkins, I. L., & Hamming, R. W. (1957). On creep and relaxation. *Journal of Applied Physics, 28*(8), 906-909.

Hutchinson, J. W. (1970). Elastic-plastic behavior of polycrystalline metals and composites. *Proceedings of the Royal Society of London, Series A, 319*, 247-272.

Iwakuma, T., & Nemat-Nasser, S. (1984). Finite elastic-plastic deformation of polycrystalline metals. *Proceedings of the Royal Society of London, Series A, 394*, 87-119.

Jefferson, A. D. (1998). Plastic-Damage Model for Interfaces in Cementitious Materials. *Journal of Engineering Mechanics, ASCE, 124*(7), 775-782

Ju, J. W. (1989). On energy-based coupled elastoplastic damage theories-constitutive modeling and computational aspects. *International Journal of Solids and Structures, 25*(7), 803-833.

Ju, J. W. (1990). Isotropic and anisotropic damage variables. *Journal of Engineering Mechanics, ASCE, 116*(12), 2764-2770.

Ju, J. W., & Chen, T. M. (1994a). Effective elastic moduli of two-phase composites containing randomly dispersed spherical inhomogeneities. *Acta Mechanica, 103*(1-4), 123-144.

Ju, J. W., & Chen, T. M. (1994b). Micromechanics and effective moduli of elastic composites containing randomly dispersed ellipsoidal inhomogeneities. *Acta Mechanica, 103*(1-4), 103-121.

Ju, J. W., Ko, Y. F., & Zhang, X. D. (2009). Multi-level elastoplastic damage mechanics for elliptical fiber reinforced composites with evolutionary fiber debonding. *International Journal of Damage Mechanics, 18*(5), 419-460.

Ju, J. W., & Sun, L. Z. (2001). Effective elastoplastic behavior of metal matrix composites containing randomly located aligned spheroidal inhomogeneities, Part I: Micromechanics based formulation. *International Journal of Solids and Structures, 38*(2), 183-201.

Ju, J. W., & Yanase, K. (2009). Micromechanical elastoplastic damage mechanics for elliptical fiber reinforced composites with progressive partial fiber debonding. *Journal of Damage Mechanics, 18*(7), 639-668.

Ju, J. W., & Yanase, K. (2010). Micromechanics and effective elastic moduli of particle-reinforced composites with near-field particle interactions. *Acta Mechanica, 215*(1), 135-153.

Ju, J. W., & Yuan, K. Y. (2012). New strain-energy based coupled elastoplastic two-parameter damage and healing models for earth moving processes. *International Journal of Damage Mechanics, 21*(7), 989-1019.

Ju, J. W., Yuan, K. Y., & Kuo, A. W. (2012). Novel strain-energy-based coupled elastoplastic damage and healing models for geomaterials-Part I: Formulations. *International Journal of Damage Mechanics, 21*(4), 525-549.

Ju, J. W., Yuan, K. Y., Kuo, A. W., & Chen, J. S. (2012). Novel Strain Energy Based Coupled Elastoplastic Damage and Healing Models for Geomaterials - Part I: Formulations. *International Journal of Damage Mechanics, 21*(4), 551-576.

Kachanov, L. M. (1958). Time of the rupture process under creep conditions. [English Translation 1999]. *Izvestiia Akademii Nauk SSSR, 8*, 26-31.

Kachanov, L. M. (1999). Rupture time under creep conditions. *International Journal of Fracture, 97*(1-4), 11-18.

Kao, W. H., Carlson, L., Yang, J. M., & Ju, J. W. (2011). US9348024B2.

Kelley, J. E., Jr. (1960). The cutting-plane method for solving convex programs. *Journal of the Society for Industrial & Applied Mathematics, 8*(4), 703–712.

Kerner, E. H. (1956). The elastic and thermo-elastic properties of composite media. *Proceedings of the Royal Society of London, Series B, 69*, 807-808.

Kessler, M. R., & White, S. R. (2001). Self-activated healing of delamination damage in woven composites. *Composites Part A- Applied Science and Manufacturing, 32*(5), 683-699.

Kessler, M. R., & White, S. R. (2002). Cure kinetics of the ring-opening metathesis polymerization of dicyclopentadiene. *Journal of Polymer Science Part A: Polymer Chemistry, 40*(14), 2373-2383. doi:10.1002/pola.10317

Khazanovich, L. (2008). The elastic–viscoelastic correspondence principle for non-homogeneous materials with time translation non-invariant properties. *International Journal of Solids and Structures, 45*(17), 4739-4747.

Khodaii, A., & Mehrara, A. (2009). Evaluation of permanent deformation of unmodified and SBS modified asphalt mixtures using dynamic creep test. *Construction and Building Materials, 23*(7), 2586-2592.

Kiefer, B., Waffenschmidt, T., Sprave, L., & Menzel, A. (2018). A gradient-enhanced damage model coupled to plasticity—multi-surface formulation and algorithmic concepts. *International Journal of Damage Mechanics, 27*(2), 253-295.

Kim, H. W., & Buttlar, W. G. (2009). Discrete fracture modeling of asphalt concrete. *International Journal of Solids and Structures, 46*(13), 2593-2604.

Kim, S. M., & Abu Al-Rub, R. K. (2011). Meso-scale computational modeling of the plastic-damage response of cementitious composites. *Cement and Concrete Research, 41*(3), 339-358.

Kim, Y. R. (2008). *Modeling of Asphalt Concrete*: McGraw-Hill Education.

Kim, Y. R., LEE, H. J., & Little, D. N. (1997). Fatigue characterization of asphalt concrete using viscoelasticity and continuum damage theory. *Journal of the Association of Asphalt Paving Technologists, 66*, 520-569.

Kim, Y. R., & Little, D. N. (1990). One-Dimensional Constitutive Modeling of Asphalt Concrete. *Journal of Engineering Mechanics, ASCE, 116*(4), 751-772.

Kim, Y. R., & Little, D. N. (2004). Linear viscoelastic analysis of asphalt mastics. *Journal of Materials in Civil Engineering, 16*(2), 122-132.

Kim, Y. R., Seo, Y., King, M., & Momen, M. (2004). Dynamic Modulus Testing of Asphalt Concrete in Indirect Tension Mode. *Transportation Research Record: Journal of the Transportation Research Board, 1891*(1), 163-173.

Ko, Y., & Ju, J. W. (2008). Micromechanical Elastoplastic Damage Modeling of Evolutionary Interfacial Arc Debonding for Fiber Reinforced Composites. *International Journal of Damage Mechanics, 14*(4), 307-356.

Ko, Y., & Ju, J. W. (2012). Effects of fiber cracking on elastoplastic-damage behavior of fiber-reinforced metal matrix composites. *International Journal of Damage Mechanics, 22*(1), 48-67.

Kovačič, S., Matskob, N. B., Ferkc, G., & Slugovc, C. (2013). Macroporous poly(dicyclopentadiene) γFe2O3/Fe3O4 nanocomposite foams by high internal phase emulsion templating. *Journal of Materials Chemistry A, 1*, 7971-7978.

Krajcinovic, D. (1983). Creep of structures - a continuous damage mechanics approach. *Journal of Structural Mechanics, 11*(1), 1-11.

Krajcinovic, D., & Fanella, D. (1986). A micromechanical damage model for concrete. *Engineering Fracture Mechanics, 25*(5-6), 585-596.

Krajcinovic, D., & Fonseka, G. U. (1981). The continuous damage theory of brittle materials: Part 1: General theory. *Journal of Applied Mechanics, 48*(4), 809-815.

Kröner, E. (1977). Bounds for effective elastic moduli of disordered materials. *Journal of the Mechanics and Physics of Solids, 25*(2), 137-155.

Ladeveze, P., & Lemaitre, J. (1984). *Damage effective stress in quasi-unilateral conditions.* Paper presented at the 16th International congress of theoretical and applied mechanics, Lyngby, Denmark.

Laws, N., & Dvorak, G. J. (1987). The effect of fiber breaks and aligned penny-shaped cracks on the stiffness and energy release rates in unidirectional composites. *International Journal of Solids and Structures, 23*(9), 1269-1283.

Leaderman, H. (1958). Viscoelasticity phenomena in amorphous high polymeric systems *Rheology* (pp. 1-61): Academic Press.

Lee, E. H. (1965). Stress analysis in visco-elastic bodies. *Quarterly of Applied Mathematics, 13*, 183-190.

Lee, H., & Pyo, S. (2007). Micromechanics-based elastic damage modeling of particulate composites with weakened interfaces. *International Journal of Solids and Structures, 44*(25), 8390-8406.

Lee, H. J., Daniel, J. S., & Kim, Y. R. (2000). Continuum damage mechanics-based fatigue model of asphalt concrete. *Journal of Material in Civil Engineering, 12*(2), 105-112.

Lee, H. J., & Kim, Y. R. (1998). Viscoelastic constitutive model for asphalt concrete under cyclic loading. *Journal of Engineering Mechanics, ASCE, 11*(3), 236-241.

Lee, J. K., Choi, S. J., & Mal, A. K. (2001). Stress analysis of an unbounded elastic solid with orthotropic inclusions and voids using a new integral equation technique. *International Journal of Solids and Structures, 38*(16), 2789-2820.

Lee, J. K., Ku, D. Y., & Mal, A. K. (2011). Elastic analysis of a half-plane with multiple inclusions using volume integral equation method. *Engineering Analysis with Boundary Elements, 35*(3), 564-574.

Lee, J. K., & Mal, A. K. (1995). A volume integral equation technique for multiple scattering problems in elastodynamics. *Applied Mathematics and Computation, 67*(1-3), 135-159.

Lee, J. K., & Mal, A. K. (1997). A Volume Integral Equation Technique for Multiple Inclusion and Crack Interaction Problems. *Journal of Applied Mechanics, 64*(1), 23-31.

Lemaitre, J. (1971). *Evaluation of dissipation and damage in metals submitted to dynamic loading.* Paper presented at the Proceedings of International Congress of Methametics, Kyoto, Japan.

Lemaitre, J. (1985). A Continuous Damage Mechanics Model for Ductile Fracture. *Journal of Engineering Materials and Technology, 107*(1), 83-89.

Lemaitre, J. (1992). *A Course on Damage Mechanics*. Berlin: Springer-Verlag.

Levine, H. S. (1982). A two-surface plastic and micro cracking model for plain concrete. *Nonlinear Numerical Analysis of Reinforced Concrete, Proceedings Winter Annual Meeting, ASME*, 27-47.

Li, G. Q., Li, Y. Q., Metcalf, J. B., & Pang, S. S. (1999). Elastic modulus prediction of asphalt concrete. *Journal of Materials in Civil Engineering, 11*(3), 236-241.

Li, J., & Weng, G. J. (1994). Strain-Rate Sensitivity, Relaxation Behavior, and Complex Moduli of a Class of Isotropic Viscoelastic Composites. *Journal of Engineering Materials and Technology, 116*(4), 495–504.

Lipinski, P., Barhdadi, E. H., & Cherkaoui, M. (2006). Micromechanical modeling of an arbitrary ellipsoidal multi-coated inclusion. *Philosophical Magazine, 86*(10), 1305-1326.

Lipinski, P., Naddari, A., & Berveiller, M. (1992). Recent results concerning the modelling of polycrystalline plasticity at large strains

Author links open overlay panel. *International Journal of Solids and Structures, 29*, 1873-1881.

Liu, Q., García, A., Schlangen, E., & Ven, M. (2011). Induction healing of asphalt mastic and porous asphalt concrete. *Construction and Building Materials, 25*(9), 3746-3752.

Liu, Y., & You, Z. (2011). Discrete-Element Modeling: Impacts of Aggregate Sphericity, Orientation, and Angularity on Creep Stiffness of Idealized Asphalt Mixtures. *Journal of Engineering Mechanics, ASCE, 137*(4), 294-303

Lubarda, V. A. (1994). An analysis of large-strain damage elastoplasticity. *International Journal of Solids and Structures, 31*(21), 2951-2964.

Lubarda, V. A., & Krajcinovic, D. (1994). Tensorial representation of the effective elastic properties of the damaged material. *International Journal of Damage Mechanics, 3*(1), 38-56.

Lubarda, V. A., & Krajcinovic, D. (1995). Constitutive structure of rate theory of damage in brittle elastic solids. *Applied Mathematics and Computation, 67*(1-3), 81-101.

Lubliner, J., Oliver, J., Oller, S., & Oñate, E. (1989). A plastic-damage model for concrete. *International Journal of Solids and Structures, 25*(3), 299-326.

Malcher, L., & Mamiya, E. N. (2014). An improved damage evolution law based on continuum damage mechanics and its dependence on both stress triaxiality and the third invariant. *International Journal of Plasticity, 56*, 232-261.

Málek, J., Rajagopal, K. R., & Tuma, K. (2015). A thermodynamically compatible model for describing the response of asphalt binders. *International Journal of Pavement Engineering, 16*, 297–314.

Málek, J., Rajagopal, K. R., & Tuma, K. (2018). Derivation of the Variants of the Burgers Model Using a Thermodynamic Approach and Appealing to the Concept of Evolving Natural Configurations. *Fluid, 3*(4), 69.

Martínez, E., Romero, J., Lousa, A., & Esteve, J. (2003). Nanoindentation stress–strain curves as a method for thin-film complete mechanical characterization: application to nanometric CrN/Cr multilayer coatings. *Applied Physics A-Materials Science & Processing, 7*(3-4), 419-426.

Masad, E. A., Huang, C. W., DAngelo, J., & Little, D. N. (2009). Characterization of Asphalt Binder Resistance to Permanent Deformation Based on Nonlinear Viscoelastic Analysis of Multiple Stress Creep Recovery (MSCR) Test. *Journal of the Association of Asphalt Paving Technologists, 87*, 535-566.

Maxwell, J. C. (1867). On the dynamical theory of gases. *Philosophical Transactions of the Royal Society of London, 157*(49-88).

Mazars, J. (1986). A description of micro- and macroscale damage of concrete structures. *Engineering Fracture Mechanics, 25*(5-6), 729-737.

Mazars, J., & Lemaitre, J. (1985). Application of Continuous Damage Mechanics to Strain and Fracture Behavior of Concrete. In S. S.P. (Ed.), *Application of Fracture Mechanics to Cementitious Composites. NATO ASI Series (Series E: Applied Sciences)* (Vol. 94, pp. 507-520): Springer, Dordrecht.

Mazars, J., & Pijaudier-Cabot, G. (1989). Continumm damage theory: application to concrete. *Journal of Engineering Mechanics, ASCE, 115*(2), 55-64.

McLaughlin, R. (1977). A study of the differential scheme for composite materials. *International Journal of Engineering Science, 15*(4), 237-244.

Milan, J., & Zdenek, P. B. (2001). *Inelastic Analysis of Structures*: John Wiley& Sons.

Miner, M. A. (1945). Cumulative damage in fatigue. *Journal of Applied Mechanics, 12*(3), A159-A164.

Molinari, A., Canova, G. R., & Ahzi, S. (1987). A self consistent approach of the large deformation polycrystal viscoplasticity. *Acta Metallurgica, 35*(12), 2983-2994.

Molinari, A., Houdaigui, F., & Tóth, L. S. (2004). Validation of the tangent formulation for the solution of the non-linear Eshelby inclusion problem. *International Journal of Plasticity, 20*(2), 291-307.

Monismith, C. L., Alexander, R. L., & Secor, K. E. (1966). *Rheologic behavior of asphalt concrete.* Paper presented at the Association of Asphalt Paving Technologists Proceedings.

Monismith, C. L., Secor, G. A., & Secor, K. E. (1965). *Temperature induced stresses and deformations in asphalt concrete.* Paper presented at the Association of Asphalt Paving Technologists Proceedings.

Monismith, C. L., & Secor, K. E. (1962). *Viscoelastic behavior of asphalt concrete pavements.* Paper presented at the Proceedings of the International Conference on the Structural Design of Asphalt Pavements, Ann Arbor, MI.

Mori, T., & Tanaka, T. (1973). Average stress in matrix and average elastic energy of materials with misfitting inclusions. *Acta Metallurgica, 21*(5), 571-574.

Mould, J. C. J., Levine, H. S., & Tennant, D. (1994). *Evaluation of a rate-dependent three invariant softening model for concrete.* Paper presented at the Fracture and Damage in Quasibrittle Structures, Chapman and Hall, London.

Mukherjee, S., & Paulino, G. H. (2003). The Elastic-Viscoelastic Correspondence Principle for Functionally Graded Materials, Revisited. *Journal of Applied Mechanics, 70*(3), 359-363.

Mura, T. (1987). *Micromechanics of defects in solids* (2nd ed.): Springer Netherlands.

Murakami, S., & Ohno, N. (1981). *A continuum theory of creep and creep damage*. Paper presented at the IUTAM Symposium on Creep in Structures Berlin, Heidelberg.

Narayan, S. P. A., Krishnan, J. M., Deshpande, A. P., & Rajagopal, K. R. (2012). Nonlinear viscoelastic response of asphalt binders: An experimental study of the relaxation of torque and normal force in torsion. *Mechanics Research Communications, 43*, 66-74.

Norris, A. N. (1985). A differential scheme for the effective moduli of composites. *Mechanics of Materials, 4*(1), 1-16.

Norris, A. N. (1989). An examination of the Mori-Tanaka effective medium approximation for multiphase composites. *Journal of Applied Mechanics, ASME, 56*, 83-88.

Oliver, J. (1990). IOn the discrete constitutive models induced by strong discontinuity kinematics and continuum constitutive equations. *International Journal of Solids and Structures, 37*, 7207-7229.

Oller, S., Oñate, E., Miquel, J., & Botello, S. (1996). A plastic damage constitutive model for composite materials. *International Journal of Solids and Structures, 33*(17), 2501-2518.

Olszak, W., & Perzyna, P. (1969). On thermal effects in viscoplasticity. *Journal of Applied Mathematics and Physics, 20*, 676–680.

Ortiz, M. (1985). A constitutive theory for the inelastic behavior of concrete. *Mechanics of Materials, 4*, 67-93.

Ortiz, M. (1987a). An analytical study of the localized failure modes of concrete. *Mechanics of Materials, 6*, 159-174.

Ortiz, M. (1987b). A method of homogenization of elastic media. *International Journal of Engineering Science, 25*(7), 923-934.

Ortiz, M., & Simo, J. C. (1986). An analysis of a new class of integration algorithms for elastoplastic constitutive relations. *International Journal for Numerical Methods in Engineering, 23*(3), 353-366.

Pandey, V. B., Singh, I. V., Mishra, B. K., Ahmad, S., Rao, A. V., & Kumar, V. (2019). Creep crack simulations using continuum damage mechanics and extended finite element method. *International Journal of Damage Mechanics, 28*(1), 3-34.

Park, S. W., Kim, Y. R., & Schapery, R. A. (1996). A viscoelastic continuum damage model and its application to uniaxial behavior of asphalt concrete. *Mechanics of Materials, 24*(4), 241-255.

Park, S. W., & Schapery, R. A. (1999). Methods of interconversion between linear viscoelastic material functions, Part I – a numerical method based on Prony series,. *International Journal of Solids and Structures, 3*, 1653-1675.

Perzyna, P. (1966). Fundamental problems in viscoplasticity. *Advances in Applied Mechanics, 9*(2), 243-377.

Polanco-Loria, M., & S¢rensen, S. I. (1995). Damage evolution laws for concrete - a comparative study. *Fracture Mechanics of Concrete Structures, Proceedings FRAMCOS-2*, 1027-1036.

Puissant, S., Demay, Y., Vergnes, B., & Agassant, J. F. (1994). Two-dimensional multilayer coextrusion flow in a flat coat-hanger die. Part I: Modeling. *Polymer Engineering and Science, 34*(3), 201-208.

Qiu , Y. P., & Weng, G. J. (1990). On the application of Mori-Tanaka's theory involving transversely isotropic spheroidal inclusions. *International Journal of Engineering Science, 289*, 1121-1137.

Qu, J., & Cherkaoui, M. (2006). *Fundamentals of Micromechanics of Solids*: Wiley.

Rabotnov, Y. N. (1963). On the Equation of State of Creep. *Proceedings of the Institution of Mechanical Engineers, 178*(1), 2-117-112-122.

Rajagopal, K. R., & Srinivasa, A. R. (2005). A note on a correspondence principle in nonlinear viscoelastic materials. *International Journal of Fracture, 131*(4), L47-L52.

Read, W. T. (1950). Stress analysis for compressible viscoelastic materials. *Journal of Applied Physics, 21*, 671-674.

Rice, J. R. (1971). Inelastic constitutive relations for solids: An internal-variable theory and its application to metal plasticity. *Journal of the Mechanics and Physics of Solids, 19*(6), 433-455.

Rice, J. R., & Tracey, D. M. (1969). On the ductile enlargement of voids in triaxial stress fields. *Journal of the Mechanics and Physics of Solids, 17*(3), 201-217.

Risse, W., & Grubbs, R. H. (1991). Block and graft copolymers by living ring-opening olefin metathesis polymerization. *Journal of Molecular Catalysis, 65*(1-2), 211-217.

Rizzo, F. J., & Shippy, D. J. (1971). An application of the correspondence principle of linear viscoelasticity theory. *Siam Journal on Applied Mathematics, 21*(2), 321-330.

Roque, R., & Buttlar, W. G. (1992). Development of a measurement and analysis system to accurately determine asphalt concrete properties using the indirect tensile mode. *Asphalt Paving Technology: Association of Asphalt Paving Technologists-Proceedings of the Technical Sessions, 61*, 304-333.

Roscoe, R. (1952). The viscosity of suspensions of rigid spheres. *British Journal of Applied Physics, 3*, 267-269.

Scarpas, A., Al-Khoury, R., Van Gurp, C., & Erkens, S. M. J. G. (1997). *Finite element simulation of damage development in asphalt concrete pavements*. Paper presented at the Eighth International Conference on Asphalt Pavements, Seattle, Washington.

Schapery, R. A., & Park, S. W. (1999). Methods of interconversion between linear viscoelastic material functions. Part II-an approximate analytical method. *International Journal of Solids and Structures, 36*, 1677-1699.

Schreyer, H. L. (1995). Continuum Damage Based on Elastic Projection Operators. *International Journal of Damage Mechanics, 4*(2), 171-195.

Schrock, R. R. (1994). Recent Advances in the Chemistry and Applications of High-Oxidation State Alkylidene Complexes. *Pure and Applied Chemistry, 66*(7), 1447-1454.

Sermage, J. P., Lemaitre, J., & Desmorat, R. (2000). Multiaxial creep fatigue under anisothermal conditions. *Fatigue & Fracture of Engineering Materials & Structures, 23*(2), 241-252.

Sharif-Kashani, P., Hubschman, J. P., Sassoon, D., & Kavehpour, H. P. (2011). Rheology of the vitreous gel: Effects of macromolecule organization on the viscoelastic properties. *Journal of Biomechanics, 44*, 419–423.

Shen, F., Hu, W., & Meng, Q. (2015). A damage mechanics approach to fretting fatigue life prediction with consideration of elastic–plastic damage model and wear. *Tribology International, 82*(A), 176-190.

Si, Z., Little, D. N., & Lytton, R. L. (2002). Characterization of Microdamage and Healing of Asphalt Concrete Mixtures. *Journal of Materials in Civil Engineering, 14*(6), 461-470.

Simo, J. C., & Hughes, T. J. R. (1998). *Computational Inelasticity*: Springer New York.

Simo, J. C., & Ju, J. W. (1987). Strain- and stress-based continuum damage model - I. Formulation. *International Journal of Solids and Structures, 23*(7), 821-840.

Simo, J. C., & Ortiz, M. (1985). A unified approach to finite deformation elastoplastic analysis based on the use of hyperelastic constitutive equations. *Computer Methods in Applied Mechanics and Engineering, 49*(2), 221-245.

Stevens, D. J., & Liu, D. (1992). Strain-based constitutive model with mixed evolution rules for concrete. *Journal of Engineering Mechanics, ASCE, 118*(6).

Sun, L. Z., & Ju, J. W. (2004). Elastoplastic Modeling of Metal Matrix Composites Containing Randomly Located and Oriented Spheroidal Particles. *Journal of Applied Mechanics, 71*(6), 774-785.

Sun, L. Z., Ju, J. W., & Liu, H. T. (2003). Elastoplastic modeling of metal matrix composites with evolutionary particle debonding. *Mechanics of Materials, 35*(3), 559-569.

Tai, W. H., & Yang, B. X. (1986). A new microvoid-damage model for ductile fracture. *Engineering Fracture Mechanics, 25*, 377-384.

Tarefder, R., & Faisal, H. (2013). Modeling Nanoindentation Creep Behavior of Asphalt Binder,. *Advances in Civil Engineering Materials, 2*(1), 418-440.

Tashman, L., Masad, E., Little, D. N., & Zbib, H. (2005). A microstructure-based viscoplastic model for asphalt concrete. *International Journal of Plasticity, 21*(9), 1659-1685.

Taya, M., & Chou, T. W. (1981). On two kinds of ellipsoidal inhomogeneities in an infinite elastic body: an application to a hybrid composite. *International Journal of Solids and Structures, 17*(6), 553-563.

Taya, M., & Mura, T. (1981). On stiffness and strength of an aligned short-fiber reinforced composite containing fiber-end cracks under uniaxial applied stress. *Journal of Applied Mechanics, 48*(2), 361-347.

Tehrani, F. F., Allou, F., Absi, J., & Petit, C. (2013). *Investigation on Mechanical Properties of Bituminous Materials through 2D/3D Finite Element Numerical Simulations.* Paper presented at the Multi-Scale Modeling and Characterization of Infrastructure Materials.

Tham, C. L., Zhang, Z., & Masud, A. (2005). An elasto-plastic damage model cast in a co-rotational kinematic framework for large deformation analysis of laminated composite shells. *Computer Methods in Applied Mechanics and Engineering, 194*(21-24), 2641-2660.

Thomson, W. (1852). On the universal tendency in nature to the dissipation of mechanical energy. *Philosophical Magazine, 4*(25), 304-306.

TRIP. (2016). *Urban Roads TRIP Report: Bumpy roads ahead: America's roughest rides and strategies to make our roads smoother*.TRIP.

Tschoegl, N. W. (1989). *The Phenomenological Theory of Linear Viscoelastic Behavior*: Springer-Verlag, Heidelberg.

Tschoegl, N. W. (1997). Time Dependence in Materials Properties: An Overview. *Mechanics of Time-Dependent Materials, 1*, 3-31.

Vadood, M., Johari, M. S., & Rahai, A. R. (2015). A new approach for simulation of hot mix asphalt; numerical and experimental. *Journal of Mechanics, 31*(6), 701-711.

Vallons, K., Drozdzak, R., Charret, M., & Lomov, S. (2015). *Damage development in woven glass fibre composites with tough thermoset matrix*. Paper presented at the TexComp-12, Raleigh, NC.

Voyiadjis, G. Z., Taqieddin, Z. N., & Kattan, P. (2008). Theoretical Formulation of a Coupled Elastic—Plastic Anisotropic Damage Model for Concrete using the Strain Energy Equivalence Concept. *International Journal of Damage Mechanics, 18*(7), 603-638.

Walpole, L. J. (1966a). On bounds for overall elastic moduli of inhomogeneous systems-I. *Journal of the Mechanics and Physics of Solids, 14*, 151-162.

Walpole, L. J. (1966b). On bounds for overall elastic moduli of inhomogeneous systems-II. *Journal of the Mechanics and Physics of Solids, 14*, 289-301.

Wang, H., & Hao, P. (2011). Numerical simulation of indirect tensile test based on the microstructure of asphalt mixture. *Journal of Materials in Civil Engineering, 23*(1), 21-29.

Wang, Y., Zhang, L., Sun, J., Bao, J. B., Wang, Z., & Ni, L. (2017). Dramatic Toughness Enhancement of Polydicyclopentadiene Composites by Incorporating Low Amounts of Vinyl-Functionalized SiO2. *Industrial & Engineering Chemistry Research, 56*(16), 4750-4757.

Weng, G. J. (1984). Some elastic properties of reinforced solids, with special reference to isotropic ones containing spherical inclusions. *International Journal of Engineering Science, 22*, 845-856.

Weng, G. J. (1990). The theoretical connection between Mori-Tanaka's theory and the Hashin-Shtrikman-Walpole bounds. *International Journal of Engineering Science, 28*, 1111-1120.

White, S. R., Sottos, N. R., Geubelle, P. H., Moore, J. S., Kessler, M., Sriram, S. R., . . . Viswanathan, S. (2001). Autonomic healing of polymer composites. *Nature, 409*(6822), 794-797.

Willis, J. R. (1977). Bounds and self-consistent estimates for the overall properties of anisotripic composites. *Journal of the Mechanics and Physics of Solids, 25*, 185-202.

Willis, J. R. (1991). On methods for bounding the overall properties of nonlinear composites. *Journal of the Mechanics and Physics of Solids, 39*, 73-86.

Willis, J. R. (1994). Upper and lower bounds for nonlinear composite behavior. *Materials Science and Engineering: A, 175*, 7-14.

Witczak, M. W., Kaloush, K., Pellinen, T. K., M., E.-B., & Von Quitus, H. (2002). *Simple Performance Test for Superpave Mix Design*.NCHRP Report 465, Transportation Research Board.

Wu, C. H. (1985). *Tension-compression test of a concrete specimen via a structure damage theory.* Paper presented at the Damage Mechanics and Continuum Modeling, Detroit.

Wu, Y., & Ju, J. W. (2017). Elastoplastic damage micromechanics for continuous fiber-reinforced ductile matrix composites with progressive fiber breakage. *International Journal of Damage Mechanics, 26*(1), 4-28.

Xiao, F., Amirkhanian, S., & Juang, C. H. (2007). Rutting Resistance of Rubberized Asphalt Concrete Pavements Containing Reclaimed Asphalt Pavement Mixtures. *Journal of Materials in Civil Engineering, 19*(6), 475-483.

Yan, Z. G., Zhang, Y., Ju, J. W., Chen, Q., & Zhu, H. H. (2019). An equivalent elastoplastic damage model based on micromechanics for hybrid fiber-reinforced composites under uniaxial tension. *International Journal of Damage Mechanics, 28*(1), 79-117.

Yang, R. B., & Mal, A. K. (1995). The effective transverse moduli of a composite with degraded fiber-matrix interfaces. *International Journal of Engineering Science, 33*(11), 1623-1632.

Yazdani, S. (1993). On a Class of Continuum Damage Mechanics Theories. *International Journal of Damage Mechanics, 2*(2), 162-176.

Yazdani, S., & Schreyer, H. L. (1988). An Anisotropic Damage Model with Dilatation for Concrete. *Mechanics of Materials, 7*(3), 231-244.

Yin, A. Y., Yang, X. H., Zeng, G. W., & Gao, H. (2015). Experimental and numerical investigation of fracture behavior of asphalt mixture under direct shear loading. *Construction and Building Materials, 86*, 1.

You, Z., & Buttlar, W. G. (2004). Discrete Element Modeling to Predict the Modulus of Asphalt Concrete Mixtures. *Journal of Materials in Civil Engineering, 16*(2), 140-146.

You, Z., Liu, Y., & Dai, Q. (2011). Three-Dimensional Microstructural-Based Discrete Element Viscoelastic Modeling of Creep Compliance Tests for Asphalt Mixtures. *Journal of Materials in Civil Engineering, 23*(1), 79-87.

Yuan, K. Y., Ju, J. W., Yuan, W., & Yang, J. M. (2014). Numerical predictions of mechanical behavior of innovative pothole patching materials featuring high toughness, low-viscosity nano-molecular resins. *Acta Mechanica, 225*(4-5), 1141-1151.

Yuan, W., Yuan, K. Y., Zou, L., Yang, J. M., Ju, J. W., Kao, W., . . . Stephen, T. (2012). *DCPD resin catalyzed with Grubbs catalysts for reinforcing pothole patching materials.* Paper presented at the SPIE 8347, Nondestructive Characterization for Composite Materials, Aerospace Engineering, Civil Infrastructure, and Homeland Security 2012, San Diego, California.

Yuan, W., Yuan, K. Y., Zou, L., Yang, J. M., Ju, J. W., Kao, W., . . . Aktan, A. E. (2013). *Two layer structure for reinforcing pothole repair*. Paper presented at the

Nondestructive Characterization for Composite Materials, Aerospace Engineering, Civil Infrastructure, and Homeland Security 2013.

Yuan, W., Yuan, M., Zou, L., Yang, J. M., Ju, W., Kao, W., . . . Solamon, R. (2011). *Development of high-toughness low-viscosity nano-molecular resins for reinforcing pothole patching materials.* Paper presented at the SPIE 7983, Nondestructive Characterization for Composite Materials, Aerospace Engineering, Civil Infrastructure, and Homeland Security 2011, San Diego, California.

Zhang, X., Wan, C., Wang, D., & He, L. (2011). Numerical simulation of asphalt mixture based on three-dimensional heterogeneous specimen. *Journal of Central South University of Technology, 18*(6), 2201-2206.

Zhu, H., & Sun, L. (2013). A viscoelastic–viscoplastic damage constitutive model for asphalt mixtures based on thermodynamics. *International Journal of Plasticity, 40*, 81-100.

Zhu, X. Y., Wang, X., & Yu, Y. (2014). Micromechanical creep models for asphalt-based multi-phase particle-reinforced composites with viscoelastic imperfect interface. *International Journal of Engineering Science, 76*, 34-46.

CHAPTER 7 : CONCLUSIONS AND FUTURE WORK

7.1 Conclusions

In this research, novel micromechanical-based isotropic frameworks have been proposed to predict the mechanical behavior of the asphalt concrete materials featuring high toughness, low viscosity nano-molecular resins and employed for comparisons between model predications and experimental measurements. An analytical approximation modeling methodology is established by treating the revolutionary asphalt concrete materials as an asphalt mastic composite matrix containing fine aggregates, asphalt binder, polymerized DCPD and air voids with coarse aggregates inhomogeneities distributed in it. Chapter 3 presents an initial strain energy based isotropic elastic-damage model through the net stress concept in conjunction with the hypothesis of strain equivalence, while similar damage evolution criterion is employed in Chapter 4 and 5 for elastoplastic-damage and elasto-viscoplastic-damage frameworks. In Chapter 6, an analytical formulation is proposed within the micromechanical framework based on the concept of the correspondence principle to predict the isotropic viscoelastic properties of the multiphase asphalt mastic composites. The conclusions of this dissertation are summarized below:

1. A multilevel homogenization approach is proposed to evaluate the effective elastic properties of the multi-phase composites employing an ensemble-volume averaged

micromechanical formulation. Evaluation results are compared with well-known analytical bounds and great agreement can be observed.

2. The governing isotropic initial elastic strain energy based damage evolution criterion is characterized through the net stress concept in conjunction with the hypothesis of strain equivalence.

3. Computational algorithms of coupled elastoplastic-damage/ elasto-viscoplastic-damage are developed based on a two-step operator splitting methodology by means of refined additive split of the stress tensor and the energy norm of the strain tensor.

4. The effective viscoelastic mechanical properties of multi-phase asphalt mastic composites are analytically formulated with the concept of the correspondence principle. Specifically, a simple yet accurate 4-parameter Burgers model is employed to evaluate the viscoelastic behavior of the asphalt binder phase.

5. A 3-D numerical model is constructed to simulate the actual asphalt concrete specimens. Algorithms are implemented to make sure spherical inclusions are randomly dispersed in the matrix and there is no overlapping among each other. The proposed damage evolution law and plastic/ viscoplastic return mapping correctors are carried out.

6. From the comparisons of experimental data and numerical simulations results, it is observed that the proposed elastic-damage model and elastoplastic-damage model can capture the mechanical behavior of the innovative asphalt concrete material under the

splitting tension test reasonably well. In particular, the prediction is more precise with plastic deformation taken into consideration.

7.2 Future Work

In this section, we present a plan and lay out a foundation for future research as extension of this doctoral dissertation:

1. **More Validation of the Proposed Isotropic Formulations**: Due to the limitation of associated experimental data, the proposed elastic-damage and elastoplastic-damage formulations have compared with the splitting tension test data, where reasonably good agreements are observed. In order to enhance the prediction and reliability of the proposed formulations, more validations need to be performed to the parameters, such as initial damage threshold, material-dependent damage variables, plasticity material constant. In addition, possible experiments, such as monotonic uniaxial tension tests with different strain rates at different temperatures with different volume fractions of components, can be done and compare with the proposed thermo-elastic-viscoplastic-damage framework.

2. **Characterization of Fatigue and Rutting Resistance Behavior**: To serve as pavement, the innovative asphalt concrete material will undergo perennial traffic loading, hence it is essential to characterize the fatigue and rutting resistance capacity of the material. The current time dependent framework may be adopted to estimate the mechanical responses of the material under repeated loading. Furthermore, the current correspondence

principle with the Laplace transform may be adopted with the Fourier transform to identify the complex viscoelasticity response.

3. **Evaluation of the Caging Effect by the p-DCPD Network**: A multilayer-coated particle concept was proposed in the current frameworks to consider the caging effect of the p-DCPD network locking asphalt binder to the aggregates, while an alternative, more accurate approach to evaluate the caging effect could be p-DCPD network cages distributed as the Voronoi cells. The strength enhancement due to the cages can be represented as chain stiffness, or an energy potential that requires to break one or more chains in the cells.

4. **Assessment on Effects of Irregular Coarse Aggregates**: Spheroidal, ellipsoidal and other representative shaped particles need to be evaluated besides the spherical particle. Effects of texture, angularity and orientation of coarse aggregates on the mechanical behavior also needs to be studied. By summarizing the effects of irregular coarse aggregates, a general shape factor function can be developed for assessment purposes.

5. **Application to Self-Healing Composites**: Self-healing materials are mentioned in the literature review with the concept of ability of composite materials to reduce the degradation with the aid of a healing agent by means of chemical interactions. The proposed micromechanical frameworks can be modified to predict the mechanical performance of the self-healing composites.